NOVEL-TYPE DIMERIC NAPHTHYLISOQUINOLINE ALKALOIDS FROM CONGOLESE *ANCISTROCLADUS* LIANAS: ISOLATION, STRUCTURAL ELUCIDATION, AND ANTIPROTOZOAL AND ANTI-TUMORAL ACTIVITIES

Dissertation zur Erlangung des

naturwissenschaftlichen Doktorgrades

der Julius-Maximilians-Universität Würzburg

vorgelegt von

Blaise Kimbadi Lombe

aus Kabinda,

Demokratische Republik Kongo

Würzburg 2019

Eingereicht am: _____

bei der Fakultät für Chemie und Pharmazie

1. Gutachter: _____

2. Gutachter: _____

der Dissertation

1. Prüfer: _____

2. Prüfer: _____

3. Prüfer: _____

Des Öffentlichen Promotionskolloquiums

Tag des Öffentlichen Promotionskolloquiums: _____

Doktorurkunde ausgehändigt am: _____

Die vorliegende Arbeit wurde am Institut für Organische Chemie

der Universität Würzburg angefertigt

Herrn Prof. Dr. Dr. h.c. mult. G. Bringmann danke ich

nicht nur für Seine hervorragende Betreuung bei der Durchführung dieser Arbeit,

sondern auch für Seine exzellenten Ratschläge und Seine Unterstützung,

sowohl in sozialer als auch in wissenschaftlicher Hinsicht,

seit 2008, als ich BEBUC-Stipendiat wurde.

DEDICATED TO

MY FAMILY

"Bokiebe nswa, otopa lume"

("If you want ants, you should wet yourself with dew")

Songye proverb

ABBREVIATIONS AND ACRONYMS

1 (or n) D	One (or n) dimensional
A.D.	After Death
AIDS	Acquired Immune Deficiency Syndrome
AO	Acridine Orange
ATR	Attenuated Total Reflection
AU	Absorbance Unit
B.C.	Before Christ
CD	Circular Dichroism
CH_2Cl_2	Dichloromethane
D.R. Congo	Democratic Republic of the Congo
DAD	Diode-Array Detector
DMEM	Dulbecco's Modified Eagle's Medium
DNA	Deoxyribonucleic Acid
EB	Ethidium Bromide
ECD	Electronic Circular Dichroism
ESI	Electrospray Ionization
EtOAc	Ethyl acetate
EtOH	Ethanol
FA	Formic Acid
GC	Gas Chromatography
GC-MS	Gas Chromatography coupled to Mass Spectrometry
H_2O	Water
HeLa	Immortal cervical cancer cell line taken from a female patient, Henrietta Lacks
HIV	Human Immunodeficiency Virus
HIV-1	HIV type 1 (the worldwide most prevalent type)
HIV-2	HIV type 2 (less pathogenic, mostly from West Africa)
HMBC	Heteronuclear Multiple Bond Correlation
HPLC	High-Performance Liquid Chromatography
HPLC-UV-MS-ECD	HPLC coupled to UV, MS, and ECD
HRESIMS	High-Resolution Electrospray Ionization Mass Spectrometry
HRMS	High-Resolution Mass Spectrometry
HSQC	Heteronuclear Single Quantum Correlation

IC_{50}	Half maximal inhibitory concentration
IR	Infrared
K1	Chloroquine-resistant strain of *Plasmodium falciparum*
L6	Immortalized rat cell line
LC	Liquid Chromatography
LC-UV-MS-CD	LC coupled to UV, MS, and CD
m/z	Mass-to-charge ratio
MD	Medical Doctor
Me	Methyl group
MeCN	Acetonitrile
MeOD	Deuterated methanol
MeOH	Methanol
min	Minute
MS	Mass Spectrometry
MSD	Mass Selective Detector
NDM	Nutrient-Deprived Medium
NF54	Drug sensitive strain of *Plasmodium falciparum*
NIQ	Naphthylisoquinoline
NMR	Nuclear Magnetic Resonance
NOE	Nuclear Overhauser Enhancement
NOESY	Nuclear Overhauser Enhancement Spectroscopy
PANC-1	Pancreatic cancer cells derived from a Caucasian lady suffering from a pancreatic carcinoma of ductal cell origin
PC_{50}	Concentration at which 50% of the cancer cells are killed in nutrient-deprived medium without displaying toxicity in normal, nutrient-rich medium
ROE	Rotating frame Overhauser Enhancement
ROESY	Rotating frame Overhauser Enhancement Spectroscopy
R_T	Retention time
SFB 630	Collaborative Research Center 630
SI	Selectivity Index
SSR	Simple Sequence Repeat
TFA	Trifluoroacetic acid
TIC	Total Ion Current

TLC	Thin Layer Chromatography
USA	United States of America
UV	Ultraviolet
WHO	World Health Organization

RESULTS AND DISCUSSION

1. Introduction

> *"We are in crisis mode. If resistance emergence is not addressed fully, a future with*
> *suboptimal antimicrobial chemotherapy is a real possibility.*[…]
> *New agents need to be discovered."*
> (George L. Drusano, PhD and MD, Infectious Diseases and Pharmacology)[1]

This quote from G. L. Drusano, the current Director of the Institute for Therapeutic Innovation at the University of Florida (USA), succinctly defines most disturbing and challenging issues with which the worldwide health care system is confronted. Not only are many existing drugs of limited value by their toxicity or significant side effects, low efficacy, uncomfortable or inappropriate dosing regimens,[2] but also many others are becoming ineffective and useless due to the increasing incidence of resistance.[2-4]

While drug resistance concerns an ever-increasing number of infectious[5] and tumor[6] diseases, it is in particular really worrying for major global illnesses like malaria.[7,8] The latter affects many millions of lives mainly in the tropics and subtropics, killing each year about half a million of people. In 2017, for example, the World Health Organization (WHO) counted 219 million of malaria cases and the estimated number of deaths due to this parasitic sickness reached 435,000.[9] *Plasmodium falciparum*, the most harmful malaria causing pathogen,[10] has meanwhile developed resistance to nearly all existing antimalarials, now even including artemisinin (**1**) and its analogs such as artemether (**2**).[11-14] These drugs have served for decades as the most efficient antimalarial therapy.[15] Effective vaccines for this life-threatening illness are not yet available, which is also true for many other infectious and tumor diseases. The development of new powerful therapies is therefore urgently needed.
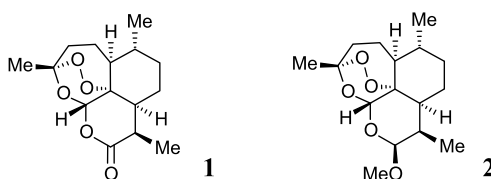
Figure 1. The natural antimalarial artemisinin (**1**) and its likewise antimalarial derivative artemether (**2**).

With respect to the big challenge to introduce new therapeutical strategies to cure infectious and tumoral diseases in order to step off the resistance treadmill, a number of research groups are currently committed in the search for novel and powerful agents. Many of these groups target particularly the plant kingdom as a potential source of new drugs. This interest in plants is related to the fact that already since very ancient time, long before the Christian era, plants have been the cornerstone of the human health care.[16-20] The medicinal use of plants for many centuries can be found in virtually all human communities and there exist many written records evidencing such an ancient utilization of plant extracts. The use of phytomedicines is documented, for example, in the *Ebers Papyrus* (a plant-medicine encyclopedia that was found in Egypt and estimated to have been written around 1,500 B.C.),[21] the *Sheng Nong's Herbal Classic* (the oldest herbal classic in China, written around 221 B.C. to 220 A.D.),[15,22] and the *Corpus hippocratum* (a famous compilation of ancient Greek medical works attributed to Hippocrate, 460-377 B.C.).[23] Even in our modern time, plant extracts still play an important role in the medical management system, particularly in developing countries, where about 80% of the population have to rely on traditional formulations for their primary health care.[24]

Moreover, the plant kingdom is – directly or indirectly – a tremendous source of several outstanding conventional medicines currently used.[19,25,26] Perennial highlights of such plant-derived drugs are, for example, the aforementioned artemisinin (**1**),[15,27,28] discovered in the plant *Artemisia annua* L. (Asteraceae) in 1972, the antimalarial quinine (**3**), isolated from the plant *Cinchona succirubra* PAVON (Rubiaceae) in 1820,[29,30] the analgesic and soporific morphine (**4**), isolated from *Papaver somniferum* L. (Papaveraceae) in 1806,[31,32] and the anti-inflammatory salicin (**5**), isolated in 1828 from willow trees (*Salix* sp., Salicaceae). Aspirin (**6**), one of the most popular and widely used pharmaceutical agents, has been developed from salicin (**5**).[33,34]
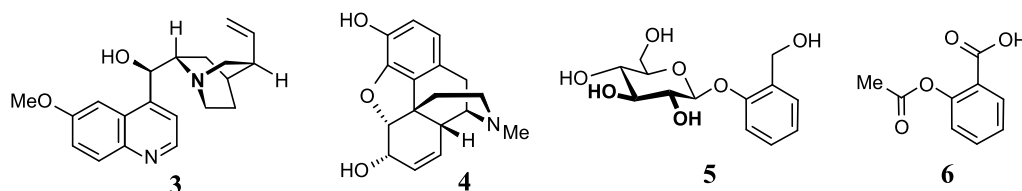
Figure 2. The plant-derived drugs quinine (**3**), morphine (**4**), and salicin (**5**); and aspirin (**6**), a derivative of **5**.

A special scientific interest of our group is devoted to the search for novel antiparasitic and antitumoral natural products in the plant kingdom, focusing particularly on the two phylogenetically related plant families Ancistrocladaceae and Dioncophyllaceae.[35-38] These families are endemic to tropical forests across Africa and Southeast Asia,[39,40] where some of the species are traditionally used by natives for the treatment of several diseases, among them malaria.[41-43]
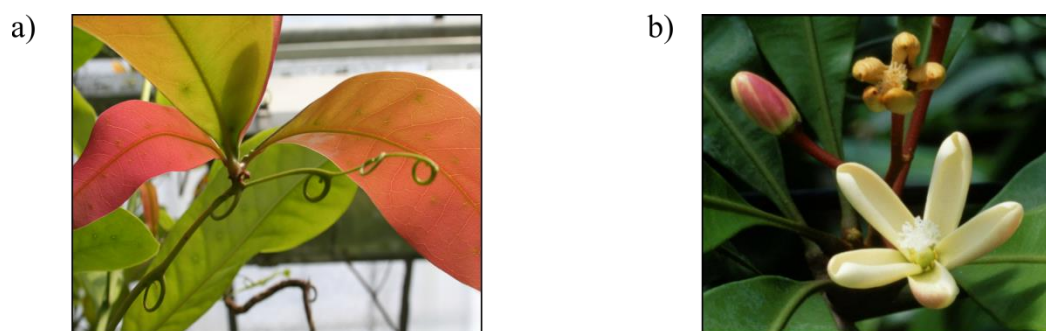
Figure 3. a) The tropical plant *Ancistrocladus congolensis* J. LÉONARD (Ancistrocladaceae); and b) the liana *Triphyophyllum peltatum* (HUTCH. & DALZ.) AIRY SHAW (Dioncophyllaceae). Credit photos: AK Bringmann.

Phytochemical studies on Ancistrocladaceae and Dioncophyllaceae plants revealed that their medicinal properties are due to the presence of naphthylisoquinoline alkaloids (NIQs),[44,45] a class of compounds that are remarkable in many respects:

- Structurally, because of the presence of both, chiral axes and stereogenic centers in their unique molecular scaffolds consisting of a naphthalene portion and an isoquinoline part, connected by a *C*,*C*- or an *N*,*C*-linkage (see examples in Figure 4);
- Biosynthetically, because they are the first (and as yet only) isoquinolines that do not originate from aromatic amino acids, as usual for the tetrahydroisoquinoline alkaloids such as morphine (**4**),[46,47] but rather from polyketide precursors;[48,49]
- Pharmacologically, because some of them exhibit strong antiprotozoal or antitumor activities, depending on their individual structures;[50-52] and
- Chemotaxonomically, because of their restricted occurrence only in the aforementioned two plant families, so that they serve as excellent phylogenetic markers.

Some prominent examples of NIQs are the antimalarial dioncophylline C (**7**),[53,54] the antitrypanosomal ancistrolikokine B (**8**),[55] the antileishmanial ancistrocladinium A (**9**),[56] and the antileukemic dioncophylline A (**10**).[57-60]
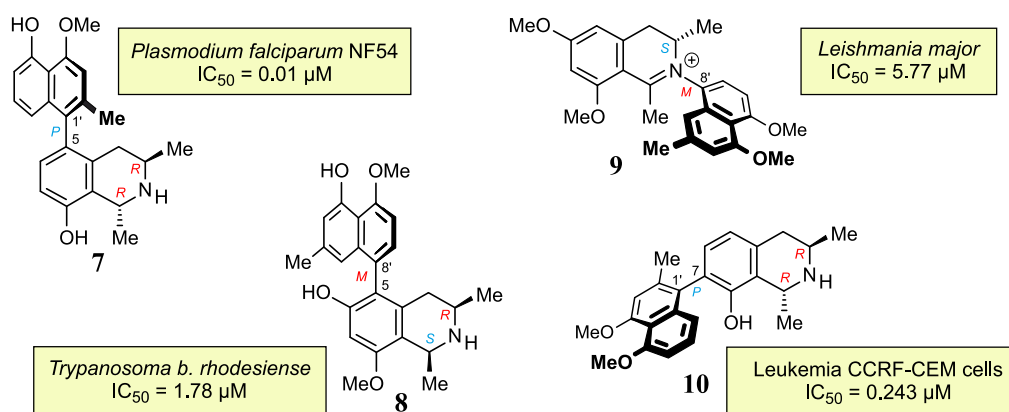
Figure 4. Selected metabolites highlighting the strong pharmacological properties and intriguing structural – in particular stereochemical – peculiarities of the class of NIQs: dioncophylline C (**7**), ancistrolikokine B (**8**), ancistrocladinium A (**9**), and dioncophylline A (**10**).

Structurally and pharmacologically most intriguing are the dimeric NIQs. Not only do they possess complex molecular architectures, with at least twice the number of elements of chirality, but they also display pronounced bioactivities. The very first NIQ dimers, the michellamines A (**11a**) and B (**11b**) (Figure 5), both with four stereocenters and two chiral biaryl axes, were isolated from *Ancistrocladus korupensis* D. W. THOMAS & GEREAU (Ancistrocladaceae) in the early 1990s.[61,62] These two metabolites were found to exert strong antiviral activities. Particularly remarkable was the quateraryl **11b**, which showed most impressive anticytopathic effects against both, HIV-1 and HIV-2, and even against other resistant strains of the AIDS-causing virus.[61-63] These remarkable anti-HIV properties, in combination with the unique structural features, triggered numerous syntheses of michellamine-type quateraryls[64-71] and the directed search for such dimers in different *Ancistrocladus* species, including even those that were botanically as yet undescribed.[72-74]

By 2001 a total of eight natural dimers were known, comprising seven quateraryls from *A. korupensis*, the michellamines A-F[62,75] and korundamine A (**12**),[76] and ancistrogriffithine A (**13**) from *A. griffithii* PLANCH.[72,77] These eight metabolites were all coupled via the sterically least hindered C-6′ positions of both naphthalene portions, so that the central binaphthalene axis was freely rotating and, thus, did not constitute an additional element of chirality. Among these 6′,6″-coupled dimers were constitutionally symmetric compounds, consisting of two 5,8′- or 7,8′-linked NIQ portions, like e.g., compounds **11a**, **11b**, and **13**, but also constitutionally unsymmetric representatives, such as the alkaloid **12**, which was a cross-coupling product of a 5,8′- and a 7,8′-linked NIQ portion.
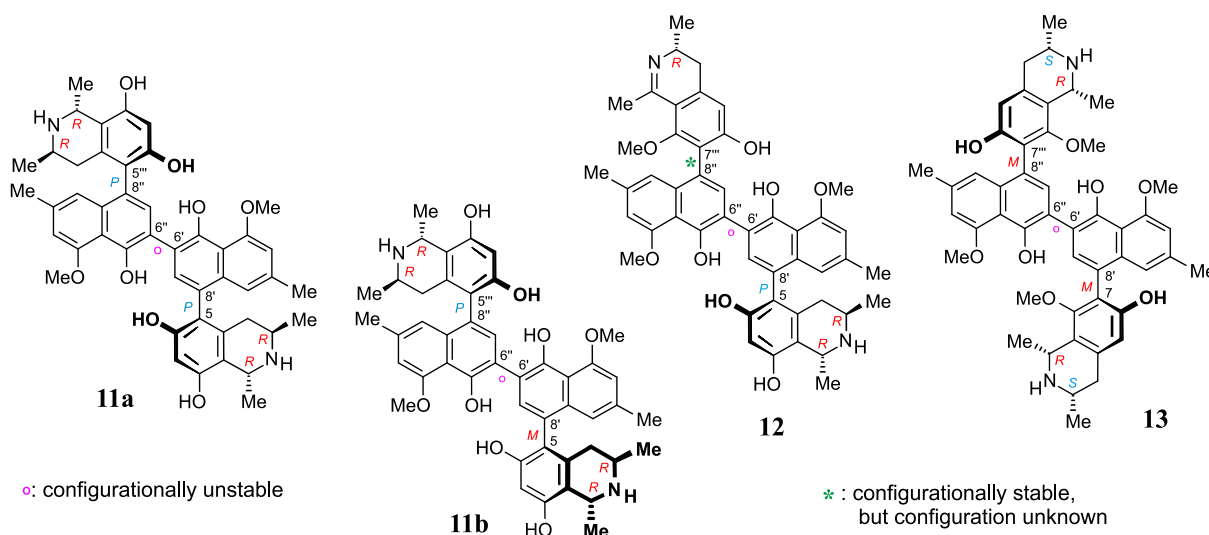
Figure 5. Michellamines A (**11a**) and B (**11b**), the first NIQ dimers discovered in nature, and two of their 6′,6″-coupled dimeric NIQ analogs, korundamine A (**12**) and ancistrogriffithine A (**13**).

In the early 2010s, the structural variety of dimeric NIQs was further enlarged by the discovery of five[78] new representatives in the Chinese species *A. tectorius* (LOUR.) MERR. and an additional one[79] in a botanically as yet unidentified *Ancistrocladus* species from the Democratic Republic of the Congo (D.R. Congo), all of them exhibiting unique molecular frameworks. These six quateraryls, among them shuangancistrotectorine D (**14**) and jozimine A₂ (**15**), were the first compounds linked via the sterically far more congested 1′,1″- or 3′,3″-positions of the naphthalene units. Consequently, their central biaryl axes were rotationally hindered, leading to the presence of three consecutive chiral biaryl axes. Some of these dimeric compounds displayed most remarkable antiprotozoal activities, with jozimine A₂ (**15**) showing extraordinary antiplasmodial properties (IC_{50} = 0.001 μM) against *P. falciparum* NF54, which, combined with its low cytoxicity (IC_{50} = 15.9 μM) against L6 cells,[79] made it a potential candidate for drug development.
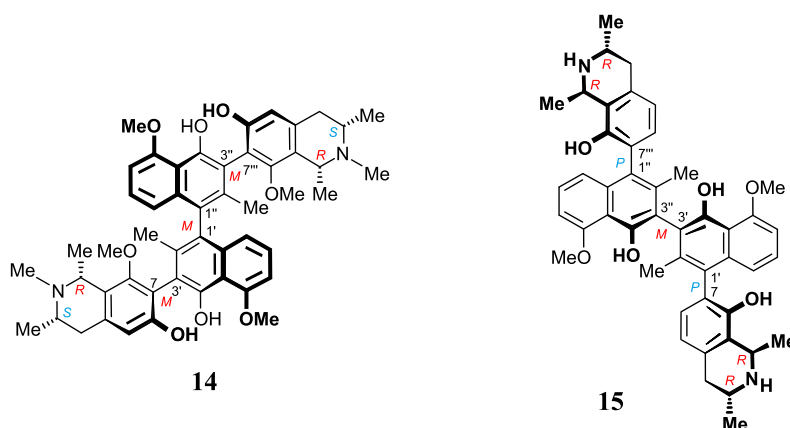
Figure 6. The first examples of symmetrically coupled NIQ dimers with three consecutive chiral axes: shuangancistrotectorine D (**14**) and jozimine A₂ (**15**).

Most recently in the course of the master studies of the author of the present thesis, a most exciting discovery in the field of dimeric NIQs was accomplished: The isolation of two structurally unusual compounds, named mbandakamines A (**16a**) and B (**16b**), consisting – similar to the aforementioned michellamines – of two 5,8′-coupled monomeric NIQs.[80] These quateraryls, different from all the previously known ones, were unsymmetrically coupled at the central biaryl axis. They showed an exceptional 6′,1″-coupling, in the *peri*-position neighboring one of the outer axes, leading to an extremely high steric hindrance at the central axis. Their hairpin-like curved molecular scaffolds, pressing some of the molecular subunits against each other, suggested that biosynthetic follow-up reactions could take place, leading to further, structurally even more original molecular scaffolds. Moreover, the two NIQs dimers exhibited pharmacologically interesting properties, among them strong antiplasmodial activities,[80] as described in more details later below.
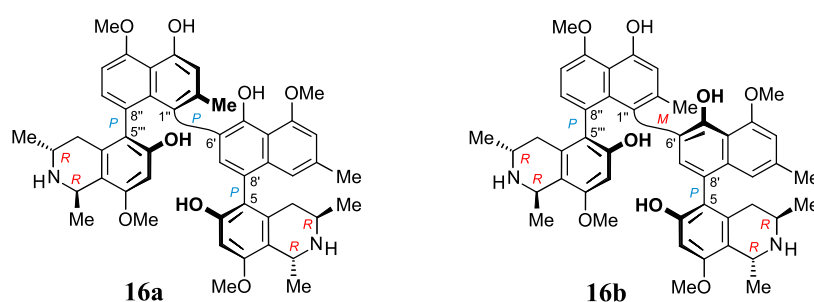
Figure 7. The first unsymmetrically coupled and highly condensed NIQ dimers, the mbandakamines A (**16a**) and B (**16b**).

The structurally unprecedented mbandakamines A (**16a**) and B (**16b**) were isolated from the leaves of a botanically as yet unidentified Congolese *Ancistrocladus* liana growing in the region around the town Mbandaka.[80] Genetic analyses based on microsatellite fingerprinting performed in cooperation with the group of Prof. G. Heubl (University of Munich, Germany) suggested that this liana might indeed represent a new, as yet undescribed *Ancistrocladus* species or subspecies.[81] This phylogenetic hint, in combination with the novel-type structural peculiarities of **16a** and **16b**, raised great interest, making it rewarding to investigate the metabolite profile of this phytochemically as yet unexplored *Ancistrocladus* plant more closely.

Therefore, the present PhD project aimed at a more-in-depth study on the NIQ pattern of this *Ancistrocladus* liana from the Mbandaka region, with the specific objectives being:

- The LC-UV-MS-CD-assisted search for further novel-type dimeric NIQs,
- Their directed isolation and the elucidation of their absolute stereostructures, and
- The evaluation of their pharmacological properties.

Apart from these outlined objectives, a further goal of this PhD project was the phytochemical and chemotaxonomic investigation of two other Congolese, likewise botanically as yet undescribed *Ancistrocladus* lianas.

2. The Plant Families Producing NIQs – an Overview

2.1. Morphology, Regional Distribution, and Phylogenic Relationship

As already mentioned, the Ancistrocladaceae and Dioncophyllaceae plant families are the only known natural producers of NIQs. All species belonging to these families are flowering scandent shrubs or woody lianas, native to the paleotropics. The Dioncophyllaceae are endemic to the coastal evergreen rainforests of West Africa,[39] whereas the Ancistrocladaceae are characterized by a disjunctive occurrence in the tropical forests of West, Central, and East Africa and South-Central and Southeast Asia,[40] as shown in Figure 8.
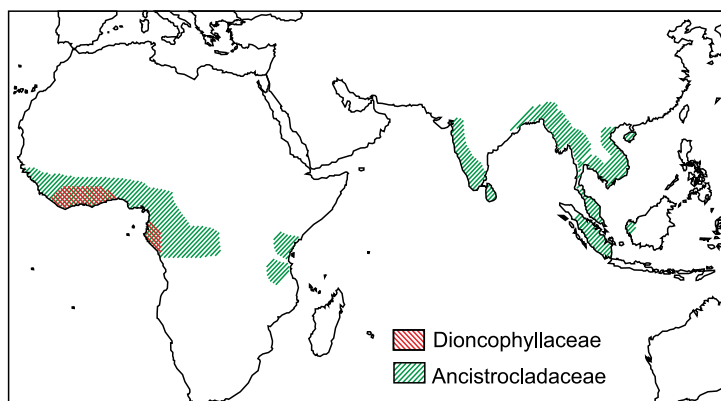
Figure 8. Distribution of Ancistrocladaceae and Dioncophyllaceae plants.

The Ancistrocladaceae family consists of just one genus, *Ancistrocladus* Wall., comprising 18 species.[40,82,83] The real number of taxa may, however, be actually much higher, as will be explained in more detail below. All of the lianas studied more closely regarding their metabolite profiles within this thesis belong to this group of plants.

The Dioncophyllaceae family is very small, too; it contains three genera, each composed of only one species: *Dioncophyllum thollonii* (genus: *Dioncophyllum* BAILL.), *Habropetalum dawei* (genus: *Habropetalum* AIRY SHAW), and *Triphyophyllum peltatum* (genus: *Triphyophyllum* AIRY SHAW).[39] Among these, *T. peltatum* is the best-known species, particularly due to the fact that during a certain period of its life it develops glandular leaves that capture insects.[84,85] This carnivorous character, however, seems to have completely gone lost in the other two species, *D. thollonii* and *H. dawei*, during evolution.[86] Phylogenetic investigations have firmly assigned the Dioncophyllaceae to the non-core Caryophyllales as a member of the carnivorous lineage, to which belong three further carnivorous plant families,

namely the Droseraceae, the Nepenthaceae, and the Drosophyllaceae (Figure 9).[86] The Ancistrocladaceae have likewise been affiliated to this carnivorous lineage as a sister clade of the Dioncophyllaceae. Carnivory has, however, never been observed for Ancistrocladaceae plants; maybe it existed long ago and went lost in the course of evolution, as for the two aforementioned Dioncophyllaceae taxa *D. thollonii* and *H. dawei*.
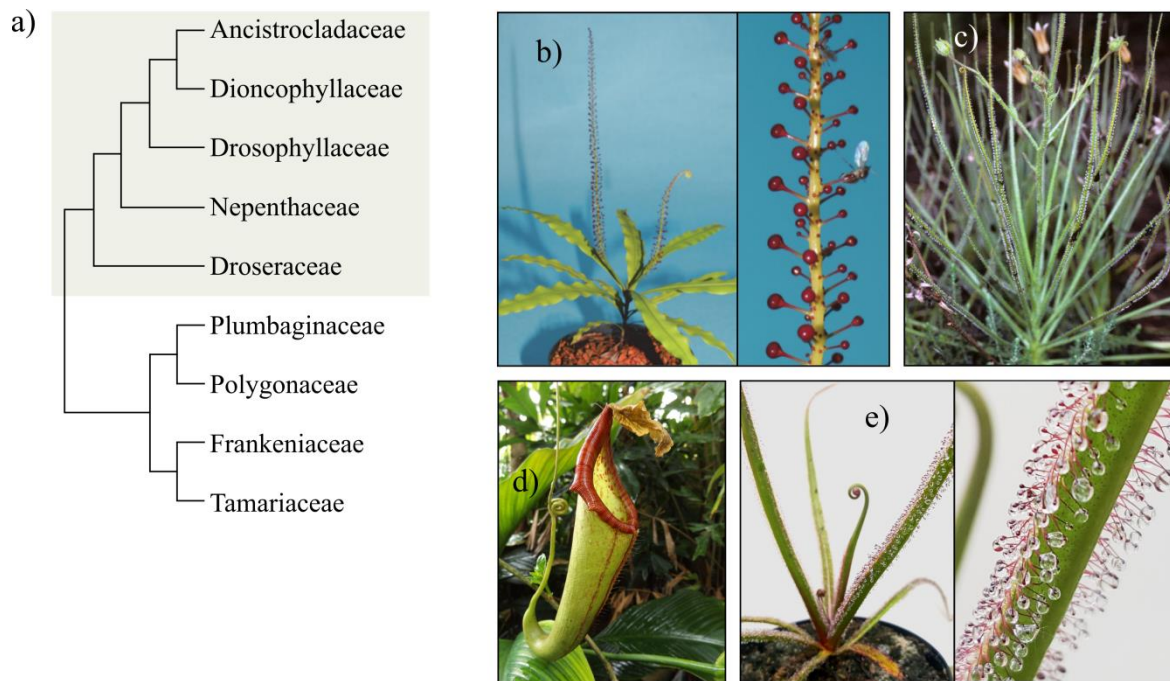
Figure 9. a) Phylogenetic relationship[86] within the non-core clade Caryophyllale (the carnivorous lineage is highlighted with a gray box); and representative carnivorous species: b) *Triphyophyllum peltatum* (Dioncophyllaceae); c) *Drosophyllum lusitanicum* (Drosophyllaceae); d) *Nepenthes* sp. (Nepenthaceae); and e) *Drosera regia* (Droseraceae). Credit photos: AK Bringmann (b), D. L. Nickrent (c),[87] and the author of this thesis (d and e).

2.2. *Ancistrocladus* Plants – Botanical Features, Habitats, and Taxonomy

Ancistrocladus plants are usually encountered as woody lianas climbing high into the canopy of the forest. The *Ancistrocladus* individuals, however, begin their life as erect, self-supporting monopodial saplings (Figure 10a) and become vigorous sympodial lianas only in their adult stage (Figure 10b and c).[40] They are equipped with characteristic recurved shoots forming woody hooks that serve as grapnels, helping the lianas to anchor to the surrounding vegetation (Figure 10d-f). The name *Ancistrocladus* reflects this botanical peculiarity: It comes from the Greek words *ankistro* (= hook) and *klados* (= shoot).[88] These ascending plants are further characterized by inflorescences (Figure 10g), possessing glands that

occasionally produce a white waxy exudate.[40] Their bisexual flowers are quite small, with four to five sepals, four to five colorful (reddish, yellow, or white) petals, five to 15 stamens, and three stigmas on either a united style or three separate styles (Figure 10h).[40] Likewise morphologically distinctive for *Ancistrocladus* lianas are their fruits, which look like nuts bearing five large lobes in the form of 'wings' (Figure 10i).[40,44,89] The leaves are simple, entire, and alternate, typically with small epidermal pits.[40]

Figure 10. Morphology of *Ancistrocladus* species: a) an erect, self-supporting sapling of a Congolese *Ancistrocladus* species; b) mature woody liana of a Congolese *Ancistrocladus* species; c) a fully developed individual of *A. likoko*; d) branch of *A. ealaensis* with the typical curved hook; e) and f) branches of a Congolese *Ancistrocladus* sp. (in f, the hook anchors to a branch of another plant, thus supporting the liana to further climb or develop); g) inflorescences of *A. likoko*; h) a flower of *A. abbreviatus*; and i) a fruit of a Congolese *Ancistrocladus* sp. with their emblematic five enlarged lobes. With the exception for picture h, which was taken in the Botanical Garden of Würzburg (credit photo: AK Bringmann), all the other pictures (a-g, and i) were recorded in the natural habitats, the Congolese rainforests, by the author of this thesis.

The typical habitats of *Ancistrocladus* plants are swamps, riversides, roadsides, and other troubled areas (Figure 11) across dry to wet evergreen forests that are found in two main areas. The first and largest one is in Africa; it extends from Senegal to D.R. Congo, and the other is located in Southeast Asia, ranging from Malaysia, Singapore, Sumatra, and (in part) Borneo, through China (Hainan Island), Vietnam, Laos, Cambodia, Thailand, Myanmar, and the Andaman and Nicobar Islands of India (Figure 8).[40] An additional small number of locally disseminated outliers has also been reported in Tanzania, Kenya, Sri Lanka, and India,[40] as indicated in Figure 8 above.

Figure 11. Typical natural habitats of *Ancistrocladus* plants – here in the tropical rainforest near the village Bonsolerive, located close to the town Mbandaka in the northwestern part of D.R. Congo (for the map of D.R. Congo, see Figure 13). Credit photos: the author of this thesis.

The taxonomy of *Ancistrocladus* plants is somehow problematic and there have long been controversial debates both on the higher systematic positioning of the genus and on the distinction between species. These discussions started already in the early 19th Century, when N. Wallich identified four species from India and Southeast Asia and grouped them into a

genus that he named *Ancistrocladus*,[90] while a few other related taxa were previously described and given other names (for an overview, see ref.[40]). In 1849, the *Ancistrocladus* genus was thoroughly described and was, for the very first time, included into the monogeneric family Ancistrocladaceae by M. J.-E. Planchon.[91] This family classification was, however, not recognized by several other botanical scientists, who rather assigned the *Ancistrocladus* taxa to a variety of other families, among them the Dipterocarpaceae, the Annonanceae, the Combretaceae, the Malpighiaceae, the Myristicaceae, and the Symplocaceae.[40,92] It is only in the beginning of the 20th Century that the Ancistrocladaceae family started to be generally accepted, as more convincing distinctive anatomical and morphological features became available.[40] The assignment of the Ancistrocladaceae family to a superior classification category, however, remained very unclear, also in the following decades. Some authors like E. F. Gilg (in 1925) placed it within the order Parietales,[93] whereas others such as A. Cronquist (in 1981) included it within the Violales.[94] Phylogenetic studies performed during the past 20 years have eventually positioned the Ancistrocladaceae family within the non-core Caryophyllales, together with the Dioncophyllaceae and some further carnivorous plant families, as already mentioned and illustrated in Figure 9.[40,95-100]

At a species level, there have been long controversies, too. A total of 27 *Ancistrocladus* taxa had been described for Africa and Asia. Some of them, however, have subsequently been reduced to taxonomic synonymy, following a comprehensive and meticulous revision of the whole Ancistrocladaceae family, published in 2005 by C. M. Taylor and colleagues.[40] This revision – the latest one regarding this plant family – recognized 16 valid *Ancistrocladus* species, among them eleven from Africa and five from Asia. Investigations by our group together with the team of Prof. G. Heubl in Munich have meanwhile resulted in the discovery of two additional *Ancistrocladus* species. One of them is *A. benomensis* RISCHER & G. BRINGMANN, growing in the Southeast of peninsular Malaysia,[83] and the other one is *A. ileboensis* HEUBL, MUDOGO & G. BRINGMANN,[82] discovered in the south-central part of the Congolese rainforest. Thus, 18 *Ancistrocladus* taxa have actually been acknowledged botanically (Table 1).

Table 1. *Ancistrocladus* species that are currently accepted botanically.

Name of species	Regional distribution (countries)	Former taxa or subspecies
A. abbreviatus AIRY SHAW	West Africa (Sierra Leone to Ghana, Nigeria)	*A. lateralis*
A. barteri SCOTT-ELLIOT	West Africa (Senegal to Ghana)	*A. pachyrrhachis* AIRY SHAW
A. grandiflorus CHEEK	West and Central Africa (Cameroon)	
A. guineensis OLIV.	West and Central Africa (Nigeria to Gabon)	*A. uncinatus* HUTCH. & DALZIEL
A. korupensis D. W. THOMAS & GEREAU	West and Central Africa (Nigeria to Cameroon)	
A. letestui PELLEGR.	West and Central Africa (Nigeria to Congo-Brazzaville)	
A. congolensis J. LÉONARD	Central Africa (Gabon to D.R. Congo)	
A. ealaensis J. LÉONARD	Central Africa (Gabon to D.R. Congo, Central African Republic)	
A. likoko J. LÉONARD	Central Africa (D.R. Congo)	
A. ileboensis HEUBL, MUDOGO & G. BRINGMANN	Central Africa (D.R. Congo)	
A. robertsoniorum J. LÉONARD	East Africa (Kenya)	
A. tanzaniensis CHEEK & FRIM.	East Africa (Tanzania)	
A. hamatus (VAHL) GILG	Central Asia (Sri Lanka)	*A. thwaitesii* TIEGHEM
A. heyneanus WALL. ex J. GRAHAM	Central Asia (India)	
A. attenuates DYER	South-East Asia (India, Myanmar)	
A. benomensis RISCHER & G. BRINGMANN	South-East Asia (Malaysia)	
A. griffithii PLANCH.	South-East Asia (India, Myanmar to Vietnam)	

A. tectorius (LOUR.) MERR.	South-East Asia (Myanmar to Vietnam, China, Malaysia to Singapore, India, Indonesia)	*A. carrallioides* CRAIB *A. cochinchinensis* GAGNEP. *A. extensus* WALL. ex. PLANCH. *A. hainanensis* HAYATA *A. harmandii* GAGNEP. *A. pinangianus* WALL. ex. PLANCH.

The real number of *Ancistrocladus* species may, however, be actually much higher, as demonstrated most recently by phylogenetic[81,88] and phytochemical studies.[56,79,80,101-104] In Southeast Asia, for example, recent investigations on nuclear and chloroplast DNA sequences and fingerprints of *Ancistrocladus* samples from Thailand and Malaysia strongly evidenced that the number of valid species in these regions is far underestimated.[88] Many Asian *Ancistrocladus* species or subspecies have thus been overlooked, or just wrongly assigned to the morphologically similar ones, which frequently happens when the botanical identification relies on specimens that do not contain all diagnostic characters.

Actually, most of the *Ancistrocladus* specimens available usually consist of few representative leaves and/or twigs. The anatomical and morphological traits of these vegetative materials, however, are in most cases not specific for a single *Ancistrocladus* species.[40,105] The leaves, for instance, are known to display a high plasticity; their morphology and diagnostic traits vary, depending on whether the leaves are from a juvenile plant (sapling phase) or from an adult liana. And even in the adult stage, stem leaves on the secondary sympodial shoots usually differ diagnostically from those on the branchlet apex.[40] Thus, leaves and stems have at best a very limited diagnostic value, while being useless for species identification when the information on the stage of the plant from which they were collected is not recorded. By contrast, the characters of the generative parts (i.e., flowers and fruits) are more reliable and, thus, serve as the basis for the species identification within the genus *Ancistrocladus*.[40] These reproductive organs, however, are not easy to obtain, due to the fact that flowering and fruiting of *Ancistrocladus* plants is in general less abundant and very irregular. In addition, flowers and fruits are frequently inconspicuous, very often hidden in the forest canopy,[40,81] where they are in most cases very challenging to reach (Figure 12).

Figure 12. Search for flowers and fruits of *Ancistrocladus* plants in the rainforest near the town Mbandaka in D.R. Congo – here the author of this thesis climbing into the forest canopy following *Ancistrocladus* lianas. Photos by A. Elangu (top) and L. Loleka (bottom).

Likewise contributing to the poor taxonomical knowledge about *Ancistrocladus* plants are the practical difficulties in reaching their habitats.[81] This is particularly true for some African countries like D.R. Congo, where field trips are very restrained by the lack of infrastructures (and poor quality, if they exist at all), political instability, recurrent civil wars and the resulting hazards. Besides these human-caused hard conditions, the *Ancistrocladus* habitat is itself also naturally challenging to access. In the Congolese rainforests, for example, some of the *Ancistrocladus* lianas occur in very dense vegetation, whereas others grow in dangerous swampy grounds, which are, in addition, often inundated at the time of flowering (about May-August). For most of these Congolese *Ancistrocladus* plants, it is indeed too demanding to collect plant specimens comprising all fertile organs essential for a reliable botanical description. Many herbarium collections from D.R. Congo therefore do not contain diagnostically relevant organs, so that the morphology-based species identification is in most cases impossible.[40,81] It is hence not astonishing that only very little is known about the diversity and delimitation of *Ancistrocladus* species in the Congolese rainforests, which represent an extremely vast area, so rich in biodiversity, as explained in the following section.

2.3. Overview on Congolese *Ancistrocladus* Species – Untangling Diversity and Delimitation of Species through Phytochemistry and Phylogenetics

The rainforests of D.R. Congo constitute the main part (ca. 60%) of the Congo Basin, the world's second-largest tropical forest, which covers over two million km^2, spanning across six countries, namely D.R. Congo, Central African Republic, Cameroon, Congo-Brazzaville (or Republic of the Congo), Equatorial Guinea, and Gabon.[106] The Congolese rainforests are therefore among the few most important and largest wilderness areas left on the Earth.[107] Old inventories estimated that the Congolese forests contain about 11,000 higher plant taxa, including over 1,000 endemic ones.[108] The actual number of the hosted plant species, however, remains uncertain, as there have not yet been thorough and specific botanical campaigns covering the entire, wide Congolese forest. The probability of finding unreported, botanically as yet undescribed species therein is still high, as evidenced by the recent discovery of many new taxa, belonging to the plant families Moraceae,[109] Rubiaceae,[110] Sapindaceae,[111] Zingiberaceae,[112] and Euphorbiaceae.[113]

The chance of discovering new *Ancistrocladus* species or subspecies in the Congolese rainforests is also very high, given in particular the above explained multi-faceted challenges related to their taxonomy. As outlined in Table 1, there are so far only four botanically

identified *Ancistrocladus* taxa occurring in D.R. Congo. Three of them, *A. congolensis* J. LÉONARD, *A. ealaensis* J. LÉONARD, and *A. likoko* J. LÉONARD, have been known for a long time, since 1949.[114] The fourth one is the aforementioned taxon *A. ileboensis*, which has recently been described for the first time by our group and the team of Prof. G. Heubl in 2010. Remarkably, its discovery was triggered by phytochemical investigations.[82] It started with the collection of leaves, twigs as well as root and stem bark from an *Ancistrocladus* liana found in the rainforest close to the town Ilebo, in the South-Central part of D.R. Congo. This plant was initially identified – based on a sterile specimen – as *A. letestui* PELLEGR., a species that is distributed from Nigeria to Congo-Brazzaville (Table 1). The collection was thus believed to be the first record of the occurrence of *A. letestui* in D.R. Congo.[82] Phytochemically, *A. letestui* is known as a rich source of dioncophylline A (**10**).[115] Preliminary phytochemical studies of the material from near the town Ilebo by HPLC and capillary electrophoresis coupled to mass spectrometry, however, did not result in the identification of **10**, but rather led to the isolation of a series of 5,1′- and 7,1′-coupled monomeric NIQs, some of which had previously been unknown.[101] This phytochemical divergence, indicating that the liana from the Ilebo region was chemotaxonomically different from *A. letestui*, raised great interest, as it suggested that this plant might be a botanically as yet unknown species. Young individuals were then collected in the forest and successfully cultivated in the Botanical Garden of the University of Würzburg, providing diagnostic organs that revealed the liana to be, indeed, a truly new species. This taxon was therefore fully described botanically and was given the name *A. ileboensis*, after the Congolese town Ilebo.[82]

The discovery of the new species *A. ileboensis*, together with the continuing detection of further Congolese *Ancistrocladus* plants showing significantly different metabolite profiles compared to those of the known species,[56,79,80,101-104] renders the clarification of the actual diversity of *Ancistrocladus* species in the Congolese rainforests a rewarding task. On the other hand, addressing such an important issue by using the classic, morphology-based identification approach is highly challenging, in view of the fact that flowers and fruits (without which a morphology-based identification of specimens is impossible) are not easily accessible, as explained above. The development of a new, morphology-independent protocol for discriminating Congolese *Ancistrocladus* species and identifying sterile specimens is therefore a likewise important objective. First investigations addressing both of these valuable issues have most recently been performed by our group in cooperation with the team of Prof. G. Heubl. They focused on the development of a high-resolution DNA fingerprinting system

based on microsatellites. By these genetic studies, the occurrence of a potentially new *Ancistrocladus* species in the region around the Congolese town Mbandaka was detected and the presence of *A. letestui* in several parts of D.R. Congo was also noticed. In the following paragraphs, a succinct overview on this work is provided; further details can be found in the original paper (see ref.[81]). The author of this thesis contributed to this project by planning and executing the collection of some of the investigated *Ancistrocladus* samples in the Congolese rainforests, by monitoring post-collective procedures and conservation of the plant materials in Kinshasa, and by organizing the transfer of the collected samples to the Heubl group in Munich, via the lab in Würzburg.

Microsatellites, also referred to as Simple Sequence Repeats (SSRs), are short sequences of usually two to six nucleotides that are tandemly repeated (typically 5 to 50 times) and spread throughout the non-coding regions of the genome.[116,117] Examples of such repeat motifs are the sequence TATATATATATATA or $(TA)_7$, which is a dinucleotide microsatellite, and the series GTCGTCGTCGTCGTC or $(GTC)_5$, a trinucleotide microsatellite (with A being Adenine, C Cytosine, G Guanine, and T Thymine). SSRs are evolutionarily unstable; they mutate at a high rate, so that their length (i.e., number of repeats) at the same locus (i.e., a fixed position within the genome) for a given population typically varies from one individual to another.[118,119] Moreover, microsatellites are codominant markers, allowing distinction between homozygous loci, which exhibit the same number of repeats on both homologous chromosomes, and heterozygous loci, possessing different SSR lengths at each alleles (e.g., one allele may have 21 repeats and the other may have 17).[119] The development of a DNA fingerprinting system based on microsatellites thus refers to the identification of loci showing high variability within a given population, so that the resulting information on both, the homo- or heterozygous character and the length of SSRs at the respective loci can be used to differentiate individuals.[116,120] This methodology is widely utilized in genetic studies, with applications in many fields like forensic investigations, paternity testing, and population mapping.[116,119-121]

Based on the DNA material of an *Ancistrocladus congolensis* plant cultivated in the Botanical Garden of Würzburg, twelve microsatellite loci from a total of 99 tested ones were identified as suitable genetic markers, permitting discrimination among *Ancistrocladus* species. Their capability for distinguishing different species was first assessed for a set of 21 samples from six botanically well-characterized *Ancistrocladus* taxa from Asia and Africa, namely *A. benomensis*, *A. griffithii*, *A. tectorius*, *A. congolensis*, *A. korupensis,* and *A.*

robertsoniorum. The markers successfully produced six clearly distinct clusters, each corresponding to the respective plant species, as revealed by STRUCTURE Analysis and Principal Coordinate Analysis, the statistical methods exploring similarities or dissimilarities of data.

The markers were then applied to 74 samples from botanically as yet unidentified *Ancistrocladus* lianas collected in the rainforests of:

- Four villages surrounding the town Mbandaka (viz., Bamanya, Bonsolerive, Djombo, and Eala), located in the northwestern part of D.R. Congo (Figure 13),

- Two sites around the town Ikela (viz., Itafa-Bolonga and Yeteto), which is in the central part of D.R. Congo, and

- Four localities neighboring the town Ilebo (viz., Libongo, Tabata, Bambange, and Ikwey), lying in the south-central part of the country.

In order to be able to assign detected clusters to a specific taxon, these plant materials were fingerprinted along with samples of the four botanically known Congolese *Ancistrocladus* taxa (viz., *A. congolensis*, *A. ealaensis*, *A. likoko*, and *A. ileboensis*) and *A. letestui*, which had sometimes been assumed to occur also in D.R. Congo, as already mentioned.
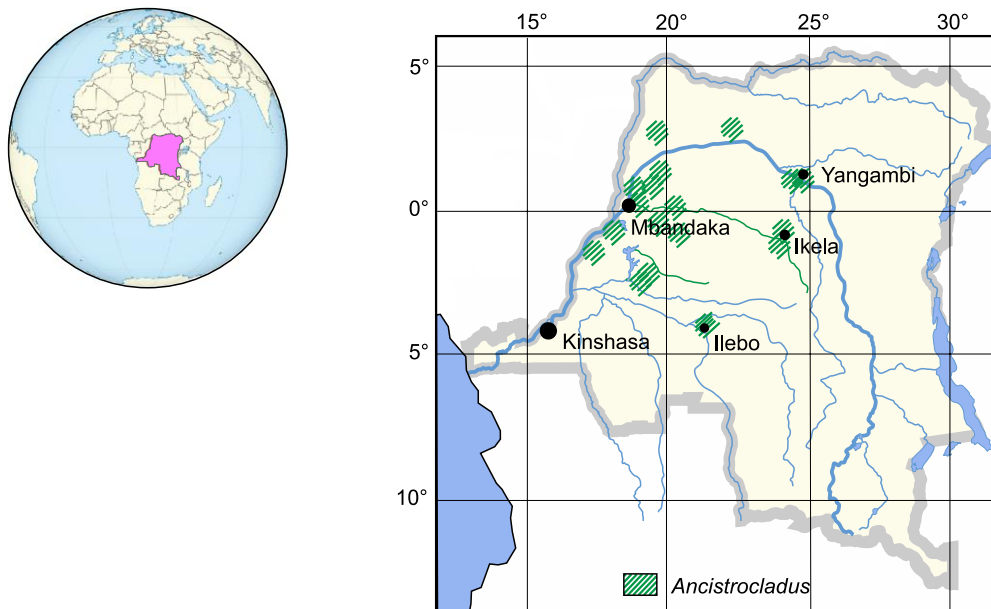
Figure 13. Distribution of botanically described *Ancistrocladus* species in D.R. Congo, based on reported collections.

Analysis of the resulting datasets for the botanically determined *Ancistrocladus* species further confirmed the differentiation ability of the microsatellite loci. These genetic markers reliably discriminated one taxon from others, except for *A. congolensis* and *A. ealaensis*,

which could not be clearly distinguished, so that they were assigned to the same cluster. A STRUCTURE examination of the 74 samples from taxonomically unidentified *Ancistrocladus* lianas revealed five distinct clusters (Figure 14), of which one unit corresponded to the tandem *A. congolensis* / *A. ealaensis*. The second cluster matched well with *A. likoko* and the third one was in accordance with *A. ileboensis*, which further firmly corroborated the species status of this recently discovered taxon. Interestingly, the fourth cluster fitted with *A. letestui*, hence strongly suggesting its presence in D.R. Congo. Most remarkably, the last cluster did not agree with any hitherto described *Ancistrocladus* taxon, thus supporting the assumption that potentially new species might be present within the plant material collected near the town of Mbandaka. First phytochemical investigations on this botanically as yet unidentified species led to the discovery of the unprecedented dimeric naphthylisoquinoline alkaloids mbandakamines A (**16a**) and B (**16b**), which are mentioned in the introduction and are further described in Chapter 3, along with other thrilling novel-type compounds.
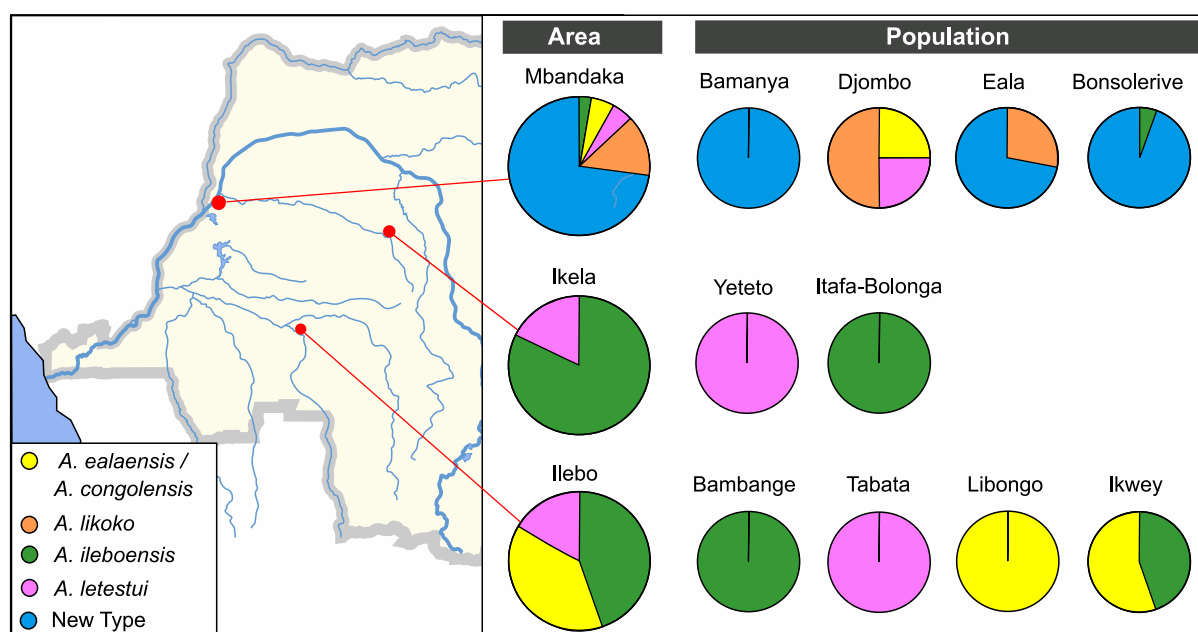
Figure 14. DNA-based cluster affiliation of *Ancistrocladus* samples collected in a total of 10 Congolese sites (Bamanya, Djombo, Eala, Bonsolerive, Yeteto, Itafa-Bolonga, Bambange, Tabata, Libongo, and Ikwey), grouped into three main areas (Mbandaka, Ikela, and Ilebo).

Moreover, our group has most recently detected further new Congolese sites of *Ancistrocladus* lianas, which have not yet been investigated phylogenetically. *Ancistrocladus* plants collected from some of these new locations have been phytochemically studied more closely for their metabolite profiles (see Chapters 4 and 5).

3. Novel-Type Dimeric NIQs from a Congolese *Ancistrocladus* Species Related to *A. ealaensis*

3.1. Introduction

The rainforests of D.R. Congo are known to host four botanically recognized *Ancistrocladus* species (viz., *A. congolensis*, *A. ealaensis*, *A. likoko*, and *A. ileboensis*),[82,114] mainly found in the northwestern part of the country (see Figure 13 above). Recent genetic investigations on plant material collected at different sites in D.R. Congo, however, have hinted at the occurrence of a potentially new species in some wilderness areas near the town Mbandaka, as explained in the preceding chapter and shown in Figure 14.[81]

From the leaves of this taxonomically as yet uncharacterized *Ancistrocladus* species, HPLC-UV-MS-ECD-assisted investigations directed to the search for structurally novel dimeric NIQs resulted in the discovery of three unprecedented types of NIQ dimers comprising:

- The first unsymmetrically coupled dimers, possessing an extremely high steric hindrance at the central biaryl axis, namely mbandakamines A (**16a**) and B (**16b**), which had been presented in the master thesis of the author of this thesis only in part, with some selected data,[122] and mbandakamines B_2 (**17**), C (**18**), and D (**19**) (Figure 15);[80,123]

- The first such compounds with oxygen bridges, leading to molecular scaffolds displaying an unusual pyran-cyclohexenone-dihydrofuran sequence and a total of eight stereogenic elements (the highest number in the class of NIQs!) viz., cyclombandakamines A_1 (**20**) and A_2 (**21**);[124] and

- The first spiro-fused dimeric NIQs, featuring a complex, cage-like molecular framework, with a five-membered carbon ring and five- and seven-membered oxygen heterocycles, named spirombandakamines A_1 (**22**) and A_2 (**23**).[123]
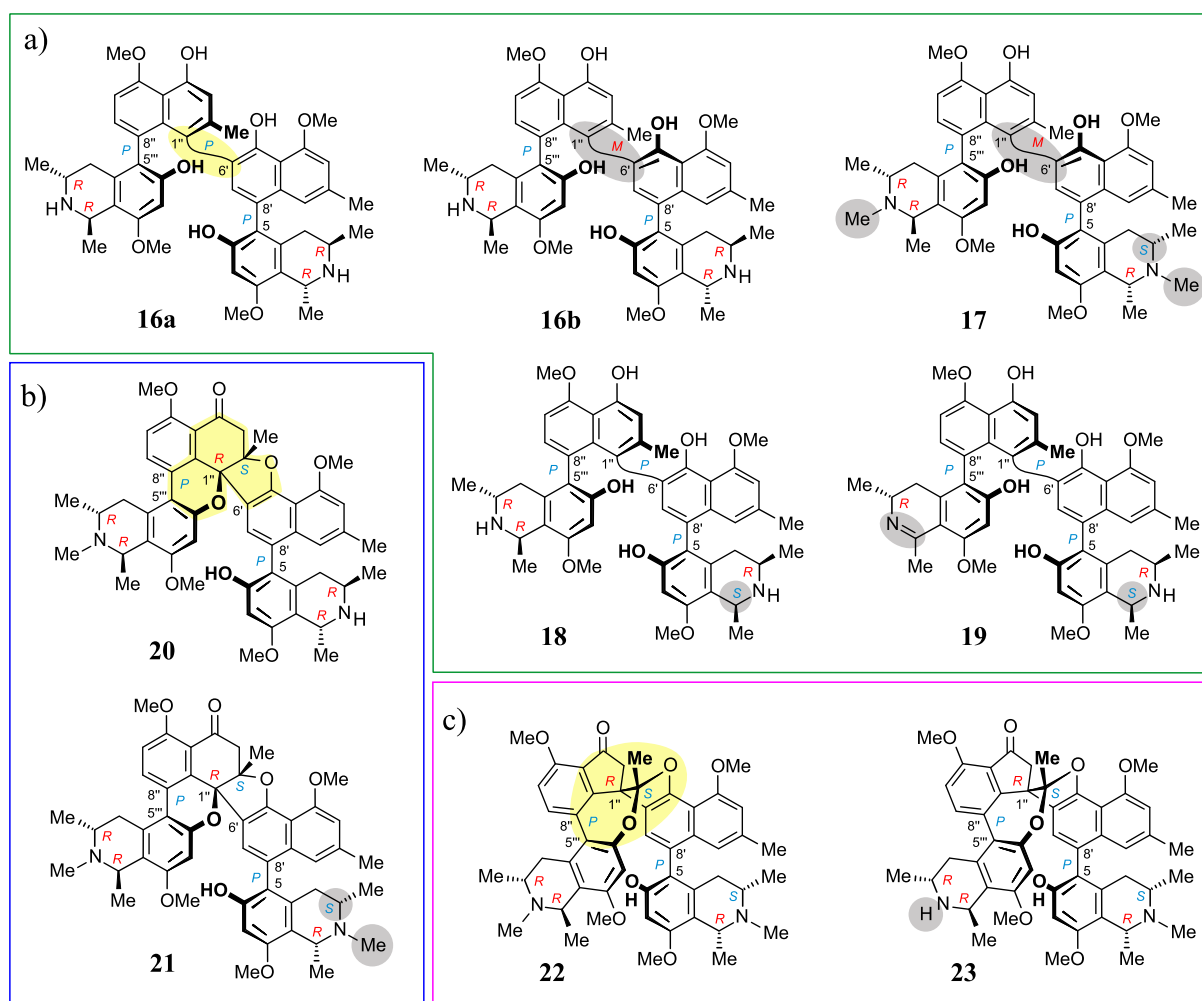
Figure 15. Three novel types of dimeric NIQs discovered in a botanically as yet unidentified Congolese *Ancistrocladus* plant: a) the mbandakamines A (**16a**), B (**16b**), B$_2$ (**17**), C (**18**), and D (**19**);[80,123] b) the cyclombandakamines A$_1$ (**20**) and A$_2$ (**21**);[124] and c) the spirombandakamines A$_1$ (**22**) and A$_2$ (**23**).[123] For each type, the unprecedented structural features are highlighted in yellow for the first member, and the structural variations within the respective subclasses are labeled in gray.

The following paragraphs provide details on the isolation, structural elucidation, and bioactivities of these thrilling novel compounds. Moreover, a plausible biosynthetic pathway to these unprecedented quateraryls is presented, and a chemotaxonomic implication of the phytochemical investigations is discussed.

Actually, the presentation of these unprecedented dimeric NIQ alkaloids is done below in the way not only to reflect the chronological order in which they have been discovered, but also to highlight the conceptual approach that guided their stepwise search and isolation from complex matrices of possibly thousands of metabolites produced by the investigated plant. Thus, the atropo-diastereomeric alkaloids mbandakamines A (**16a**) and B (**16b**) are described

first, here not just in a preliminary and partial form as done in the aforementioned master thesis,[122] but now in a comprehensive and detailed manner. This is followed by the thrilling discovery and structural elucidation of the highly novel cyclo- and spirombandakamines (**20-23**) and a discussion on a plausible concept for their biosynthetic formation. Then the detection of mbandakamine B$_2$ (**17**), which happened as a consequence of the search for potential direct precursors of the isolated cyclo- and spirombandakamines, is reported, along with some preliminary investigations on the atropisomerization and attempts for the biomimetic semi-synthesis of the cyclic mbandakamines. Then the detection of mbandakamines C (**18**) and D (**19**) is shown, followed by the chemotaxonomic discussion and the bioactivities of the isolated metabolites.

3.2.   Mbandakamines A (16a) and B (16b): the First Unsymmetrically Coupled Dimeric NIQs

3.2.1. *Discovery of Mbandakamine A (16a)*

In August 2008, a team of scientists led by Prof. V. Mudogo collected plant material from a botanically as yet unidentified *Ancistrocladus* liana in the tropical forest surrounding the village Bonsolerive, close to the town Mbandaka in D.R. Congo. A voucher specimen (No. 032) was deposited in the Herbarium Bringmann, University of Würzburg.

In cooperation with Dr. C. Steinert (who, at that time, was a PhD student in our research group),[125] HPLC-MS investigations on different plant extracts were performed, hinting at the presence of a plethora of mono- and dimeric naphthylisoquinoline alkaloids, as evidenced by the masses of their monoprotonated ions ([M+H]$^+$, *m/z*: 379 to 436 for monomers and 756 to 813 for dimers).[73] Of particular interest was the leaf extract, since LC-MS studies suggested the presence of a whole series of dimers, even occurring as the main constituents, and, thus, being available in substantial quantities (see peaks marked in red in Figure 16).
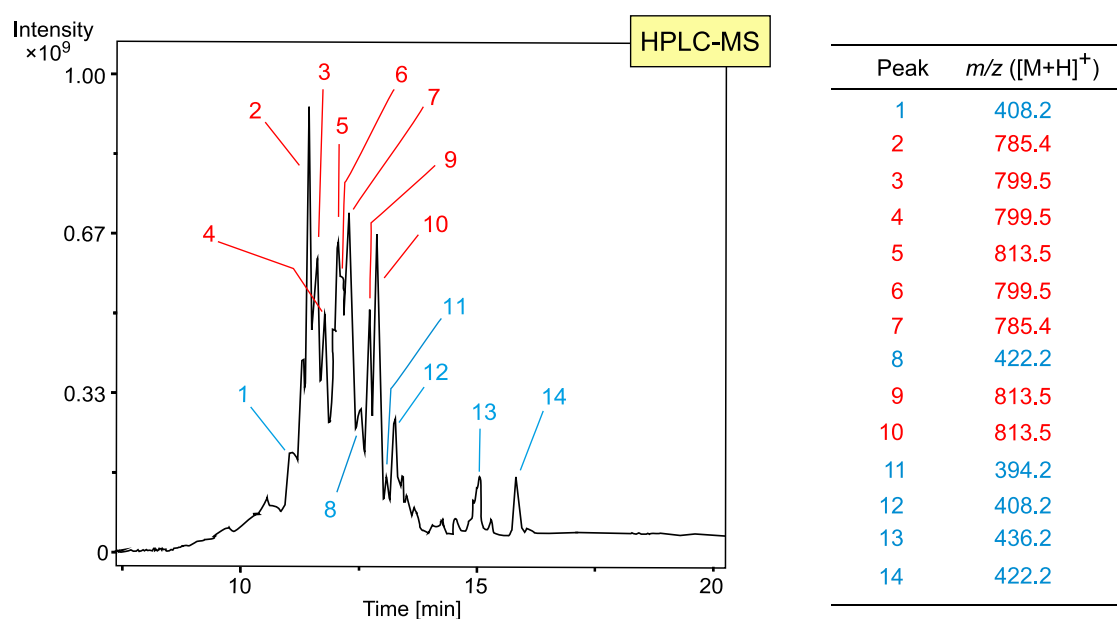
Figure 16. Total ion current (TIC) chromatogram of the leaf extract of a botanically as yet unidentified Congolese *Ancistrocladus* species (No. 032) and the corresponding masses (*m/z*). The red-highlighted masses (*m/z*) suggest the likewise red-indicated peaks to correspond to dimeric NIQs, while those in blue are characteristic for monomers.

The major compound in the crude leaf extract (Peak 2 in Figure 16) revealed a monoprotonated ion at *m/z* 785.4 ($[M+H]^+$) and a doubly protonated one at 393.2 ($[M+2H]^{2+}$), suggesting that this dimer might be ancistrogriffithine A (**13**), the only previously known dimeric NIQ with such mass spectral characteristics.[72,77] A co-elution HPLC-UV experiment with pure authentic **13**, however, led to two clearly separated peaks, revealing a difference of their retention times of ca. 0.2 min (Figure 17), thus excluding the presence of **13** in the extract. Consequently, the main constituent of the leaf extract (= Peak 2) had to be an unknown, probably novel-type dimeric NIQ, thus making its isolation and structural elucidation a rewarding task.
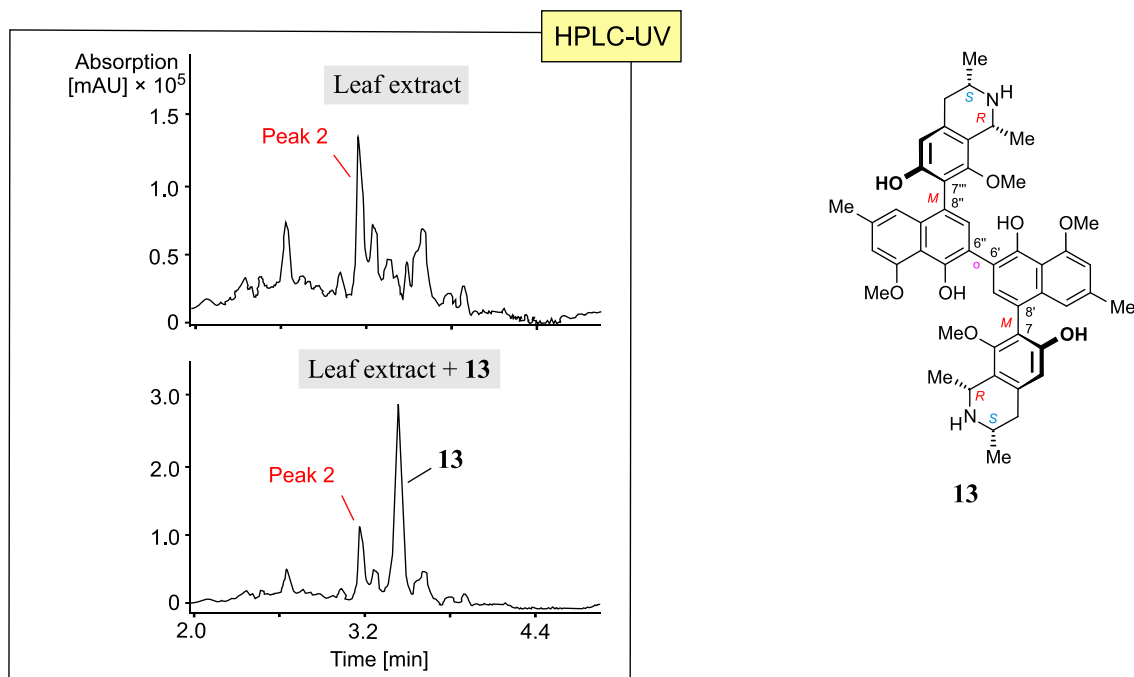
Figure 17. HPLC-UV analysis of the leaf extract of *Ancistrocladus* sp. 032, clearly revealing the absence of ancistrogriffithine A (**13**), the only previously known dimeric NIQ with an identical *m/z* (785.4 [M+H]$^+$), as obvious from co-elution experiments.

Extraction of the air-dried and powdered leaves with an acidified mixture of ethanol and dichloromethane provided a crude extract, which was neutralized with sodium hydroxide, and concentrated under reduced pressure. The resulting solid crude residue was macerated in chloroform to remove chlorophyll and other undesired lipophilic metabolites. The remaining alkaloid-enriched fraction was dissolved in methanol and resolved by reversed-phase preparative HPLC, providing Peak 2 in a pure form. The molecular formula of this compound was found to be $C_{48}H_{52}N_2O_8$, as evidenced by HRESIMS. Its ^{1}H NMR spectrum showed a full set of signals, indicative of an unsymmetric dimer, which again differentiated it from the C_2-symmetric ancistrogriffithine A (**13**),[72] showing only a half set of NMR signals. This additional divergence strongly evidenced the isolated metabolite (i.e., Peak 2) to be a new dimeric NIQ. It was henceforth named mbandakamine A (**16a**) in reference to the region Mbandaka, where the plant material had been collected.

3.2.2.   Structural Elucidation of Mbandakamine A (16a)

The ^{1}H NMR spectrum of **16a** (in deuterated methanol, MeOD) exhibited four three-proton singlets at 4.15, 4.09, 3.85, and 3.03 ppm, indicative of four methoxy groups. The compound

16a was shown by HRESIMS to have eight oxygens (see above). In view of this fact, it was obvious that the other four remaining oxygen functions present in the molecule were hydroxy groups.

One of the naphthylisoquinoline portions of **16a**, the 'southeastern' part **16a-I** (see Figure 18), showed a *meta*-coupling pattern for the two aromatic protons H-1' (6.62 ppm, *p*t, $J = 1.2$ Hz) and H-3' (6.74 ppm, d, $J = 1.2$ Hz) and the sequential ROESY correlations H-1' $\leftrightarrow$ CH$_3$-2' (2.34 ppm, d, $J = 0.7$ Hz) $\leftrightarrow$ H-3' $\leftrightarrow$ OCH$_3$-4' (4.09 ppm, s), together with HMBC correlations of a high-field shifted aromatic proton (H-7', 6.44 ppm, s) to two carbons: One (120.5 ppm) belonging to the adjacent isoquinoline part (C-5) and another one (127.8 ppm) to the naphthalene portion of the second, 'northwestern' part **16a-II** of **16a** (Figure 18). These findings suggested a 5,8'-coupling within the first naphthylisoquinoline moiety, **16a-I**, which was corroborated by the ROESY interactions of H-1' with H$_{ax}$-4 (2.52 ppm, dd, $J = 18.0, 11.7$ Hz) and of H-7' with H$_{eq}$-4 (3.89 ppm, dd, $J = 18.1, 4.5$ Hz), and by HMBC correlations from H$_{eq}$-4, H-7 (6.46 ppm, s) and H-7' to C-5 (120.5 ppm) (Figure 18). In the isoquinoline part, the HMBC interactions from H-1 (4.79 ppm, q, $J = 6.7$ Hz), CH$_3$-1 (1.57 ppm, q, $J = 6.7$ Hz) and from H-7 to C-8 (157.3 ppm), and the sequential ROESY interactions H-1 $\leftrightarrow$ OCH$_3$-8 (3.85 ppm, s) $\leftrightarrow$ H-7 proved the methoxy group to be linked to C-8 (Figure 18). The molecular portion **16a-I** therefore accounted for half of the eight detected oxygen functions, namely two methoxy groups (at C-8 and C-4') and two hydroxy functions (at C-6 and C-5').
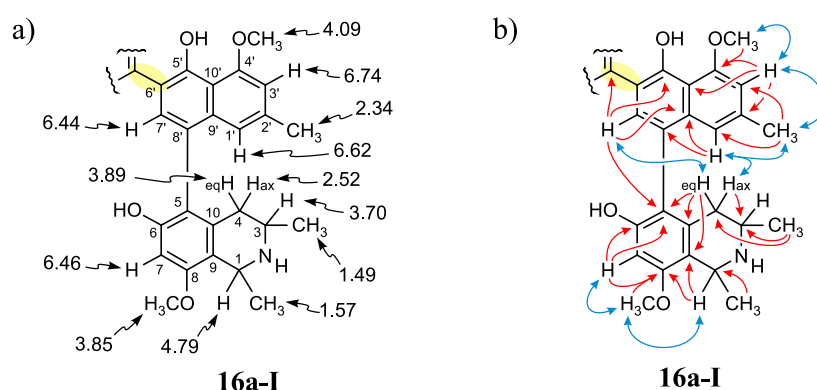
Figure 18. Selected NMR data of the 'southeastern' molecular half (**16a-I**) of mbandakamine A (**16a**): a) ^{1}H chemical shifts in ppm; and b) key HMBC (red single arrows) and ROESY (blue double arrows) interactions. The coupling position of **16a-I** to the other molecular part of **16a**, **16a-II** (see Figure 19), is highlighted in yellow.

In **16a-II**, the 'northwestern' naphthylisoquinoline part of **16a** (Figure 19), an AB spin system of two aromatic protons (7.00 ppm and 7.05 ppm, d, $J = 7.9$ Hz), the ROESY series OCH$_3$-5" (4.15 ppm, s) ↔ H-6" (7.00 ppm) ↔ H-7" (7.05 ppm), and HMBC correlations from H-7" to C-5" (158.4 ppm) and to C-9" (138.1 ppm), and from H-6" to C-8" (126.3 ppm) and to C-10" (116.2 ppm) revealed the presence of a naphthalene subunit with a methoxy group at C-5" (Figure 19). The connection of C-5''' (122.7 ppm) in the isoquinoline portion to C-8" in the naphthalene was evidenced by ROESY interactions between H-7" and H$_{ax}$-4''' (2.42 ppm, dd, $J = 18.0, 12.0$ Hz) and by HMBC correlation from H-7" to C-5''', and was further corroborated by joint HMBC correlations from H$_{ax}$-4''', H$_{eq}$-4''' (1.97 ppm, dd, $J = 18.0, 4.3$ Hz), and H-7''' (5.32 ppm, s) to C-5'''. This showed that the second naphthylisoquinoline portion, **16a-II**, was 5,8'-coupled, too, i.e., 5''',8" in the molecular context of **16a** (Figure 19). The HMBC correlations from H-1''' (4.64 ppm, q, $J = 6.7$ Hz) and from H-7''' to C-8''' (156.5 ppm) and the ROESY series CH$_3$-1''' (1.53 ppm, d, $J = 6.7$ Hz) ↔ OCH$_3$-8''' (3.03 ppm, s) ↔ H-7''' proved the methoxy group to be attached to C-8''' and the free hydroxy group to be at C-6''' (Figure 19). The remaining, fourth hydroxy group thus had to be at C-4", which, in view of the fact that the central binaphthalene linkage in all known dimeric NIQs always occurs in *ortho*- or *para*-positions to hydroxy functions (see e.g., Figures 5 and 6),[62,75,77-79,126] suggested **16a-II** to be coupled to **16a-I** either via C-3" or C-1".
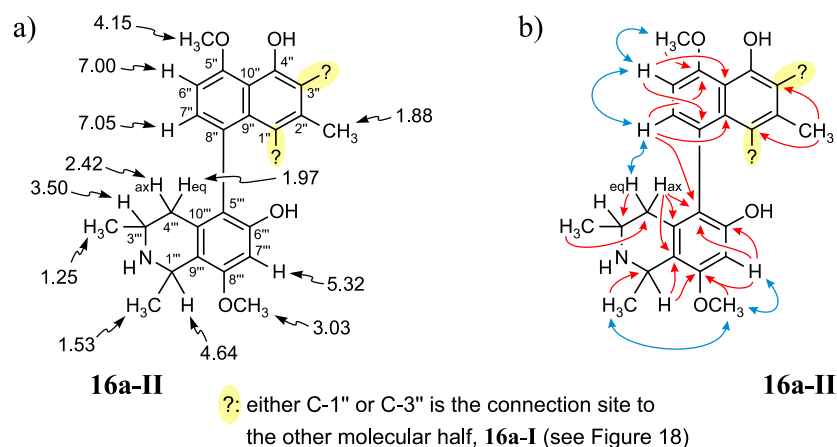
Figure 19. Key NMR data of the 'northwestern' moiety (**16a-II**) of mbandakamine A (**16a**): a) ^{1}H chemical shifts in ppm; and b) selected ROESY (double arrows in blue) and HMBC (red-highlighted single arrows) interactions.

In the first, southeastern moiety **16a-I**, the position of the inner biaryl axis was determined to be C-6′, by the already mentioned HMBC correlation from H-7′ to a carbon atom (127.8

ppm) belonging to a different naphthalene part, by the ROESY series H-1' ↔ CH$_3$-2' ↔ H-3' ↔ OCH$_3$-4' (Figure 18), and by a further ROESY interaction from H-7' to CH$_3$-2". This methyl group, located in the naphthalene part of the northwestern naphthylisoquinoline moiety **16a-II**, exhibited an up-field shifted signal of 1.88 ppm (3H, s), indicating that a second shielding substituent – viz., the naphthalene portion of **16a-I** – had to be attached in a neighboring position of **16a-II**, i.e., at C-1" or C-3", thus corroborating the aforementioned hints. Consequently, at this step of the structural elucidation, two possible constitutions were imaginable for mbandakamine A. The first one was an unprecedented 6',1"-coupling at the central axis, leading to a U-turn-like curved array, in which the isoquinoline portion of the northwestern part **16a-II** was tightly pressed against both, the naphthalene and the isoquinoline units of the southeastern half **16a-I**, so that NOE interactions between these ring systems would be expected to be observed (Figure 20a). The other plausible constitution was a 6',3"-linked dimer (at that time a likewise as yet unknown coupling type), displaying a relatively more 'relaxed', almost linear arrangement, in which the two isoquinoline portions point in opposite directions and are, thus, far away one from another, so that NOE effects between them should not be observed (Figure 20b).
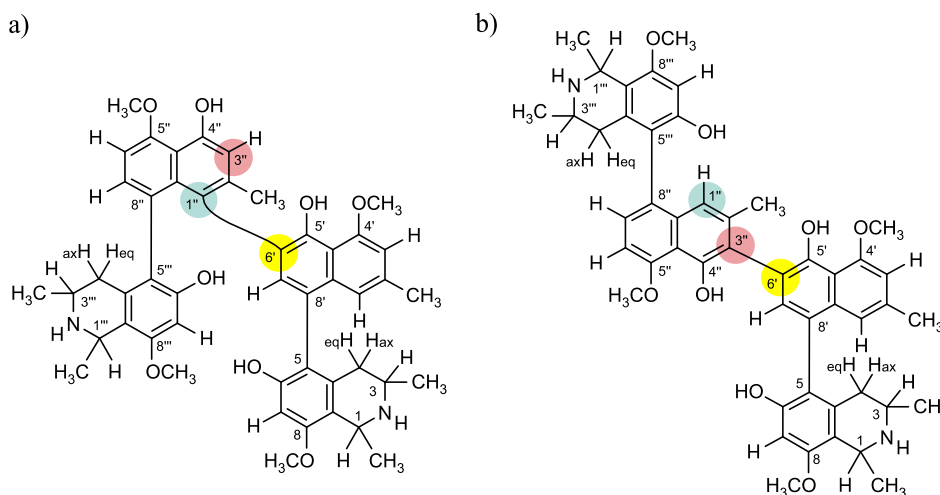
Figure 20. Two imaginable constitutions of mbandakamine A, differing one from another only by the coupling at the central biaryl axis: a) a 6',1"-coupled dimer; or b) a 6',3"-linked one.

ROESY measurements revealed numerous interactions between the naphthalene part of **16a-I** and the isoquinoline portion of **16a-II**, and even between the two isoquinoline moieties of **16a-I** and **16a-II** were observed, e.g., between H-7''' and both, H$_{ax}$-4 and H$_{eq}$-4, OCH$_3$-4' ↔ H-1''' (see the ROESY spectrum in Scheme 1), CH$_3$-3 ↔ OCH$_3$-8''', and OCH$_3$-4' ↔ OCH$_3$-8'''

(for all ROESY correlations, see Table 6 in the Experimental Part). Such interactions, which had never been observed in any dimeric naphthylisoquinoline alkaloid prior to this work, excluded the almost linear 6',3"-coupling, thus showing that the two naphthalene parts of mbandakamine A had to be connected by an unprecedented axis between C-6' and C-1" (Scheme 1).
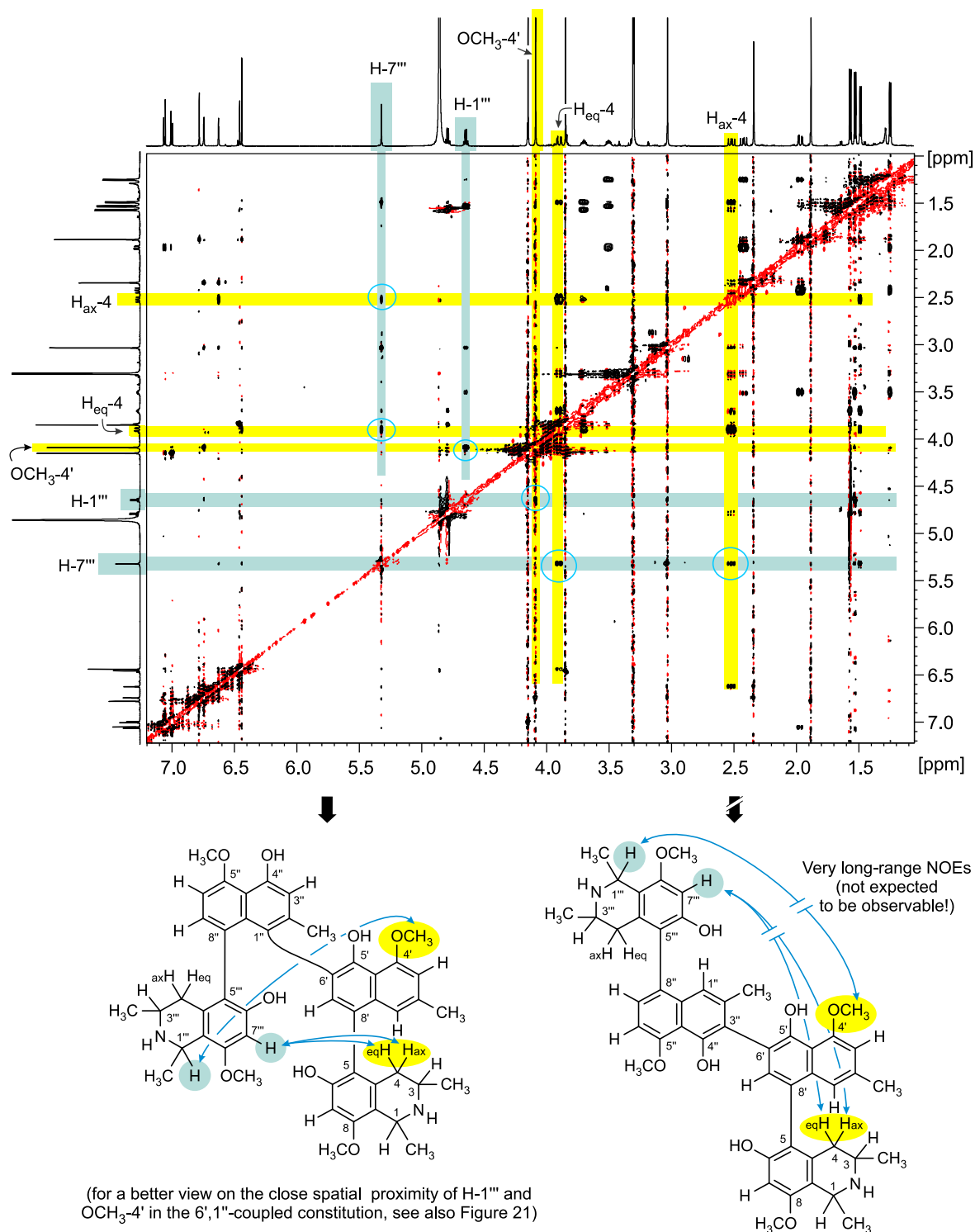
Scheme 1. Distinguishing the two possible constitutions of mbandakamine A by ROESY correlations.

With the complete constitution of mbandakamine A established, the relative and absolute configurations of the seven stereogenic elements (i.e., the four centers and three axes) remained to be assigned.

The relative configurations of the stereogenic centers in the isoquinoline parts were determined to be *trans* based on ROESY interactions between H-3 and the protons of CH$_3$-1 and between H-3''' and the protons of CH$_3$-1''' (Figure 21a). The absolute configurations at C-3 and C-3''' were established to be *R* by ruthenium-mediated oxidative degradation, which, in view of the relative *trans*-configuration, evidenced C-1 and C-1''' to be *R*-configured, too. ROESY correlations between H$_{eq}$-4 and H-7', and between H$_{eq}$-4''' and H-7'' (Figure 21a) revealed the respective nuclei to be on the same side of the molecule, which, in combination with the absolute *R*-configurations at C-1 and C-3 and at C-1''' and C-3''', assigned both outer axes to be *P*-configured. ROESY correlations between the isoquinoline portions of **16a-I** and **16a-II** and between H-1''' and OCH$_3$-4' (Figure 21a) evidenced the central axis of mbandakamine A to be *P*-configured, too. Consequently, mbandakamine A was 1*R*,3*R*,1'''*R*,3'''*R*,*PPP*-configured and thus possessed the full absolute stereostructure **16a** (Figure 21b).
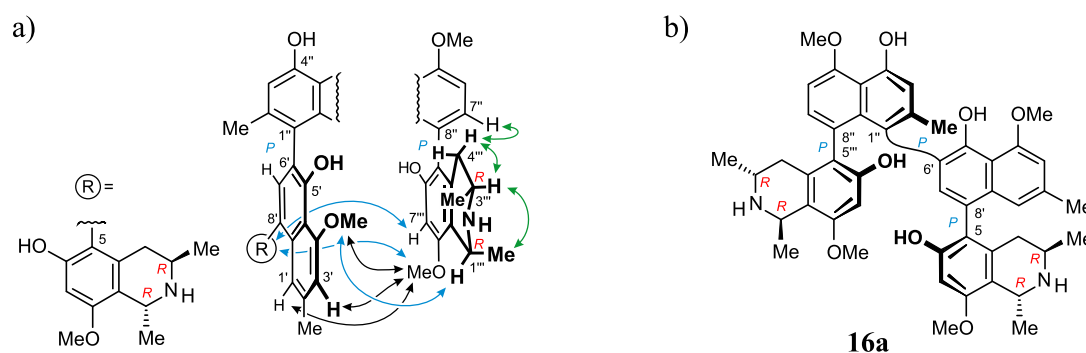
Figure 21. a) ROESY correlations between the naphthalene part of the molecular half **16a-I** (left) and the isoquinoline moiety of the second portion **16a-II** (right), evidencing the 6',1''-coupling (black arrows) and the relative configurations at the centers and at the outer axes (green arrows) and at the central biaryl linkage (blue arrows) of mbandakamine A; b) the full absolute stereostructure of mbandakamine A (**16a**).

With its 6',1''-coupling, mbandakamine A was the first natural dimeric naphthylisoquinoline alkaloid with a biaryl axis joining two naphthylisoquinoline halves in an unsymmetric way. In particular, the C-1''-position is extremely overcrowded, due to its connection to the naphthalene unit of the southeastern naphthylisoquinoline portion, which, in

turn, is jammed between the rigid methyl group at C-2" and the bulky isoquinoline substituent at C-8". The attachment of two bicyclic aryl substituents in the two neighboring *peri*-positions C-1" and C-8" created a unique array in which the ring current effect exerted by the southeastern naphthalene and isoquinoline substituents are strongly effective at the nuclei in the northwestern isoquinoline. This explains the most unusual chemical shifts of the protons H-7''' (5.32 ppm) and OCH$_3$-8''' (3.03 ppm), which are spatially very close – and, thus, highly sensitive – to the two southwestern aryl ring systems.

Moreover, mbandakamine A (**16a**) was the very first compound possessing two *peri* chiral biaryl axes ever found in nature. The only other natural products previously known with a somewhat similar structural array were the dimeric 4-phenylanthraquinones like joziknipholone A (**24**, Figure 22).[127] Although compounds such as **24** possessed two aryl substituents in *peri* positions of an anthracene-derived unit (at C-4′ and C-10′), they actually displayed only one chiral biaryl axis, the sp^2-sp^2 bond between C-4′ and C-1′′′. Furthermore, the intriguing 1,8-diarylnaphthalene unit as displayed by mbandakamine A had never been found in any other natural product before.
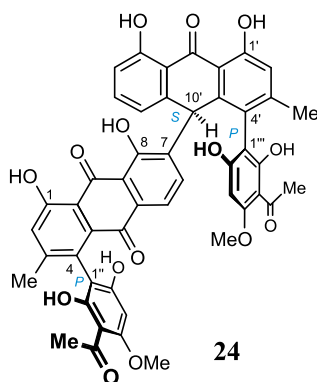
Figure 22. The natural dimeric 4-phenylanthraquinone joziknipholone A (**24**),[127] with *peri* aryl substituents, somewhat similar to that in mbandakamine A (**16a**).

The closest scaffolds to mbandakamine A (**16a**) previously known in the literature were artificial 1,8-diphenylnaphthalenes[128-130] like the trimer **25**[131] and the semi-synthetic dimeric naphthylisoquinoline jozimine B (**26**, Figure 23),[132] which appeared overall less crowded compared to **16a**, in particular regarding the relatively low steric hindrance at the central axis of **26** in comparison to that of **16a**.
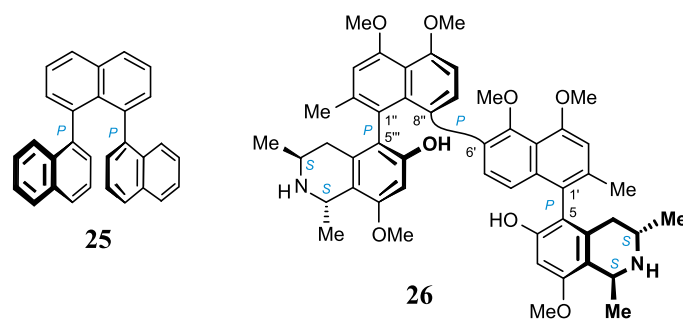
Figure 23. A simplified synthetic scaffold and a complex semi-synthetic one closely related to mbandakamine A (**16a**): the 1,8-diarylnaphthalene **25**[131] and jozimine B (**26**).[132]

3.2.3. *Isolation and Structural Elucidation of Mbandakamine B (16b)*

The discovery of mbandakamine A (**16a**) with its unprecedented highly unsymmetric structure and its multi-facetted structural novelties made the search for imaginable analogs, like atropisomers, a rewarding task. Of particular interest was the atropo-diastereomer at the central biaryl axis, as the center of originality of **16a**.

The directed screening of the extract for another dimer possessing the same mass as that of **16a** revealed Peak 7 (Figure 16), to be a potential candidate. Unfortunately, this compound was found to be present in the extract in substantially smaller quantities compared to **16a** (ca. 1:10). Moreover, it eluted together with another, unknown minor metabolite in reversed-phase HPLC. Although all the attempts to fully remove the interfering constituents were unsuccessful, repetitive reversed-phase HPLC provided Peak 7 in a significantly purified form, allowing unambiguous assignment of its full three-dimensional structure.

In HRESIMS measurement, it exhibited a monoprotonated ion at *m/z* 785.3789 and a doubly protonated one at *m/z* 393.1954, consistent with a molecular formula of $C_{48}H_{52}N_2O_8$, which was identical to that of **16a** (see above), thus confirming the two compounds to be isomers.

The coupling pattern of the ^{1}H NMR signals displayed by the second dimer was the same as that of mbandakamine A (**16a**), revealing the presence of four methoxy groups and, in the

aromatic region, four singlets, two *meta*-coupled doublets, and two *ortho*-located protons. Analysis of the 1D and 2D NMR data of this metabolite established its constitution to be identical to that of **16a**, that is, consisting of two 5,8′-linked naphthylisoquinoline halves, **16b-I** and **16b-II**, unsymmetrically connected to each other via C-6′ in **16b-I** and C-1″ in **16b-II** (Figure 24). This alkaloid was therefore the second dimer with such a highly unsymmetric, and severely strained 6′,1″-coupling at the binaphthalene core; it was henceforth named mbandakamine B.
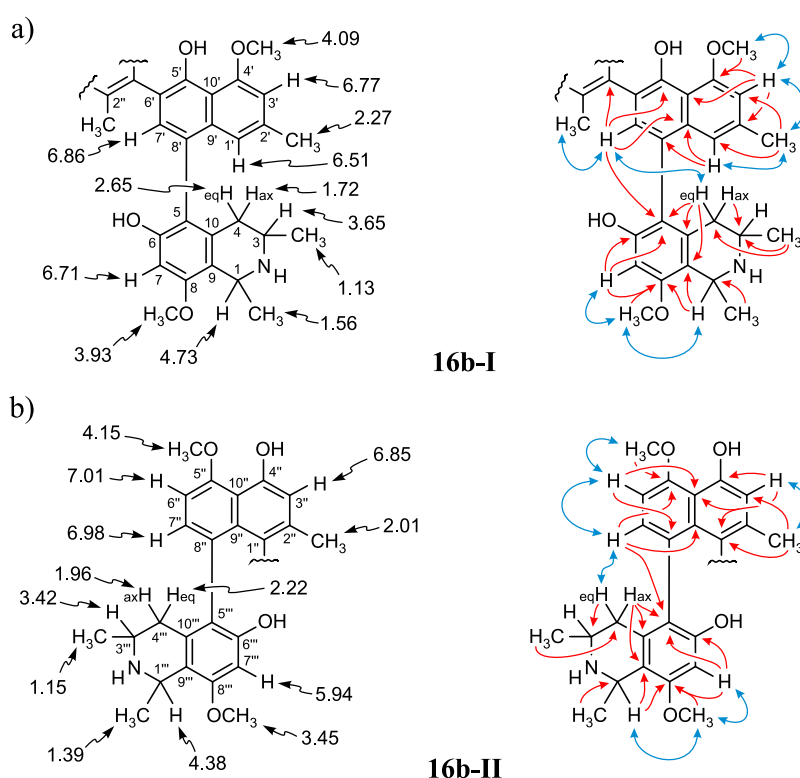
Figure 24. ¹H NMR chemical shifts (in ppm) and selected ROESY (blue double arrows) and HMBC (red double arrows) interactions of mbandakamine B (**16b**) evidencing the constitution of: a) its 'southeastern' portion **16b-I**; and b) its 'northwestern' moiety **16b-II**.

The relative configurations at the stereocenters in both isoquinoline portions of mbandakamine B were determined to be *trans* by ROE interactions between CH₃-1 and H-3 in **16b-I**, and CH₃-1‴ and H-3‴ in **16b-II** (Figure 25a). The oxidative degradation of mbandakamine B afforded 3-aminobutyric acid as its *R*-enantiomer exclusively, which demonstrated that both, C-3 and C-3‴ were *R*-configured. This, together with the aforementioned *trans*-array, evidenced that the stereogenic centers at C-1 and C-1‴ had to be *R*-configured, too, all just like in **16a**. Likewise similar to **16a** were the ROE interactions

across the outer biaryl axes (H_{eq}-4 ↔ H-7' in **16b-I**, and H_{eq}-4''' ↔ H-7'' in **16b-II**, see Figures 24 and 25a), which, in view of the absolute *R*-configurations at C-3 and C-3''', established both outer axes to be *P*-configured.

With the constitution and all the relative and absolute configurations at the stereocenters and at the outer axes of mbandakamine B being the same as that of mbandakamine A (**16a**), the only structural difference between these two dimers thus had to be opposite configurations at the central biaryl axes. This was confirmed by specific ROESY interactions between the two molecular portions of mbandakamine B, **16b-I** and **16b-II**, more exactly between H-7' and H_{ax}-4''', and between OCH_3-4' and H-7''' (Figure 25a), evidencing an *M*-configuration at the central biaryl axis. Consequently, mbandakamine B had the absolute stereostructure **16b** depicted in Figure 25b.
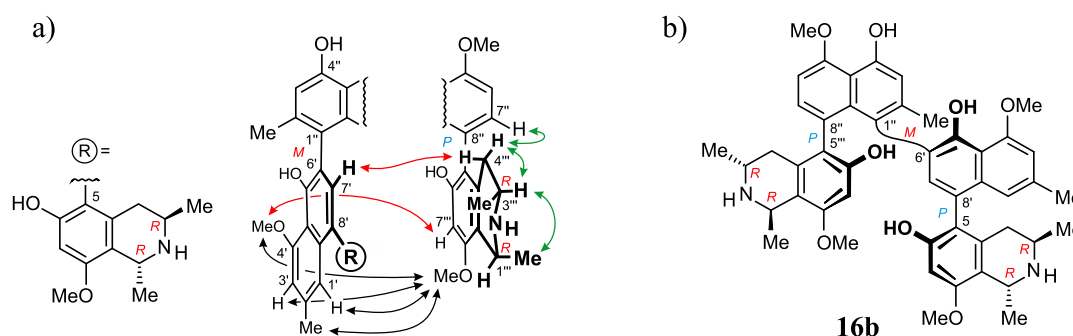
Figure 25. a) ROESY correlations between the naphthylisoquinoline halves **16b-I** and **16b-II** of mbandakamine B (**16b**), indicative of the 6',1''-coupling (black arrows) and of the relative configurations at the centers and at the outer axes (green arrows) and at the central axis (red arrows); b) full absolute stereostructure of mbandakamine B (**16b**).

The most obvious spectral differences between **16a** and **16b** were the ECD curves, which were virtually opposite to each other (Figure 26a), although **16a** and **16b** only differed in the configuration at the central axis, with all other six stereogenic elements − two axes and four centers − being identical. This demonstrated that the binaphthalene core, whose stereo-orientation is given by the configuration of the central axis, was the most important chromophore, largely dominating the ECD spectrum. This finding corroborated with the conclusions from two earlier known cases of atropo-diastereomers at the central axis, the pair shuangancistrotectorines A (**27a**) and B (**27b**)[78] and the couple jozimine A_2 (**15**) and its *P*-configured diastereomer jozibrevine A (structure not shown, for that of **15**, see Figure 6),[79]

which likewise displayed mirror-like ECD curves,[78,79] as exemplarily shown for **27a** and **27b** in Figure 26b.
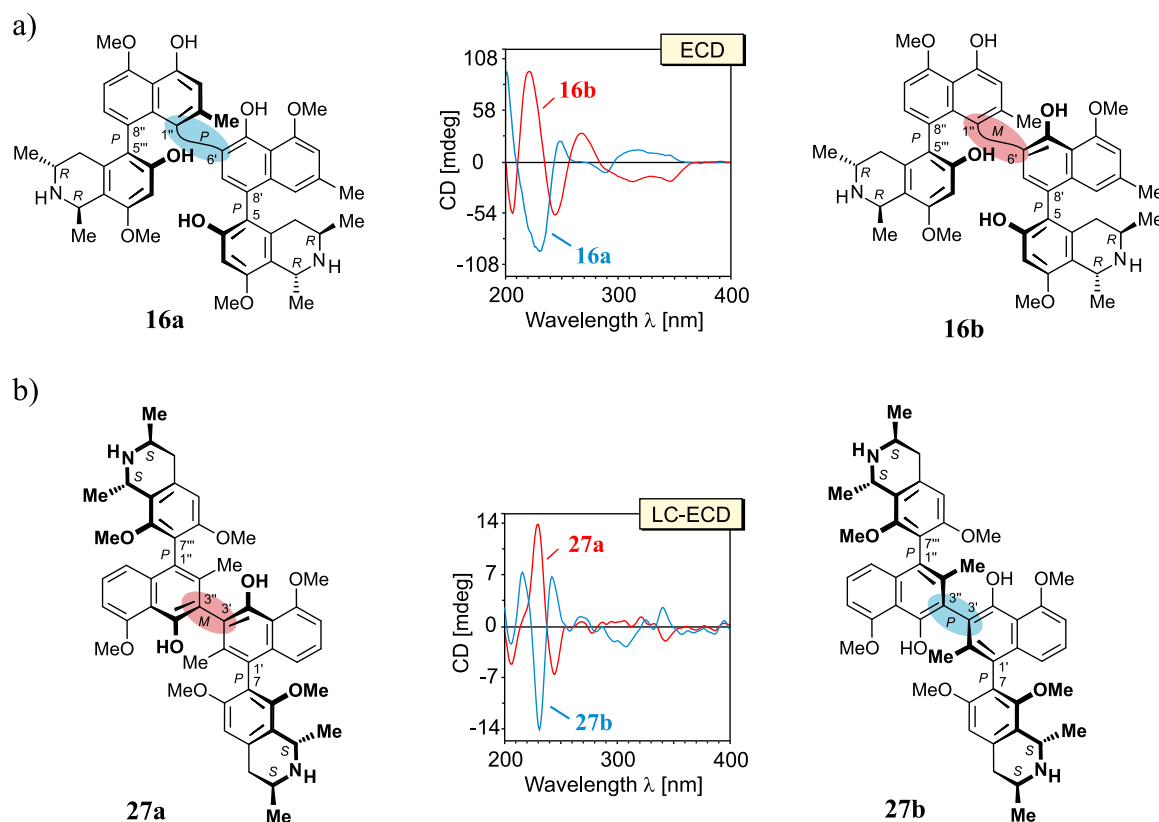
Figure 26. a) Nearly opposite ECD spectra of the atropo-diastereomers mbandakamines A (**16a**) and B (**16b**);[80] b) likewise mirror-like ECD curves displayed by the pair shuangancistrotectorines A (**27a**) and B (**27b**),[78] differing from each other only by the configuration at the binaphthalene linkage.

3.2.4. *Confirmation of the Absolute Stereostructures of Mbandakamines A (16a) and B (16b) by ECD Calculations and Biomimetic Total Synthesis*

The thrilling absolute stereostructures of mbandakamines A (**16a**) and B (**16b**) established by the fruitful interplay of HPLC, MS, NMR, ECD, and ruthenium-mediated oxidative degradation, as described above, were firmly and independently supported by ECD calculations performed by F. N. Katele (in collaboration with Dr. T. Bruhn) in our group.[133]

Both mbandakamines A (**16a**) and B (**16b**) were sequentially optimized with PM6[134] and B97D/TZVP,[135,136] leading to six relevant conformers (i.e., those with ΔE < 3 kcal mol^{-1} above the global minimum)[137] for each diastereomer. Using the semi-empirical ZINDO/S method,[138] the ECD curves of each of the six conformers found per diastereomer were

calculated and added in a Boltzmann-weighted manner, i.e., according to the population of the respective conformer, giving one average ECD curve for each of the atropo-diastereomers **16a** and **16b**. The obtained theoretical ECD spectra of **16a** and **16b** were found to fit very well with those found experimentally (see Scheme 2), thus confirming the above described stereochemical assignments.
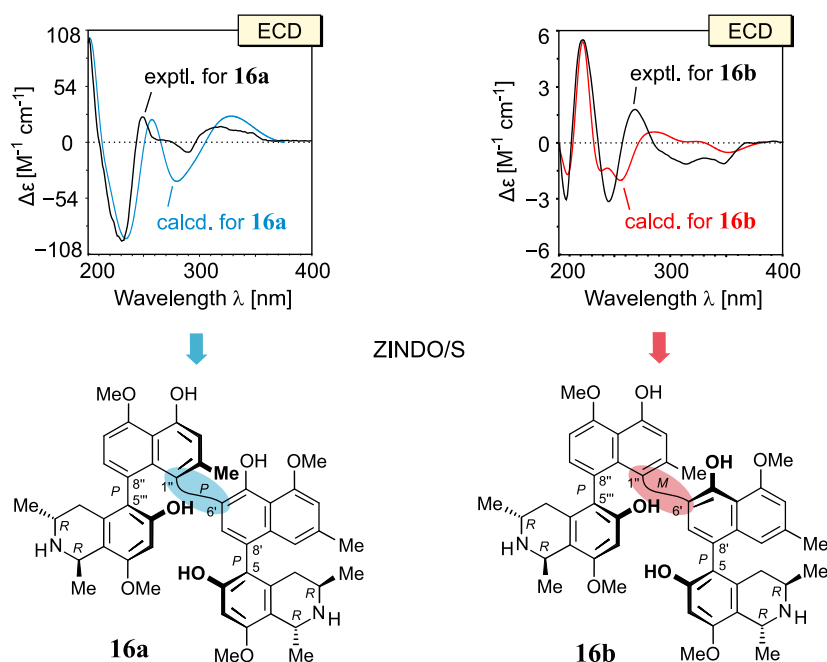
Scheme 2. Assignment of the absolute stereostructures of mbandakamines A (**16a**) and B (**16b**) by ECD calculations using ZINDO/S, performed by F. N. Katele.[133]

A further solid argument validating the aforementioned assignment is the total synthesis of mbandakamine A (**16a**), as most recently accomplished by Dr. C. Schies, in our group,[139] which was achieved by direct oxidative cross-coupling of the two constitutionally slightly different, unprotected monomeric precursors **28** and **29** (Scheme 3). The obtained synthetic material of **16a** was found to be identical with the authentic natural product in all respects – spectroscopically, physically, and chromatographically – thus further confirming the above established absolute stereostructure.[139] In this reaction, mbandakamine A (**16a**) was obtained with other, likewise expected regioisomeric coupling products, but, remarkably, with no traces of its atropo-diastereomer mbandakamine B (**16b**).[139] This apparently high atropo-diastereoselectivity actually corroborates the substantially predominant occurrence of **16a** over **16b** (ca. 10:1) in the plant material, as mentioned above (see Section 3.1.2).[80,139]
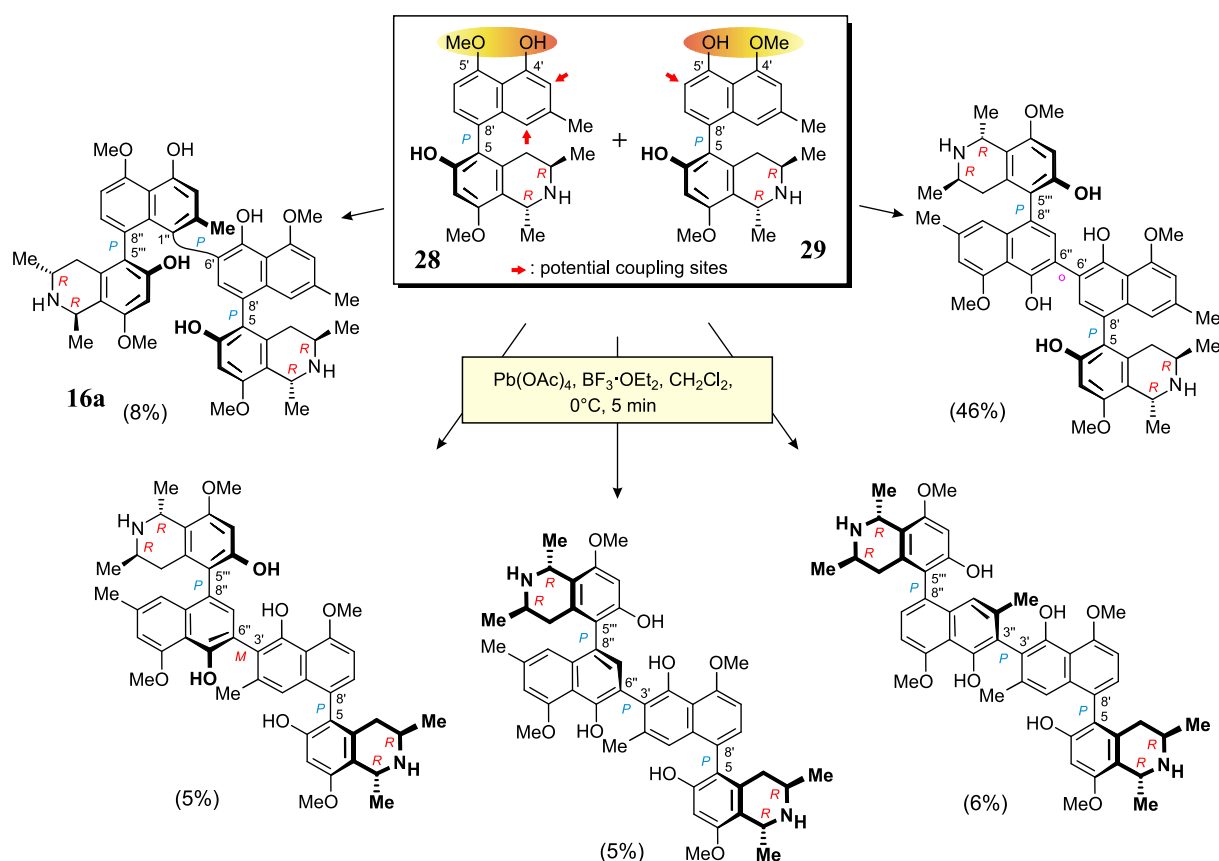
Scheme 3. Biomimetic phenol-oxidative cross-coupling of the two monomeric NIQs **28** and **29**, differing one from another only by the MeO/OH pattern at C-4′ vs C-5′, to generate mbandakamine A (**16a**) and related dimers, achieved by Dr. C. Schies.[139]

The above-presented isolation of mbandakamines A (**16a**) and B (**16b**), with their multi-facetted structural novelties within the field of NIQ (i.a., with an exceptionally high steric hindrance at the central axis, the first even drastically unsymmetric linkage in the binaphthalene core, and with the first biaryl coupling in the two neighboring *peri*-positions), made it rewarding to search for further novel NIQ dimers in the same leaf extract, as described in the following paragraphs.

3.3. Cyclombandakamines A₁ (20) and A₂ (21): the First Oxygen-Bridged NIQ Dimers

3.3.1. Discovery of Cyclombandakamine A₁ (20)

HPLC-MS investigations of different fractions obtained during the isolation of **16a** and **16b** revealed the occurrence of further, minor dimeric NIQs. Of these, particularly interesting was a compound contained in the fraction collected just before the one of **16b** by preparative

reversed-phase HPLC. It gave a monoprotonated ion at *m/z* 797.4 (in HPLC-ESIMS), which was 12 units more as compared to the above-mentioned *m/z* of **16a** and **16b**, hinting at the presence of an *N*- or *O*-methylated analog of **16a** or **16b** with one tetrahydro- and one dihydroisoquinoline units like the scaffolds exemplarily shown in Figure 27.
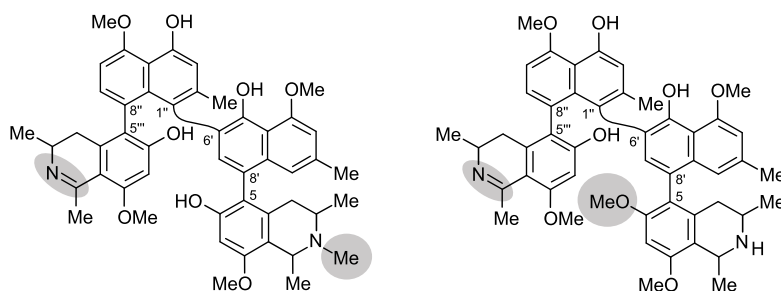
Figure 27. Examples of *N*- or *O*-methylated constitutional analogs of **16a** and **16b** with one tetrahydro- and one dihydroisoquinoline units, according to the HPLC-MS detected *m/z* (797.4). The constitutional differences as compared to **16a** and **16b** are underlaid in gray.

The online UV spectrum of this compound, however, was not in full agreement with such an assumption. As compared to the online UV curve of e.g., **16a**, it showed a hypsochromic shift in the region from 280 to 360 nm, highlighted in Figure 28, instead of a bathochromic shift or the appearance of a new band with a lower frequency, as it would have been expected for an NIQ with a dihydroisoquinoline unit.[75,78,103,140] The spectral divergences were even more appealing, particularly because the observed blue shift was suggestive of the loss of some electronic π-interactions, which might be caused e.g., by a disruption of the aromaticity in some of the aryl rings.[141,142] These assumptions drew great interest to that compound, making its isolation and structural elucidation a rewarding goal.
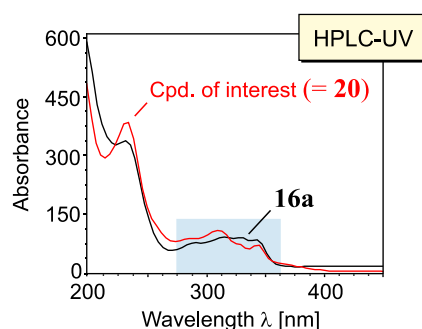
Figure 28. Comparison of the online UV spectrum of mbandakamine A (**16a**) with the one of the compound of interest, which was later (see below) established to be cyclombandakamine A$_1$ (**20**, see Figure 32). The underlaid part indicates the spectral region where the differences were particularly attracting.

Preparative HPLC on a reversed-phase column provided the targeted metabolite, as a beige amorphous powder. According to HRESIMS (*m/z* 797.3783, [M+1]$^+$), it had a molecular formula of $C_{49}H_{52}N_2O_8$. Its ^{1}H NMR spectrum displayed a full set of signals, indicative of an unsymmetric dimer, with four three-proton singlets, typical of *O*-methyl groups, as in **16a** and **16b**,[80] and one further three-proton singlet, characteristic of a methyl being attached to one of the nitrogen atoms. Mostly striking was the aromatic region (Figure 29a), showing only seven protons, instead of eight or ten as usual (see e.g., **16a** and **16b**, and **15**).[62,75-78,80] Likewise unprecedented was the presence of three (instead of two) methylene groups with diastereotopic protons, and the observation of a quaternary carbon at δ_C 196.0 ppm in ^{13}C NMR (Figure 29b), suggestive of a tetralone carbonyl carbon.[143] All these indications strongly hinted at a novel-type structure, which was subsequently elucidated, as explained in below.
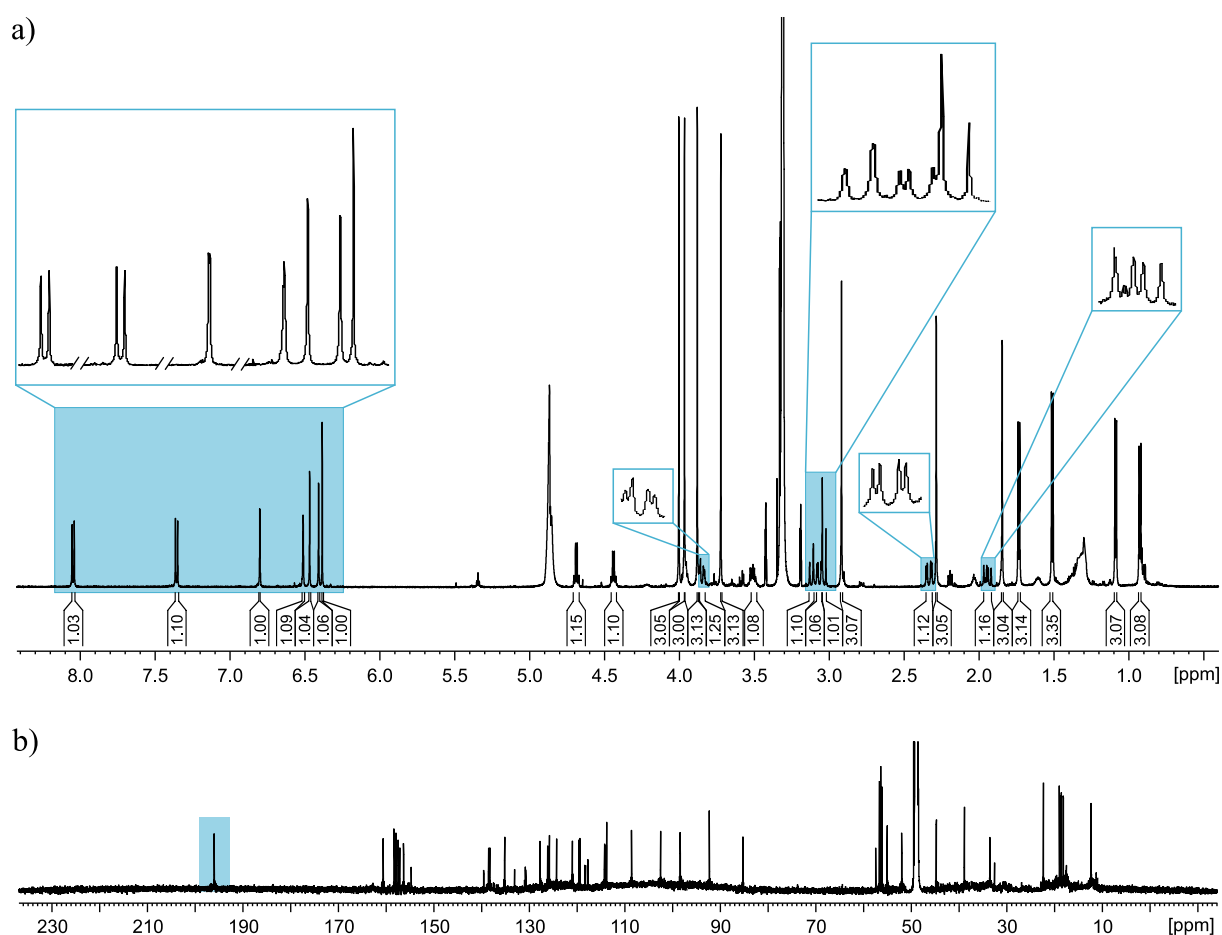
Figure 29. 1D NMR spectra of the isolated compound cyclombandakamine A$_1$ (**20**): a) ^{1}H NMR spectrum; and b) ^{13}C NMR spectrum; the highlighted – and enlarged – parts (with signals for seven aromatic protons, three pairs of diastereotopic protons, and a carbonyl group) are features uncommon in the field of NIQ.

3.3.2. *Structural Elucidation of Cyclombandakamine A₁ (20)*

Similar to mbandakamines A (**16a**) and B (**16b**), one of the naphthylisoquinoline portions of **20**, the southeastern part, denoted as **20-I** (Figure 30), showed NMR signals typical of a 5,8′-coupled monomeric naphthylisoquinoline, with the other, northwestern part, **20-II**, linked via C-6′.[80] The pattern included a *meta*-coupling of the two aromatic protons, H-1′ (6.51 ppm, *p*t, *J* = 1.1 Hz) and H-3′ (6.80 ppm, d, *J* = 1.2 Hz), sequential ROESY interactions H-7′ (6.38 ppm, s) ↔ H$_{eq}$-4 (2.33 ppm, dd, *J* = 17.9, 4.9 Hz) ↔ H$_{ax}$-4 (1.94 ppm, dd, *J* = 17.9, 11.4 Hz) ↔ H-1′ ↔ CH₃-2′ (2.29 ppm, *p*d, *J* = 0.3 Hz) ↔ H-3′ ↔ OCH₃-4′ (4.00 ppm, s), and HMBC correlations from H-7 (6.41 ppm, s), H$_{eq}$-4, and H-7′ to C-5 (119.7 ppm). An HMBC interaction of H-7′ (colored in green, Figure 30) to a quaternary carbon (δ_C 85.3 ppm) belonging to **20-II** established C-6′ (δ_C 121.0 ppm) as the connection site of **20-I** to **20-II**. The location of a methoxy group at C-8 in the isoquinoline of **20-I** was evidenced by the ROESY series H-3 (3.52 ppm, m) ↔ CH₃-1 (1.51 ppm, d, *J* = 6.7 Hz) ↔ OCH₃-8 (3.88 ppm, s) ↔ H-7 (6.41 ppm, s), corroborated by joint HMBC correlations from H-1 (4.68 ppm, q, *J* = 6.8 Hz), OCH₃-8, and H-7 to C-8 (157.5 ppm), as illustrated in Figure 30.
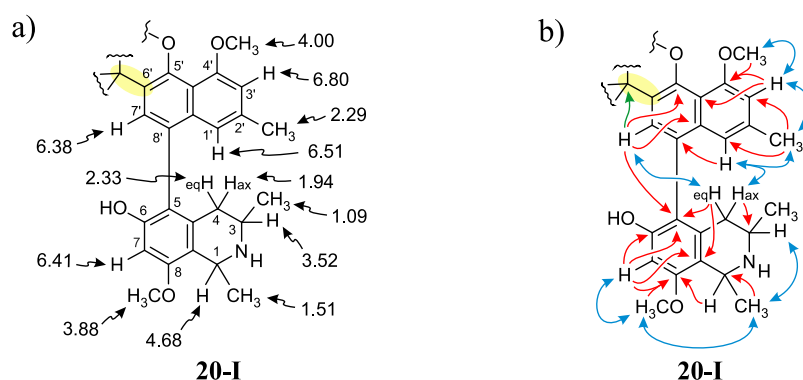
Figure 30. Selected NMR data of the southeastern molecular half (**20-I**) of cyclombandakamine A₁ (**20**): a) ¹H chemical shifts in ppm; and b) key HMBC (red single arrows) and ROESY (blue double arrows) correlations; the crucial HMBC demonstrating C-6′ to be the coupling position of **20-I** to C-1″ in the other molecular part of **20**, **20-II** (see Figure 31), is shown in green.

The northwestern part **20-II** (Figure 31) was spectroscopically more complex. It possessed an *N*-methylated isoquinoline portion with a methoxy group (3.72 ppm, s) at C-8‴ (158.0 ppm). This was evidenced by a series of ROESY correlations CH₃-3‴ (0.93 ppm, d, *J* = 6.7 Hz) ↔ CH₃-*N* (2.92 ppm, s) ↔ CH₃-1‴ (1.73 ppm, d, *J* = 6.6 Hz) ↔ OCH₃-8‴ ↔ H-7‴ (6.47 ppm, s), together with HMBC correlations of CH₃-*N* with C-1‴ (57.9 ppm) and C-3‴

(55.1 ppm), and of H-1‴, H-7‴, and OCH$_3$-8‴ jointly to C-8‴. An AB spin system of H-7″ (8.04 ppm, d, *J* = 9.0 Hz) and H-6″ (7.35 ppm, d, *J* = 9.0 Hz), ROESY interactions of H-6″ with OCH$_3$-5″ (3.97 ppm, s), and HMBC correlations from H-7″ to C-5″ (160.6 ppm) and C-9″ (138.3 ppm), from OCH$_3$-5″ to C-5″, and from H-6″ to C-10″ (119.4 ppm) proved the position of OCH$_3$-5″, and, thus, evidenced the aforementioned carbonyl group to be at C-4″ (Figure 31). This assignment was corroborated by the low-field shifts of the diastereotopic protons at C-3″ (3.12 ppm, dd, *J* = 0.7, 14.6 Hz, and 3.03 ppm, d, *J* = 14.6 Hz), by their ROESY interactions with CH$_3$-2″ (1.85 ppm, *p*d, *J* = 0.3 Hz), and by their HMBC correlations with CH$_3$-2″, C-4″, and C-10″. From HMBC correlations of H-7″, H-7‴, and H$_{eq}$-4‴ (3.06 ppm, dd, *J* = 17.1, 4.51 Hz) to C-5‴, the northwestern half (**20-II**) was found to be 5‴,8″-coupled, like the southeastern part, **20-I** (Figure 30). Joint HMBC correlations of H-7′, CH$_3$-2″, and of both protons at C-3″ to a quaternary carbon (δ_C 85.3) proved this C-atom to be C-1″ (Figure 31), hence indicating that the two molecular portions, **20-I** and **20-II**, were coupled through C-6′ and C-1″, respectively, as already in **16a/b**.[80]
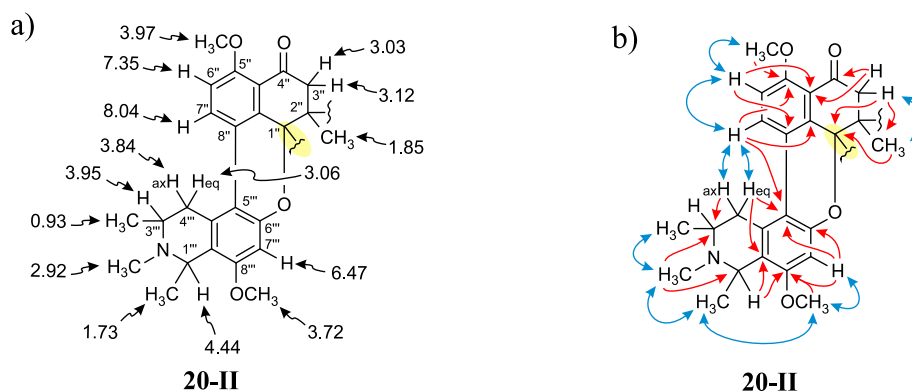
Figure 31. Key NMR data of the northwestern moiety (**20-II**) of cyclombandakamine A$_1$ (**20**): a) ^{1}H chemical shifts in ppm; and b) selected ROESY (double arrows in blue) and HMBC (red-highlighted single arrows) interactions.

In contrast to **16a** and **16b** – and to all other known naphthylisoquinoline alkaloids – ROE interactions between H-7″ and both diastereotopic protons, H$_{eq}$-4‴ (for the NMR data, see also Table 11 in the Experimental Part) and H$_{ax}$-4‴ (3.84 ppm, dd, *J* = 17.1, 5.4 Hz), were observed (Figure 31, **20-II**), suggesting that the two moieties in that northwestern half were not orthogonal to each other, but nearly co-planar, much closer than usual, firmly pressed against one another, apparently by being part of a tight ring. This was due to an ether bond between O-6‴ and C-1″, which, furthermore, explained the observed downfield shift of this

carbon (85.3 ppm). In a similar way, the chemical shift of C-2″ (92.3 ppm) indicated that this atom was involved in an ether bond with the spatially close oxygen, O-5′, like the above-mentioned linkage between C-1″ and O-6‴, thus establishing the northern part of **20-II** to be a tetralone subunit (Figure 31). Hence, the isolated dimer was found to be the first cyclized, since twofold oxygen-bridged, *N*-methyl analog of **16a** or **16b**. It was therefore named cyclombandakamine A$_1$.

This novel-type naphthylisoquinoline dimer was also stereochemically thrilling: it did not only possess the usual two stereocenters in each of the isoquinoline moieties and a stereogenic axis in the southeastern half, but, for the first time, also two additional stereocenters in the tetralone moiety in the northwestern part. Furthermore, the *C,C*-axis linking the two northwestern bicyclic aryls (C-5‴ to C-8″) remained a further potential stereogenic element.

The relative configurations at the stereocenters in the two isoquinoline moieties were determined to be *trans* from ROESY interactions between CH$_3$-1 and H-3 and between CH$_3$-1‴ and H-3‴ (Figure 32), but also between CH$_3$-3‴ and H-1‴. The latter, quite unusual interaction hinted at the presence of a second, less common conformation in the western isoquinoline part, presumably as a consequence of the repulsive van der Waals interactions of the tightly pressed H-4‴ and H-7″. The ruthenium-mediated oxidative degradation established the absolute configuration to be *R* at both, C-3 and C-3‴, which, with respect to the above assigned relative *trans*-configuration, evidenced *R*-configurations at C-1 and C-1‴, too. From ROESY interactions of H$_{ax}$-4 with H-1′, and of H$_{eq}$-4 with H-7′ (Figure 32) and based on the above-established absolute *R*-configurations at C-3 and C-1, the axis in the southeastern naphthylisoquinoline half, **20-I**, was determined to be *P*-configured, as also in **16a/b**.
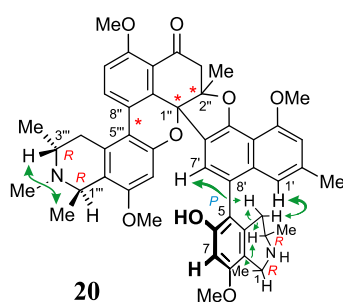
Figure 32. ROESY correlations evidencing the relative and − based on the results of the oxidative degradation − absolute configurations at the 'classical' stereogenic elements (i.e., centers in the isoquinoline portions, and the southeastern biaryl axis) of cyclombandakamine A$_1$ (**20**).

In the tetralone subunit, the linkage of O-6‴ with C-1″ sterically fixes the western axis, making its absolute configuration and that of C-1″ interdependent: a *P*-configuration at the western biaryl axis and *R* at C-1″ entailing each other, like *M* implying *S*. This phenomenon reduced the number of remaining possible stereoisomers from eight (as expected for three independent stereogenic elements) to only four, two of them with a *cis*-array of the dihydrofuran-cyclohexene system (see **20-A** and **20-B**, Figure 33), and two with a *trans*-junction, which, however, would be severely strained (see **20-C** and **20-D**). Indeed, an ROE interaction between CH₃-2″ and H-7‴ (Figure 33) indicated the dihydrofuran and cyclohexene rings to be *cis*-fused, thus further reducing the number of possible diastereomers to only two, with 1″*R*,2″*S*,8″*P*- and 1″*S*,2″*R*,8″*M*-configurations, i.e., **20-A** and **20-B**.
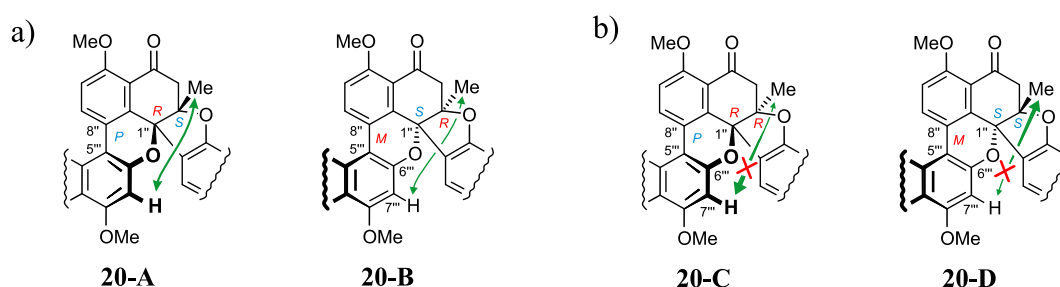
Figure 33. The only four possible absolute configurations of the three stereogenic elements in the pyran-cyclohexenone-dihydrofuran sequence of **20** with the key ROESY interaction (Me-2″ ↔ H-7‴) indicative of the relative configurations: a) the *cis*-fused isomers **20-A** and **20-B**; and b) the severely strained *trans*-fused analogs **20-C** and **20-D**. The red cross illustrates that the ROESY interaction in the respective scaffold should not be expected to be observed.

The two remaining isomers, **20-A** and **20-B**, were distinguished by the ROESY interactions observed between CH₃-3‴ and H-7′, and between CH₃-3‴ and H-7 (see Figure 34a, magenta arrows), which showed that C-1″, C-2″, and the western C-8″– C-5‴ biaryl axis were *R*-, *S*-, and *P*-configured, respectively. In the other possible diastereomer, with 1″*S*,2″*R*,8″*M*-configuration, CH₃-3‴ would point to the opposite direction (Figure 34b), and would, thus, be far away from H-7′ and H-7, so that no spatial interactions between these nuclei would be expected. Consequently, cyclombandakamine A₁ was 1*R*,3*R*,5*P*,1″*R*,2″*S*,8″*P*, 1‴*R*,3‴*R*-configured, i.e., with the full absolute stereostructure **20-A** presented in Figure 34.
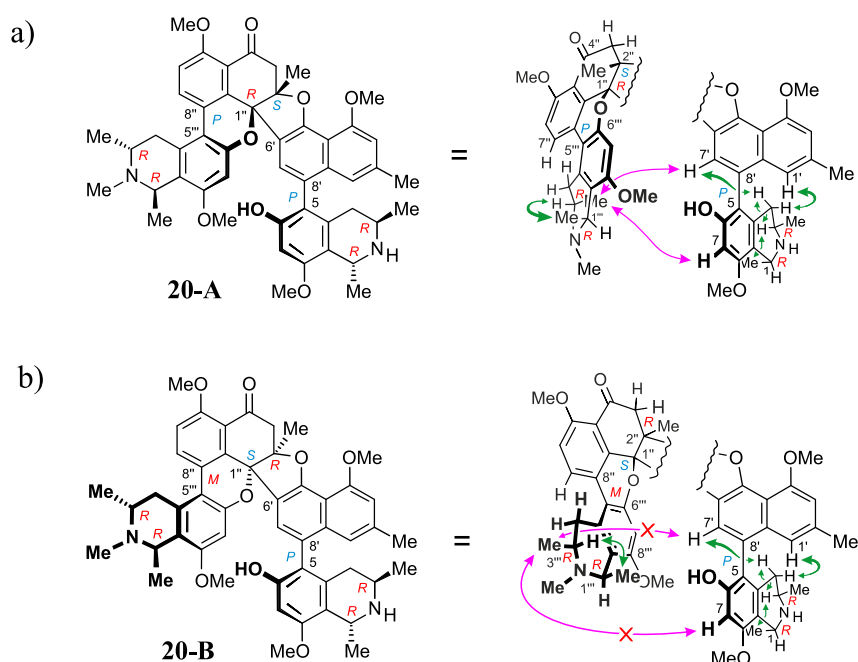
Figure 34. Structures of the two possible absolute configurations of cyclombandakamine A_1 and the key ROESY interactions (in magenta) allowing their distinction: a) the 1*R*,3*R*,5*P*,1″*R*,2″*S*,8″*P*,1‴*R*, 3‴*R*-configured scaffold (**20-A**); and b) the 1*R*,3*R*,5*P*,1″*S*,2″*R*,8″*M*,1‴*R*,3‴*R*-configured molecular framework (**20-B**). The red cross illustrates that the interaction would not be expected to be observed for the respective scaffold.

To further verify the experimental assignment, both imaginable diastereomers **20-A** and **20-B** were optimized by using the B97-D3[144] functional in combination with the basis set def2-TZVP,[145] as implemented in ORCA.[146] Due to the rigidity of the central structural core of cyclombandakamine A_1, only the global minima were determined for each of the two above-mentioned diastereomers, as performed by Dr. T. Bruhn in our group. The experimentally observed ROE interactions matched well only with the ones predicted for the optimized structure of the 1″*R*,2″*S*,8″*P*-isomer (i.e., **20-A**). Moreover, the ECD spectrum calculated for **20-A**, by using TDCAM-B3LYP/def2-TZVP,[147] showed a good agreement with the experimental one of the isolated product, while that of the 1″*S*,2″*R*,8″*M*-diastereomer, i.e., **20-B**, was virtually opposite (Scheme 4). This confirmed cyclombandakamine A_1 to have the above-established full absolute stereostructure **20-A** and indicated that its ECD curve was largely dominated by the chiral tetralone chromophore.
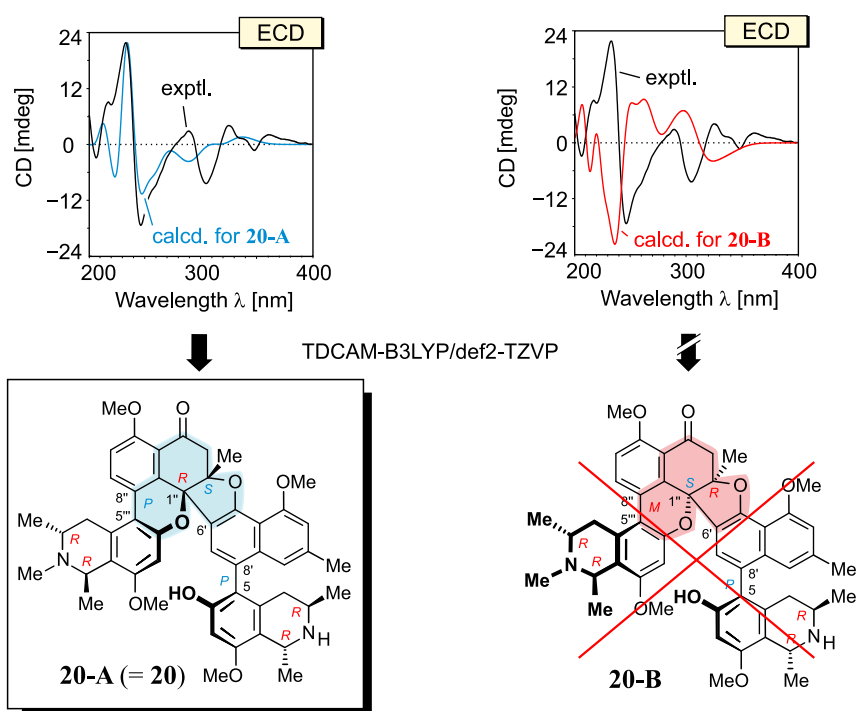
Scheme 4. Investigation of the absolute configuration of cyclombandakamine A$_1$ (**20**) by quantum-chemical ECD calculations. The experimental ECD spectrum was compared with the ones calculated for the two most probable stereostructures according to NMR and the oxidative degradation, **20-A** (with a 1″*R*,2″*S*,8″*P*-configuration in the tetralone unit) and **20-B** (displaying a 1″*S*,2″*R*,8″*M*-array). The theoretical ECD curves were calculated only for one – arbitrarily chosen low-energy – conformer of each diastereomer **20-A** and **20-B**.

The structure of cyclombandakamine A$_1$ (**20**), hence fully elucidated, was remarkable in many respects. It displayed two ether bonds linking a cyclohexenone subunit to a naphthalene and an isoquinoline moiety, as never seen before in the field of NIQs, thus making it the first dimeric NIQ to possess oxygen bridges. Even more thrilling were the stereochemical features of **20**, since its rigid, annulated molecular architecture, with eight consecutive condensed rings, showed a total of eight stereogenic elements (six centers and two axes, one of them thermodynamically dictated) – the highest number ever encountered in any NIQ before. Moreover, the fused pyran-cyclohexenone-dihydrofuran core (see the highlighted part in **20-A** or **20-B**, Scheme 4) was unprecedented among all previously known compounds (including the natural and artificial ones!); even as a partial substructure, this framework had not formerly been detected, which made **20** the very first chemical substance with such a structural unit. Biosynthetically, it seemed evident that the polycyclic dimeric alkaloid cyclombandakamine A$_1$ should have originated from an unusual pathway. As explained later below (see Section 3.5), this novel scaffold apparently resulted from the oxidation-induced

cyclization of an *N*-methyl derivative of mbandakamine A (**16a**) or B (**16b**), a process that had previously not been known for NIQs. Pharmacologically, cyclombandakamine A_1 was interesting, too: It exhibited potent antiprotozoal activities (see Section 3.10).

The isolation and complete structural elucidation of cyclombandakamine A_1 (**20**) thus was a very important discovery, opening new doors for synthetic, biosynthetic, analytical, theoretical, and pharmacological investigations.

3.3.3. Search for O-Bridged Dimeric NIQs in Plant Materials from Other Congolese *Ancistrocladus species*

The structural peculiarities of cyclombandakamine A_1 (**20**), together with its presumed biosynthetic origin and its pharmacological properties, made the search for related compounds an important goal. Directed, HPLC-UV-MS-assisted screening of the fractions hinted at the presence of further *O*-bridged dimeric NIQs, which, unfortunately, were found only in much smaller quantities. This insignificant occurrence, combined with the lack of further plant materials from the Congolese liana *Ancistrocladus* sp. 032, hampered the isolation of the detected promising candidates, triggering the search for such compounds in plant materials from other Congolese *Ancistrocladus* species available in the laboratory. From a total of seven different Congolese *Ancistrocladus* lianas investigated by HPLC-UV-MS (viz., *A. congolensis*, *A. likoko*, *A. ealaensis*, *Ancistrocladus* sp. 002A, *Ancistrocladus* sp. 002B, *Ancistrocladus* sp. 015, and *Ancistrocladus* sp. 114), only *A. ealaensis* and *Ancistrocladus* sp. 114 provided some hints (i.e., UV spectrum and *m/z*) at the occurrence of the targeted *O*-bridged dimeric compounds. This is exemplarily illustrated in Figure 35, showing an HPLC-UV chromatogram of an alkaloid-enriched fraction from *A. ealaensis*, with Peaks A and B being potential candidates, based on their online UV spectra, which were very similar to the one of **20**.
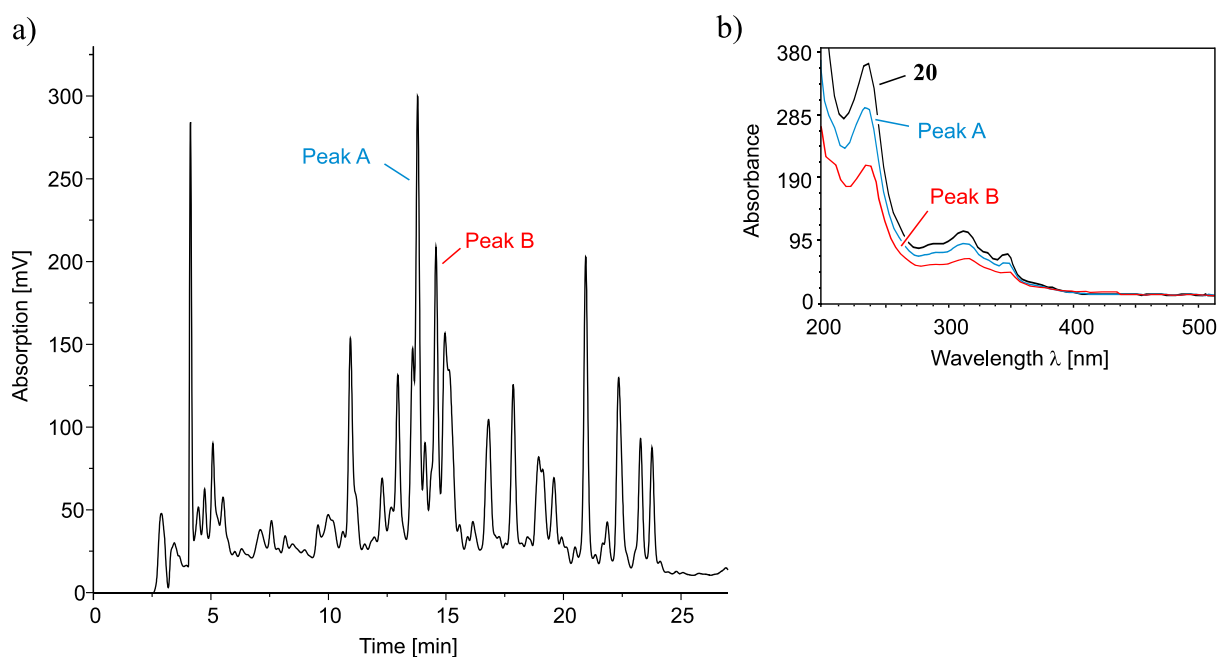
Figure 35. a) Chromatogram of an alkaloid-enriched fraction from the leaves of *A. ealaensis*; and b) comparison of online UV spectrum of cyclombandakamine A_1 (**20**) with the ones of Peaks A and B, suggesting the latter to be *O*-bridged compounds.

Due to the very restricted quantities of plant material of these two promising lianas available in the lab, and to the fact that the two plant species were already being phytochemically investigated by other researchers in our group, Dr. D. T. Tshitenge and J. P. Mufusama, no targeted isolation work was performed on these plants, thus warranting the collection of additional plant material from the Congolese liana *Ancistrocladus* sp. 032. Therefore, another field trip to the rainforests near the Congolese village Bonsolerive was conducted by the author of this thesis in August 2015, which, with the assistance of a GPS, permitted collection of further plant material from an *Ancistrocladus* liana growing at the same location as previously documented for *Ancistrocladus* sp. 032. An authentication procedure by HPLC-UV and HPLC-MS showed the freshly collected materials to be similar to the previously collected ones. A voucher specimen (No. 104) for the new collection has been deposited at the Herbarium Bringmann, University of Würzburg.

3.3.4. *Isolation and Structural Elucidation of Cyclombandakamine A_2 (21)*

Investigations on the crude leaf extract of the newly collected plant material by HPLC-UV suggested the occurrence of a second possible *O*-bridged dimer, as evidenced from its online UV spectrum, which was very similar to the one of cyclombandakamine A_1 (**20**) presented

above (see e.g., Figure 35b). Fractionation of the crude extract by liquid-liquid and liquid-solid extraction and subsequent directed resolution of the alkaloid-enriched fraction by preparative HPLC on a reversed-phase achiral C-18 column yielded a beige amorphous powder. It had a molecular formula of $C_{50}H_{55}N_2O_8$, as demonstrated by HRESIMS (*m/z* 811.3952, [M+1]$^+$), thus showing a molecular weight with 14 units more than **20**. Its ^{1}H and ^{13}C spectra revealed close similarities to those of **20**: the presence of seven aromatic protons and three methylene groups with diastereotopic protons, and of a carbonyl function, but with one additional CH_3 group (δ_H 2.96 and δ_C 41.5 ppm). The 1D and 2D NMR data (Figure 36) proved that the extra methyl group was linked to the nitrogen of the southeastern naphthylisoquinoline half (i.e., **21-I**). This *N*-methyl group was the only constitutional difference as compared to **20**.
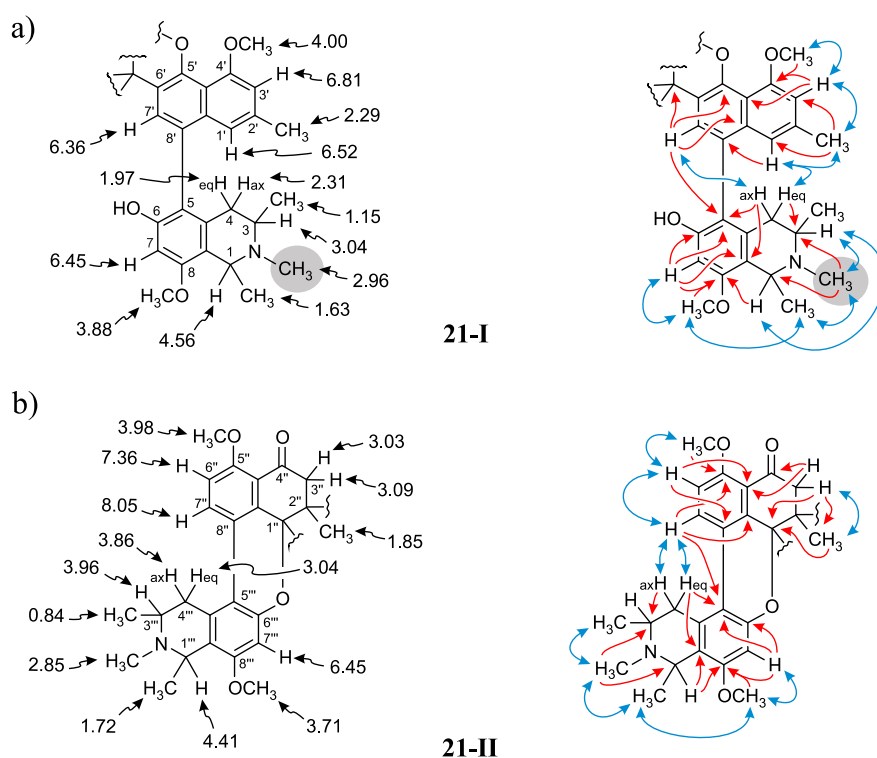
Figure 36. ^{1}H NMR chemical shifts (in ppm) and selected ROESY (blue double arrows) and HMBC (red double arrows) of cyclombandakamine A$_2$ (**21**) evidencing the constitution: a) in the southeastern portion **21-I**; and b) in the northwestern moiety **21-II**. The constitutional difference of **21** compared to cyclombandakamine A$_1$ (**20**), the extra *N*-methyl group, is highlighted in gray.

Additional differences between the two alkaloids were found in the configuration of the southeastern half **21-I** (Figure 37). In this molecular part, the proton at C-3, which was axial, as obvious from the coupling constants of H$_{ax}$-4 (2.31 ppm, dd, *J* = 17.5, 11.9 Hz) and H$_{eq}$-4

(1.97 ppm, dd, J = 17.5, 2.9 Hz), showed a ROESY interaction with H-1, thus indicating a *cis*-configuration at C-1 *versus* C-3 instead of *trans* as in the respective part of **20**, **20-I**. In addition, this second *O*-bridged alkaloid displayed ROESY interactions between H_{ax}-4 and H-7′, and between H_{eq}-4 and H-1′, opposite to the ones observed for **20-I** (see Figure 30). This demonstrated that **21-I** had to be either 1*R*,3*S*,5*P*-configured or 1*S*,3*R*,5*M*. In the northwestern half (Figure 37), the relative configurations at all stereogenic elements were identical to those in **20-II**, i.e., *trans*-configuration for both, C-3‴ *versus* C-1‴ and C-1″ relative to C-2″, so that the configurations in this part were either 1″*R*,2″*S*,8″*P*,1‴*R*,3‴*R*, as in **20**, or 1″*S*,2″*R*,8″*M*,1‴*S*,3‴*S*, i.e., the opposite. ROESY interactions observed between the two subunits of the new alkaloid were all identical to the ones displayed by the molecular parts of **20**. These spatial correlations, in particular those between CH_3-3‴ and both, H-7 and H-7′, indicated that a *P*-configuration at the southeastern biaryl axis would entail a *P*-configuration at the biaryl linkage in the northwestern unit, leading to the 1*R*,3*S*,5*P*,1″*R*,2″*S*,8″*P*,1‴*R*,3‴*R*-configured scaffold **21-A**, while a 5*M*-configured biaryl axis would give an overall 1*S*,3*R*,5*M*,1″*S*,2″*R*,8″*M*,1‴*S*,3‴*S*-configuration, i.e., the enantiomer (*ent*-**21-A**) (Figure 37).
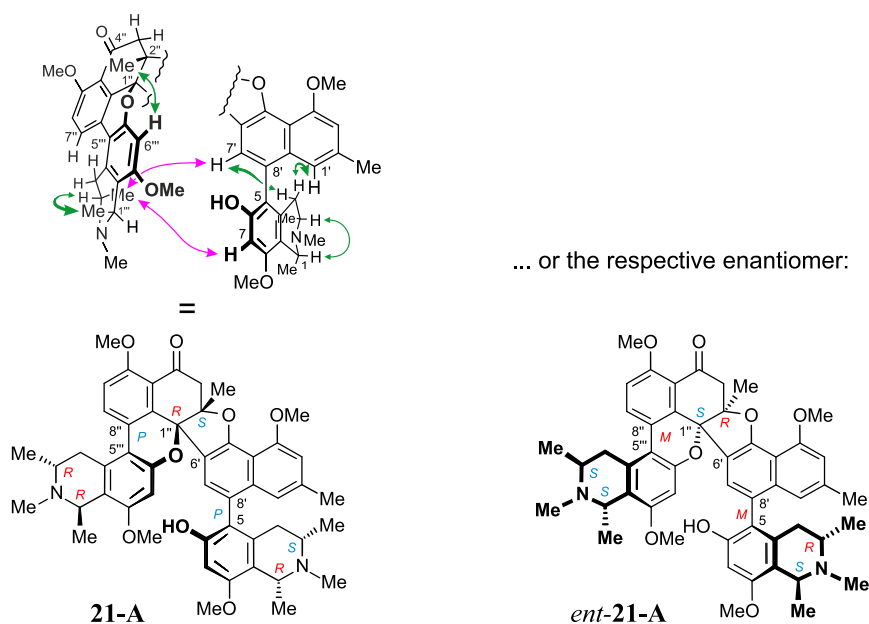
Figure 37. ROESY interactions indicating the relative configuration of the second *O*-bridged dimeric NIQ (i.e., cyclombandakamine A₂, **21**), and the two corresponding possible absolute stereostructures, **21-A** or *ent*-**21-A**.

The ruthenium-mediated oxidative degradation provided a ca. 1:1 ratio of *R*- and *S*-configured *N*-methyl-3-aminobutyric acid, thus indicating opposite configurations at C-3 and C-3‴. This confirmed the above stereochemical assignment, but it left open the (more tricky)

question of whether the molecule was 3*S*,3'''*R*-configured (= **21-A**) or 3*R*,3'''*S* (= *ent*-**21-A**). Particularly noteworthy, this was the very first time in the field of NIQ dimers that the oxidative degradation, although unambiguously showing that one molecular half had 3*S* and one had 3*R*, failed to tell which configuration was in which half. In all other cases there had been clarity about the location either because one was dealing with monomers, which of course only contain one "C-3", or in dimers for which the two stereogenic centers were identically configured, or in heterochiral dimers, where constitutional differences (*N*-H or *N*-Me) gave clarity, while here, in **21**, both halves gave rise to *N*-methyl-3-aminobutyric acid, so that other, addtional methods had to be applied.

Comparison of the ECD spectrum of the second *O*-bridged dimeric NIQ with the one of cyclombandakamine A$_1$ (**20**) revealed a close similarity (Scheme 5), thus excluding the presence of the stereostructure *ent*-**21-A**, which, in view of its 1''*S*,2''*R*,8''*M*-configuration in the tetralone unit that is opposite to the one in **20** (1''*R*,2''*S*,8''*P*), would have been expected to exhibit a virtually mirror-image ECD curve, as evidenced above in the case of **20**. The ECD similarity therefore firmly established the new alkaloid to possess the absolute stereostructure **21-A**, i.e., with 1*R*,3*S*,5*P*,1''*R*,2''*S*,8''*P*,1'''*R*,3'''*R*-configuration. The new *O*-bridged compound was henceforth named cyclombandakamine A$_2$.
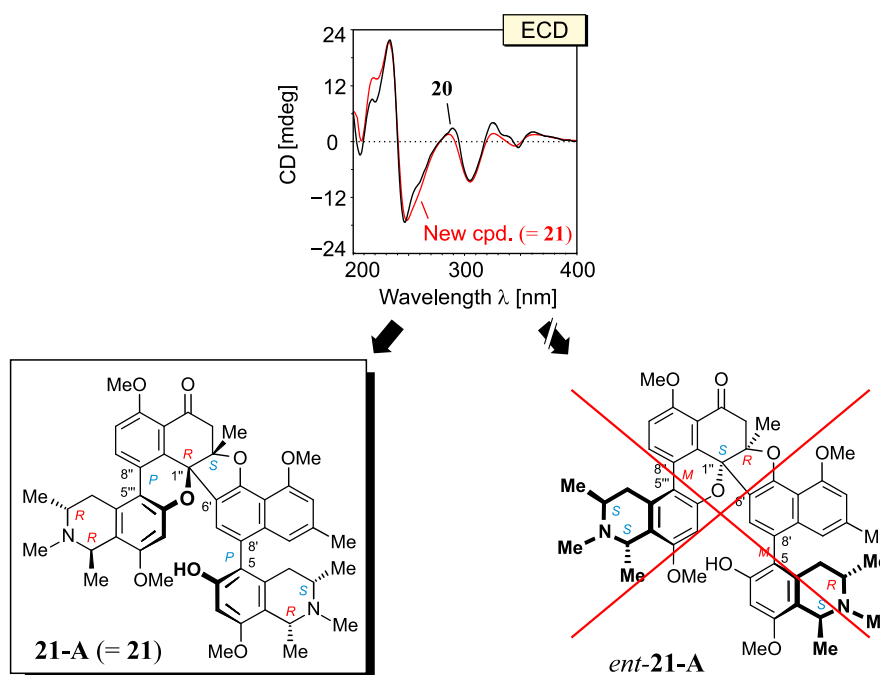
Scheme 5. Comparison of the ECD spectrum of the new alkaloid, cyclombandakamine A$_2$ (**21**), with the one of cyclombandakamine A$_1$ (**20**), evidencing cyclombandakamine A$_2$ to have the absolute stereostructure **21-A**, i.e., with 1*R*,3*S*,5*P*,1''*R*,2''*S*,8''*P*,1'''*R*,3'''*R*-configuration.

The fruitful interplay of chromatographic (HPLC), spectroscopic (UV, MS, NMR), chemical (the ruthenium-mediated oxidative degradation with GC-MSD analysis), and chiroptical (ECD) methods, combined with quantum-chemical ECD calculations, hence permitted detection, directed isolation, and full stereochemical elucidation of the very first oxygen-bridged dimeric naphthylisoquinoline alkaloids, cyclombandakamines A_1 (**20**) and A_2 (**21**). Besides their novel-type scaffolds, with the highest number of stereogenic elements ever found in the field of NIQs (viz., six centers and two biaryl axes), and their intriguing biosynthetic origin, as described later (see Section 3.5), these two compounds were also pharmacologically interesting. They showed strong antiprotozoal activities (see Section 3.10). Moreover, the hints at the occurrence of such dimeric NIQs in the Congolese liana *A. ealaensis* as above-presented were subsequently corroborated by the isolation of a series of seven further cyclombandakamines by Dr. D. T. Tshitenge,[148] thus enlarging this subclass of dimeric alkaloids, and showing that their – long-overlooked – occurrence is not a single event and that, hence, a true new subclass of NIQs was discovered in this work.

3.4. Spirombandakamines A_1 (22) and A_2 (23): the First Spiro-Fused NIQ Dimers

3.4.1. *Discovery of Spirombandakamine A_1 (22)*

The isolation of mbandakamines A (**16a**) and B (**16a**), with their unprecedented, most sterically crowded 6′,1″-axis, making them the first highly unsymmetrically coupled dimeric NIQs, already indicated that *Ancistrocladus* liana from the vicinity of the town Mbandaka to be phytochemically most remarkable. With the identification of the very first *O*-bridged dimeric NIQs, cyclombandakamines A_1 (**20**) and A_2 (**21**), displaying unusual annulated scaffolds possessing eight stereogenic elements, this Congolese *Ancistrocladus* species had now gained further phytochemical importance by being a rich source of structurally intriguing compounds. These findings warranted the search for further novel NIQ dimers in the leaf extract from that plant, leading this time to the discovery of yet another structurally most complex subclass, the spiro-fused dimeric NIQs, as described below.

By HPLC-MS, another fraction was found to contain a compound showing a monoprotonated ion that possessed the same mass (*m/z* 811.3, [M+H]$^+$) as cyclombandakamine A_2 (**21**), making it a potential diastereomer of **21**. Its online UV spectrum, however, was different compared to that of **21**, with most significant divergences in

the region from 280 to 380 nm (Figure 38a), where the compound did not show an hypsochromic shift as in **21**, but rather a slight bathochromic one, reminiscent of a dimeric NIQ with a dihydroisoquinoline unit).[62,75-78,80] Likewise notably divergent were the ECD curves of the two alkaloids, as recorded in an online stop-flow mode on HPLC-ECD (Figure 38b). All these features suggested that the structures of the two metabolites were substantially different.
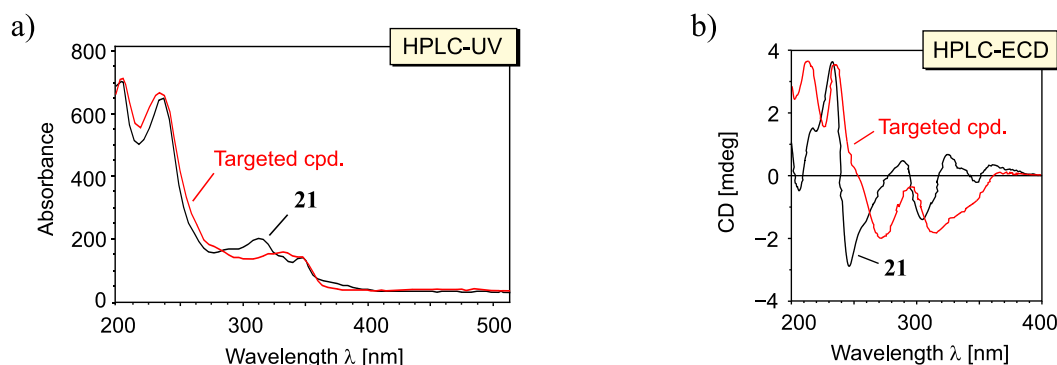
Figure 38. Comparison of: a) the online UV curve of the targeted compound (i.e., spirombandakamine A$_1$, **22**) with that of cyclombandakamine A$_2$ (**21**); and b) their respective online ECD spectra.

Resolution by preparative HPLC provided the compound as an optically active colorless powder. Its molecular formula C$_{50}$H$_{55}$N$_2$O$_8$, as deduced from HRESIMS (*m/z* at 811.3973, [M+H]$^+$), was indeed the same as that of **21**. Most surprisingly, its ^{1}H and ^{13}C NMR spectra were also very similar to those of **21** (signals for seven aromatic protons, three methylene groups with diastereotopic protons, two *N*-methyl groups, four methoxy groups, six methyl groups, and a carbonyl carbon) – as if it was a diastereomer of **21**, in contrast to the aforementioned hints from the UV and ECD data. These puzzling features made the structural elucidation of the compound a most tricky, but also highly rewarding task.

3.4.2. *Structural Elucidation of Spirombandakamine A$_1$ (22)*

1D and 2D NMR measurements revealed the first, southeastern part of **22**, denoted as **22**-**I** (Figure 39), to be an *N*-methylated 5,8′-coupled naphthylisoquinoline, with C-6′ (δ$_C$ 126.3) being the coupling position to the other half, **22**-**II**, as in **21**. Key interactions indicative of the coupling site within **22**-**I** included HMBC correlations from H-7′ (6.46 ppm, s), H-7 (6.55 ppm, s), and H$_{ax}$-4 (2.32 ppm, dd, *J* = 17.3, 11.4 Hz) to C-5 (119.4 ppm), ROESY correlations

of H-7′ with H$_{ax}$-4 and of H$_{eq}$-4 (1.88 ppm, dd, J = 17.3, 2.9 Hz) with H-1′ (6.53 ppm, s), and HMBC interactions from H-7′ to a quaternary carbon atom (58.7 ppm) belonging to the other molecular portion of **22**, **22-II** (see the green-highlighted interaction, Figure 39b). The location of a methoxy group at C-8 (157.5 ppm) was evidenced by HMBC interactions from H-7 and OCH$_3$-8 (3.87 ppm, s) to C-8, together with a ROESY effect between OCH$_3$-8 and both, CH$_3$-1 (1.61 ppm, d, J = 6.6 Hz) and H-1 (4.58 ppm, q, J = 6.6 Hz). The other methoxy group of this moiety was at C-4′ (157.4 ppm), as deduced from the HMBC interaction of its protons (4.01 ppm, s) and of H-3′ (6.70 ppm, s) to this carbon atom, in conjunction with the ROESY interactions between its protons and H-3′. The *N*-methyl group (2.96 ppm, s) exhibited HMBC correlations with both, C-1 and C-3 (60.5 ppm) (Figure 39).
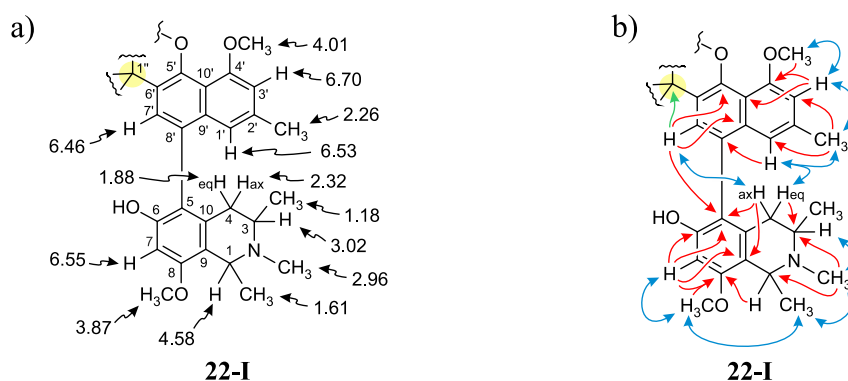
Figure 39. Key NMR data of the southeastern moiety (**22-I**) of the new dimer, spirombandakamine A$_1$ (**22**): a) ^{1}H chemical shifts in ppm; and b) selected ROESY (blue double arrows) and HMBC (red and green single arrows) interactions. The yellow part indicates the connection site in the other molecular portion, **22-II** (see also Figure 40).

The isoquinoline portion of the second, 'northwestern' part of **22**, **22-II** (Figure 40),[149] was constitutionally similar to the one of **21**, since it possessed a methoxy group (3.78 ppm, s) at C-8‴ (157.6 ppm), an *N*-methyl group (2.10 ppm, s), and C-5‴ (123.4 ppm) as the connecting point to the northern naphthalene-derived portion. In ROESY experiments, the *N*-methyl group of this isoquinoline moiety was found to interact with both, the isoquinoline and the naphthalene portions of the first half, via H-7 and H-7′, as in **21**. But, in contrast to **21**, this *N*-methyl showed an additional, most unusual interaction with H-1′, hinting at the presence of an unprecedented structure. An AB spin system [H-7″ (7.86 ppm, d, J = 8.7 Hz), H-6″ (7.23 ppm, d, J = 8.7 Hz)], together with an HMBC correlation of H-7″ to C-5‴, indicated that the second half (**22-II**) was 5‴,8″-coupled, like in the first half, **22-I**. HMBC interactions of H-7″ and of a methoxy group (4.03 ppm, s) jointly to C-5″ (158.4 ppm), in conjunction with a

ROESY interaction of this *O*-methyl group with H-6″, established it to be linked to C-5″. The aforementioned carbonyl group thus had to be C-4″ (203.2 ppm). Adjacent to it, at C-3″ (52.4 ppm), there was a methylene group with diastereotopic protons, as indicated by their typical[124,143] chemical shifts [H$_a$ (2.66 ppm, d, *J* = 19.5 Hz) and H$_b$ (3.49 ppm, d, *J* = 19.5 Hz)] and by joint HMBC correlations from H-6″ and both, H$_a$-3″ and H$_b$-3″ to C-10″ (125.7 ppm). A weak, four-bond HMBC interaction from CH$_3$-2″ (1.94 ppm, s) to C-3″, together with an unusually high chemical shift of C-9″ (157.8 ppm) and an HMBC interaction from H$_a$-3″ to C-9″, indicated the presence of a cyclopentenone ring. HMBC interactions of CH$_3$-2″ and both, H$_a$-3″ and H$_b$-3″, to a carbon atom at 58.7 ppm (Figure 40), together with the aforementioned HMBC from H-7′ to the same carbon (see Figure 39), showed this atom to be C-1″ and, at the same time, evidenced a 6′,1″-coupling of the two molecular halves of **22**. This connection was further supported by an HMBC correlation from H$_a$-3 to C-6′, as also shown and highlighted in green in Figure 40. The chemical shift of C-2″ (125.6 ppm) suggested it to be doubly oxygenated, evidencing the presence of an acetal function. This shift, together with ^4J HMBC from CH$_3$-2″ to both, C-5′ (154.4 ppm) and C-6‴ (154.3 ppm) and a ROESY interaction between CH$_3$-2″ and H-7‴, indicated C-2″ to be linked to the oxygen at C-5′ and the one at C-6‴, thus revealing the presence of an unprecedented spiroacetal-fused molecular skeleton. The compound was therefore named spirombandakamine A$_1$.
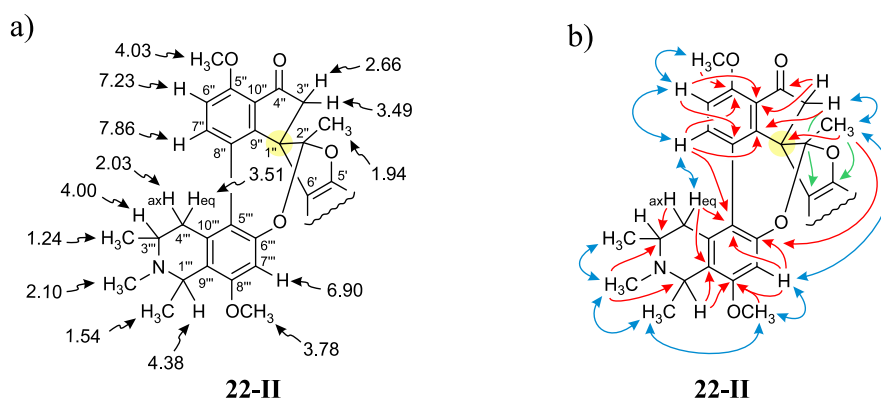
Figure 40. NMR data indicating the constitution of the molecular moiety **22-II**: a) ^{1}H chemical shifts in ppm; and b) decisive HMBC (single arrows) and ROESY (double arrows) interactions, including the key HMBC correlations between the two molecular subunits **22-I** and **22-II** (in green), which prove their *C,C*- and *C,O*-connections.

With the constitution of spirombandakamine A$_1$ hence established, it remained the task to determine the configurations at the eight elements of chirality present in the molecule.

H-3 (3.02 ppm, m) exhibited a ROESY correlation with H-1, while H_{eq}-4 revealed a cross-peak with H-1′, and H_{ax}-4 with H-7′ (Figure 41). These relationships, showing a *cis*-configuration of C-1 *versus* C-3 (60.5 ppm), indicated that the southeastern moiety (**22-I**) was either 1*S*,3*R*,5*M*- or 1*R*,3*S*,5*P*-configured.
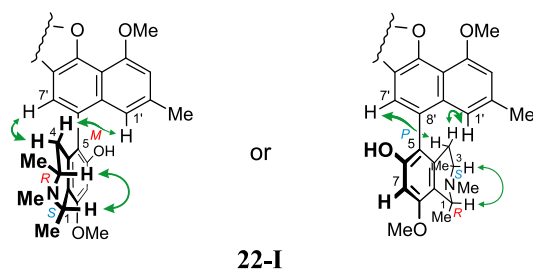
Figure 41. The two possible stereo-arrays of the southeastern half **22-I**, as evidenced by ROESY interactions (double arrows).

In the other, northwestern part of **22** (**22-II**), the relative configuration at the stereocenters C-1‴ (58.6 ppm) and C-3‴ (50.6 ppm) was determined to be *trans* by a ROESY interaction of CH$_3$-1‴ (1.54 ppm, d, *J* = 6.8 Hz) with the axial H-3‴ (4.00 ppm, m) (Figure 42). This correlation, in conjunction with the one between H_{eq}-4‴ (3.51 ppm, dd, *J* = 18.3, 4.9 Hz) and H-7″, revealed the configurations at the outer stereogenic elements of **22-II** to be either 1‴*S*,3‴*S*,5‴*M* or 1‴*R*,3‴*R*,5‴*P*.
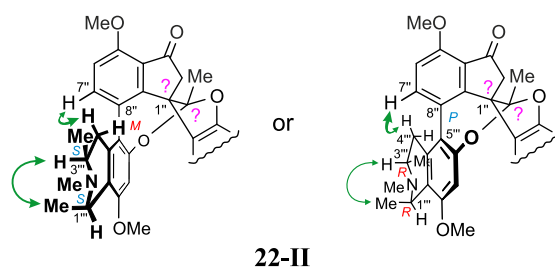
Figure 42. The two possible partial stereo-arrays of the northwestern half **22-II**, as evidenced by ROESY interactions at the outer stereogenic elements (i.e., the centers in the isoquinoline portion and the biaryl axis).

Considering the two stereocenters in the spiro-fused core of the molecule (i.e., at C-1″ and C-2″), up to four configurational combinations were imaginable, namely 1″*R*,2″*R*-, 1″*R*,2″*S*-, 1″*S*,2″*S*-, or 1″*S*,2″*R*-arrangements. These combinations, together with the above determined two possible partial configurations at the other stereogenic elements of **22-II** (i.e.,

1‴*S*,3‴*S*,5‴*M* or1‴*R*,3‴*R*,5‴*P*), led to a total of eight stereo-arrays conceivable for **22-II** (Figure 43a-b). Among these, four would thermodynamically be impossible or very unstable (Figure 43a), since being extremely strained. The number of possible absolute configurations of the northwestern portion was thus reduced from a total of 32 (as would have been expected for five independent stereogenic elements) to only four, shown in Figure 43b.
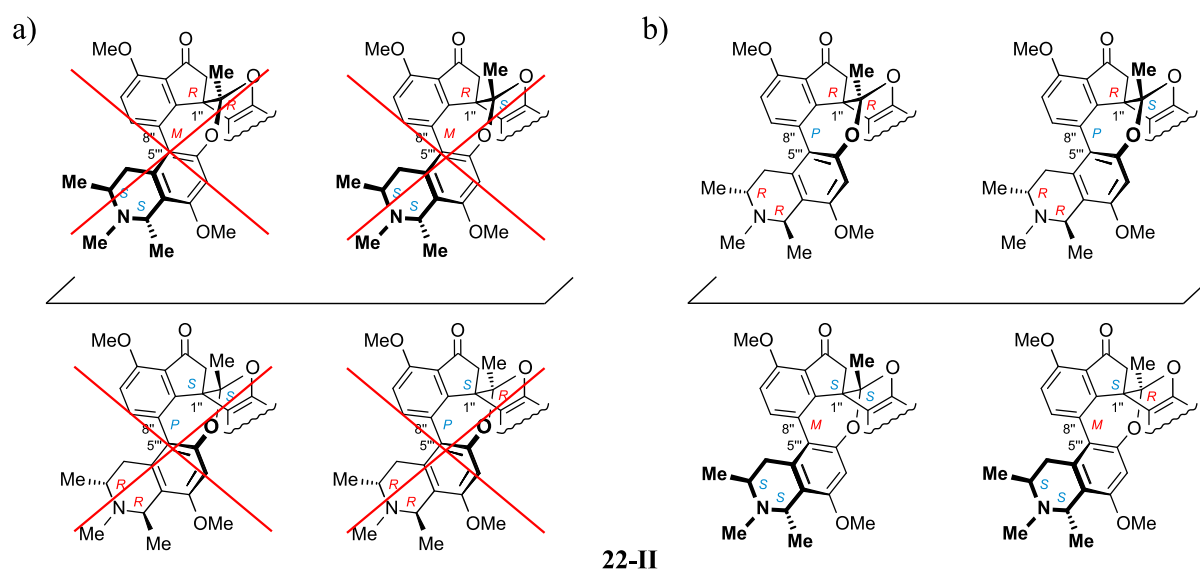
Figure 43. The eight stereo-arrays of the northwestern half **22-II** still imaginable at this point of the investigation: a) the four extremely strained and, thus, expectedly impossible stereo-arrays (as indicated by the red crosses); and b) the four possible ones.

ROESY interactions between CH$_3$-2″ and H-7‴ (Figure 44) revealed the five- and seven-membered oxygen-containing rings to be *cis*-fused, hence indicating the northern portion to be either 1″*R*,2″*S*- or 1″*S*,2″*R*-configured. In the case of a *trans*-array, i.e., for a 1″*R*,2″*R*- or a 1″*S*,2″*S*-configuration, CH$_3$-2″ and H-7‴ would be pointing in opposite directions (either 'down and up' or 'up and down', relative to the acetal carbon atom), making them too far away to each other so that a ROE interaction between them would not be expected to be observed. This further reduced the number of possible stereo-arrays of **22-II** to now just two.
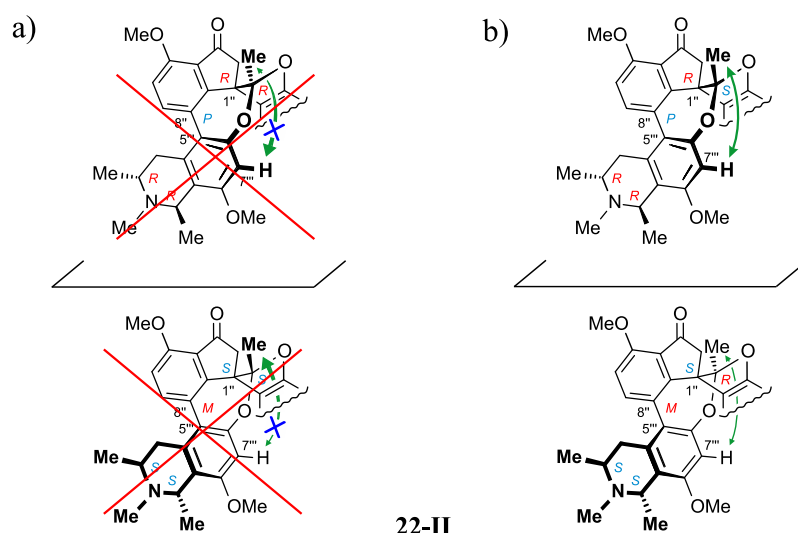
Figure 44. An observed ROESY interaction between Me-2″ and H-7‴ (green arrow) discriminating the only four possible absolute configurations of the northwestern half **22-II**: a) the two *trans*-fused stereoisomers, in which such an ROE should not be observed (as shown by a small blue cross), thus being excluded as indicated by the red crosses; and b) the two *cis*-fused scaffolds, in which that ROE should be expected to be detected.

With now two possible absolute stereo-arrays remaining for each of the molecular halves of **22**, namely 1*R*,3*S*,5*P* (referred to as **Ia**, Figure 45) or 1*S*,3*R*,5*M* (**Ib**) for the southeastern portion **22-I**, and 1″*R*,2″*S*,1‴*S*,3‴*S*,5‴*M* (**IIa**) or 1″*S*,2″*R*,1‴*R*,3‴*R*,5‴*P* (**IIb**) for the northwestern moiety **22-II**, there were up to four imaginable combinations to give the entire spirombandakamine A₁, constituting two pairs of diastereomers and their respective enantiomers: **Ia-IIa** and **Ib-IIb**, as well as **Ia-IIb** and **Ib-IIa**.
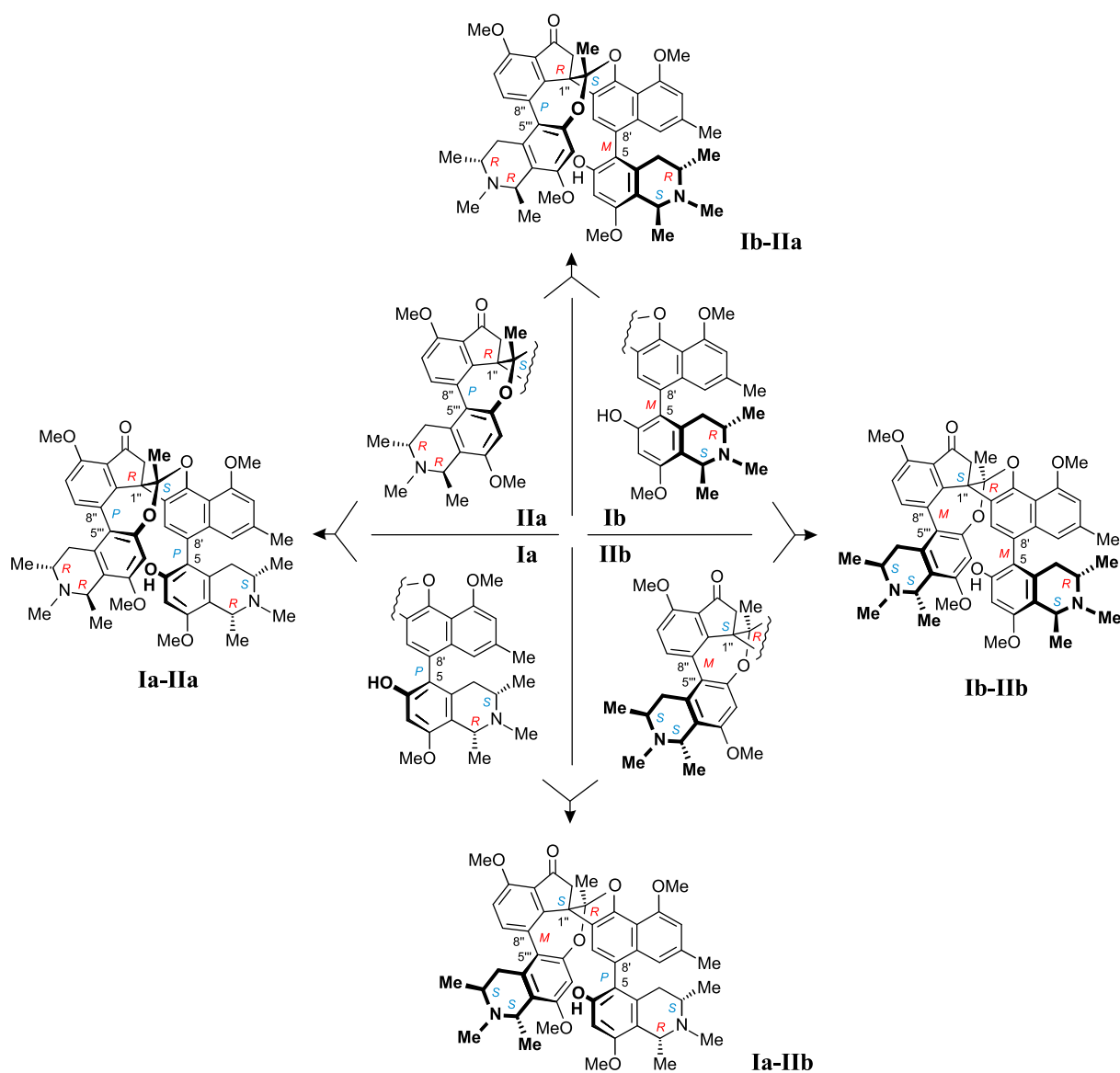
Figure 45. Combination of the possible molecular halves of spirombandakamine A₁ (**Ia**, **Ib**, **IIa**, and **IIb**), leading to four plausible full absolute stereostructures (viz., **Ia-IIa**, **Ib-IIa**, **Ib-IIb**, or **Ia-IIb**).

Again the discrimination between the two enantiomeric pairs came from ROE analysis. Indeed, spatial interactions between the *N*-methyl group of the northwestern half (**22-II**) and both, H-7 and H-7′, and also between H_{ax}-4‴ and H-7′ (Figure 46, magenta arrows) were detected, which indicated that a *P*-configuration at the eastern biaryl axis would necessitate a *P*-configuration at the northwestern biaryl axis, thus leading to the overall 1*R*,3*S*,5*P*,1‴*R*,3‴*R*,5‴*P*-configuration, i.e., the scaffold **Ia-IIa**. An *M*-configured eastern axis would, in turn, lead to a 1*S*,3*R*,5*M*,1‴*S*,3‴*S*,5‴*M*-configuration, i.e., to **Ib-IIb**, the enantiomer of **Ia-IIa**. In the case of the other enantiomeric pair (i.e., **Ia-IIb** and **Ib-IIa**), their unlike *P*- and *M*-axial configurations would keep the aforementioned *N*-methyl group and H-7

far away from each other, so that any ROE correlations between them should not be observed (Figure 46). Thus, spirombandakamine A_1 had to possess either the absolute stereostructure **Ia-IIa** – or of course its enantiomer **Ib-IIb** (not shown, all fully mirror-imaged).
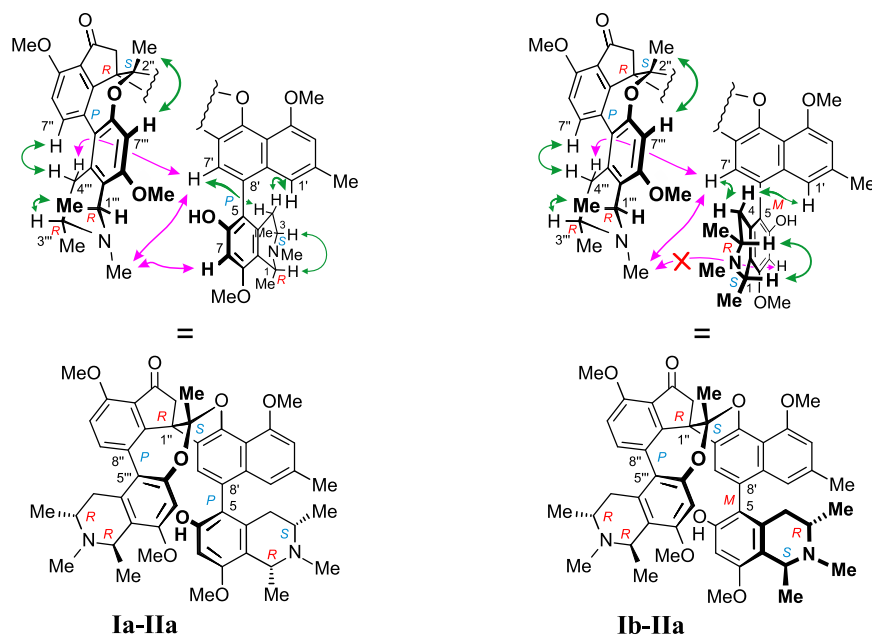
Figure 46. Key ROESY interactions evidencing the overall relative configuration of spirombandakamine A_1, including the crucial correlations between the molecular moieties (magenta double arrows), which allowed discrimination between the two enantiomeric pairs – here exemplarily represented by the diastereomers **Ia-IIa** and **Ib-IIa**. The red cross illustrates that the spatial interaction in the respective stereoisomer should not be observed.

The relative configuration of spirombandakamine A_1 hence determined was supported by ruthenium-mediated oxidative degradation, which yielded both, *R*- and *S*-configured *N*-methyl-3-aminobutyric acid, thus proving opposite configurations at C-3 and C-3‴. Whether the molecule was 3*R*,3‴*S*- (leading to **Ia-IIa**) or 3*S*,3‴*R*-configured (giving **Ib-IIb**) could, however, not be figured out by these NMR and chemical methods. A similar case – that the oxidative degradation could not give clarity on the exact absolute configurations at the stereocenters in the isoquinoline units – had been encountered for the first time in the above-described cyclombandakamine A_2 (**21**), and had been overcome by comparing its ECD curve with the one of its structurally well-established analog cyclombandakamine A_1 (**20**). Here, however, in the case of spirombandakamine A_1, it was particularly tricky, as this metabolite was the first NIQ dimer with a highly original spiro-fused scaffold, so that its ECD spectrum could not be compared with any such curve of the previously known compounds. This,

combined with the failure of all crystallization attempts, made once more quantum-chemical ECD calculations the method of choice for the determination of the absolute stereostructure of spirombandakamine A_1.

Of the two remaining possible stereoisomers **Ia-IIa** and **Ib-IIb**, the latter was arbitrarily selected, then modeled and optimized with B3LYP-D3/def2-TZVP. For this scaffold, the ECD spectrum was calculated using ωB97XD3/def2-TZVP(-f) with the full TDDFT approach. The predicted ECD curve of its enantiomer (i.e., **Ia-IIa**) was obtained by reflecting the calculated spectrum of **Ib-IIb** with respect to the zero line. These computational studies were performed by Dr. Bruhn. As a result, the experimental ECD spectrum matched well with the one simulated for **Ia-IIa** (Scheme 6), while being virtually opposite to the one calculated for **Ib-IIb**. Thus, spirombandakamine A_1 had the full absolute stereostructure **Ia-IIa** (= **22**), i.e., with $1R,3S,5P,1''S,2''R,1'''R,3'''R,5'''P$ configuration.
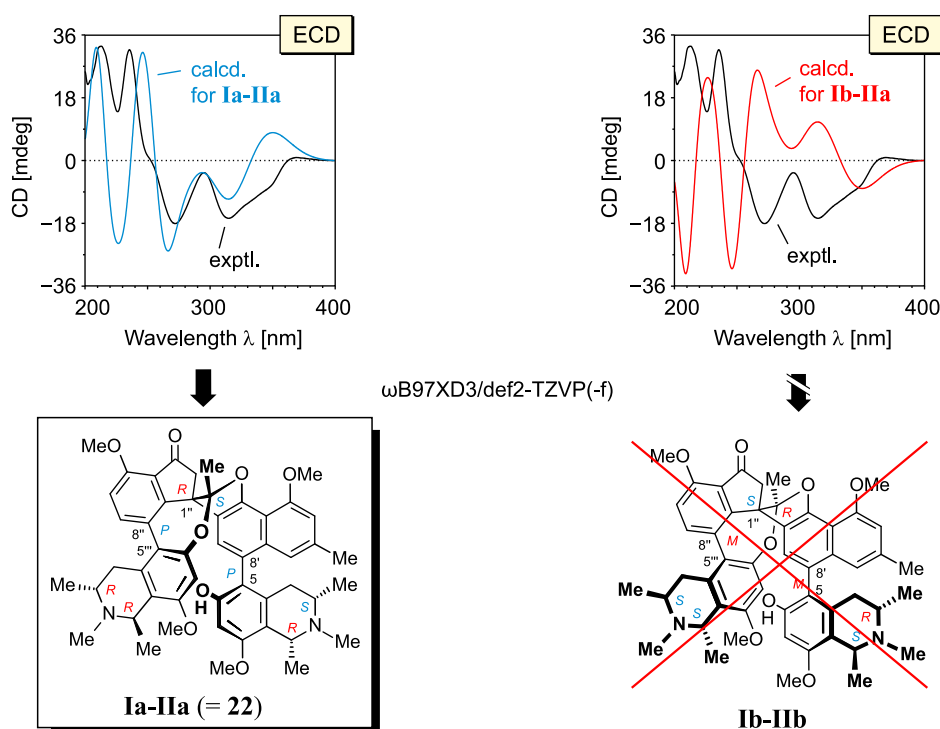
Scheme 6. Assignment of the absolute configuration of spirombandakamine A_1 (**22**), by comparison of its experimental ECD curve with the spectra calculated for both enantiomers, **Ia-IIa** (i.e., with $1R,3S,5P,1''R,2''S,1'''R,3'''R,5'''P$-configuration) and **Ib-IIb** ($1S,3R,5M,1''S,2''R,1'''S,3'''S,5'''M$), by using ωB97XD3/def2-TZVP(-f) with the full TDDFT approach.

3.4.3. Isolation and Structural Elucidation of Spirombandakamine A₂ (23)

The thrilling, unprecedented absolute stereostructure of spirombandakamine A₁ (**22**) raised great interest, triggering the search for further such compounds. Additional LC-UV-MS-assisted screening of the same plant extract led to the discovery of a very similar minor metabolite, isolated by reversed-phase preparative HPLC. It had the molecular formula $C_{49}H_{52}N_2O_8$, as deduced from HRESIMS (m/z = 797.3753 [M+H]⁺), hinting at an *O*- or *N*-demethylated analog of **22**. Its ¹H and ¹³C NMR spectra, closely related to those of **22**, suggested the missing methyl group to be the one linked to the nitrogen atom in the northwestern portion of **22** (**22-II**), which was confirmed by the 1D and 2D NMR data (Figure 47). Key evidence of this was provided by the upfield shifts of C-1‴ (48.3 ppm) and C-3‴ (45.6 ppm) compared to those in **22** (58.6 and 50.6 ppm, respectively). The new dimeric alkaloid was henceforth named spirombandakamine A₂.
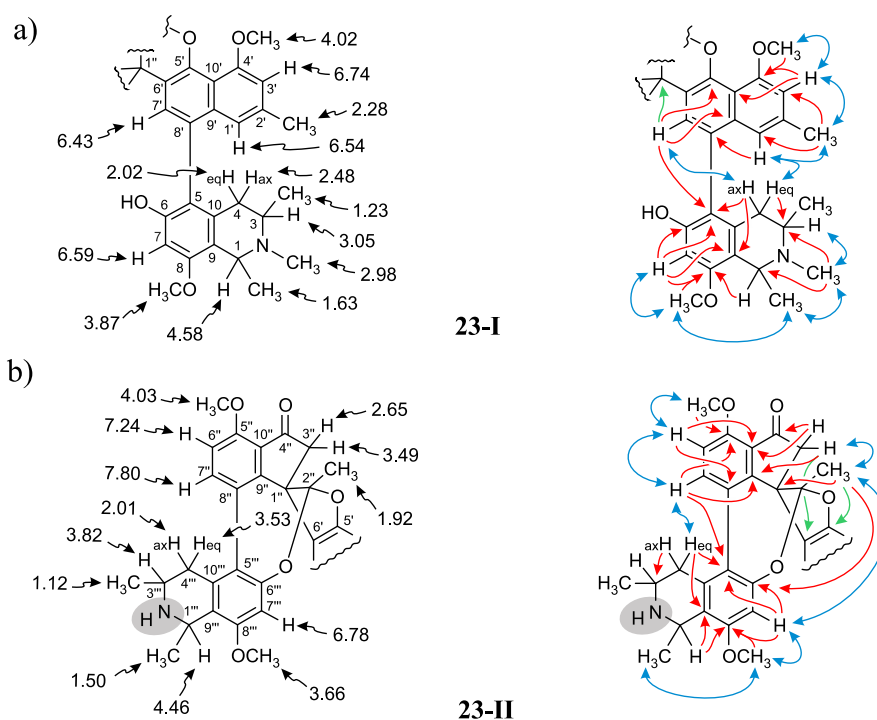
Figure 47. ¹H NMR chemical shifts (in ppm) and selected ROESY (blue double arrows) and HMBC (red double arrows) of spirombandakamine A₂ (**23**) evidencing the constitution in: a) its southeastern portion **23-I**; and b) its northwestern moiety **23-II**. The difference in the constitution of **23** as compared to that of spirombandakamine A₁ (**22**) is highlighted in gray.

The relative configurations at the stereocenters in the isoquinoline portions in spirombandakamine A₂ were the same as in **22**: *cis* in the southeastern portion and *trans* in the

northwestern part (Figure 48a). Its oxidative degradation provided both, (*R*)- and (*S*)-3-aminobutyric acid, thus, as for **22**, evidencing opposite configurations at C-3 and C-3‴. The concomitant formation of *N*-methyl-3-aminobutyric acid only as its *S* enantiomer, however, proved that the *S*-configured center was the one near to the *N*-methyl group (i.e., C-3), while C-3‴ was, thus, *R*-configured. This, together with the above-stated *cis*-configuration at C-3 *versus* C-1 and the *trans*-array at C-3‴ relative to C-1‴, indicated that both, C-1 and C-1‴ were *R*-configured. Consequently, for spirombandakamine A$_2$ (and in contrast to **22**) an unambiguous assignment of the full absolute configurations including all stereocenters in the isoquinoline portions was possible even without quantum-chemical ECD calculations. At the axes and at the stereocenters C-1″ and C-2″, the ROESY interactions were all similar to those in **22**, which, as described in the case of **22** (see above) and as also illustrated in Figure 48a, demonstrated that both axes of spirombandakamine A$_2$ were *P*-configured, and C-1″ and C-2″ were *R*- and *S*-configured, respectively, given the absolute *S* configuration at C-3 and *R* at C-3‴ as established by the oxidative degradation. Therefore, spirombandakamine A$_2$ was unambiguously assigned to be 1*R*,3*S*,5*P*,1″*S*,2″*R*,1‴*R*,3‴*R*,5‴*P*-configured, like **22**, and had the absolute stereostructure **23** shown in Figure 48b.
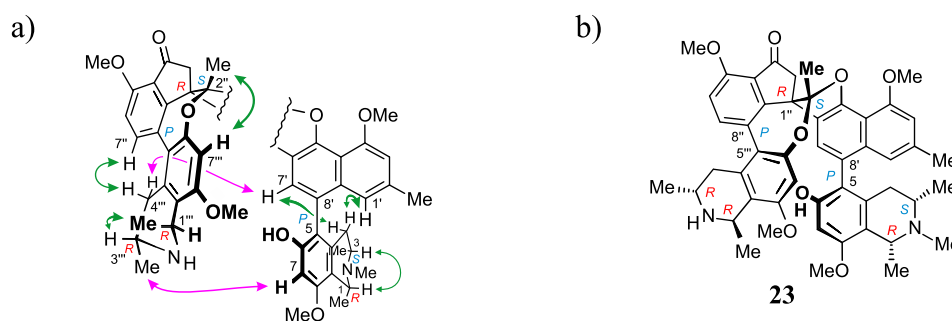
Figure 48. a) ROESY correlations within each of the two molecular moieties **23-I** and **23-II** (green double arrows), and between them (magenta double arrows), evidencing the relative and, thus (given the results of the oxidative degradation), absolute configurations of spirombandakamine A$_2$; and b) the absolute stereostructure of spirombandakamine A$_2$ (**23**).

In accordance with the close structural similarities of spirombandakamines A$_1$ (**22**) and A$_2$ (**23**), their ECD spectra were nearly identical (Figure 49), thus providing further independent confirmation of the absolute stereostructure of **22** as determined by computational investigations.
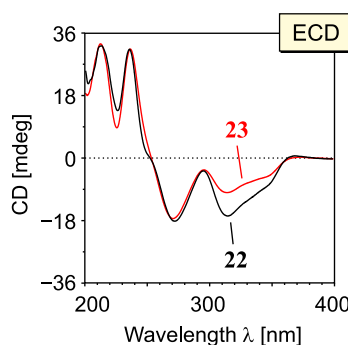
Figure 49. Comparison of the ECD spectra of spirombandakamines A$_1$ (**22**) and A$_2$ (**23**).

Spirombandakamines A$_1$ (**22**) and A$_2$ (**23**) hence structurally fully elucidated were remarkable in many respects. They were the first naphthylisoquinoline alkaloids (including dimers and monomers) possessing a five-membered isocyclic ring. Moreover, the fusion of this uncommon cycle with two, likewise unusual, acetal-fused five- and seven-membered oxygen heterocycles created a unique structural core, which had not been found in any other natural or synthetic compound. In addition, with two chiral biaryl axes and six stereocenters, they had overall eight stereogenic elements – the highest total number for NIQs, so far displayed only by the likewise novel scaffold of the cyclombandakamines (see Section 3.2). Their exceptional biosynthetic formation is discussed in the following Section, along with the pathways of the cyclombandakamines.

3.5. Possible Biosynthetic Pathways to "Open-Chain" Mbandakamines, Cyclo- and Spirombandakamines

Dimeric NIQs most evidently arise from phenol-oxidative *C,C*-coupling of two identical or different monomeric NIQs, which, in turn, are formed from two molecular subunits, the naphthalene part and the isoquinoline moiety. These portions are built up separately from common polyketidic precursors, and then joined together regio- and stereoselectively, following the same principle of a – now mixed – phenol-oxidative coupling.[44,45,126]

This biosynthetic pathway was formulated in more detail and substantiated by biomimetic cyclization reactions[150-152] – and was finally firmly proven for dioncophylline A (**10**) by feeding experiments with $^{13}C_2$-labeled acetate (Scheme 7) during the past decade.[48,49,153,154] Accordingly, both molecular portions, **32** and **33**, originate from six acetate-malonate units each, via an identical hexaketide chain **30**, and a joint monocyclic diketone **31**, which then divergently undergoes yet another aldol condensation to give the naphthalene **32** or, with

reductive nitrogen incorporation, the dihydroisoquinoline **33**. The two building blocks, **32** and **33**, are then convergently cross-coupled to deliver a complete naphthyldihydroisoquinoline alkaloid, which, after *trans*-selective 1,2-dihydrogenation and twofold *O*-methylation, gives, e.g., dioncophylline A (**10**) and related monomers like **34** – or dimers such as the C_2-symmetric compound jozimine A_2 (**15**), as plausibilized by biomimetic chemical reactions.[79]
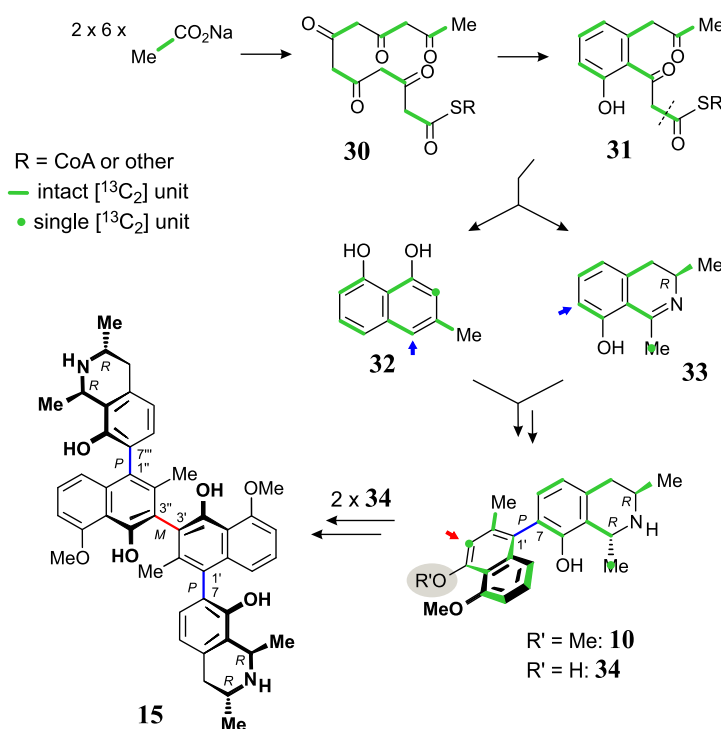
Scheme 7. Acetate-malonate pathway to mono- and dimeric NIQs: evidences of the polyketidic nature of dioncophylline A (**10**) deduced from the pairwise $^{13}C,^{13}C$ correlations after feeding sodium $[^{13}C_2]$-acetate to cell cultures of *Triphyophyllum peltatum* (Dioncophyllaceae).[48,49,154] The blue and red arrows exemplarily indicate the positions for the cross-linkage of **32** and **33** to yield **10** or **34** and for the homo-coupling of **34** to give jozimine A_2 (**15**), as succeeded biomimetically, by oxidative dimerization of (not ^{13}C-labeled) **34**.[79]

The biosynthetic origin of the novel, "open-chain" NIQ dimers mbandakamines A (**16a**) and B (**16b**) is very similar to the one described above for jozimine A_2 (**15**). As sketched in Scheme 8, the formation of **16a** and **16b** obviously proceeds via an enzymatically catalyzed phenol-oxidative cross-coupling of two constitutionally slightly divergent 5,8′-linked monomeric NIQs **28** and **29** through the drastically different 1′- and 6′-positions (indicated by red arrows). And the route to the compounds **28** and **29** is, without any doubt, the same as solidly established for dioncophylline A (**10**), involving an acetate-malonate initiated series of cyclization and condensation reactions leading to the building blocks **32** and now, with an

oxygen function at C-6, to **35**, which, after the respective follow-up reactions (i.a., phenol-oxidative *C,C*-coupling and regio-divergent *O*-methylation in the naphthalene portion), should give the full monomeric NIQ building blocks **28** and **29**, which would then be oxidatively coupled to give **16a** and **16b**. This biosynthetic pathway has most recently been supported by the already mentioned biomimetic total synthesis of **16a** from **28** and **29** (see Scheme 3).[139]
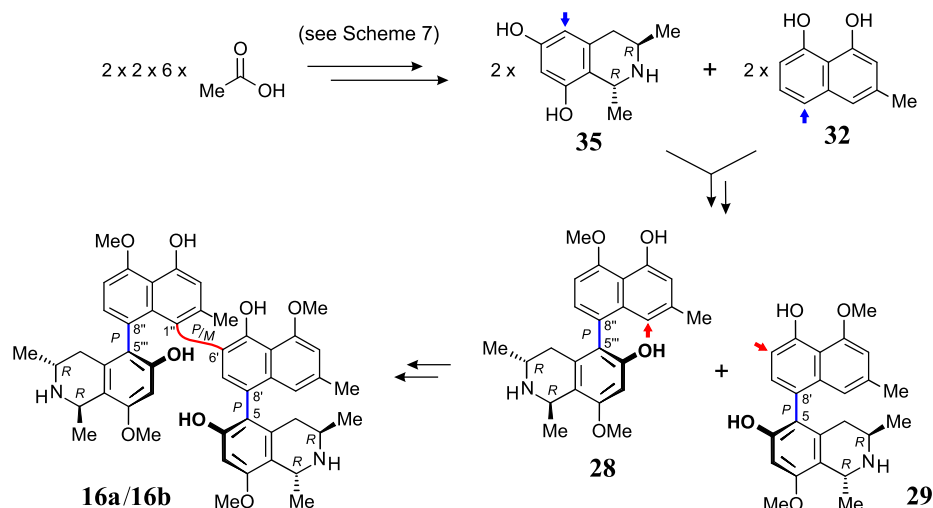
Scheme 8. Plausible biosynthetic origin of 'open-chain' dimeric NIQs, with a highly unsymmetric 6,1′-coupling, here sketched for mbandakamines A (**16a**) and B (**16b**). The short red and blue arrows exemplarily illustrate the coupling positions in the respective molecular entity.

The unprecedented bridged NIQ dimers, cyclo- and spirombandakamines, are apparently the products of an oxidation-induced cyclization of the 'open-chain' mbandakamine-type dimers. An early hypothesis for the biosynthesis of cyclombandakamines, such as cyclombandakamines A$_1$ (**20**) (Scheme 9),[124] suggested the direct biogenetic precursor of **20** to be an *N*-methylated derivative of **16a/b**, like compound **37**. This dimer should arise from three oxidative coupling steps, viz., those linking naphthalene portions and isoquinoline subunits to give the two monomers **29** and **36** (blue axes), differing only in their *O*- and *N*-methylation patterns, and one oxidative cross-coupling of **29** and **36** to yield the mbandakamine analog **37** (red axis). Compound **37** could then be further oxidized to give enone **39** through another phenol-oxidative activation via the double phenoxy radical **38**, now leading to an intramolecular C–O coupling (green C–O bond). In this step, a *P*-configuration at the northwestern axis would create the observed *R*-configuration at C-1″. Subsequent intramolecular Michael addition of the phenolic oxygen function at C-5′ (inducing the observed *cis*-array and hence the *S*-configuration at C-2″) would then give **20**. Thus,

cyclombandakamine A_1 (**20**) would arise from four consecutive oxidative coupling steps (forming the two bonds highlighted in blue, and then the red and green ones) – the highest total number for a naphthylisoquinoline alkaloid to date. In a similar manner, **21** might originate from a doubly *N*-methylated 3-*epi*-derivative of **16a/b**.
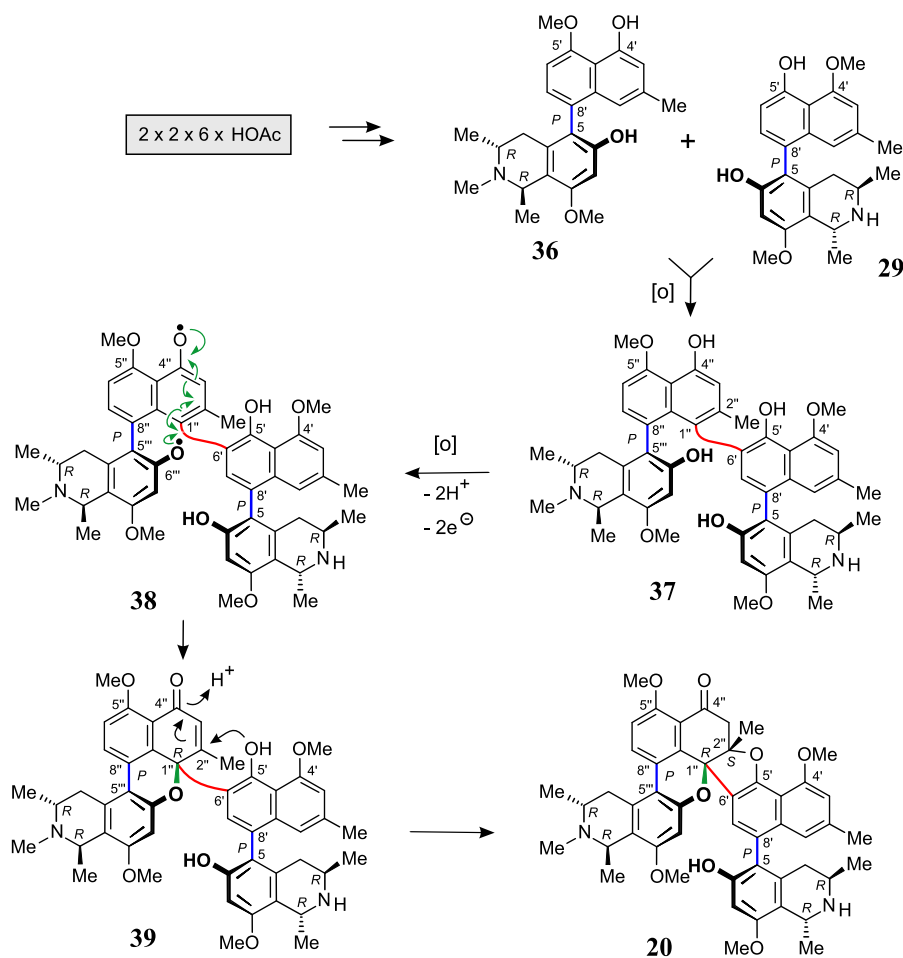
Scheme 9. Possible biosynthetic pathway to cyclombandakamines via phenoxy radicals – here exemplarily illustrated for cyclombandakamine A_1 (**20**).[124]

A short time after the isolation of the cyclombandakamines, the discovery of the polycyclic molecular architectures of spirombandakamines A_1 (**22**) and A_2 (**23**) suggested that cyclo- and spirombandakamines might also arise from joint epoxide precursors.[123] This hypothesis was stimulated by the fact that cyclombandakamine A_2 (**21**) and spirombandakamine A_1 (**22**), although being, at first sight, so different from each other, share a lot: They have the same southeastern half and similar northwestern isoquinoline portion, and the intact northern aryl ring is identical, too. According to this biosynthetic concept, as sketched in Scheme 10, **21** and **22** might both result from a doubly *N*-methylated 3-*epi*-derivative of **16a/b**, such as

compound **17**, by an epoxidation in the highly strained C-1″–C-2″ region, which, by the conversion of these two atoms from sp^2 to sp^3, should lead to a substantial decrease of steric hindrance. For stereoelectronic reasons, the configuration of the resulting epoxide **40** ("oxygen down", i.e., **40a**, or "up", **40b**) should be of importance for the further course of the reaction. The epoxide with the oxygen being "down", **40a**, should be cleaved through an attack by O-6‴, leading to **41** and subsequently to **21**, while **40b** (with the oxygen "up") would be opened by the C-2″–C-3″ electron pair to provide **42** and then **22**. In view of the high specificity of enzymes, it is also imaginable that the epoxidation of **17** by a monoxygenase takes place stereoselectively, possibly only from the bottom side, to give **40a**. In that case, the resulting intermediate **41** might, alternatively, also lead to **22**, with the correct configuration at C-1″, but then the rearrangement would not profit from the epoxide opening as a driving force, as in the direct reaction of **40b** to **42**.
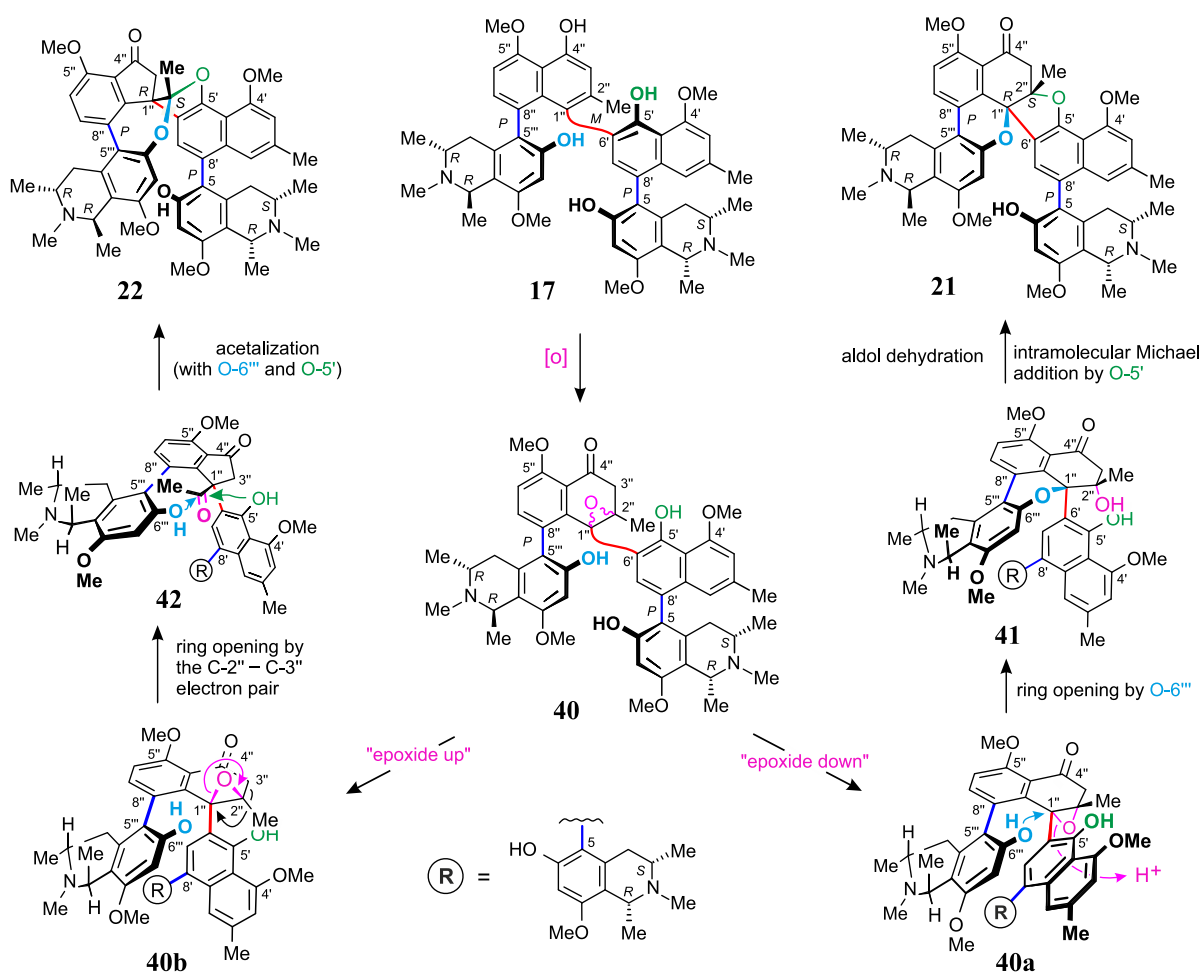
Scheme 10. Hypothetic biosynthetic origin of cyclo- and spirombandakamines by epoxidation of open-chain mbandakamines – here exemplarily shown for the formation of cyclombandakamine A$_2$ (**21**) and spirombandakamine A$_1$ (**22**), via the epoxides **40**.[123]

This plausible biosynthetic pathway to cyclo- and spirombandakamines, witnessing a thrilling follow-up chemistry (as never been observed in any other type of NIQ dimers!), is undoubtedly a consequence of the particular, U-turn-shaped and highly condensed structure of the open-chain mbandakamine-type quateraryls, in which three of the phenolic parts (the two naphthalene portions and the western isoquinoline unit) are tightly pressed against each other. The reaction would, thus, be driven by the decrease of steric strain at the critical C-1″ position, from sp^2 to sp^3. This high functional density would therefore facilitate the suggested cascade of reactions to give the bridged compounds, which would explain why such follow-up products were never found for the other, more 'linearly' coupled NIQ dimers.

3.6.   Search for Potential Direct Biogenic Precursors of Cyclo- and Spirombandakamines: Discovery of Mbandakamine B$_2$ (17)

The unprecedented absolute stereostructures of the cyclo- and spirombandakamines, together with their thrilling presumable biosynthetic formation as presented above, made the search for putative precursors – such as compound **17** (Scheme 10) – a rewarding task not only for their possible biomimetic semi-synthesis, but also for investigating the impact of the follow-up cyclization cascade reactions on the bioactivities of the mbandakamines.

HPLC-UV-MS-assisted investigations of the same plant extract hinted at the occurrence of a candidate precursor to both, cyclombandakamine A$_2$ (**21**) and spirombandakamine A$_1$ (**22**). On C$_{18}$-HPLC (operating in reversed-phase mode), it was strongly retained as compared to **21** and **22**, so that it eluted after a longer retention time. Its UV spectrum was typical of a mbandakamine-type dimer, and the *m/z* of its monoprotonated molecule (813.4) was two units more than the ones of **21** and **22**, which suggested the compound to be an open-chain mbandakamine. Directed preparative HPLC resolution provided a white amorphous powder, possessing a molecular formula of C$_{50}$H$_{57}$N$_2$O$_8$ (HRESIM, *m/z* 813.4106 [M+H]$^+$). Its proton NMR spectrum showed a full set of signals (eight aromatic protons, two methylene groups with diastereotopic protons, two *N*-methyl groups, four methoxy groups, and six methyl groups), indicative of an unsymmetrically coupled quateraryl. 1D and 2D NMR data confirmed the compound to be a new mbandakamine-type dimer, consisting of two 5,8′-coupled *N*-methylated NIQ portions (**17-I** and **17-II**) connected to each other via C-6′ and C-1″ (Figure 50).
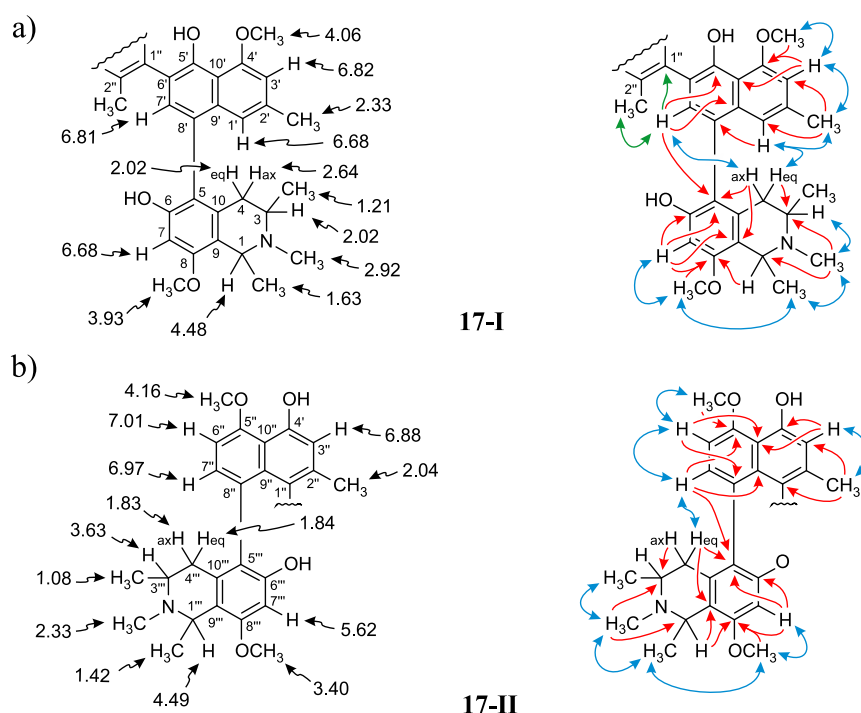
Figure 50. ¹H NMR chemical shifts (in ppm) and selected ROESY (blue double arrows) and HMBC (red arrows) interactions of the potential biosynthetic precursor to **21** or **22**, mbandakamine B₂ (**17**), evidencing the constitution in: a) its southeastern portion **17-I**; and b) its northwestern moiety **17-II**. The green-highlighted HMBC (single arrow) and ROESY (double arrow) interactions are those establishing the 6′,1″-connectivity between **17-I** and **17-II**.

In the southeastern moiety **17-I**, ROE interactions at the stereocenters and across the naphthalene-isoquinoline axis were the same as the ones observed for **22-I** (i.e., H-1 ↔ H-3, H$_{ax}$-4 ↔ H-7′, and H$_{eq}$-4 ↔ H-1′), which indicated that **17-I** was either 1*R*,3*S*,5*P*-configured, like **22-I**, or 1*S*,3*R*,5*M*. In the other molecular portion **17-II**, the ROESY correlations H-3‴ ↔ CH₃-1‴ and H$_{ax}$-4 ↔ H-7′ were identical to the ones detected for **22-II**, indicating **17-II** to be either 1‴*R*,3‴*R*,5‴*P*-configured, similar to **22-II**, or 1‴*S*,3‴*S*,5‴*M* (Figure 51). This, together with ROESY interactions between H-1‴ and H-7, and between the *N*-methyl group of the northwestern half **17-II** and H-7′, H-7, and OCH₃-8 in the southeastern moiety **17-I**, correlated an *M*-configuration at the western outer axis with a *P*-configured central axis and an *M*-configuration at the other outer, eastern axis, therefore leading to 1*S*,3*R*,5*M*,6′*P*,1‴*S*,3‴*S*,5‴*M* (Figure 51). In turn, an *M*-configured western axis would entail the opposite overall configuration, 1*R*,3*S*,5*P*,6′*M*,1‴*R*,3‴*R*,5‴*P*, i.e., this would be the enantiomer.
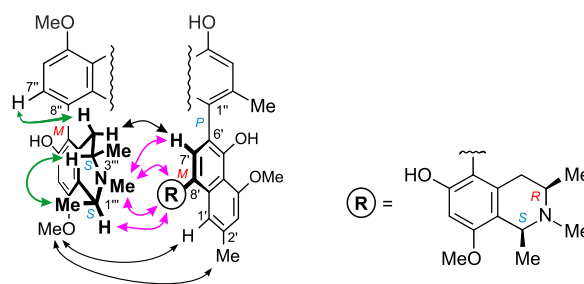
Figure 51. ROESY correlations of the potential precursor of **21** and **22**, mbandakamine B$_2$ (**17**) relevant for the relative configuration at its outer stereogenic elements (in green) and at its central biaryl axis (in magenta), and the ones further confirming its central 6′,1″-coupling (in black) – here exemplarily illustrated for the enantiomer 1*S*,3*R*,5*M*,6′*P*,1‴*S*,3‴*S*,5‴*M*.

Ruthenium-mediated oxidative degradation[155,156] yielded both, *R*- and *S*-configured *N*-methyl-3-aminobutyric acid, thus confirming opposite configurations at C-3 and C-3‴, but it left unanswered the question of whether the compound was 3*R*,3‴*S*-configured – or 3*S*,3‴*R*. Taking advantage of the fact that in the case of dimeric NIQs with three biaryl chiral axes, the spatial array at the binaphthalene chromophore gives the by far strongest contribution to the overall ECD spectrum (as explained above),[78,80,123,126] the absolute configuration at the central biaryl axis of the new dimeric alkaloid was determined by comparing its ECD curve with those of the constitutionally and stereochemically related compounds mbandakamines A (**16a**) and B (**16b**).[80] As shown in Scheme 12, the ECD spectrum of the isolated new metabolite was almost opposite to the one of mbandakamine A (**16a**), while being closely similar to that of mbandakamine B (**16b**). This indicated that the new compound was *M*-configured at the central binaphthalene linkage. And given the aforementioned correlation between an *M*-configuration at the central axis and *P*-configuration at both outer axes, the absolute axial configuration of the new dimeric NIQ was thus *P,M,P* (like in mbandakamine B), which was consistent with the overall 1*R*,3*S*,5*P*,6′*M*,1‴*R*,3‴*R*,5‴*P*-array. Therefore, the new compound was found to possess the full absolute stereostructure **17**, and was named mbandakamine B$_2$.[123]
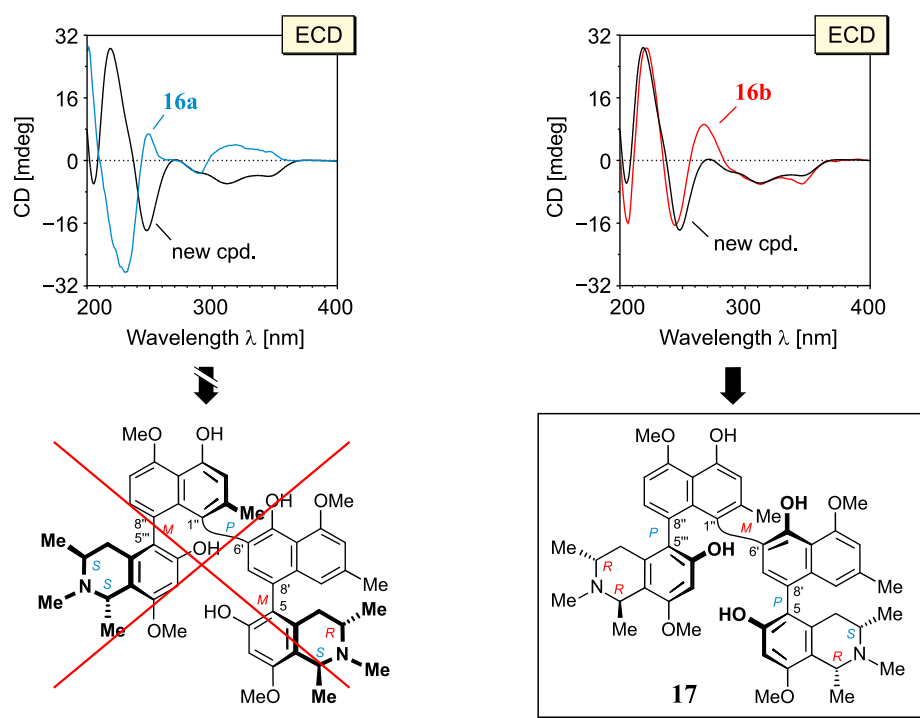
Scheme 12. Comparison of the ECD curve of the new compound, mbandakamine B$_2$ (**17**), with the related spectra of mbandakamines A (**16a**) and B (**16b**), evidencing the central axis of the new compound to be *M*-configured, leading to the overall absolute stereostructure **17**.

3.7. Atropisomerization of Mbandakamine B$_2$ (17) and Biomimetic Semi-Synthesis of Cyclombandakamine A$_2$ (21) and Spirombandakamine A$_1$ (22): Preliminary Investigations

With a few milligrams of mbandakamine B$_2$ (**17**) in hands, it was attractive to qualitatively check the aforementioned hypothetic origin of the cyclized dimeric compounds **21** and **22** from **17**. While planned chemical experiments towards this goal were as yet unexplored, it was unexpectedly found that treatment of **17** with aqueous acids generated cyclombandakamine A$_2$ (**21**) and spirombandakamine A$_1$ (**22**). These findings were in fact a consequence of the preliminary studies on the acid-catalyzed atropisomerization of **17**, as explained in the following paragraphs.

Mbandakamine B$_2$ (**17**) was always obtained with trace quantities of an unidentified NIQ alkaloid that was not baseline resolved (and, thus, was hardly removable), as visible in Figure 52a. Under "normal" conditions (viz., at ambient temperature and neutral pH), the quateraryl **17** was stable. When an acidified solution of this dimer in acetonitrile (TFA, pH: 2-4) was warmed up to 50°C for 10 h or was left at ambient temperature over several days, however, it was very slowly converted into another compound, referred to as **17F2** (Figure 52b), which was evidenced to be isomeric to **17** by HPLC-MS measurement.
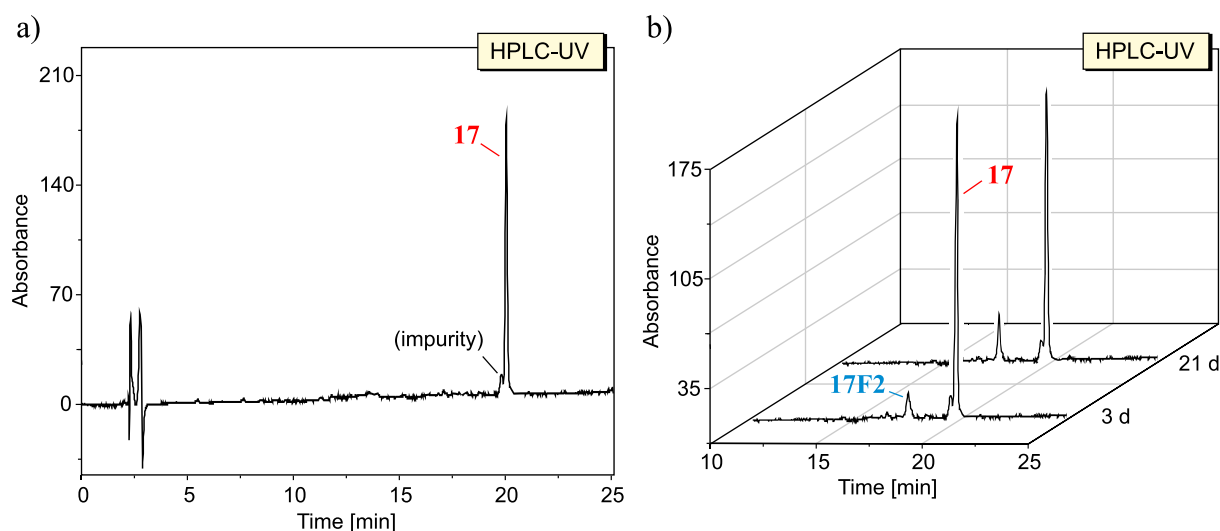
Figure 52. HPLC chromatograms of mbandakamine B$_2$ (**17**) in acidic acetonitrile (TFA, pH: 2-4): a) at t = 0 h; and b) after 21 days (kept at ambient temperature).

The online ECD curve of the generated isomer **17F2** was virtually opposite to the one of **17** (Figure 53a), which, given the already mentioned fact that ECD spectra of dimeric NIQs with three consecutive chiral biaryl axes are strongly dominated by the stereo-array at the binaphthalene chromophore,[78,80,123,126] and in view of the *M*-configuration at the central axis of **17**, indicated the binaphthalene linkage in **17F2** to be *P*-configured. This axial *P*-configuration was further corroborated by the observation that the online ECD and UV curves of **17F2** matched very well with those of mbandakamine A (**16a**) – likewise possessing a *P*-configuration at the binaphthalene linkage (Figure 53). The observed conversion was thus found to involve an atropisomerization of **17** at the central axis, i.e., at the most hindered one!
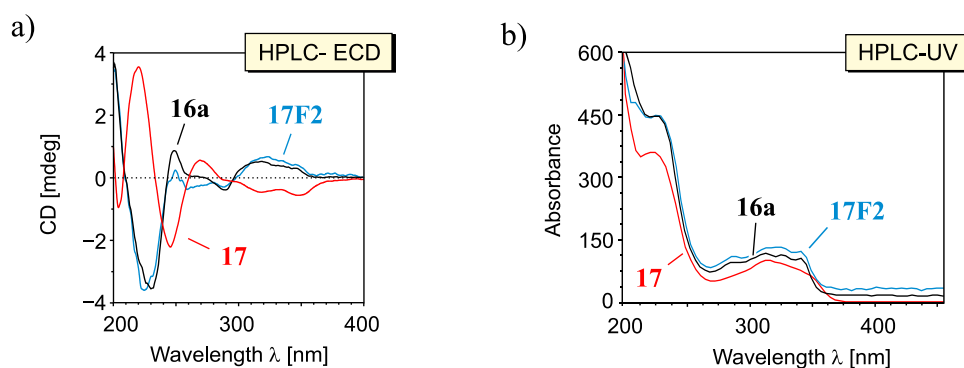
Figure 53. Comparison of: a) online ECD curves; and b) online UV spectra of **17F2** and mbandakamines B$_2$ (**17**, central axis: *M*) and A (**16a**, central axis: *P*), evidencing *P*-configuration at the central axis of **17F2**. Note that the intensities of the UV curves of **16a** and **17F2** were fitted to the ones of **17** for better comparability.

While the opposite configuration at the central axis could clearly be evidenced by ECD investigations, the question of whether the isomerization affected the outer axes or not could not be unanswered. Likewise unanswered remained the question regarding the reversibility of the conversion process. To address these issues, **17F2** was required in a pure form – or at least in a mixture in which **17F2** was the major component. This necessity, together with the small available quantity of **17** and the very slow atropisomerization of **17** warranted attempts to speed up the isomeric interconversion. For this reason, an acidic acetonitrile solution of mbandakamine B$_2$ (**17**) was heated to 60°C for two days, leading to a mixture, now exhibiting more peaks than the two expected ones (Figure 54). Of these, the peak that would correspond to **17F2** based on the retention time (ca. 17.7 min), i.e., Peak 1 (Figure 54), appeared to be only slightly increased one compared to the experiment presented above in Figure 52b. In addition, the UV curves within Peak 1 were not similar to each other: The spectrum at the right slope was the same as the one previously detected and shown in Figure 53b (closely related to the one of mbandakamine A, **16a**), but the curve at the left side was characteristic of cyclombandakamines. This suggested that Peak 1 contained **17F2** and another, cyclic dimeric compound (referred to as **17F3**), whose retention time and UV spectrum were both reminiscent of those of cyclombandakamine A$_2$ (**21**). Moreover, the UV curve and the retention time of the minor product eluting just before Peak 1, quoted as **17F4**, were indicative of the presence of spirombandakamine A$_1$ (**22**).

Resolution of the obtained mixture on a semi-preparative HPLC column provided sub-milligram quantities of these three compounds of interest (namely, **17F2**, **17F3**, and **17F4**). By co-elution and LC-MS measurements, **17F4** and **17F3** were corroborated to be spirombandakamine A$_1$ (**22**) and cyclombandakamine A$_2$ (**21**), respectively. Thus, the first biomimetic semi-synthesis of both spiro- and cyclombandakamines from open-chain mbandakamine was accomplished – as an unexpected outcome of these preliminary atropisomerization studies. Further, in-depth investigations for the optimization of the detected reaction conditions will be rewarding. In addition, since these studies were not conducted in an inert atmosphere, it is probable that the presence of air oxygen played an important role in the oxidation of **17**; this likewise needs to be thoroughly investigated.
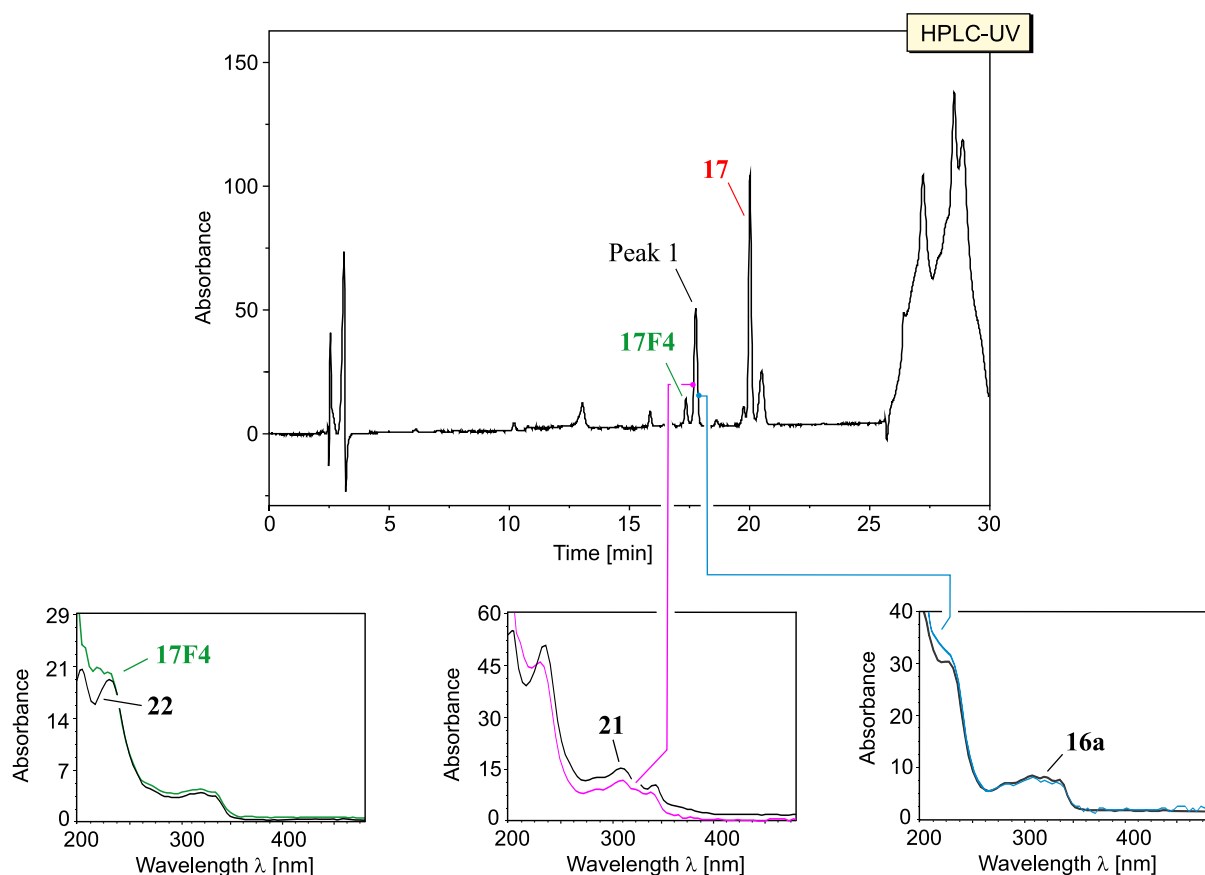
Figure 54. HPLC chromatogram of mbandakamine B$_2$ (**17**) in acidic acetonitrile (TFA, pH: 2-4) heated at 60°C for 2 d, and UV curves, indicating the presence of three different mbandakamine-type dimers: spiro-fused (**17F4**), *O*-bridged (occurring in the 'western', faster part of Peak 1) and the atropo-diastereomer of **17** (present in the slow, 'eastern' part of Peak 1). Note that for better comparability the intensities of the UV spectra of **16a**, **21**, and **22** were fitted to the ones of the respective peak.

The obtained sub-milligram quantities of the isomer of mbandakamine B$_2$ (**17**) with a *P*-configured central axis, **17F2**, were insufficient for NMR measurements that could help to address the question regarding the configuration exchange at the outer biaryl linkages. However, they provided the opportunity to further investigate the isomerization process. As shown in Figure 55, when left under acidic conditions, **17F2** was also very slowly converted into mbandakamine B$_2$ (**17**).
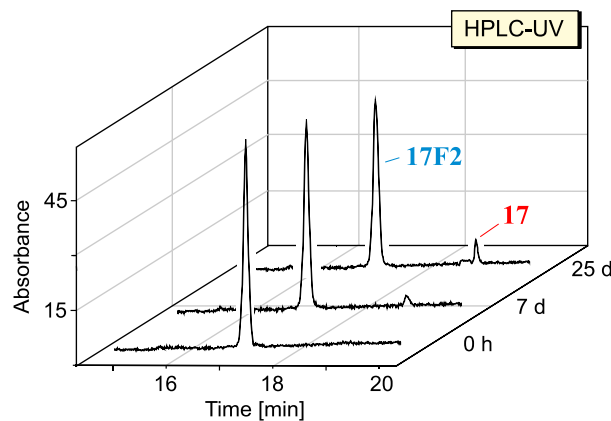
Figure 55. HPLC chromatograms of **17F2** in acidic acetonitrile (TFA, pH: 2-4, kept at ambient temperature), evidencing its slow conversion into mbandakamine B$_2$ (**17**).

Atropisomerization is a long-known process, which can be physically or chemically induced.[157-160] In the field of dimeric NIQs, an axial-configuration conversion was already reported for the three atropisomers michellamines A-C (**11a-c**)[62] and also noticed for the couple shuangancistrotectorines A and B (**27a** and **27b**).[78] Yet, its occurrence in the case of mbandakamine B$_2$ (**17**), as above presented, was quite astonishing, in view of the extraordinary steric congestion at the central axis of the mbandakamines. Such an atropo-diastereomerization, against strongest steric load, was most likely not physical, but a chemically induced one, certainly triggered by the presence of the acid. Following a generally accepted acid-catalyzed mechanism,[161-163] the atropisomerization of **17** (Scheme 12, Path **A**) might have proceeded via the protonation of the highly strained (and, thus, most reactive) sp^2-configured atom C-1″, leading to the formation of the monoprotonated intermediate **I**, which then have undergone a rotation about the now sp^3 - sp^2 bond (i.e., the 6′,1″-linkage), with subsequent deprotonation back to an sp^2 - sp^2 central biaryl axis with, in part, *M*- and now also, in part, *P*-configuration.

The isomerization at the axial stereo-array of **17** may have also followed a most recently formulated protocol by Genaev *et al.*,[164] according to which **17** (Scheme 12, Path **B**) would pass through the intermediate **II**, possessing a central 6′,1″-linkage that involved two sp^3-configured C-atoms (one resulting from a protonation and the other by tautomerization), making it sterically much less hindered and, thus, most favorable for a rotation about that 6′,1″-bond. A likewise imaginable atropisomerization mechanism (Pathway **C**) would be that protonation might occur at both, C-1″ and C-6′, leading to the dication **III**, which, as in the case of **II**, would make the rotation about the central axis much easier. Similar doubly

protonated species had been shown to be intermediates in the atropisomerization of 1,1′-bi-2-naphthol in superacids.[164] Despite the absence of a superacid here, in the atropisomerization of mbandakamines, such a mechanism, via twofold C-protonated intermediates of type **III**, would, nonetheless, be imaginable, due to the electron-rich character as a consequence of the presence of additional methoxy groups in the two naphthalene ring systems.
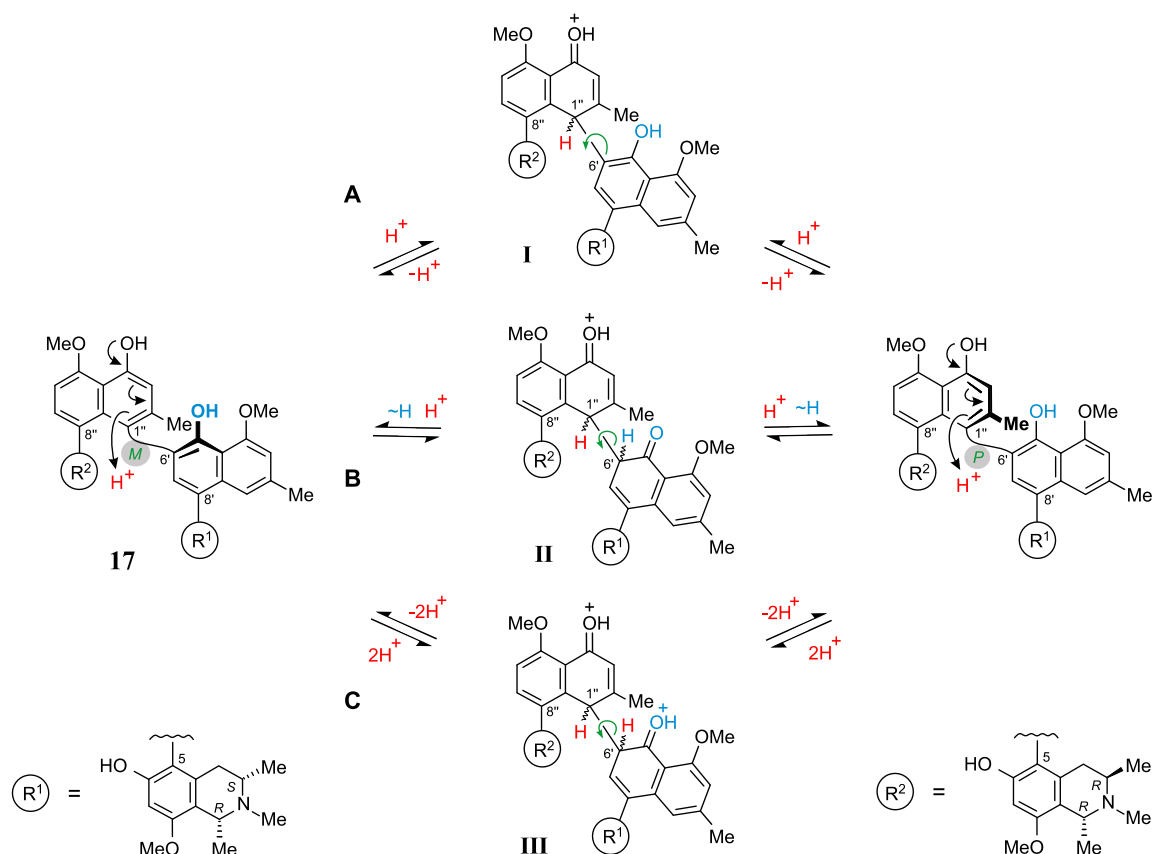
Scheme 12. Plausible mechanisms of the acid-catalyzed atropisomerization at the central biaryl axis of mbandakamine B$_2$ (**17**).

These preliminary studies on the atropisomerization of mbandakamines opened the door for interesting research options, like the optimization of the conditions to generate significant quantities of the desired atropisomers for further structural studies, for their directed search in plant extracts, and for the assessment of their bioactivities.

3.8.   Further Isolated Mbandakamine-Type Dimeric NIQs

Besides the above-described novel open-chain and cyclized mbandakamine-type dimers, which were all isolated through a directed, HPLC-UV-MS-CD-assisted approach, two further related dimeric compounds were discovered in the dimer-enriched fraction. These were the new open-chain mbandakamines **18** and **19**, which were identified in the course of parallel phytochemical work on *A. ealaensis* by Dr. D. T. Tshitenge in our group.[165,166] Both compounds, **18** and **19**, possessed a central *P*-configured axis, making them stereochemically closest to mbandakamine A (**16a**), with **18** being just an epimer of **16a** at C-1. The structural elucidation of these two metabolites, named mbandakamines C (**18**) and D (**19**), has most recently been published.[165,166]
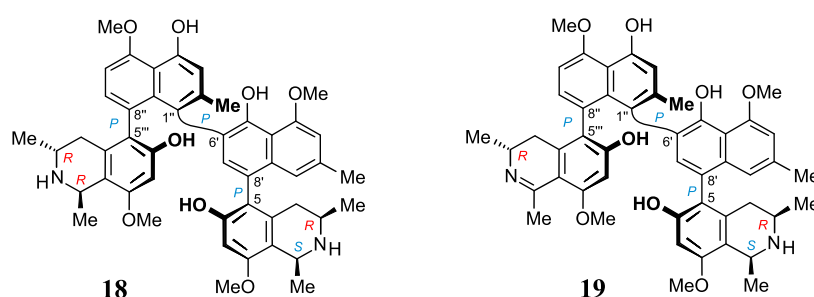
Figure 56. Structures of mbandakamines C (**18**) and D (**19**).

3.9.   Chemotaxonomic Relevance of the Discovered Metabolites

Besides being highly remarkable from their structures, their biosynthetic origin, and their bioactivities (as presented below), the obtained open-chain and cyclized dimeric NIQs were botanically relevant, too. They provided valuable insight into the chemotaxonomic position of the investigated botanically as yet unidentified Congolese *Ancistrocladus* liana with respect to the well-known related species from the Congo rainforests. During the past years, intense phytochemical investigations on the four taxonomically recognized Congolese *Ancistrocladus* species (viz., *A. likoko*, *A. congolensis*, *A. ealaensis*, and *A. ileboensis*)[82,114] had revealed the NIQ patterns to differ from one taxon to another. This established the comparison of NIQ profiles as a useful strategy to acquire preliminary information about the species status of some botanically as yet unidentified *Ancistrocladus* samples.

According to these studies, *A. likoko* typically produced only 5,8′-coupled monomeric NIQs in large quantities, along with a few 6′,6″-coupled dimeric compounds (referred to as

michellamine-type dimers), which occurred in very low concentrations.[55,167-170] *A. congolensis* likewise produced 5,8′-linked monomeric NIQs and michellamine-type dimers, but it additionally provided 5,1′- and 7,1′-coupled monomers.[171,172] *A. ileboensis* and *A. ealaensis*, by contrast, were much more creative, both at a monomeric and dimeric level. The former one was shown to contain a number of 7,1′-, 5,1′-, 5,8′-, and 7,8′-connected monomers, and the symmetric 3′,3″- and the unsymmetric 3′,6″-coupled dimers of 7,1′-linked monomers.[60,101,173] *A. ealaensis* was evidenced to yield 5,8′-, 7,8′-, and *N,C*-coupled monomers, and representatives of four subclasses of dimeric NIQs: michellamine-type, korundamine-type (i.e., 6′,6″-coupled dimer with two different, 5,8′- and 7,8′-connectivities at the outer axes), open-chain mbandakamine-type, and cyclombandakamine-type dimers.[148,165,166,174]

Considering this picture of NIQ types produced by distinct well-known Congolese *Ancistrocladus* species, it was thus clear that the liana from Bonsolerive – the plant from which the nine above-presented open-chain and cyclized mbandakamine-type dimers were isolated – was chemotaxonomically more close to *A. ealaensis* than to any other botanically recognized Congolese taxon. This close proximity was also supported by some morphologic features such as its relatively small leaves, the golden-yellow petals, and a single style with three stigmas, all characteristic of *A. ealaensis*.[40,114][175] There were, however, some facts suggesting the liana from Bonsolerive to diverge from *A. ealaensis*. From a chemotaxonomic point of view, the first observation was that the spiro-fused mbandakamines discovered from this plant were not detected in *A. ealaensis*, although the clear majority of dimers isolated from this species belonged to the mbandakamine types: four open-chain mbandakamines and seven cyclombandakamines, out of a total of 15 isolated dimers. Moreover, HPLC-UV-assisted investigations of both, the crude extract and the alkaloid-enriched fraction from the Bonsolerive liana provided no hints at the presence of 6′,6″-coupled dimers and *N,C*-linked monomers, not even in traces. Genetically, the DNA fingerprinting based on microsatellites clearly distinguished samples of *A. ealaensis* from the ones of the liana from Bonsolerive, as presented in Chapter 2 (see above). Thus, the *Ancistrocladus* plant here investigated seemed to be a new species or at least subspecies, and further investigations are therefore needed to firmly ascertain or contradict its taxonomic status.

3.10. Bioactivities of the Isolated Metabolites

3.10.1. Antiprotozoal Activities

Due to the previously reported pronounced antiprotozoal activities of some mono- and dimeric NIQs,[44,50,52,126,176] the novel open-chain and cyclized mbandakamines, **16a/b-23**, were tested *in vitro* against the NF54 strain of *Plasmodium falciparum*, the protozoan parasite causing the devastating tropical disease malaria. These biological tests were carried out in the group of Prof. R. Brun (in Basel, Switzerland). As shown in Table 2, all the test compounds showed significant antiplasmodial properties, with half-maximal inhibitory concentrations (IC_{50}) being in the submicromolar range. Particularly impressive was mbandakamine B_2 (**17**), which exhibited a remarkably low IC_{50} value of 17 nM, placing it among the most active mono- and dimeric NIQs ever found.[44,50,126] With this inhibitory activity, the open-chain dimer **17** was considerably more effective (more than three times) than the corresponding cyclized analogs cyclombandakamine A_2 (**21**) and spirombandakamine A_1 (**22**), which displayed IC_{50} values of 60 and 40 nM, respectively. Thus, the aforementioned biosynthetic cyclization process from **17** to **21** and **22** in the plant (see Section 3.5) reduced the antiplasmodial properties. Also interesting for structure-activity relationship were the IC_{50} values of the two atropisomeric mbandakamines A (**16a**) and B (**16b**), which substantially differed one from another (43 and 148 nM, respectively), hence showing the impact of axial chirality on the bioactivity. Likewise noteworthy was the *N*-methylation degree, which seemed to play a crucial role on the antiplasmodial properties of spirombandakamines, as witnessed by the IC_{50} value of **22** (40 nM), which was more than five times better than the one of its *N*-demethylated analog **23** (226 nM).

In a most recent bioassay against a different, chloroquine-resistant K1 strain of *Plasmodium falciparum*, three tested compounds, mbandakamine B_2 (**17**), spirombandakamines A_1 (**22**) and A_2 (**23**), displayed pronounced activities, too (Table 2). Again, mbandakamine B_2 (**17**) showed the lowest IC_{50} (4 nM), which is so far the best one ever found for mono- and dimeric NIQ alkaloids. The excellent antiplasmodial activity of **17**, together with its high selectivity index (SI) of 343, makes it most promising candidate for further pharmacological investigations.

Apart from the evaluation of their antiplasmodial properties, the obtained metabolites were also tested against *Trypanosoma brucei rhodesiense*, the pathogenic agent causing acute trypanosomiasis in humans. Only mbandakamine B_2 (**17**) and its cyclized analog

cyclombandakamine A$_2$ (**21**) were found to be effective, displaying excellent IC$_{50}$ values (5 and 10 nM, respectively), with high selectivity indices (274 and 1076, respectively), making them promising lead structures. All the other tested compounds were virtually inactive. Moreover, in the bioassay carried out against *Trypanosoma cruzi*, the agent causing Chagas' disease, and *Leishmania donovani*, one of the parasites causing leishmaniosis, all the test compounds showed virtually no activities, thus indicating these alkaloids to be pathogen-specific.

Table 2. Antiprotozoal activities of the novel mbandakamine-type dimers **16a/b**, **17-23**.

Cpd.	IC$_{50}$ (SI)[a,b]					
	P. falciparum		*T. brucei rhodesiense* STIB900	*T. cruzi* Tulahuen C2C4 Lac Z	*L. donovani* axenic amastigotes MHOM/ ET/67/L82	Cytotoxicity (L6 cells)
	NF54	K1				
Standard	0.007[c]	0.309[c]	0.003[d]	2.48[e]	0.18[f]	0.017[g]
16a[h]	0.043 (158)	n.d.	2.43 (2.6)	9.22 (<1)	n.d.	6.32
16b[h]	0.148 (260)	n.d.	n.d.	n.d.	n.d.	39.04
17	0.017 (81)	0.004 (343)	0.005 (274)	2.98 (<1)	94.23 (0)	1.37
18[g]	0.047 (338)	0.064 (248)	1.8 (9)	41.8 (<1)	>100	15.9
19[g]	0.337 (26)	0.126 (70)	4.1 (2)	n.d	>100	8.87
20	0.043 (397)	n.d.	1.085 (16)	31.74 (0.54)	105.7 (0.16)	17.09
21	0.055 (196)	n.d.	0.010 (1076)	7.71 (1.40)	>120	10.76
22	0.040 (89)	0.007 (509)	0.691 (5)	5.54 (<1)	>100	3.56
23	0.226 (37)	0.094 (80)	0.296 (28)	16.94 (<1)	>100	8.42

[a] Values are given in µM; [b] SI: Selectivity Index (it is calculated as the ratio of the IC$_{50}$ value for the L6 cells to the IC$_{50}$ data against the respective pathogen); [c] Chloroquine; [d] Melarsoprol; [e] Benznidazole; [f] Miltefosine; [g] Podophyllotoxin; [h] as the diacetate; **g** values reported from ref.[166]; n.d.: not determined.

3.10.2. Antitumor Activities of Mbandakamine A (16a) against Human Pancreatic Cancer PANC-1 Cells and Cervical Cancer HeLa Cells

Pancreatic cancer is one of the most dreadful cancer types, with only less than 5% of patients surviving the first five years after diagnosis.[177-180] In 2018, it caused over 432,000 deaths worldwide.[181] Even more worrying is its strongly increasing incidence, with estimations predicting it to be among the top leading cancer diseases by 2030.[179,182,183] Surgery remains a potential cure, but it is in many cases impossible since the disease is usually detected quite late, at a more advanced stage of an already rapidly progressing metastasis.[179,184,185] Moreover, the treatment of this malignant cancer disorder with conventional chemotherapeutic agents severely suffers from the rapid development of multidrug-resistance of the tumor cells[184,186] and from the fact that the pancreatic cancer cells have a remarkable inherent tolerance to extreme nutrition starvation, enabling them to survive and proliferate aggressively under hypovascular and hypoxic conditions.[187] Therefore, the development of new treatment strategies against pancreatic cancer is an urgent need.

The antiausterity strategy is an emerging approach in the field of anticancer drug development, aiming at the discovery of new agents that inhibit the growth of cancer cells preferentially in nutrient-deprived medium (NDM).[187-191] This preferential cytotoxicity, also referred to as antiausterity activity, is represented by PC_{50} values, i.e., the concentration at which 50% of the pancreatic cancer cells are killed in NDM without displaying toxicity in normal, nutrient-rich Dulbecco's modified Eagle's medium (DMEM).

Initiated by the author of this thesis, a cooperation for testing the antiausterity potential of NIQs and analogs was established between our research group and the team of Prof. S. Awale (University of Toyama, Japan), a pioneer and leader in the field of antiausterity agents. The team of Prof. Awale is particularly renowned for their discovery of arctigenin (**43**, Figure 57a), a highly promising antiausterity drug candidate isolated from the seeds of the plant *Arctium lappa* L.;[191] this compound has even successfully passed an early phase II human clinical trial.[192] As part of the cooperation with his group, several natural and synthetic compounds were tested,[103,104,167,169,173,193,194] among them the open-chain dimer mbandakamine A (**16a**) (the other isolated novel mbandakamine-type compounds were not tested because of their very limited availability). As shown in Figure 57b, mbandakamine A (**16a**) strongly inhibited the growth of PANC-1 cells in a concentration-dependent manner, both in DMEM (IC_{50} = 4.31 µM) and in NDM (IC_{50} = 4.19 µM). Its cytotoxic potency, however, was not preferential to NDM, as visible by the virtually identical IC_{50} values recorded in NDM and in DMEM. Thus,

16a could not be regarded as a potential antiausterity agent, in contrast to some other potent new NIQs described later below (see Sections 4.5 and 5.5). On the other hand, its detected strong cytotoxic properties made it rewarding for further investigations on other cancer cells. In a standard, classically operated bioassay against the cervical cancer HeLa cell line, **16a** exhibited impressive growth-inhibitory activity (Figure 57c), with an IC_{50} value of 1.39 µM, which was far better than that of the anticancer agent 5-fluorouracil[195] (**44**, IC_{50} = 13.9 µM), used as reference.
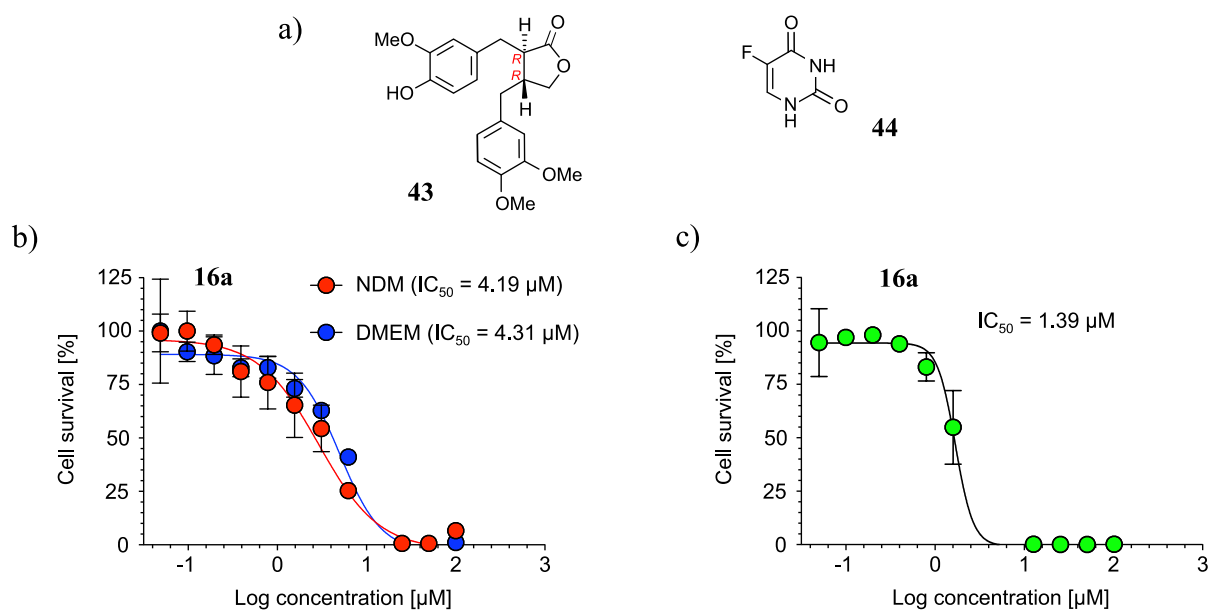
Figure 57. a) Structures of the anticancer agents arctigenin (**44**) and 5-fluorouracil (**43**), and cytotoxic activity of mbandakamine A (**16a**) against: b) the PANC-1 human pancreatic cancer cell line in nutrient-deprived medium (NDM) and Dulbecco's modified Eagle's medium (DMEM), and c) against cervical cancer HeLa cells.

4. Michellamine-Type Dimers and Further Monomeric NIQs from a Congolese *Ancistrocladus* Liana Related to *A. likoko*

4.1. Introduction

During the aforementioned field trip to the rainforests close to the Congolese village Bonsolerive in August 2015, the author of this thesis discovered another *Ancistrocladus* liana, occurring in the same site as the potentially new *Ancistrocladus* species investigated and presented in the preceding chapter. Particularly striking were its leaves, which were much larger (about 57 cm long and 12 cm wide) than those of any other *Ancistrocladus* plant species found nearby. This liana had hooked-like inflorescences, which, together with the aforementioned large size of the leaves, were reminiscent of *A. likoko*, the only known Congolese taxon with similar – yet different – morphological characteristics.[40,114] Comparative HPLC-UV-MS profiling of the leaf alkaloid pattern of this liana and that of an authentic sample of *A. likoko*, however, revealed substantial phytochemical differences between the two samples. This metabolic divergence and the fact that *A. likoko* had so far not been found to occur in that sampling area indicated that the liana might belong to a new, as yet undescribed plant species or subspecies. The isolation and structural elucidation of its alkaloids thus became a rewarding task, not only for the chemotaxonomic characterization of this liana and its possible delineation from other *Ancistrocladus* taxa, but also for their biological evaluation.

The following paragraphs describe the isolation and structural elucidation of eleven mono- and dimeric naphthylisoquinoline alkaloids from the leaves of this yet unidentified *Ancistrocladus* liana (Figure 58). The isolated metabolites comprise six previously unknown compounds, including michellamines A_6 (**45**) and A_7 (**46**), which are the first dimers of 5,8′-coupled naphthylisoquinoline alkaloids with *cis*-configured stereocenters in both tetrahydroisoquinoline subunits, michellamines B_4 (**47**) and B_5 (**48**), ancistrobonsoline A_1 (**49**) and its 6-*O*-methyl derivative, ancistrobonsoline A_2 (**50**). The five other obtained metabolites were described from earlier work on other *Ancistrocladus* plants: ancistroealaine C (**51**),[166] korupensamines A (**52a**) and B (**52b**),[196] and michellamines A_2 (**53**)[172] and E (**54**).[75] This work provided the basis for a discussion of the chemotaxonomic position of this liana relative to other *Ancistrocladus* species. Furthermore, the bioactivities of the isolated metabolites are presented and also discussed.
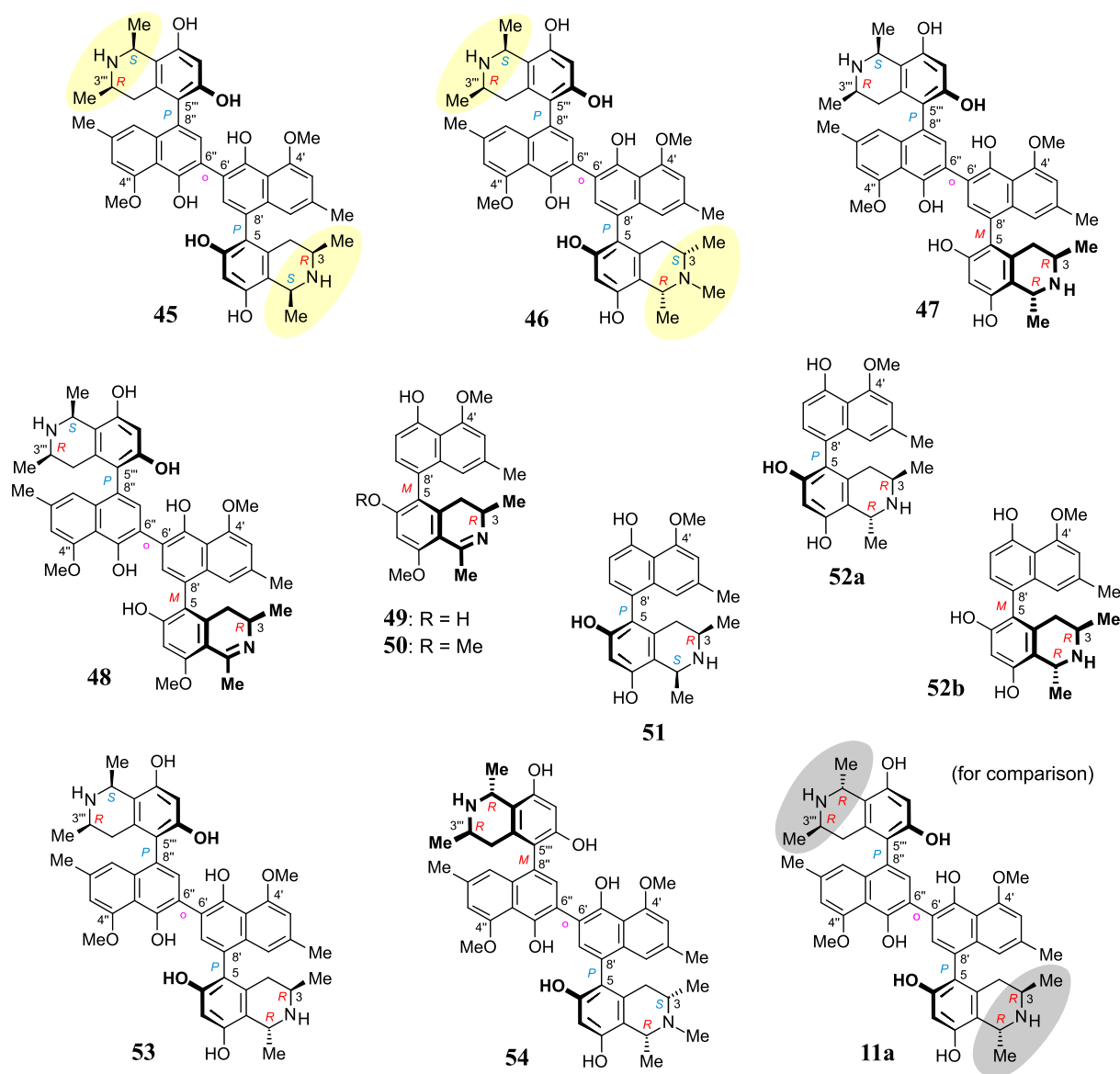
Figure 58. Metabolites isolated from an as yet unidentified Congolese *Ancistrocladus* liana, among them six new compounds: michellamines A_6 (**45**), A_7 (**46**), B_4 (**47**), and B_5 (**48**), ancistrobonsolines A_1 (**49**) and A_2 (**50**), and five previously known ones: ancistroealaine C (**51**), korupensamines A (**52a**) and B (**52b**), and michellamines A_2 (**53**) and E (**54**). Yellow ellipses on **45** and **46** highlight the combination of two 1,3-*cis*-configurations, never observed in any other related dimer; for reason of comparison, see the structure of the well-known michellamine A (**11a**) with its 1,3-*trans*-configurations (underlaid in gray) in both molecular halves – this compound is not produced by the investigated Congolese liana.

4.2.   Isolation and Identification of Known Compounds

Extraction of the air-dried leaves with a mixture of methanol and dichloromethane (1:1), followed by concentration under reduced pressure, provided a crude residue, which was then submitted to a cation-exchange column to remove undesired, non-basic metabolites. The

resulting alkaloid-enriched fraction was partitioned between water and dichloromethane, and monitored by HPLC (Figure 59).
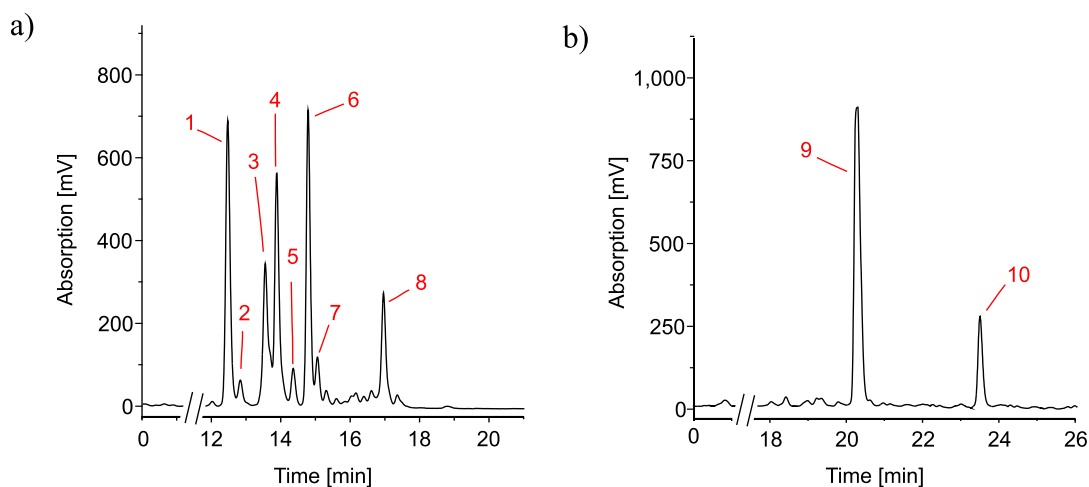
Figure 59. HPLC profiles of: a) H_2O-derived alkaloid-enriched subfraction; and b) CH_2Cl_2-derived alkaloid-enriched subfraction from the leaves of the Congolese *Ancistrocladus* plant morphologically related to *A. likoko*.

Resolution of the water-phase subfraction on a preparative HPLC column permitted isolation of nine pure constituents, obtained as amorphous solids. The fastest-eluting compound (Peak 1, Figure 59a) was found to be ancistroealaine C (**51**), earlier known from *Ancistrocladus ealaensis*.[165] The second alkaloid (Peak 2) was korupensamine A (**52a**), while Peak 3 contained two alkaloids overlapping each other, korupensamine B (**52b**) and michellamine A$_2$ (**53**), and Peak 7 corresponded to michellamine E (**54**). These four metabolites (**52a/b**-**54**) had previously been isolated from other *Ancistrocladus* species, yet only from Central Africa: The korupensamines A (**52a**) and B (**52b**), first known from the Cameroonian plant *A. korupensis*[196] as well as michellamine E (**54**),[75] had both also been reported from *A. likoko*,[55,167] where they occur as major metabolites. Korupensamine A (**52a**) is likewise the main naphthylisoquinoline alkaloid in *A. congolensis*,[171,172] in which michellamine A$_2$ (**53**) was discovered[172] before its more recent detection as a minor constituent of *A. likoko*.[167] The other four remaining compounds from the aqueous subfraction (Peaks 4, 5, 6, and 8, Figure 59a), as well as those from the dichloromethane subfraction (Peaks 9 and 10, Figure 59b), were as yet unknown.

4.3.   Structural Elucidation of the New Compounds

4.3.1.   Michellamine A_6 (45)

The first new metabolite, compound **45** (Peak 4, Figure 59a), had a molecular formula $C_{46}H_{48}N_2O_8$, as evidenced from HRESIMS (757.3486, $[M+H]^+$). ^1H and ^{13}C NMR measurements showed only a half set of signals, which indicated that this metabolite consisted of two equivalent molecular portions, but left open the question of whether the two halves were homomorphous or enantiomorphous to each other. The latter possibility (i.e., the presence of an achiral *meso* compound) was excluded by the optical activity of **45**, showing that it was C_2-symmetric.

The ^1H NMR spectrum exhibited four aromatic protons. Two of them displayed a *meta*-coupling (6.84 ppm, *p*t, *J* = 0.9 Hz; 6.86 ppm, *p*d, *J* = 1.3 Hz), typical of protons at C-1′ and C-3′,[75,172,196] while the other two appeared as singlets (6.47 and 7.29 ppm), which suggested the presence of a symmetric dimer of 5,6′-, 5,8′-, 7,6′-, or 7,8′-coupled naphthylisoquinoline monomers. The aliphatic region, with two three-proton doublets (1.82 ppm, *J* = 6.5 Hz; 1.26 ppm, *J* = 6.5 Hz), signals for two aryl substituents (2.37 ppm, s; 4.10 ppm, s), a quartet (4.64 ppm, *J* = 6.5 Hz), a multiplet (3.27 ppm), and two doublet of doublets (2.64 ppm, *J* = 17.3, 3.3 Hz; 2.27 ppm, *J* = 17.3, 12.0 Hz), was, however, closely similar to that of the likewise isolated known[165] ancistroealaine C (**51**), so that a 5,8′-coupled molecular framework was expected. In agreement with this assumption, one of the two aromatic singlets was assigned as H-7 (6.47 ppm), from its HMBC correlations with C-6 (156 ppm), C-8 (156.5), and C-9 (113.0) (Figure 60). This showed that the other, remaining singlet (7.29 ppm) had to be at C-7′ (134.9 ppm) and, hence, clearly excluded any biaryl linkage involving C-7 (102.9 ppm).

The two remaining possible coupling types (5,6′ or 5,8′) were further discriminated by joint correlative HMBC signals from H-7 and H-1′ (6.84 ppm, *p*t, *J* = 0.9 Hz) to C-8′ (124.3 ppm) (Figure 60), which excluded a 5,6′-coupling, where such interactions would not have been observed. Thus, the naphthalene and isoquinoline portions were linked to each other by a 5,8′-axis, and the two monomeric naphthylisoquinoline halves were therefore connected via C-6′ (120.4 ppm). These couplings, in particular the 6′,6″-linkage between the naphthalene portions, were further corroborated by the chemical shifts of C-6′ and of the surrounding nuclei, C-5′ (152.4 ppm) and C-7′ (134.9 ppm), which were near-identical to those of other dimers with similar molecular frameworks (e.g., in the case of michellamine A_2 (**54**): 120.3 ppm for C-6′, 152.3 ppm for C-5′, and 134.7 ppm for C-7′).[172] The location of the methoxy

group (4.10 ppm for protons and 57.1 ppm for the carbon atom) at C-4′ (158.2 ppm) was deduced from NOE interactions of its protons with H-3′ (6.86 ppm, *p*d, *J* = 1.3 Hz), in conjunction with joint HMBC correlations from both, *O*-methyl protons and H-3′ to C-4′ (Figure 60).
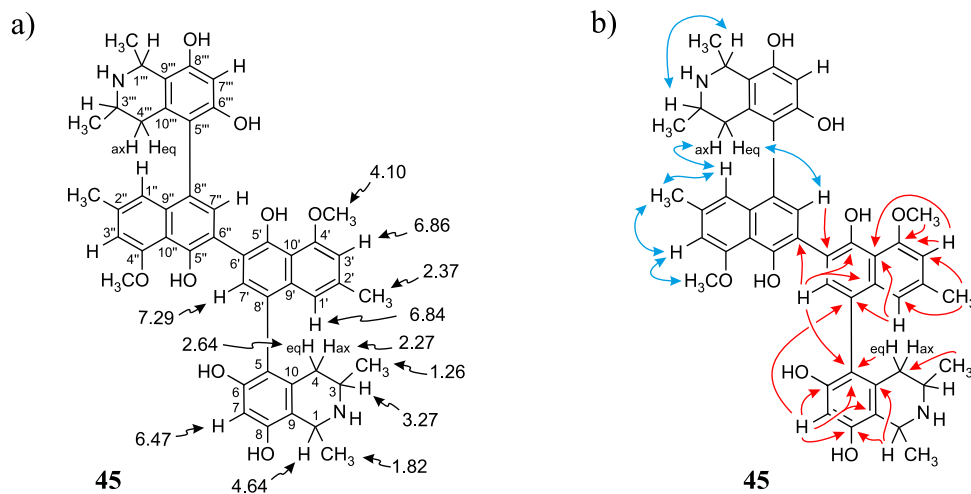
Figure 60. Selected NMR data of michellamine A$_6$ (**45**): a) ^{1}H chemical shifts in ppm; and b) key HMBC (red single arrows) and ROESY (blue double arrows) correlations.

Based on NOESY interaction of the proton at C-3 with the one at C-1 (Figure 61a), the relative configuration at the stereocenters C-1 and C-3 was determined to be *cis*. Ruthenium-mediated oxidative degradation[156] of this alkaloid led to the *R*-enantiomer of 3-aminobutyric acid (derived from C-3), as monitored by GC-MSD analysis of the Mosher derivatives. This revealed C-3 to be *R*-configured and thus, given the aforementioned relative *cis*-configuration, C-1 had to be *S*-configured.

At the naphthalene-isoquinoline biaryl axes, within the 5,8′-coupled monomeric halves, the stereo-array was determined by NOESY interactions of the proton at C-7′ with the equatorial proton (2.64 ppm; *J* = 17.3, 3.3 Hz) at C-4 (33.3 ppm) and between the axial proton (2.27 ppm; *J* = 17.3, 12.0 Hz) and the aromatic proton at C-1′ (119.3 ppm). This, in conjunction with the absolute *R*-configuration at C-3 (51.0 ppm), as depicted in Figure 61a, indicated *P*-configuration at the outer axes, revealing these portions to be structurally identical to the known, co-isolated ancistroealaine C (**51**). Hence, the metabolite was found to be the 6′-homocoupling product of **51**, with the absolute stereostructure **45** presented in Figure 61b. This was further confirmed by the similarity of the ECD spectrum of **45** with that of the co-

occurring, likewise *P,P*-configured michellamine A_2 (**53**) (Figure 61c). Owing to this combination of two *P*-configured outer biaryl axes, the new compound was included in the 'series A' of michellamines – which so far comprised michellamines A-A_5 – and was thus named michellamine A_6. It differed from michellamine A_2 (**53**) only by the configuration at C-1, so that it can also be referred to as 1-*epi*-michellamine A_2. Its 1,3-*cis*-configurations in both tetrahydroisoquinoline portions, as highlighted in Figure 58, was a unique structural feature that had not been found in any other similarly coupled naphthylisoquinoline dimers.
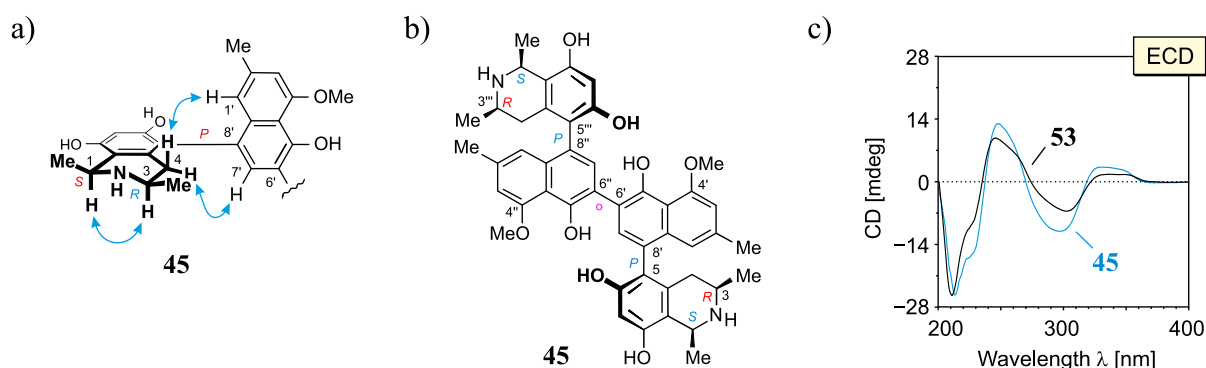
Figure 61. a) Key ROESY (blue double arrows) indicating the relative and – given the results of oxidative degradation – absolute configurations of the two identical portions (= ancistroealaine C, **51**) of michellamine A_6 (**45**); b) the absolute stereostructure of michellamine A_6 (**45**); c) comparison of the ECD curve of **45** with the one of the known, co-occurring *P,P*-configured michellamine A_2 (**53**), corroborating the established molecular scaffold of **45**.

4.3.2. Michellamine A_7 (46)

The second new alkaloid, compound **46**, corresponding to Peak 5 in Figure 59a, had a molecular weight 14 units larger than that of **45**, matching with the molecular formula $C_{47}H_{50}N_2O_8$ (*m/z* 771.3655, HRESIMS). Its UV spectrum, which was very similar to that of **45**, indicated that **46** was a 6′,6″-coupled dimer, too. This was further supported by its ^1H NMR spectrum, which closely resembled that of the co-isolated michellamine A_2 (**53**), except for the presence of one additional three-proton singlet at 3.04 ppm. In the HSQC experiment, this extra methyl signal correlated with the carbon atom at 41.4 ppm, thus indicating **46** to be an *N*-methylated michellamine-type dimer. Further 1D and 2D NMR data revealed that methyl group to be attached to the nitrogen atom in the 'southeastern' portion (Figure 62). Key evidence of the exact location of this *N*-methyl group were the HMBC correlations from its protons to both, C-1 and C-3 and the signals of these methine carbons, which appeared deshielded (62.6 ppm for C-1 and 60.6 ppm for C-3) as compared to those of the *N*-

demethylated congeners – like, for example, in the case of **45** (Figure 60). This assignment was further supported by the ROESY series CH$_3$-1 (1.77 ppm, d, *J* = 6.7 Hz) ↔ *N*-Me ↔ CH$_3$-3 (1.33 ppm, d, *J* = 6.6 Hz) (Figure 62), which, in addition, revealed a 1,3-diaxial relationship of H-1 (4.64 ppm, q, *J* = 6.6 Hz) and H-3 (3.23 ppm, m) and, thus, a relative *cis*-configuration at the stereocenters C-1 and C-3. For the stereocenters in the other, 'northwestern' part of **46**, a relative *cis*-configuration was observed, too, again evidenced by the ROESY interactions of H-1‴ (4.64 ppm, q, *J* = 6.6 Hz) with H-3‴ (3.29 ppm, m), as in **45** (Figure 61a).

Figure 62. Selected NMR data of michellamine A$_7$ (**46**): a) ^{1}H chemical shifts in ppm; and b) key HMBC (red single arrows) and ROESY (blue double arrows) correlations; the constitutional differences between the two molecular halves of **46** are highlighted in gray.

The ruthenium-mediated oxidative degradation of **46** yielded both, *R*- and *S*-configured 3-aminobutyric acids, showing that this alkaloid was either 3*R*,3‴*S*- or 3*S*,3‴*R*-configured. The simultaneous formation of the *N*-methylated analog of 3-aminobutyric acid only as its *S*-enantiomer, however, clearly indicated that the *S*-configured stereocenter was located next to the *N*-methyl group, i.e., at C-3. Thus, the isolated compound had to be 3*S*,3‴*R*-configured, which, given the relative *cis*-configurations in both halves as mentioned above, showed that C-1 and C-1‴ (52.5 ppm) were *R*- and *S*-configured, respectively.

From ROESY interactions between H$_{ax}$-4 (2.69 ppm, dd, *J* = 18.0, 11.4 Hz) and H-7′ (7.33 ppm, s), and between H$_{eq}$-4 (2.36 ppm)[197] and H-1′ (6.78 ppm, s) (Figure 63a), and based on the above-assigned *S*-configuration at C-3, the configuration at the southeastern axis was

determined to be *P*, thus revealing this portion of **46**, **46-I**, to correspond to korupensamine D, a known naphthylisoquinoline alkaloid from *A. korupensis*.[196] At the other, northwestern axis of **46**, the ROESY interactions were complementary: H_{ax}-4‴ (2.28 ppm, dd, *J* = 17.8, 12.2 Hz) with H-1″ (6.85 ppm, s) and H_{eq}-4‴ (2.65 ppm, dd, *J* = 17.8, 4.3 Hz) with H-7″ (7.29 ppm, s), which, together with the opposite *R*-configuration at C-3‴ (51.0 ppm) established above, indicated that axis to be *P*-configured, too, as in **45** (Figure 61a). This metabolite thus had to be a cross-coupling product of ancistroealaine C (**51**) and korupensamine D (its structure corresponds to **46-I** with a proton at C-6′),[196] and hence possessed the absolute structure **46** presented in Figure 63b. The assigned 3D molecular architecture of **46**, and in particular the *P*-stereo-array at the stereogenic axes, was further supported by its ECD spectrum, which showed similar Cotton effects as **45** (Figure 63c). With the *P,P*-configured outer biaryl axes, this new quateraryl NIQ belonged to the 'series A' of michellamine-type dimers, too, and was henceforth named michellamine A7. It is the second dimer of 5,8′-coupled naphthylisoquinolines that possess the unusual combination of two 1,3-*cis*-configured halves.

Figure 63. a) Relevant ROESY (blue double arrows) correlations indicating the relative and – given the results of oxidative degradation – absolute configurations of the southeastern portion of michellamine A7 (**46**), **46-I** (the northeastern moiety of **46** is identical to the portion sketched in Figure 61a for **45**, i.e., ancistroealaine C, **51**); b) the absolute stereostructure of michellamine A7 (**46**); and c) comparison of the CD spectra of **46** and **45**, corroborating their *P,P*-stereo-arrays.

4.3.3. Michellamine B4 (47)

Compound **47**, with a slightly longer retention time than those of **45** and **46** (Peak 6, Figure 59a), was revealed to be isomeric to **45** by mass spectrometry (HRESIMS: *m/z* 757.3475 [M+H]+, molecular formula: $C_{46}H_{48}N_2O_8$). Its ^{1}H and ^{13}C NMR spectra displayed full sets of

signals, which showed that, different from **45**, it consisted of two non-identical molecular halves.

The ^{1}H NMR spectrum of **45** matched the half-set of signals of **47** nearly perfectly ($\Delta\delta_H \leq$ 0.02), which suggested that the two compounds had one molecular portion in common. Further analysis of the 1D and 2D NMR data of **47** established the constitution of **47** to be identical to that of **45**, that is, two 5,8′-coupled naphthylisoquinoline halves connected to each other via C-6′ (Figure 64).

Figure 64. Selected NMR data of michellamine B$_4$ (**47**): a) ^{1}H chemical shifts in ppm; and b) HMBC (red single arrows) and ROESY (blue double arrows) correlations relevant for the constitution.

In one of the two molecular portions of **46**, in the northwestern part, the relative configuration at the stereocenters C-1′′′ *versus* C-3′′′ was deduced to be *cis* from ROE interactions of H-1′′′ and H-3′′′, as also (even twice) in **45** (Figure 61a). In the southeastern part of **47** (**47-I**), however, the stereocenters were *trans*-configured, as evidenced from ROESY interactions between H-3 and CH$_3$-1 (Figure 65a). The ruthenium-mediated oxidative degradation of **47** yielded 3-aminobutyric acid as its *R*-enantiomer exclusively, which demonstrated that both, C-3 and C-3′′′ were *R*-configured. This, together with the aforementioned *cis*- and *trans*-arrays, established the absolute configurations at C-1′′′ and C-1 to be *S* and *R*, respectively.

From ROESY interactions of H$_{ax}$-4′′′ with H-1′′ and of H$_{eq}$-4′′′ with H-7′′, and in view of the absolute *R*-configuration at C-3′′′, the absolute axial configuration in the northwestern half was assigned to be *P*, revealing this portion to be identical to **51**, as in **45** (Figure 61a). In the

other, southeastern part, the respective protons interacted in a complementary way: H_{ax}-4 with H-7′ and H_{eq}-4 with H-1′, as shown in Figure 65a. These correlations, together with the known *R*-configuration at C-3 (see above), evidenced the southeastern biaryl axis to be *M*-configured, thus showing the corresponding moiety to have the same structure as the likewise isolated korupensamine B (**52b**). Therefore, compound **47** had to be the 6′,6″-cross-coupling product of ancistroealaine C (**51**) and korupensamine B (**52b**), with the absolute stereostructure given in Figure 65b. It was named michellamine B_4, in continuation of the series of michellamines with opposite configurations at the two outer biaryl axes (type B). It differs from the well-known michellamine B (**11b**)[62] only the configuration at C-1 in the *P*-configured molecular portion.

Figure 65. a) Key ROESY (blue double arrows) correlations indicating the relative and − given the results of oxidative degradation − absolute configurations of the southeastern portion of michellamine B_4 (**47**), **47-I** (the northeastern moiety of **47** is identical to the portion sketched in Figure 61a for **45**, i.e., ancistroealaine C, **51**); b) the absolute stereostructure of michellamine B_4 (**47**); and c) the molecular architecture of the structurally closely related, well-known michellamine B (**11b**). The gray labeling indicates the structural difference between **46** and **11b**.

Particularly noteworthy in the case of michellamine B_4 (**47**) was the fact that its ECD spectrum was not really similar to that of its analog michellamine B (**11b**) (Figure 66a). But, in agreement with the known feature[126,198] that an ECD spectrum of a given michellamine-type dimer is virtually equivalent to the curve obtained from a simple addition of the individual ECD spectra of the corresponding monomers, the ECD curve of **47** was found to be comparable to the one of a 1:1 mixture of its co-occurring monomers, ancistroealaine C (**51**) and korupensamine B (**52b**) (Figure 66b), thus further corroborating the assigned stereostructure of **47**.
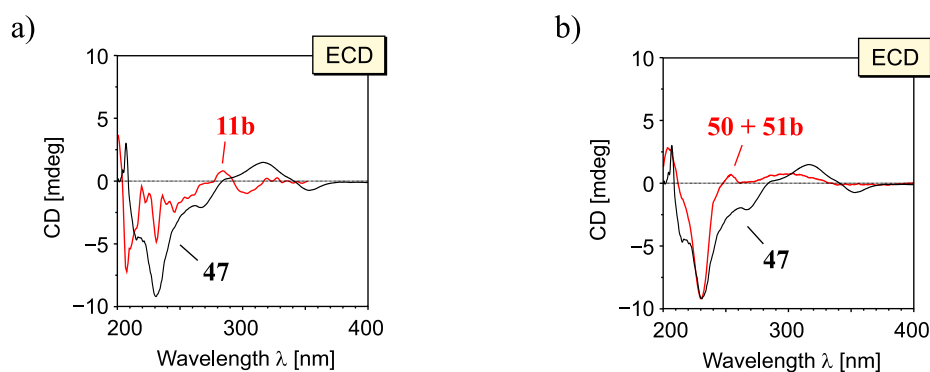
Figure 66. comparison of ECD spectrum of michellamine B$_4$ (**47**) with: a) the ECD curve of michellamine B (**11b**);[172] and b) the one of the 1:1 mixture of the monomeric NIQs ancistroealaine C (**51**) and korupensamine B (**52b**).

4.3.4.   Michellamine B$_5$ (48)

Compound **48**, the slowest-eluting major metabolite in the aqueous fraction (Peak 8, Figure 59a), gave a monoprotonated molecule at *m/z* 769.3484 in HRESIMS, i.e., 12 units more than **47**. Its ^{1}H NMR spectrum displayed a full set of signals, with one quartet (instead of two), thus indicating that this metabolite consisted of one naphthyl-1,3-dimethyl*tetra*hydro- and one naphthyl-1,3-dimethyl*di*hydroisoquinoline subunit. In addition, this dimer had three methoxy functions (4.11, 4.10, and 4.03 ppm), i.e., one *O*-methyl group more than the other three compounds, **45**-**47**. Comparison of its ^{1}H NMR spectrum with those of **45**-**47** showed that these four metabolites had one common, nearly perfectly matching half-set of signals, corresponding to the northwestern portions of **45**-**47**, which were equivalent to ancistroealaine C (**51**). The northwestern portion of **48** was therefore expected to be identical to **51**, too, and its southeastern part was assumed to be the naphthyl-1,3-dimethyl*di*hydroisoquinoline moiety, possessing two methoxy groups.

This assumption was corroborated by 1D and 2D NMR data, which led to a molecular architecture similar to that of **48**, but with one additional methyl group attached to the oxygen function at C-8 and a double bond between C-1 and the adjacent nitrogen atom in the southeastern portion (Figure 67). Key NMR features of the location of the methoxy function at C-8 (165.8 ppm) were the joint HMBC interactions from H-7 (6.69 ppm, s) and OCH$_3$-8 (4.03 ppm, s) to C-8, and the ROESY series H-7 ↔ OCH$_3$-8 ↔ CH$_3$-1 (2.77 ppm, d, *J* = 1.4 Hz).
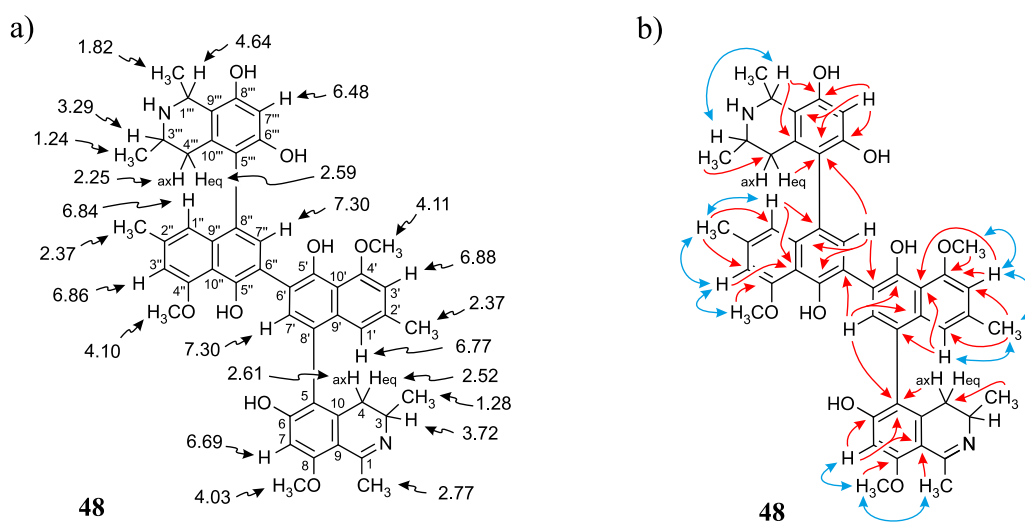
Figure 67. Selected NMR data of michellamine B$_5$ (**48**): a) ^{1}H chemical shifts in ppm; and b) HMBC (red single arrows) and ROESY (blue double arrows) correlations relevant for the constitution.

The oxidative degradation procedure delivered aminobutyric acid only in its *R*-configured form, showing that both, C-3 and C-3$'''$ were *R*-configured. In the northwestern portion, ROESY interactions at the stereocenters C-1$'''$ *versus* C-3$'''$ and across the naphthalene-isoquinoline linkage were the same as in **45** (Figure 61a), so that C-1 was *S*-configured and the biaryl axis had the *P*-configuration. In the southeastern portion, the ROESY interaction between H$_{ax}$-4 and H-7$'$ indicated these two spin systems to be on the same side of the molecule, as depicted in Figure 68a, which evidenced an *M*-configuration at the biaryl axis. Therefore, this metabolite possessed the absolute stereostructure **48**, as shown in Figure 68b. It was named michellamine B$_5$, due to its stereochemical similarity with michellamine B$_4$ (**47**). Within a list of now 18 known natural michellamine-type dimers, it was only the third example that possessed a dihydroisoquinoline ring system; the two other previously described analogs with such a structural peculiarity were the *P,M*-configured michellamine F (**55**)[75] and michellamine A$_4$, which had a hydroxy function at C-8 (instead of the methoxy group, as in **48** and **55**) and a *P*-configuration at both outer axes.[172] Michellamines B$_5$ (**48**) and F (**55**) differ one from another only by the configuration at C-1 in the tetrahydroisoquinoline unit.
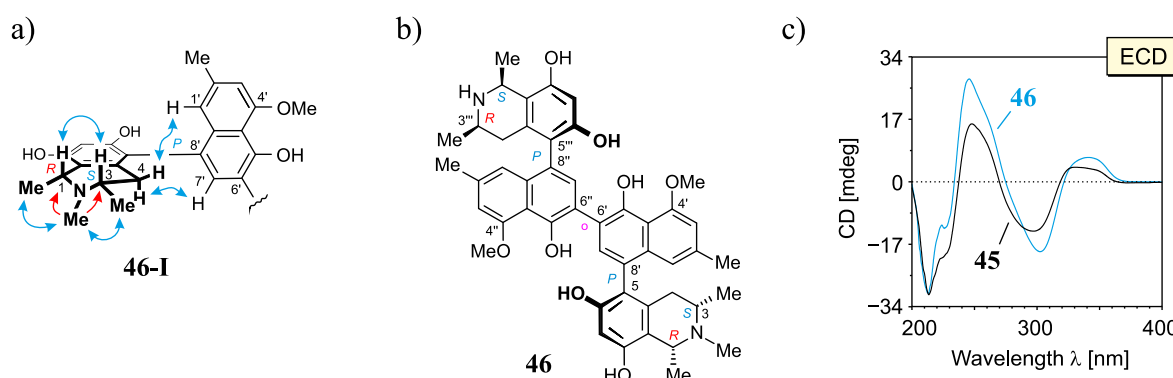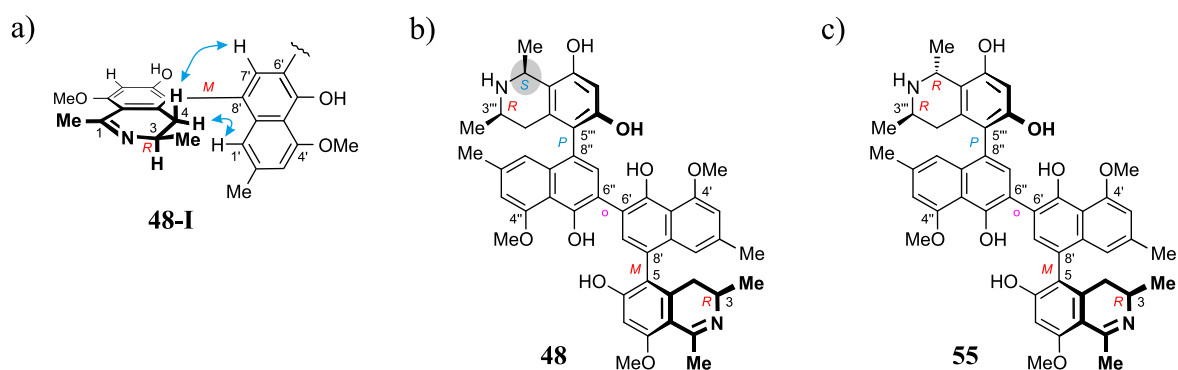
Figure 68. a) Main ROESY (blue double arrows) interactions indicating the relative and – given the results of oxidative degradation – absolute configurations at the axis in the southeastern portion of michellamine B$_5$ (**48**), **48-I** (the northeastern moiety of **48** is identical to the portion sketched in Figure 61a for **45**, i.e., ancistroealaine C, **51**); b) the absolute stereostructure of michellamine B$_4$ (**48**); and c) of the previously known structurally closely analog michellamine F (**55**). The gray labeling indicates the structural difference between **48** and **55**.

4.3.5. Ancistrobonsoline A$_1$ (49)

The dichloromethane subfraction contained two major, readily separated metabolites (Figure 59b). They were obtained as amorphous solids by resolution on a preparative reverse-phase HPLC column. The more polar one (Peak 9, Figure 59b), compound **49**, gave an *m/z* at 392.1843 [M+H]$^+$, corresponding to the molecular formula C$_{24}$H$_{25}$NO$_4$. In the ^{1}H NMR spectrum, the presence of two methoxy signals, together with the absence of a quartet around 4.5 ppm, which typically indicated a proton located at C-1, hinted at a naphthyl-1,3-dimethyldihydroisoquinoline alkaloid, presumably equivalent to the southeastern portion of **49**. This was further corroborated by the fact that the signals in the aliphatic region of the ^{1}H NMR spectrum of **49** matched very well with those assigned to the protons of the southeastern half of **48**. Detailed analysis of the 1D and 2D NMR spectra of this monomeric alkaloid established it to have the same molecular skeleton as the southeastern portion of **48**, yet with an additional proton at C-6′ (Figure 69).
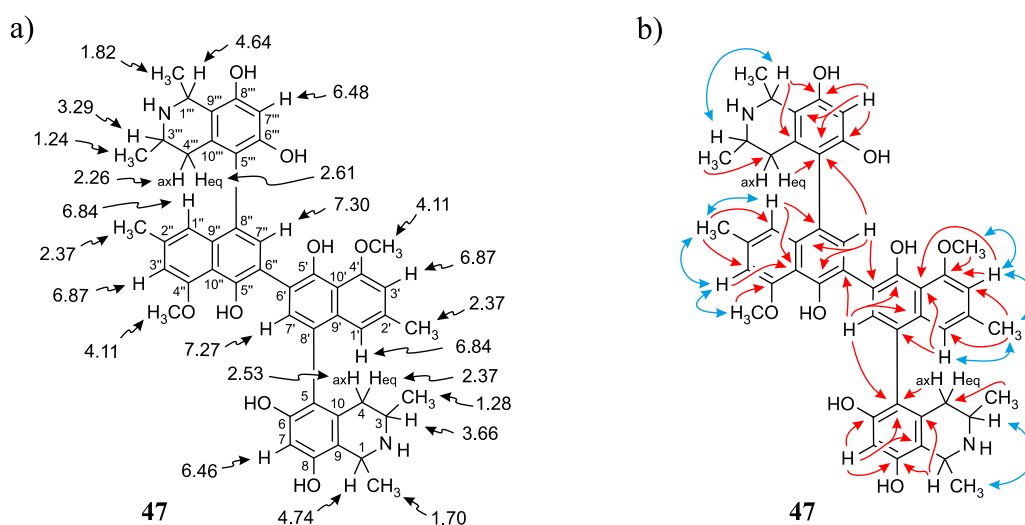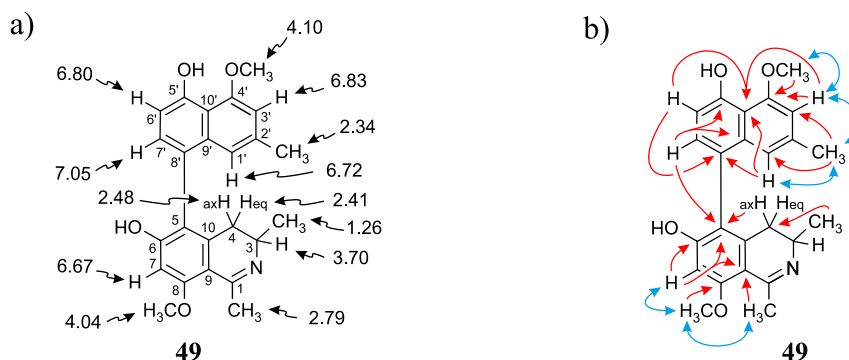

Figure 69. Selected NMR data of ancistrobonsoline A$_1$ (**49**): a) ^{1}H chemical shifts in ppm; and b) HMBC (red single arrows) and NOESY (blue double arrows) correlations relevant for the constitution.

The ROESY interactions across the biaryl axis of **49** were all similar to those in the southeastern portion of **48** (Figure 70a), as also the results of the oxidative degradation. This monomeric alkaloid thus possessed the absolute stereostructure **49**, as presented in Figure 70b. It was, consequently, the as yet undescribed enantiomer of the known alkaloid 6,5′-*O,O*-didemethylancistroealaine A (*ent*-**49**).[102] The two compounds **49** and the *ent*-**49** thus constituted one the very rare cases of NIQ enantiomeric pair. In agreement with their opposite absolute configurations, their ECD spectra were fully mirror-image like (Figure 70c). Instead of the rational, but long name *ent*-6,5′-*O,O*-didemethylancistroealaine A, the new compound was named ancistrobonsoline A$_1$, after the Congolese village Bonsolerive, where the plant had been collected.
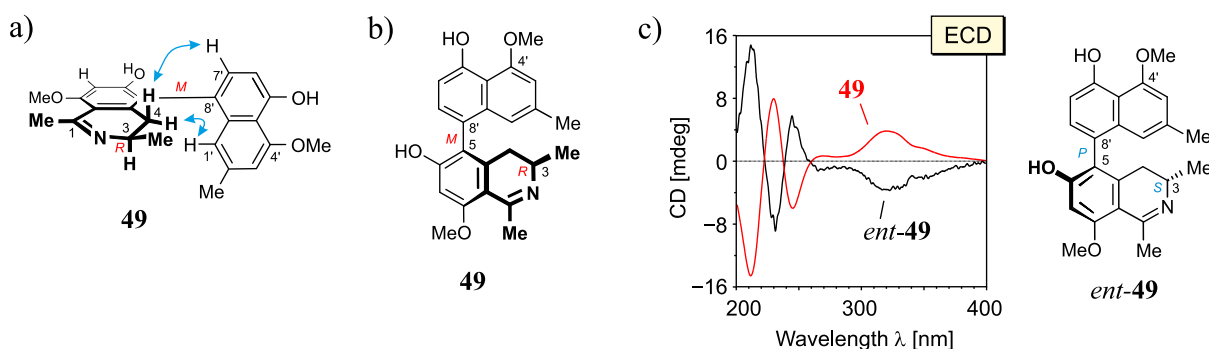
Figure 70. a) NOESY (blue double arrows) interactions indicating the relative and − given the results of oxidative degradation − absolute configurations of ancistrobonsoline A$_1$ (**49**); b) absolute stereostructure of ancistrobonsoline A$_1$ (**49**); and c) comparison of the ECD spectrum of **49** with that of its previously known natural enantiomer, *ent*-**49** (= 6,5′-*O,O*-didemethylancistroealaine A),[102] further confirming the absolute stereostructure of **49**.

4.3.6. Ancistrobonsoline A$_2$ (50)

The sixth new compound discovered during these investigations (Peak 10, Figure 59b) was attributed the molecular formula $C_{25}H_{27}NO_4$ according to the observation of its mono-protonated molecule at *m/z* 406.2013 in HRESIMS. Its ^{1}H NMR spectrum was very similar to that of **49**, indicating the presence of a 1,3-dimethyldihydroisoquinoline, yet with the signal of an additional *O*-methyl group at 3.83 ppm, linked either to *O*-6 or to *O*-5′. NOE interactions of the protons of that *O*-methyl group with H-7, together with their joint HMBC correlations to C-6, clearly located that methoxy function to be at C-6 (Figure 71).
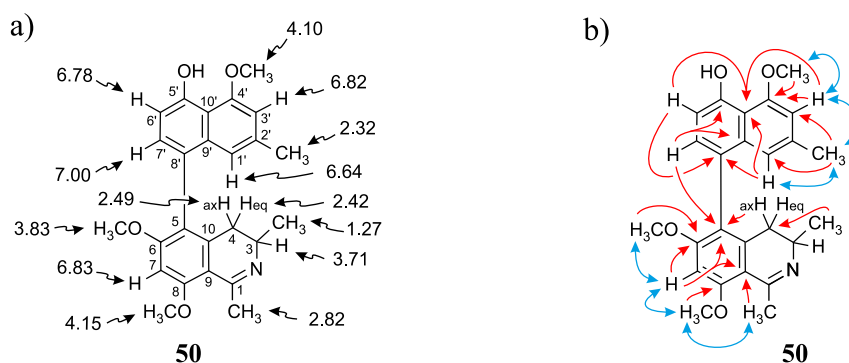
Figure 71. Selected NMR data of ancistrobonsoline A$_2$ (**50**): a) ^{1}H chemical shifts in ppm; and b) HMBC (red single arrows) and NOESY (blue double arrows) correlations relevant for the constitution.

The absolute configuration at the stereocenter C-3 of **50** was determined to be *R* by oxidative degradation, which, as in the case of **49**, provided (*R*)-3-aminobutyric acid. Across the biaryl axis, the specific relationships between the diastereotopic protons at C-4 and the aromatic protons H-1′ and H-7′ were the same as in **49** (Figure 72a): H$_{ax}$-4 ('up') interacted with H-7′ and H$_{eq}$-4 ('down') with H-1′, which was consistent with an *M*-configuration at the 5,8′-axis. This absolute stereochemical assignment was further corroborated by the close similarity of the ECD spectrum of **50** with that of **49** (Figure 72b). Therefore, the new alkaloid had to possess the absolute stereostructure **50**, as presented in Figure 72c, and was, thus, the 6-*O*-methylated derivative of **49**. It was named ancistrobonsoline A$_2$. With their *R*-configuration at the stereocenter and *M* at the biaryl axis, ancistrobonsolines A$_1$ (**49**) and A$_2$ (**50**) belong to a very small subgroup of naphthyldihydroisoquinolines displaying such stereochemical features, with previously only one single representative, ancistrolikokine F, which differs from **49** only by the position of the *O*-methyl group in the naphthalene portion, which is at C-5′, instead of C-4′ as in **49**.[167]
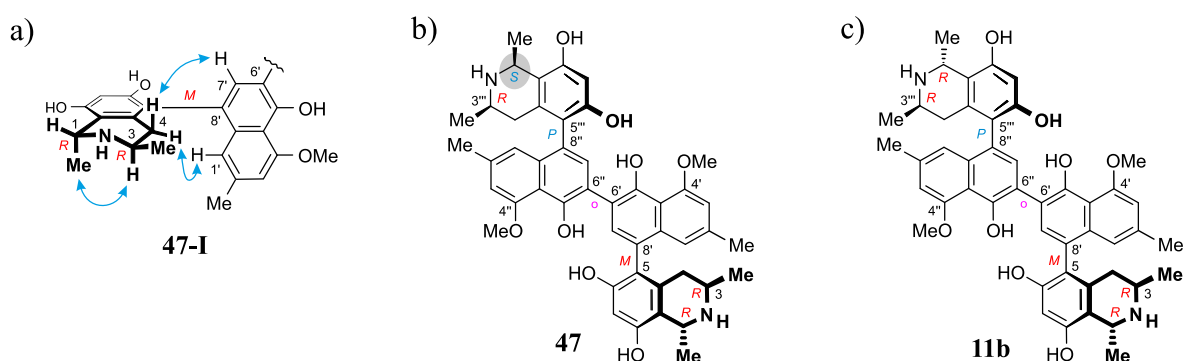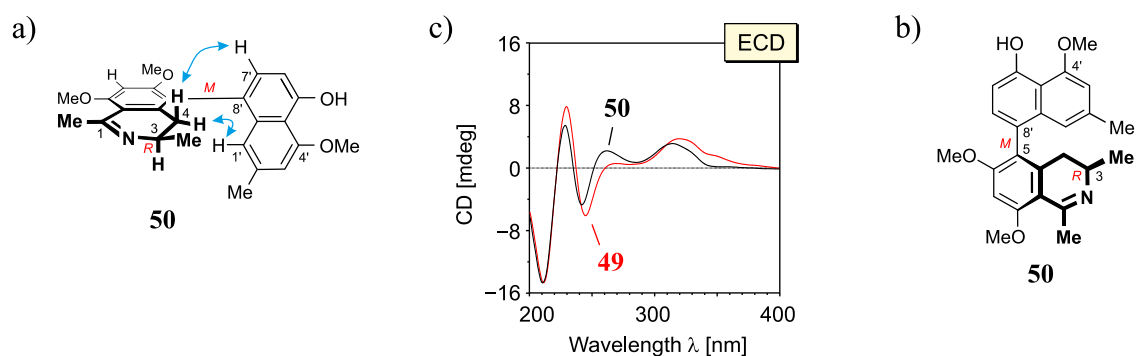

Figure 72. a) NOESY (blue double arrows) interactions indicating the relative and – given the results of the oxidative degradation – absolute configurations of ancistrobonsoline A$_2$ (**50**); b) comparison of the ECD spectrum of **50** with that of the structurally related, co-occurring ancistrobonsoline A$_1$ (**50**); and c) absolute stereostructure of ancistrobonsoline A$_2$ (**49**).

4.4.   Chemotaxonomic and Biosynthetic Significance of the Isolated Metabolites

The molecular architectures of the alkaloids thus isolated from this as yet unidentified *Ancistrocladus* taxon were remarkable in many respects. Firstly, it was striking that all of these compounds belonged to the same 5,8′-coupling type and, where dimers were concerned, they are all based on a central 6′,6″-axis. Such a specific phenol-oxidative coupling – and, thus strict enzymic assistance – had so far been observed only in *A. likoko*.[55,167-170]

These findings thus revealed a close phylogenetic relationship between the two taxa (in addition to their aforementioned morphological similarities), but delineated one from the other by the fact that the naphthalene moieties of the metabolites produced by the plant from the proximity of Bonsolerive were, all of them, *O*-methylated only at C-4′ (and at C-4″, in the case of dimers), not at C-5′ (nor at C-5″). And their configuration at C-3 (or/and at C-3‴, for dimeric compounds) was always *R*, except for the *N*-methylated isoquinoline portions, where an exclusive *S*-configuration was observed (Figure 58). Such a regioselective *O*-methylation in the naphthalene subunits and a stereospecificity at C-3 (and/or at C-3‴) were not known from *A. likoko* (nor from any other related plant). Likewise demarcating these two taxa was the fact that *A. likoko* was a virtually exclusive producer of monomeric alkaloids: out of more than 35 metabolites, only six dimers had so far been isolated from this species, and if so, only obtained as minor, or even as trace metabolites.[55,167-170] The plant investigated here, by contrast, was a rich source of dimeric compounds.

Moreover, the remarkable occurrence of dimers with a symmetric 6′,6″-coupling at the central axis chemotaxonomically delineated this taxon from the other – likewise still unidentified – liana species that occurs in the same area (see Chapter 3).[81] The latter was known to produce a drastically different metabolic pattern, including novel dimers with unsymmetric, 6′,1″-coupled central axes,[80] with additional oxygen bridges[124] and/or acetal linkages,[123] (i.e., open-chain, cyclo- , and spirombandakamines), but so far with no symmetric, 6′,6″-coupled ones, not even in traces, as described the Chapter 3.

Secondly, it is particularly noteworthy that this liana produced the 1,3-*trans*-configured korupensamine A (**52a**) only in small quantities (Peak 2, Figure 59a) and showed no hints at the presence of its dimer, michellamine A (**11a**), not even in traces.[62] This is exceptional, since all of the plants known to produce michellamine-type alkaloids, viz., *A. korupensis*,[62,75] *A. congolesis*,[172] and *A. likoko*,[167,168] always contained michellamine A (**11a**) as one of the main dimeric compounds. Moreover, **11a** was always accompanied by its monomer,

korupensamine A (**52a**), likewise occurring as a major metabolite in those plants.[62,75,172] For this reason, it had even been suggested[172] that other (minor) dimeric analogs differing from michellamine A (**11a**) by the configurations at the stereocenters may originate from the preformed 'parent' dimer michellamine A (**11a**), i.e., by modification after the dimerization step. In the case of the metabolites of the plant investigated here, however, one of the main constituents (Peak 4, Figure 59a), michellamine A_6 (**45**), was twofold 1,3-*cis*-configured and could be regarded as a bis-epimer of michellamine A (**11a**) at C-1 and C-1‴. Since **45** was accompanied by an unusually large quantity of its – likewise *cis*-configured – monomer (Peak 1, Figure 59a), ancistroealaine C (= 1-*epi*-korupensamine A) (**51**), it seemed likely that **45** (as also **46**) originated from the correspondingly preformed *cis*-monomers.

4.5.   Biological Activities of the Isolated Metabolites

4.5.1.   *Antiprotozoal Properties*

Like in the case of the novel mbandakamine-type dimers (presented in Chapter 3), which were tested against the pathogens causing malaria (*Plasmodium falciparum*), human African sleeping sickness (*T. b. rhodesiense*), Chagas' disease (*T. cruzi*), and visceral leishmaniosis (*L. donovani*), the two new monomers ancistrobonsolines A_1 (**49**) and A_2 (**50**) were also assessed against these parasites. These antiprotozoal tests were carried out in the group of Prof. R. Brun (Basel, Switzerland), as already mentioned. The other isolated new michellamine-type dimeric NIQs **45-48** were not evaluated, since their analogs had previously been found inactive.[75,196] As shown in Table 3, compounds **49** and **50** exhibited weak-to-moderate inhibitory properties. Of particular interest were the results of **49** and **50**, which revealed the MeO/OH substitution pattern to play a crucial role for the bioactivities: an *O*-methylation seemed to be favorable for the antiplasmodial and antitrypanosomal activities, but disadvantageous for the antileishmanial activity. This finding complemented previous results on the antileishmanial activities of related alkaloids, yet with *P*-configuration at the axis and *S* at C-3.[102] Likewise interesting were the antiprotozoal activities of **49** and its enantiomer (Table 3), which were – in the case of *T. cruzi* drastically – different from one to another, documenting, once again, the impact of the absolute stereostructure on the bioactivity.

Table 3. Antiprotozoal activities of the new monomeric NIQs **49** and **50**, and previously reported[102] data of the enantiomer of **49**.

Cpd.	IC_{50} $(SI)^{a,b}$					
	P. falciparum		*T. brucei rhodesiense* STIB900	*T. cruzi* Tulahuen C2C4 Lac Z	*L. donovani* axenic amastigotes MHOM/ ET/67/L82	Cytotoxicity (L6 cells)
	K1	NF54				
Standard	0.31^c	0.01^c	0.04^d	5.69^e	1.08^f	0.01^g
49	2.7 (43)	2.1 (54.7)	44.4 (2.6)	109.3 (1)	87.9 (1)	114.9
ent-**49**^{h}	5.4	n. d.	24.8	16.3	43.4	>230
50	1.8 (29.3)	2.4 (22)	12.6 (4.6)	80.1 (>1)	246.6 (<1)	52.8

^{a} Values are given in μM; ^{b} SI: Selectivity Index; ^{c} Chloroquine; ^{d} Melarsoprol; ^{e} Benznidazole; ^{f} Miltefosine; ^{g} Podophyllotoxin; ^{h} previously reported values (see ref. [102]); n.d.: not determined.

4.5.2. *Anti-HeLa Cells Potential: Cytotoxicity and Effects on Cell Morphology*

In the framework of the already mentioned cooperation with the group of Prof. S. Awale, for investigating the potential of NIQs towards different cancer cell lines, the isolated compounds were tested for their cytotoxic activity against HeLa human cervical cancer cells (Table 4). Interestingly, the new twofold 1,3-*cis*-configured quateraryl compounds, michellamines A$_6$ (**45**) and A$_7$ (**46**), and the likewise new monomeric NIQ alkaloids, ancistrobonsolines A$_1$ (**49**) and A$_2$ (**50**), displayed strong cytotoxic activity, with IC_{50} values between 14.8 and 21.5 μM. The most potent cytotoxicity (IC_{50} = 8.8 μM) was displayed by michellamine E (**54**), which was even more active than the positive control 5-fluorouracil (**44**) (IC_{50} = 13.9 μM), an anticancer drug in clinical use.

Michellamine E (**54**) was, therefore, investigated for its effects on cell morphology and apoptosis using two distinct staining methods, the Hoechst 33342 staining and the ethidium bromide-acridine orange (EB-AO) double-staining assay. In the Hoechst 33342 staining, the dye penetrates through the cell membrane and intercalates with DNA and emits blue fluorescence.[199] As shown in Figure 73, untreated HeLa cells (the control) displayed regular cell morphology with the intact nuclei. However, treatment with 12.5 μM of **54** induced nuclear fragmentation, suggestive of cells undergoing apoptosis, as indicated by fragmented nuclei exemplarily shown by white arrows in Figure 73. The EB-AO assay, on the other hand,

allows visualizing the cellular morphology as well as the distinction between the live and dead cells. Acridine orange (AO) is a cell-membrane permeable dye emitting bright-green fluorescence in live cells, while ethidium bromide (EB) penetrates only the membrane of dying or dead cells staining them red.[199] As shown in Figure 74, untreated HeLa cells (the control) displayed intact, regular cell morphology with exclusive bright green fluorescence in AO-EB staining. Treatment of the tumor cells with 12.5 μM of **54**, however, disrupted the cellular integrity leading to rounding of the cell membrane, membrane rupture, and disintegration of cellular contents resulting in an increased population of red EB fluorescence of dead cells (Figure 74).

Table 4. Growth-inhibitory activities of the isolated compounds **45-54** against HeLa cervical cancer cells (IC_{50}) and, following the antiausterity strategy, against the human PANC-1 pancreatic cancer cell line (PC_{50}).

Cpd.	HeLa (IC_{50} in μM)	PANC-1 (PC_{50} in μM)
Standard	13.9^a	0.8^b
45	14.8	54.2
46	20.6	24.3
47	46.3	50.3
48	29.8	60.2
49	14.3	7.5
50	21.5	12.1
51	30.5	>100
52a	48.3	>100
52b	37.8	94.9
53	32.1	19.3
54	8.8	18.9

^{a} 5-Fluorouracil (**44**)　　^{b} Arctigenin (**43**)
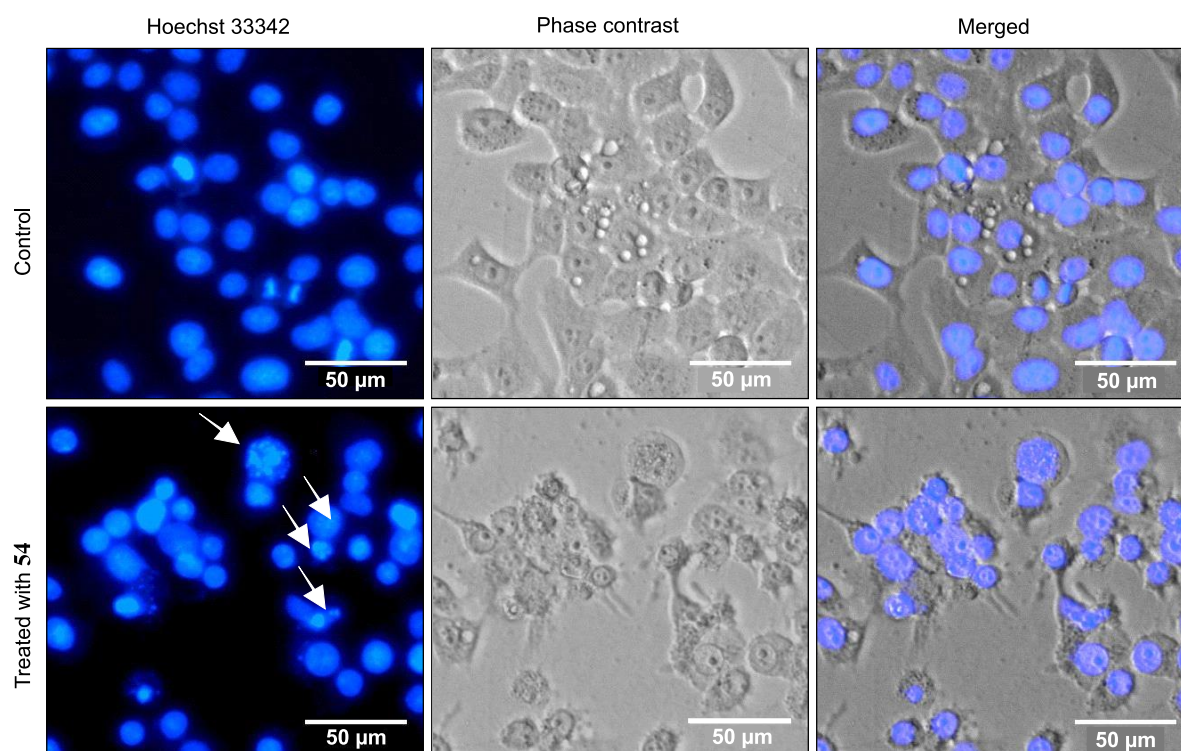
Figure 73. Hoechst 33342 nuclei staining revealing the morphological changes of HeLa human cervical cancer cells induced by 12.5 µM of michellamine E (**54**) in comparison to untreated control.
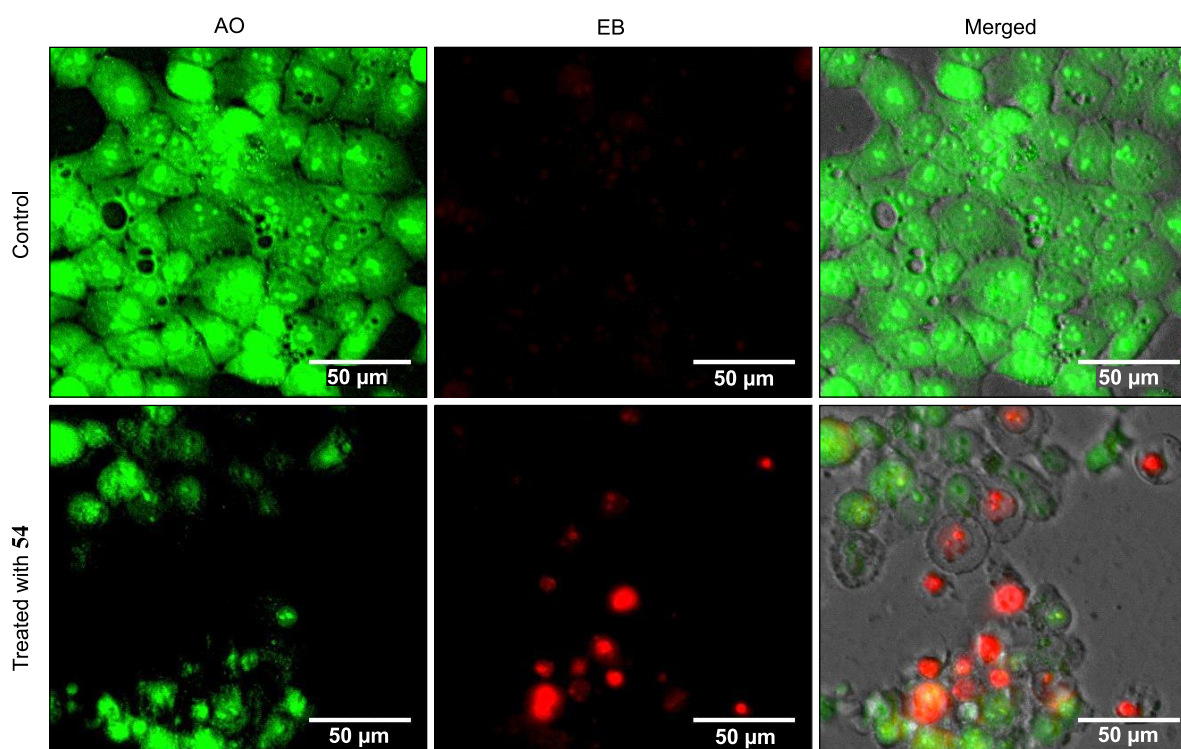
Figure 74. Morphological alterations of HeLa human cervical cancer cells induced by 12.5 µM of michellamine E (**54**) in comparison to untreated control, as revealed by the double acridine orange (AO) – ethidium bromide (EB) staining assay.

4.5.3. *Preferential Cytotoxicity against PANC-1 Human Cancer Cells and Effects on Cell Morphology*

Following the recently developed antiausterity strategy,[187,189-191] as explained above (see Section 3.10.2), the isolated NIQs **45–54** were tested against PANC-1 pancreatic cancer cells. The new dimer michellamine A_7 (**46**) and its previously known analogs michellamines A_2 (**53**) and E (**54**) exhibited significant preferential cytotoxicities against PANC-1 cells in a concentration-dependent manner, as exemplarily illustrated in Figure 75. Their PC_{50} values (i.e., the concentration at which 50% of the cells are preferentially killed under nutrient-deprived conditions, without cytotoxicity in normal, nutrient-rich medium) ranged from 18.9 to 24.3 µM, but were surpassed by the even higher activities of the new monomeric compounds ancistrobonsolines A_1 (**49**) and A_2 (**50**), with PC_{50} values of 7.5 and 12.1 µM, respectively (Table 4, see above).
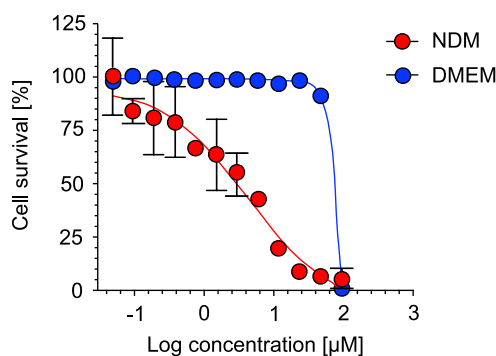
Figure 75. Cytotoxic activity of the new compound ancistrobonsoline A_2 (**50**) against the PANC-1 human pancreatic cancer cell line in nutrient-deprived medium (NDM) and Dulbecco's modified Eagle's medium (DMEM); and b) cervical cancer HeLa cells.

The effects of ancistrobonsolines A_1 (**49**) and A_2 (**50**), as representatives of the compounds showing potent antiausterity activities, on the cell morphology and on apoptosis were further investigated by the EB-AO double-staining fluorescence assay as described above. As shown in Figure 76 (A and A′), the untreated PANC-1 cells, serving as the control, emitted the typical bright-green color, characteristic of living cells, exhibiting an intact cellular morphology. This, however, changed significantly when the cells were treated with 12.5 µM of **49** and **50**, as revealed by the yellow fluorescence resulting from the overlapping of light emitted by AO (green) and EB (red) (Figure 76, B′ and D′). With 25 µM, both compounds

induced a dramatic morphological alteration and disintegration of cellular organelles, leading to total cell death as illustrated by the virtually exclusive red stain in Figure 76 (C′ and E′).
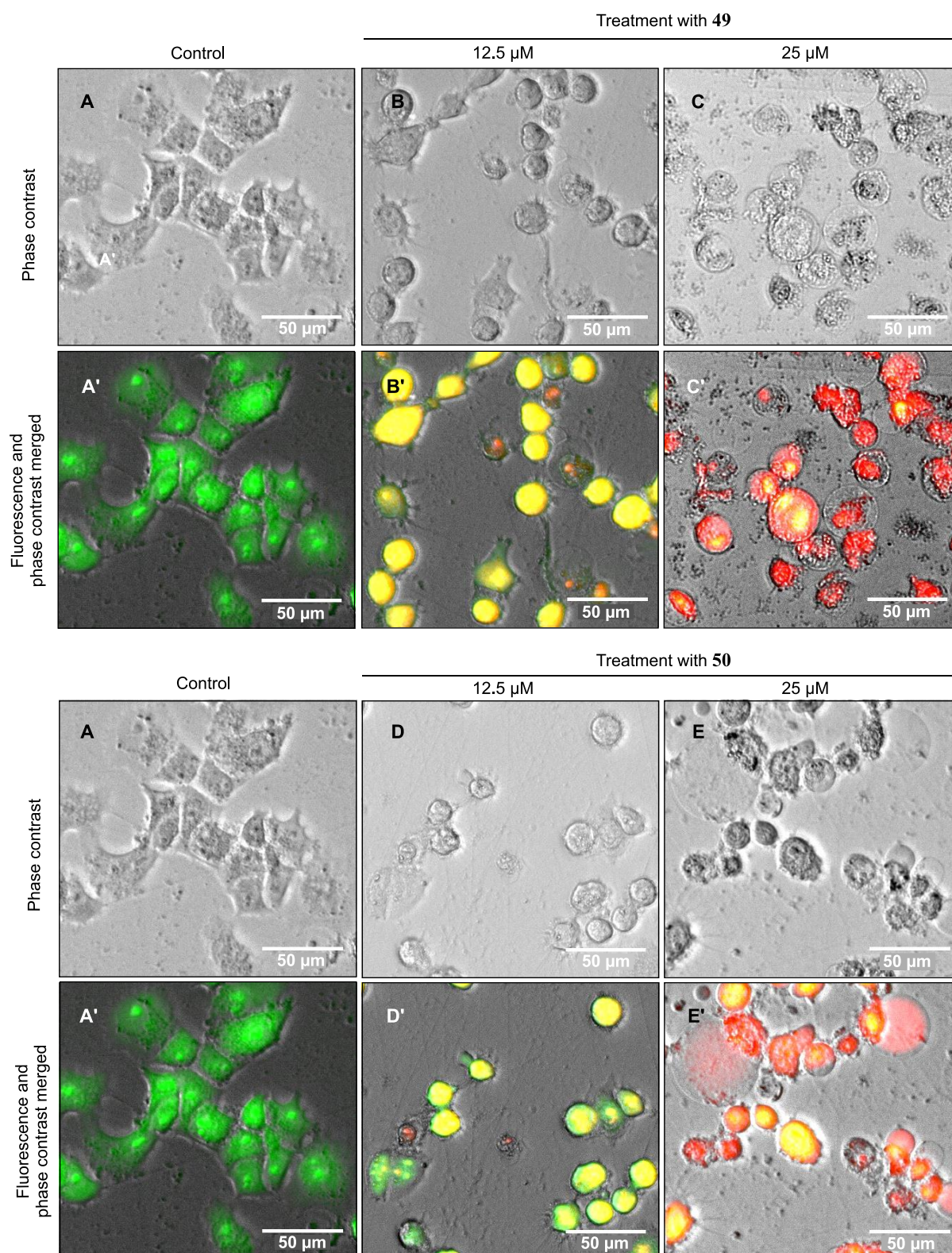
Figure 76. Morphological variations of PANC-1 human pancreatic cancer cells induced by the new compounds ancistrobonsolines A$_1$ (**49**) and A$_2$ (**50**) compared to the untreated ones (control).

Particularly noteworthy, the atropisomer of the new compound ancistrobonsoline A$_2$ (**50**), ancistrolikokine E$_3$, most recently been isolated from the twigs of the Congolese liana *A. likoko*, was found to be a much more promising antiausterity agent.[169] It displayed excellent preferential cytotoxicity against PANC-1 cells under nutrient-deprived conditions, with a PC$_{50}$ value of 2.5 μM, making it five times more effective than **50**.[169] Further, advanced investigations revealed this alkaloid to be capable of significantly preventing PANC-1 cell migration and colony formation in a concentration-dependent manner.[169] These properties were pharmacologically most important, as they demonstrated the potential of a particular compound for inhibiting the process of tumor metastasis formation. Mechanistic investigations suggested that ancistrolikokine E$_3$ inhibited the activation of the Akt/mTOR pathway and the expression levels of the key autophagy regulators Atg5, Atg12, Beclin-1, LC3-I, and LC3-II.[169]

All these results suggested that NIQs were promising lead structures for anticancer drug development.

5. Phytochemical Studies on a Congolese *Ancistrocladus* Species Related to *A. congolensis*

5.1. Introduction

During a field trip conducted in December 2014, S. M. Kavatsurwa (currently working as a PhD student at the University of Pretoria, under the co-supervision of Prof. G. Bringmann) discovered an *Ancistrocladus* liana occurring in the remote area of the village Yafunga, close to the north-central Congolese town Yangambi (for the map, see Figure 13). The size and shape of the leaves of this liana (up to ca. 28 cm long, 10.5 cm wide, elliptic to elliptic-obovate) as well as its fruits were all reminiscent of *A. congolensis*,[40,114] the only *Ancistrocladus* species reported to grow in that area and known to have similar morphological traits.[114] Phytochemically, *A. congolensis* is recognized as a rich source of both, mono- and michellamine-type dimeric naphthylisoquinolines.[172] Analysis of different plant extracts of the liana from Yafunga by HPLC-UV-MS, as performed by S. M. Kavatsurwa in collaboration with the author of this thesis, however, showed no hints at the presence of dimers, not even in traces. Moreover, the ruthenium-mediated oxidative degradation[156] of the alkaloid-enriched extract from this liana hinted at the occurrence of naphthylisoquinoline alkaloids that were exclusively *S*-configured at C-3 in the isoquinoline subunit, which clearly distinguished this *Ancistrocladus* plant from *A. congolensis*, and also from the other botanically described Congolese species, all known to produce both, 3*R*- and 3*S*-configured alkaloids.[60,167,172,174] These substantial phytochemical differences thus indicated that the liana might belong to a new, as yet undescribed plant species or subspecies. Besides further planned taxonomic investigations, including DNA fingerprinting,[81,88,200] the isolation and structural characterization of the alkaloids of this so far botanically unknown plant became a rewarding task, not only for a detailed chemotaxonomic description of the liana and its possible demarcation from other *Ancistrocladus* species, but also for the evaluation of the bioactivities of its constituents.

First phytochemical studies on this liana performed by Kavatsurwa resulted in the isolation and structural elucidation of the full three-dimension structures of four NIQs,[201] among them one new 5,8′-coupled alkaloid, named ancistroyafungine A (**56**), and three previously known metabolites: 6,5′-*O*,*O*-didemethylancistroealaine A (*ent*-**49**), and ancistrocladinium A (**9**) and B (**68**) (Figure 77). Subsequent isolation work, now performed by the author of this thesis, provided additional material of the above-mentioned metabolites for biological tests, and

yielded eleven further NIQs. Of these, three were previously unknown and were named ancistroyafungines B-D (**57-59**). The other remaining eight compounds were already known[56,102,202-204] from earlier investigations on related African and Asian *Ancistrocladus* species: 6-*O*-methylhamatine (**60**), 4′-*O*-demethylancistrocladine (**61**), ancistroguineine A (**62**), ancistrobertsonine A (**63**), ancistrobrevine B (**64**), ancistrotectoriline A (**65**), 6-*O*-demethylancistroealaine A (**66**), and 7-*epi*-ancistrobrevine D (**67**).

The following paragraphs report on the isolation and structural elucidation of these metabolites and discuss the geo- and chemotaxonomic position of this *Ancistrocladus* sp. with respect to other African and Asian *Ancistrocladus* species. Moreover, the antiausterity activities of the isolated compounds against human pancreatic cancer PANC-1 cells are presented.
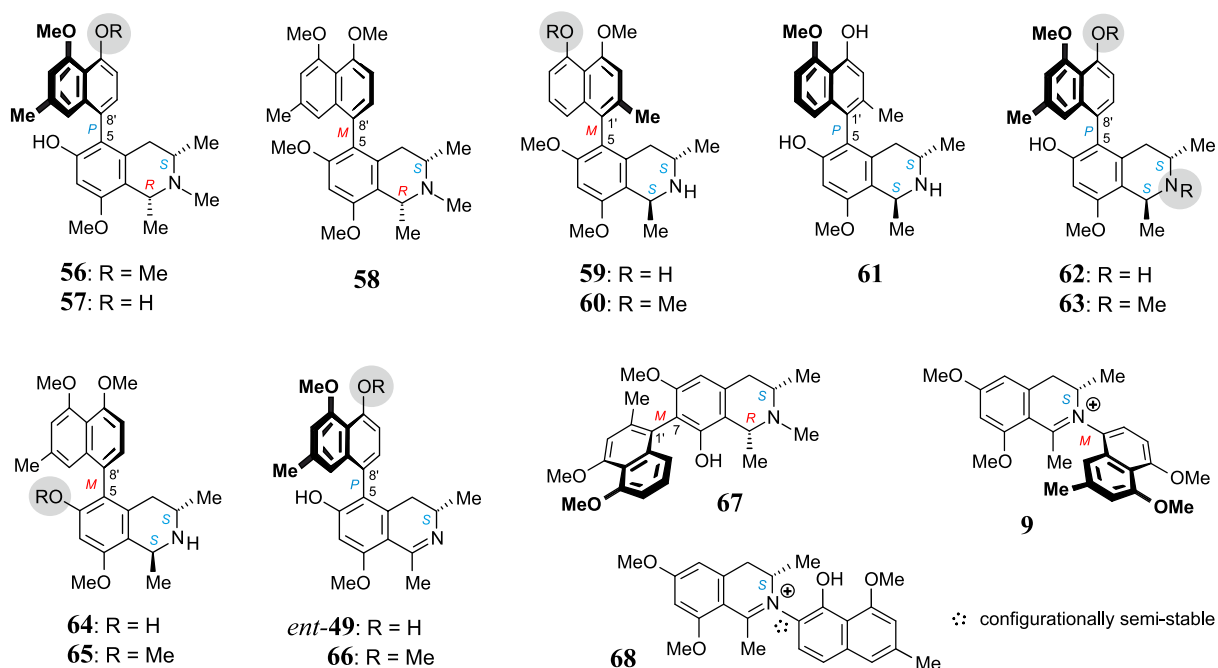
Figure 77. Metabolites isolated from an as yet unidentified Congolese *Ancistrocladus* plant discovered near the village Yafunga, among them four new compounds, ancistroyafungines A-D (**56-59**), and eleven known ones, 6-*O*-methylhamatine (**60**), 4′-*O*-demethylancistrocladine (**61**), ancistroguineine A (**62**), ancistrobertsonine A (**63**), ancistrobrevine B (**64**), ancistrotectoriline A (**65**), 6,5′-*O,O*-didemethylancistroealaine A (*ent*-**49**), 6-*O*-demethylancistroealaine A (**66**), 7-*epi*-ancistrobrevine D (**67**), and ancistrocladinium A (**9**) and B (**68**).

5.2.   Isolation and Identification of Known Compounds

Air-dried stem bark material of a botanically as yet unidentified *Ancistrocladus* species from the rainforest near the Congolese village Yafunga was ground and macerated in a mixture of dichloromethane and methanol (1:1). After filtration and evaporation of the solvent under reduced pressure, the crude extract was sonicated in water and the resulting aqueous filtrate was extracted with dichloromethane. The organic phase was evaporated to dryness, dissolved in methanol, and submitted to preparative reversed-phase HPLC, yielding 13 fractions. Further resolution of the obtained fractions on a semi-preparative HPLC column provided 15 alkaloids, which subsequently were structurally elucidated.

The first two metabolites, obtained from the two slowest-eluting fractions, were identified to be the cationic *N,C*-coupled ancistrocladinium A (**9**) and B (**68**), previously known from Congolese,[56,165] Vietnamese,[205] and Chinese[206] *Ancistrocladus* species. The third compound was revealed to be the 7,1′-coupled 7-*epi*-ancistrobrevine D (**67**), earlier known from investigations on *A. cochinchinensis*[207] and *A. tectorius*.[208] The fourth alkaloid was found to be the aforementioned enantiomer of the new, herein described NIQ ancistrobonsoline A$_1$ (**49**) (see chapter 4). This isomer (i.e., *ent*-**49**) had previously been detected from an as yet botanically uncharacterized Congolese *Ancistrocladus* species.[102] The fifth compound was established to be the 5′-*O*-methyl analog of *ent*-**49**; this derivative (i.e., alkaloid **66**) had been discovered along with *ent*-**49** in the same above-cited Congolese *Ancistrocladus* taxon.[102] The sixth isolated constituent was evidenced to be ancistrobrevine B (**64**), well-known as the very first monomeric NIQ with a 5,8′-axis, described in 1992 from *A. abbreviatus*.[204] It has meanwhile been found in other related African species, among them *A. congolensis*[172] and *A. robertsonium*.[209] The seventh compound was found to be the 6-*O*-methyl derivative of **64**, ancistrotectoriline A (**65**), previously reported from *A. tectorius*,[210,211] *A. tanzaniensis*,[212] and *A. ealaensis*.[166] The eighth and ninth alkaloids were likewise 5,8′-coupled, identical to ancistroguineine A (**62**) and ancistrobertsonine A (**63**), earlier known to be produced by *A. guineënsis*[213] and *A. robertsonium*,[203] respectively. The tenth compound was demonstrated to be identical to 4′-*O*-demethylancistrocladine (**61**), a 5,1′-linked metabolite known to be produced by the Asian taxa *A. tectorius*[202,214] and *A. cochinchinensis*.[205] The eleventh metabolite was identified to be 6-*O*-methylhamatine (**60**), formerly detected in *A. tectorius*[214] and in some Congolese *Ancistrocladus* taxa, including *A. congolensis*[172] and *A. ileboensis*.[102] The remaining four obtained compounds were as yet unknown; their structural elucidation is thus described in the following parts.

5.3.   Structural Elucidation of the New Compounds

5.3.1.   *Ancistroyafungine A (56)*

The first of these new metabolites had a molecular formula of $C_{26}H_{31}NO_4$, as deduced from its monoprotonated molecule at *m/z* 422.2333 by HRESIMS, which, together with the UV spectrum, suggested it to be a naphthyltetrahydroisoquinoline alkaloid. This was further corroborated by its ^{1}H NMR spectrum. In the aliphatic region, it exhibited a quartet (H-1, 4.65 ppm, *J* = 6.6 Hz), a multiplet (H-3, 4.65 ppm), two diastereotopic protons (H_{ax}-4, 2.58 ppm, *J* = 17.2, 11.5 Hz; H_{eq}-4, 2.21 ppm, *J* = 17.2, 3.1 Hz), and three *O*-methyl groups (3.92, 3.93, and 3.96 ppm). Likewise observed in that spectral part were two three-proton doublets (1.26 ppm, *J* = 6.5 Hz; 1.72 ppm, *J* = 6.5 Hz), characteristic of CH_3-3 and CH_3-1, and two three-proton singlets: one at 2.31 ppm, evidencing an aryl-methyl group (CH_3-2′), and the other one at 3.02 ppm, suggesting the presence of an *N*-methyl group. In the aromatic region of the spectrum, the existence of two *meta*-coupled protons (6.69 and 6.79 ppm, *J* = 0.9 Hz), together with one singlet (6.60 ppm) and an AB spin system (6.94 and 7.16 ppm, *J* = 7.9 Hz), indicated that the coupling site of the naphthalene moiety was either C-8′ or C-6′. The latter possibility was excluded due to the fact that one of the AB spin system protons (the doublet signal at 6.79 ppm) was evidenced to be at C-6′ (106.9 ppm), by HMBC correlations from both, H-6′ and CH_3O-5′ (3.96 ppm, s) to the carbon atom C-5′ (158.6 ppm), so that the biaryl axis in this molecular portion had to be located at C-8′ (Figure 78).

In the isoquinoline part, the coupling position was deduced to be C-5, based on the joint HMBC correlations from the diastereotopic protons (H_{ax}-4 and H_{eq}-4) and H-7′ (7.16 ppm, d, *J* = 7.9 Hz) to C-5 (120.3 ppm). These interactions were complemented by another long-range HMBC coupling between the same carbon atom (C-5) and the aromatic singlet proton H-7 (6.60 ppm). The aforementioned hint at the presence of an *N*-methyl group was further confirmed by the deshielded chemical shift of the carbon signal corresponding to that methyl group (41.9 ppm), and by the HMBC cross-peaks between the *N*-methyl protons and both, C-1 (62.4 ppm) and C-3 (60.9 ppm) (Figure 78). Further HMBC signals involving a methoxy group at 3.92 ppm, H-7, and H-1, all of them with a deshielded quaternary carbon at 157.6 ppm, evidenced the latter nucleus to be C-8, to which that *O*-methyl substituent was linked. The remaining, third *O*-methyl group (3.93 ppm) was deduced to be located at C-4′ (158.9 ppm), based on its ROESY interactions with H-3′ (6.79 ppm, s) and the joint HMBC correlations of the 4′-*O*-methyl protons and H-3′ with C-4′ (Figure 78).

Figure 78. Selected NMR data of ancistroyafungine A (**56**): a) ^{1}H chemical shifts in ppm; and b) key HMBC (red single arrows) and NOESY (blue double arrows) correlations.

The relative configuration at the stereocenters C-1 and C-3 was determined to be *cis* from NOESY interactions between H-1 and H-3 (Figure 79a). Ruthenium-mediated oxidative degradation[156] of the compound yielded *N*-methyl-3-aminobutyric acid exclusively as in the form of *S*-enantiomer, as assessed by GC-MSD analysis of its the Mosher derivatives. This clearly indicated that the stereocenter C-3 of the alkaloid was *S*-configured and, in view of the above-assigned *cis*-array of the two methyl groups at the chiral centers, C-1 had to be *R*-configured (Figure 79a).

In NOESY experiments, the equatorial proton at C-4 and the aromatic proton at C-1' were found to interact with each other. This through-space correlation showed the involved spin systems (H_{eq}-4 and H-1′) to be on the same side of the isoquinoline 'plane', which, given the above-established *S*-configuration at C-3, should be the upper face, as illustrated in Figure 2B, so that the configuration at the biaryl axis should be *P*. This stereochemical assignment was further corroborated by the complementary dipolar coupling of H_{ax}-4 with H-7′, both underneath, i.e., on the bottom side of the isoquinoline 'plane' (Figure 79a). Further confirmation came from the ECD curve of this compound, which was very similar to that of the likewise *P*-configured co-isolated alkaloid ancistrobertsonine A (**63**) (Figure 79b). Therefore, the isolated metabolite had the absolute stereostructure **56**, as presented in Figure 79c, and was named ancistroyafungine A, after the Congolese village Yafunga, where the plant material had been collected. It may also be referred to as the 6-*O*-demethylated analog of ancistrobertsonine C[209] or as the 1-epimer of ancistrobertsonine A (**63**).
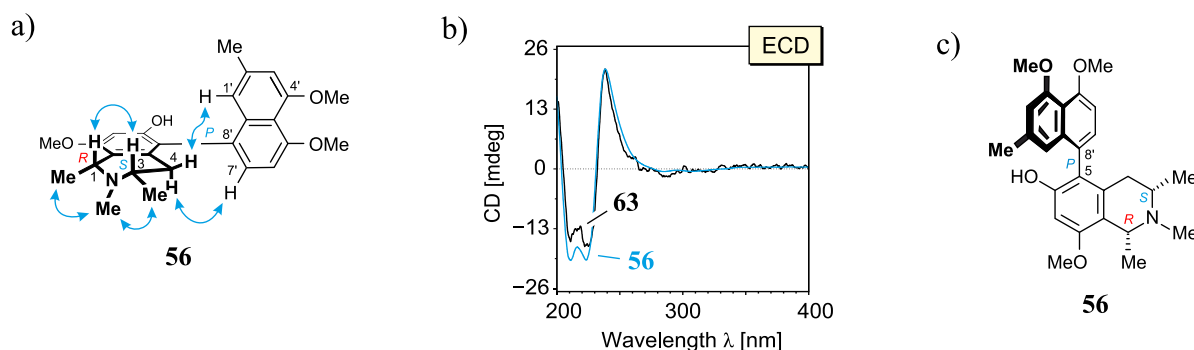
Figure 79. a) NOESY (blue double arrows) interactions indicating the relative and – given the results of the oxidative degradation – absolute configurations of ancistroyafungine A (**56**); b) comparison of the ECD spectrum of **56** with that of the known,[203] co-occurring ancistrobertsonine A (**63**); and c) absolute stereostructure of ancistroyafungine A (**56**).

5.3.2. Ancistroyafungine B (57)

The second new alkaloid was found to possess the molecular formula $C_{25}H_{29}NO_4$, as evidenced by HRESIMS measurement (*m/z* 408.2167 [M+H]$^+$). Its ^{1}H NMR spectrum was very similar to that of ancistroyafungine A (**56**), except for the fact that it had two methoxy groups (4.09 and 3.91 ppm), i.e., one *O*-methyl signal fewer than **56**, which indicated that it was an *O*-demethylated analog of **56** (Figure 80). The missing methyl group, as compared to the structure of **56**, was anticipated to be the one at *O*-5′, based on the fact that while superposing the proton NMR spectrum of **56** and that of the new alkaloid, the signal of H-6 of both compounds appeared to be the most affected one among all aromatic protons ($\Delta\delta_{H-6}$ = 0.13 and $\Delta\delta$ of other protons ≤ 0.06 unit). Further analysis of the 1D and 2D NMR spectra of the second new compound confirmed the above deduced constitution, being similar to that of **56**, but with a free phenolic hydroxy function at C-5′, instead of a 5′-methoxy group.
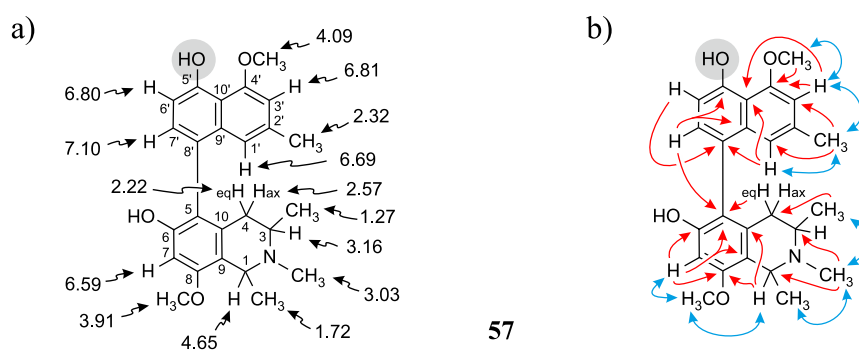
Figure 80. Selected NMR data of ancistroyafungine B (**57**): a) ^{1}H chemical shifts in ppm; and b) key HMBC (red single arrows) and NOESY (blue double arrows) correlations. The gray labeling indicates the structural difference as compared to **56** (see Figure 78).

In the NOESY experiment, the interactions of the protons at C-1 and C-3, and of those across the biaryl axis (Figure 81a), were all the same as in compound **56**: H-1 (4.65 ppm, q, J = 6.4 Hz) interacted with H-3 (3.16 ppm, m), H_{ax}-4 (2.57 ppm, dd, J = 17.3, 11.4 Hz) with H-1′ (6.69, pt, J = 1.1 Hz), and H_{eq}-4 (2.22 ppm, dd, J = 17.3, 3.1 Hz) with H-7′ (7.10, d, J = 7.9 Hz), so that the full absolute configuration of the isolated metabolite had to be either 1*R*,3*S*,5*P*, as in **56**, or 1*S*,3*R*,5*M*, i.e., fully opposite. The oxidative degradation provided (*S*)-*N*-methyl-3-aminobutyric acid, which showed that C-3 was *S*-configured, and the overall absolute configuration consequently had to be 1*R*,3*S*,5*P*, i.e., the same as that of **56**. This assignment was further corroborated by the fact that the ECD curve of the alkaloid was closely similar to that of **56**, as shown in Figure 81b. Hence, the second new alkaloid had the absolute stereostructure **57** as given in Figure 81c. It was, thus, the 5′-*O*-demethyl analog of **56** and was named ancistroyafungine B. It could likewise be addressed as 8-*O*-methylkorupensamine D.[196]
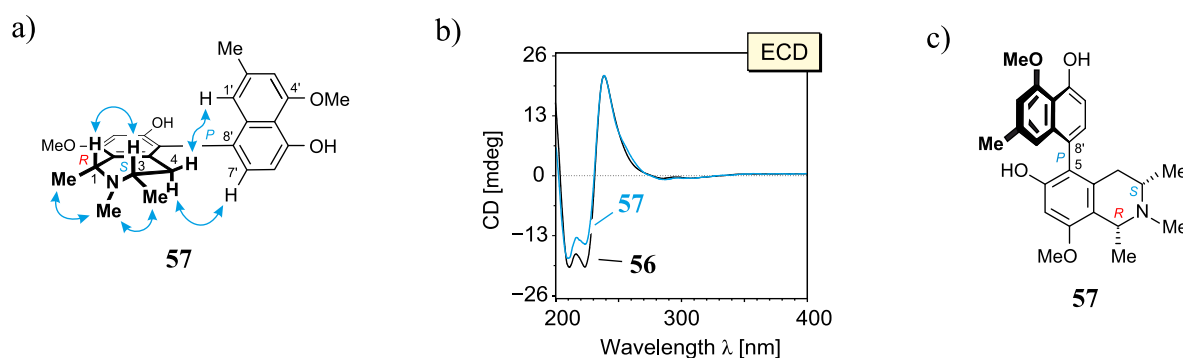
Figure 81. a) NOESY (blue double arrows) interactions indicating the relative and – given the results of the oxidative degradation – absolute configurations of ancistroyafungine B (**57**); b) comparison of the ECD spectrum of **57** with that of the above-described new compound ancistroyafungine A (**56**); and c) absolute stereostructure of ancistroyafungine B (**57**).

5.3.3. *Ancistroyafungine C (58)*

The third previously unknown metabolite had 14 mass units more than ancistroyanfugine A (**56**), consistent with a molecular formula of $C_{27}H_{33}NO_4$ (HRESIMS *m/z* 436.2486 [M+H]$^+$), which corresponded to a fully *O*- and *N*-methylated naphthyltetrahydroisoquinoline alkaloid. In its ^{1}H NMR spectrum, the presence of an AB spin system (H-6′, 6.91 ppm, d, J = 8.5 Hz) and H-7′ (7.10 ppm, d, J = 8.0 Hz) and of an aryl methyl singlet at 2.30 ppm suggested that the alkaloid again belonged to the 5,8′-coupling pattern, as already compounds **56** and **57**. This was confirmed by joint HMBC correlations from H_{eq}-4 (2.49 ppm, dd, J = 17.8, 3.5 Hz), H-7 (6.79 ppm), and H-7′ to C-5 (122.0 ppm) (Figure 82).
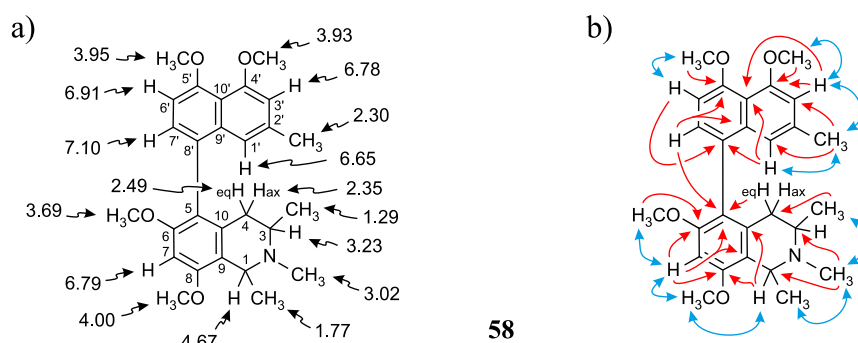
Figure 82. Selected NMR data of ancistroyafungine C (**58**): a) ^{1}H chemical shifts in ppm; and b) key HMBC (red single arrows) and NOESY (blue double arrows) correlations.

From NOESY interactions between H-1 and H-3, the relative configuration at the stereocenters C-1 *versus* C-3 was determined to be *cis* (Figure 83a), as in the cases of **56** and **57**. Likewise similar to **56** and **57** was the outcome of the oxidative degradation, which gave (*S*)-*N*-methyl-3-aminobutyric acid, showing that C-3 was *S*-configured and C-1 *R*-configured, as a consequence of the above mentioned *cis*-configuration. The correlations across the biaryl axis were, however, opposite to those observed in **56** and **57**, since now H$_{eq}$-4 interacted with H-7′, and H$_{ax}$-4 with H-1′, so that the axial configuration had to be opposite, too, i.e., *M*, as shown in Figure 83a. This was strongly supported by the ECD curve of **58**, which, displaying a negative ECD couplet, as expected for an *M*-array, was very similar to that of the co-occurring, likewise *M*-configured ancistrotectoriline A (**65**) (Figure 83b). Thus, this metabolite had the new absolute stereostructure **58**, as presented in Figure 83c, and was named ancistroyafungine C, in continuation of the series of new alkaloids isolated from this as yet unknown Congolese *Ancistrocladus* liana. It was, thus, the atropo-diastereomer of ancistrobertsonine C known from the Kenyan plant *A. robertsoniorum*.[209]
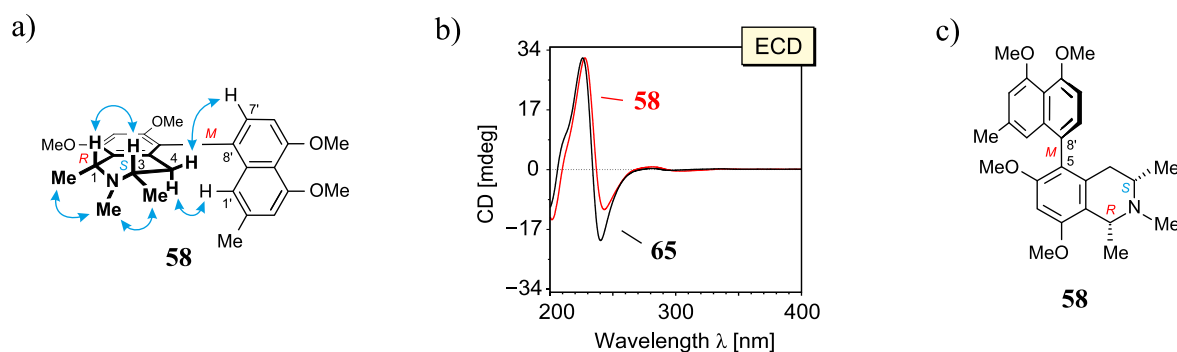
Figure 83. a) NOESY correlations establishing the relative and, together with the results of the oxidative degradation, the absolute configuration of ancistroyafungine C (**58**); b) further assignment of the axial configuration of **58** by comparison of its ECD curve with that of the co-occurring, likewise *M*-configured ancistrotectoriline A (**10**);[210] and c) absolute structure of ancistroyafungine C (**58**).

5.3.4. *Ancistroyafungine D (59)*

The fourth new compound discovered during these investigations was found to be isomeric to **57** by HRESIMS ($C_{25}H_{29}NO_4$, *m/z* 408.2168 $[M+H]^+$). Its ^1H NMR spectrum exhibited five aromatic protons, including two singlets (6.92 and 6.78 ppm) and an AMX spin system (7.11 ppm, dd, *J* = 7.7, 8.4 Hz; 6.70 ppm, dd, *J* = 1.0, 7.7 Hz; 6.54 ppm, dd, *J* = 1.1, 8.4 Hz), which suggested it to be a 7,1′-, 7,3′-, 5,1′-, or 5,3′-coupled naphthylisoquinoline alkaloid. In the aliphatic region, the CH$_3$-3 doublet signal appeared upfield (1.20 ppm), like in **56-58**, indicating the location of the biaryl axis in the isoquinoline portion to be at C-5 (156.3 ppm), and not at C-7 (as in the co-isolated compound **67**, see Figure 77), in which the ring current effect exerted by the naphthalene substituent would be effective at CH$_3$-3 only marginally.

In agreement with the above-mentioned findings, one aromatic singlet (6.78 ppm) was located at C-7 (95.6 ppm), based on the joint HBMC correlations from this proton and H-1 (4.80 ppm, q, *J* = 6.8 Hz) to an *O*-substituted aromatic carbon atom, C-8 (158.1 ppm) (Figure 84). The other aromatic singlet (6.92 ppm) was evidenced to be H-3′ by its NOESY interactions with the protons of one of the three *O*-methyl groups displayed by this compound (4.12 ppm), which was complemented by joint HMBC interactions from these nuclei (CH$_3$O-4′ and H-3′) to C-4′ (157.1 ppm). Therefore, this metabolite, different from the three new alkaloids described above, belonged to the subclass of 5,1′-coupled naphthylisoquinolines. The two remaining methoxy groups were found to be located at C-6 (159.7 ppm) and C-8 (158.1 ppm), based on the joint HMBC cross peaks from CH$_3$O-6 (3.68 ppm, s) and H-7 (6.78 ppm, s) to C-6 (159.7 ppm), and from H-7, H-1 (4.80 ppm, q, *J* = 6.8 Hz), and CH$_3$O-8 (4.01 ppm, s) to C-8 (158.1 ppm), together with the NOESY series CH$_3$O-6 ↔ H-7 ↔ CH$_3$O-8 ↔ CH$_3$-1 (1.64 ppm, d, *J* = 6.9 Hz).
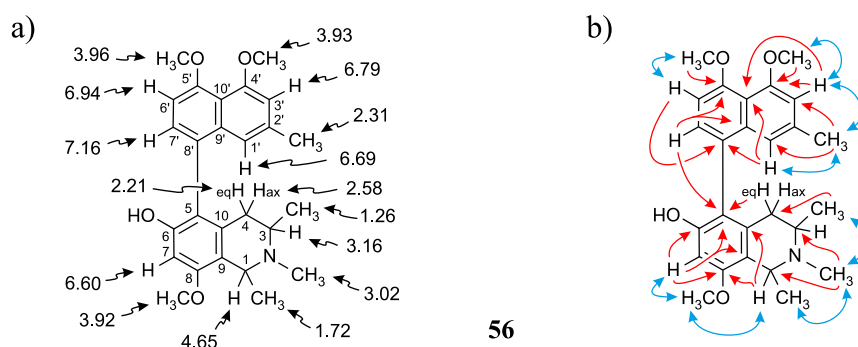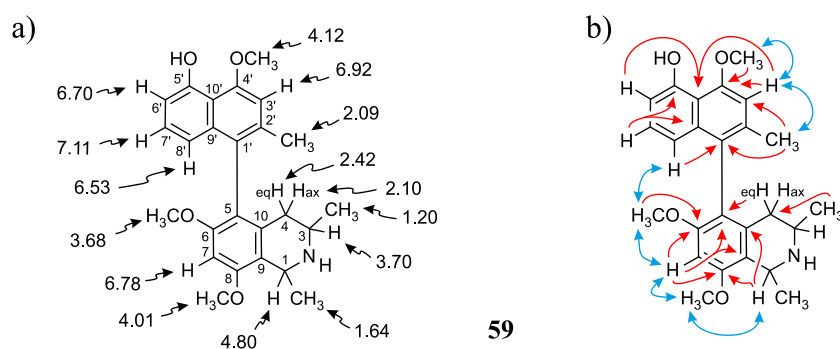

Figure 84. Selected NMR data of ancistroyafungine D (**59**): a) ^1H chemical shifts in ppm; and b) key HMBC (red single arrows) and NOESY (blue double arrows) correlations.

From an NOE correlation between H-3 and Me-1, the relative configuration at the stereocenters C-1 *versus* C-3 was deduced to be *trans* (Figure 85a). The oxidative degradation procedure provided the *S*-enantiomer of 3-aminobutyric acid, which revealed that C-3 was *S*-configured, and, due to the above-mentioned *trans*-arrangement of the methyl groups at the chiral centers, C-1 had to be *S*-configured, too. From NOESY interactions between H-8′ and H$_{ax}$-4, the naphthalene-isoquinoline biaryl axis was shown to be *M*-configured (Figure 85a). The great similarity of the ECD curve of this alkaloid with that of the known[102] and co-isolated, likewise 1*S*,3*S*,5*M*-configured 6-*O*-methylhamatine (**60**) (Figure 85b) confirmed the stereochemical assignment at the biaryl axis. Thus, the compound had the absolute stereostructure **59**, as presented in Figure 85c, and, hence, was the new 5′-*O*-demethyl-6-*O*-methyl analog of the well-known alkaloid hamatine, which occurs in various African and Asian *Ancistrocladus* species.[44,79,172,203,208] The new compound was named ancistroyafungine D.
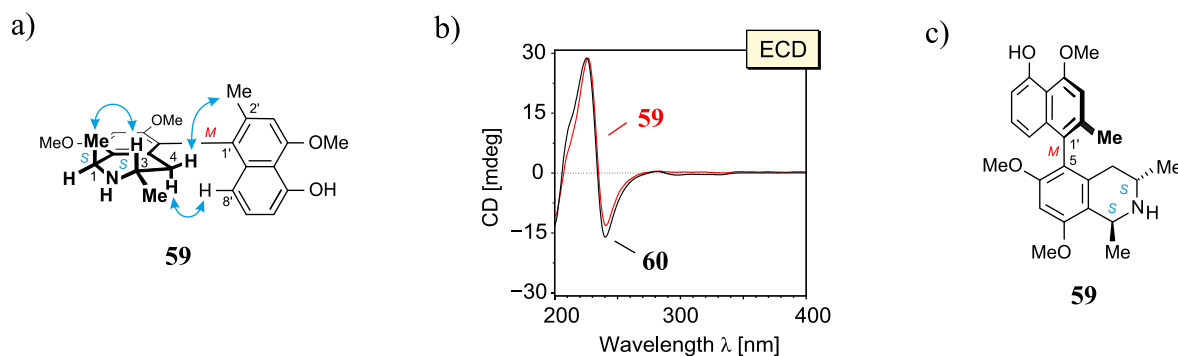
Figure 85. a) NOESY couplings establishing the relative and, with the results of the oxidative degradation, absolute configuration of ancistroyafungine D (**59**); b) the similarity between the ECD curve of **59** and that of the well-known,[102] likewise 1*S*,3*S*,5*M*-configured 6-*O*-methylhamatine (**60**), further corroborating the assigned absolute stereostructure of **59**, shown in c).

5.4.   Geo- and Chemotaxonomic Significance of the Isolated Metabolites

The stereostructures of the alkaloids obtained from this as yet unidentified Congolese *Ancistrocladus* liana were remarkable in many respects. The phytochemical results presented here corroborated the already mentioned preliminary hints at the absence of dimeric compounds, and strongly supported the initial detection of alkaloids with an exclusive *S*-configuration at C-3 in the alkaloid-enriched plant extract. The findings now clearly demarcated chemotaxonomically this liana from its morphologically most related species, *A. congolensis*, and from all the other botanically recognized Congolese *Ancistrocladus* taxa,

since they produced 3*R*- and 3*S*-configured alkaloids and a number of dimers.[148,166,167,172,173] This delineation is further highlighted by the variety of isolated compounds, showing five different coupling types, viz., 5,8′, 5,1′, 7,1′, *N*,6′, and *N*,8′. None of the known Congolese species has as yet shown such a structural diversity.

Furthermore, all the 15 isolated metabolites possessed an oxygen function at C-6, which, together with the 3*S*-configuration, assigned them to belong to the subclass of "Ancistrocladaceae-type" alkaloids,[44] typical of *Ancistrocladus* plants from Asia and East Africa.[44,50] Thus, the investigated liana appeared to occupy a special phylogenetic position within the Ancistrocladaceae family: from the geo- and chemotaxonomic point of view, it ranged between the naphthylisoquinoline-producing species from Asia and East Africa and the *Ancistrocladus* lianas from the Congo Basin; with the latter plants it shared morphological similarities.

Besides this plant, only one other liana, likewise yet undescribed and morphologically related to *A. congolensis*,[102] had so far been identified to occupy a similar position as a geo- and chemotaxonomic link between the Central African species and the East African taxa, with distinct similarities in particular to *A. robertsonium* from Kenya. From the latter, and from those two as yet unidentified Congolese species, a series of 5,1′-linked naphthylisoquinoline alkaloids related to ancistrocladine and hamatine had been isolated, along with a large number of 5,8′-coupled alkaloids. Some of the metabolites discovered in the two unknown Congolese lianas were analogs of the two main constituents of *A. robertsonium*, viz., ancistrobertsonines A (**63**) and C. But there were also clear differences in the metabolic profiles of those two as yet unidentified plants, as obvious from comparative HPLC-UV-MS investigations and, in particular, from the discovery of the new ancistroyafungines A-D (**56-59**) in the liana, as presented herein. This metabolic divergence and the fact that the two unidentified plants occur in two different regions (one was found in the central part of the Congolese rainforest near the city of Ikela, and the other – the plant here investigated – was collected far away, in the north-central Congolese village Yafunga) suggested that these lianas might represent different, but closely related new species or subspecies. Further botanical investigations are in progress.

5.5.   Antiausterity Activity against Human Pancreatic Cancer PANC-1 Cells: Cytotoxicity and Effects on Cell Morphology

Encouraged by the promising results on the antiausterity properties of some NIQs against human PANC-1 pancreatic cancer cells, as presented in the previous Chapter (see Section 4.5.3), and in order to gain more insight into the anticancer potential of this class of natural products, the alkaloids **56**-**65**, *ent*-**49**, **66**, and **67** isolated from this Congolese *Ancistrocladus* liana were tested for their preferential cytotoxicity against the human PANC-1 pancreatic cancer cell line. As shown in Table 5, all of the tested compounds showed moderate to strong antiausterity activities against PANC-1 cancer cells, in a concentration-dependent manner (Figure 86). Their PC_{50} values were at a micromolar level, ranging from 7.6 to 67.8 μM. Within this series of alkaloids, the new compounds ancistroyafungines B (**57**) and D (**59**) were the most potent representatives, and their PC_{50} values (7.6 and 9.7 μM, respectively) were even comparable to those of the most active monomeric alkaloids identified in previous studies.[103,167]

Table 5. Preferential cytotoxicity of the NIQs isolated from a Congolese *Ancistrocladus* species related to *A. congolensis* against human pancreatic cancer PANC-1 cells in NDM.

Cpd.	PC_{50}[a]	Cpd.	PC_{50}[a]
56	22.7	**63**	11.8
57	7.6	**64**	20.2
58	15.0	**65**	67.8
59	9.7	*ent*-**49**	9.8
60	31.9	**66**	14.0
61	11.2	**67**	29.9
62	15.8	Arctigenin (**43**)[b]	0.8

[a] Values are given in μM; [b] the positive control.

The test results showed that the degree of *O*-methylation in the naphthalene portion played a crucial role for the cytotoxic activities of NIQs. Ancistroyafungine A (**56**, PC_{50} = 22.7 μM), with two methoxy functions at C-5′ and C-4′, was found to be almost three times less active than its 5′-*O*-demethyl analog ancistroyafungine B (**57**, PC_{50} = 7.6 μM), which indicated that an MeO/OH pattern seemed favorable for the antiausterity activities. This tendency was also

supported by the activity of 6-*O*-methylhamatine (**60**, PC_{50} = 31.9 µM), which was less pronounced than that of its 5′-*O*-demethyl analog ancistroyafungine D (**59**, PC_{50} = 9.7 µM).
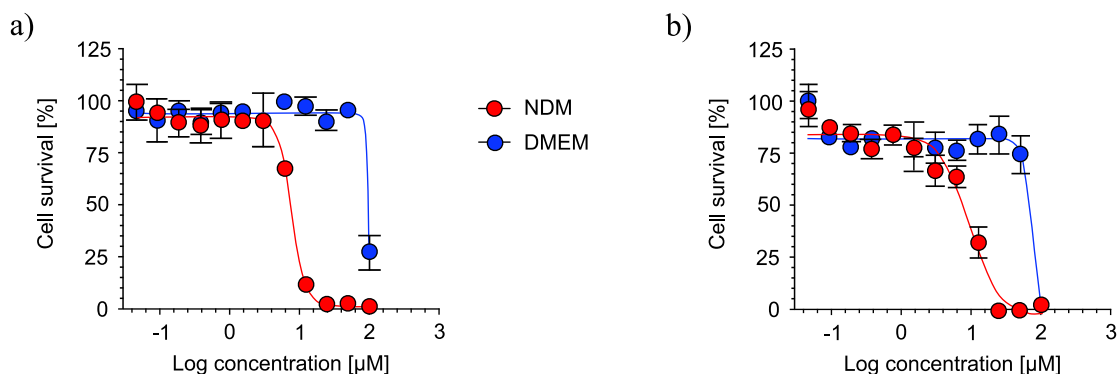
Figure 86. Cytotoxic activities of: a) ancistroyafungine B (**57**); and b) ancistroyafungine D (**59**) against the PANC-1 human pancreatic cancer cell line in nutrient-deprived medium (NDM) and in Dulbecco's modified Eagle's medium (DMEM).

In a similar manner, the substitution pattern of the isoquinoline portion seemed to play an important role for the cytotoxic activity of the alkaloids, too. This became evident from the activity of ancistrobrevine B (**65**, PC_{50} = 20.2 µM), possessing a mixed 6-OH/8-MeO substituted tetrahydroisoquinoline subunit, as compared to that of ancistrotectoriline A (**65**, PC_{50} = 67.8 µM), equipped with two methoxy groups at C-8 and C-6. This finding complemented previous results obtained for the two related alkaloids ancistrolikokines E and E$_2$,[167] yet both with *P*-configuration at the axis and *R*-configuration at C-3. The impact of stereochemical features on the preferential cytotoxicity thus evidenced was also highlighted by the different PC_{50} values of the 1-epimers ancistroyafungine A (**56**, PC_{50} = 22.7 µM) and ancistrobertsonine A (**63**, PC_{50} = 11.8 µM).

Another structural feature likewise showing a strong influence on the bioactivity was the location of the biaryl axis: The cytotoxic effect of 6-*O*-methylhamatine (**60**, PC_{50} = 31.9 µM), a 5,1′-coupled alkaloid, was more than two times stronger as compared to that of its 5,8′-coupled analog ancistrotectoriline A (**65**, PC_{50} = 67.8 µM). On the other hand, compounds **60** and **65** could also be considered as regioisomers with respect to the methyl group at C-2′ – being in the axis-bearing naphthalene ring of **60**, or once in the remote ring in the case of **65**.

The most active compound, ancistroyafungine B (**57**), was further studied for its effects against PANC-1 cell morphology under nutrient-deprived conditions using the ethidium bromide (EB) – acridine orange (AO) double-staining fluorescence assay. PANC-1 cells were

treated with 20 μM of **57**, and incubated in NDM, along with an untreated control. After 24 h of incubation, both treated and untreated cells were stained with the EB/AO reagents,[103] as in in the case of the new and potent NIQs ancistrobonsolines A_1 (**49**) and A_2 (**50**) described in the preceding chapter. AO emits bright green fluorescence in living cells, while EB is permeable only in dead or dying cells through ruptured cell membrane, and emits red fluorescence. As shown in Figure 87, control PANC-1 emitted bright green fluorescence with intact cell morphology. However, those treated with 20 μM of ancistroyafungine B (**57**) emitted red fluorescence exclusively (Figure 87), with a dramatic change in PANC-1 cell morphology. Therefore, ancistroyafungine B (**57**) was further studied for its effects against PANC-1 cells in NDM in real time using a live-cell imaging system. PANC-1 cells were treated with 20 μM of compound **57** in NDM and incubated in a stage-top humidified incubator at 37 °C and 5% CO_2; images were captured every 10 min on an EVOS FL digital cell imaging system for 19 h. The dynamic responses of the PANC-1 cells against the treatment with the alkaloid **57** can be viewed in the captures of the movie[104][215] shown in Figure 88. PANC-1 cells at the start of the test (T_0) had an intact morphology. Then, however, the cells lost the membrane integrity within 4 h and showed membrane blebbing and rounding, followed by rupture of cell membrane, leading to total cell death within 10 h.
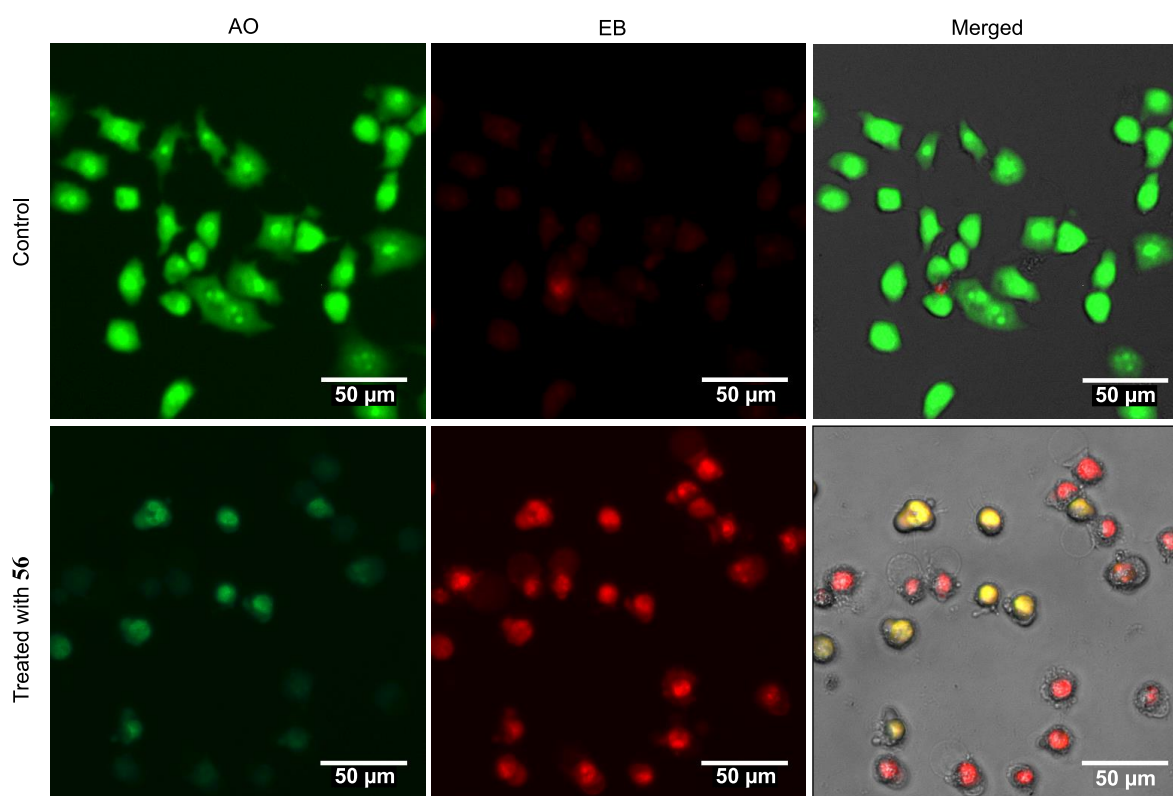
Figure 87. Morphological changes of PANC-1 cells induced by 20 μM of the new alkaloid ancistroyafungine B (**57**) in comparison with the untreated control.
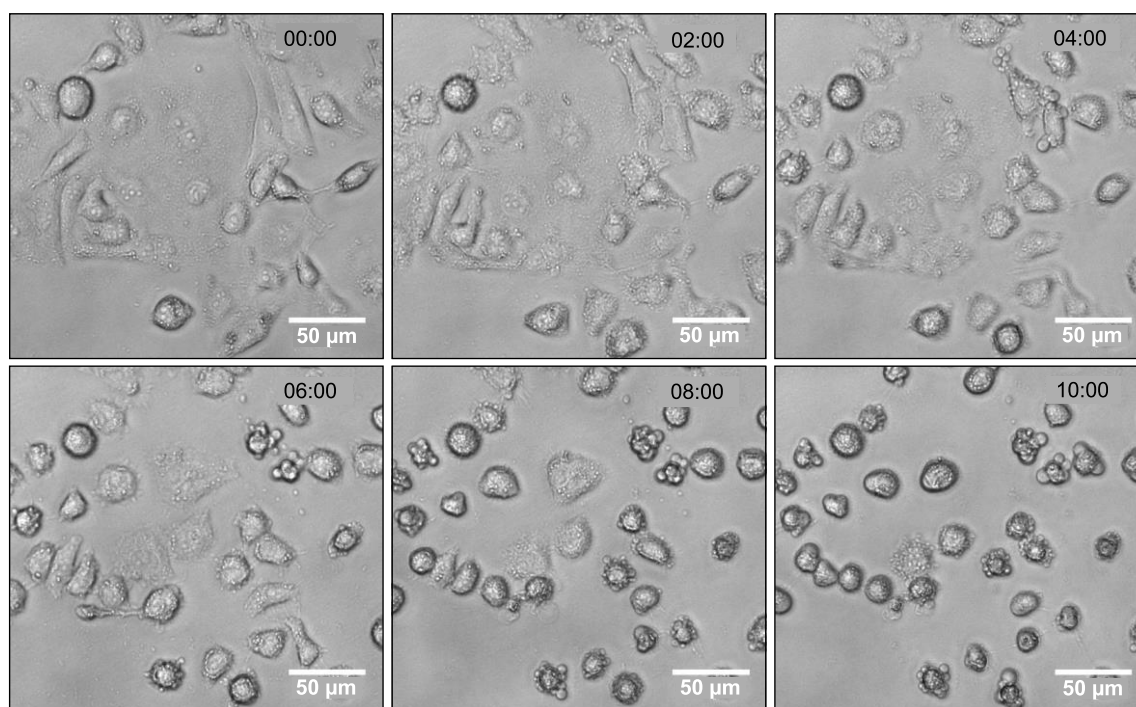
Figure 88. Captures of the live imaging of the effect of 20 µM of ancistroyafungine B (**57**) on PANC-1 cells at different intervals of time (hour : minute). For the authentic video, see https://vimeo.com/283591161.

The results obtained from these investigations and from previous studies evidenced preferential cytotoxicities of NIQs against pancreatic cancer cells,[103,167,173] thus suggesting that these natural products were promising lead structures for anticancer drug development. The metabolites of this as yet botanically unknown Congolese *Ancistrocladus* species, as presented here provided valuable information for the ongoing SAR investigations. Further, more-in-depth studies regarding the anti-cancer potential of NIQs are presently in progress.

6. Summary

Naphthylisoquinoline alkaloids (NIQs) are the only known plant-derived isoquinolines that do not originate from aromatic amino acids, but from polyketide precursors. They display unique molecular scaffolds, consisting of a naphthalene and an isoquinoline moiety connected by a *C,C*- or an *N,C*-axis, which is usually rotationally hindered and, thus, an element of chirality. They also exist as dimers, which show up to three consecutive chiral biaryl axes and four stereocenters. Depending on their individual structures, some of them exhibit promising antiprotozoal, antiviral, or antitumoral activities.

The occurrence of NIQs is as yet restricted to the small West African plant family Dioncophyllaceae, with only three monotypic genera, *Dioncophyllum* BAILLION, *Habropetalum* A. SHAW, and *Triphyophyllum* A. SHAW, and to the closely related family Ancistrocladaceae, with only one genus, *Ancistrocladus* WALLICH.

The vast tropical rainforest of the Democratic Republic of the Congo (DRC) is known to host four *Ancistrocladus* species, namely *A. congolensis* J. LÉONARD, *A. ealaensis* J. LÉONARD, *A. likoko* J. LÉONARD, and *A. ileboensis* HEUBL, MUDOGO & G. BRINGMANN. Most recent discoveries of new locations of *Ancistrocladus* lianas in DRC and genetic analyses on plant material collected at different sites in the country, however, hint at the presence of further, botanically as yet undescribed *Ancistrocladus* species. Phytochemical investigations on these potentially new species are thus a rewarding task, not only for the chemotaxonomic characterization of the lianas and their possible delineation from other *Ancistrocladus* taxa, but also for the evaluation of the biological activities of their constituents.

The aim of the present work was the isolation, full stereochemical assignment, and antiprotozoal and antitumoral testing of novel-type dimeric NIQs and related metabolites from three taxonomically as yet undescribed Congolese *Ancistrocladus* species. Based on these findings, another objective was to gain an improved knowledge on the chemotaxonomic relationships to the botanically recognized *Ancistrocladus* taxa.

In detail, the following results were obtained:

1) From the leaves of the first, taxonomically as yet uncharacterized Congolese *Ancistrocladus* species ("*Ancistrocladus* sp. 032/104"), HPLC-UV-MS-ECD investigations focused on the search for structurally novel dimeric NIQs resulted in the discovery of three unprecedented types of NIQ dimers.

- The first discovered subclass comprised mbandakamines A (**16a**), B (**16b**), B$_2$ (**17**), C (**18**), and D (**19**), all with a novel 6′,1″-coupling type at the central axis, making them the first unsymmetrically linked dimeric NIQs. Even more remarkable, these were the very first compounds ever found in nature with a naphthalene unit bearing two aryl systems in two neighboring *peri*-positions, at C-1″ and C-8″. These exceptional aryl connections created a hairpin-like curved molecular array, in which three of the four bulky bicyclic ring systems (the two naphthalene parts and one of the two isoquinoline portions) were strongly pressed against each other, leading to an extremely high steric hindrance at the central axis and a total of seven stereogenic elements. The elucidation of the full three-dimensional structures of these unique metabolites succeeded due to the fruitful interplay of spectroscopic, chemical, and chiroptical methods. The assigned absolute stereostructures were further corroborated by ECD calculations performed by F. N. Katele for **16a** and **16b** and by chemical total synthesis of **16a**, as most recently accomplished by Dr. C. Schies in our group.
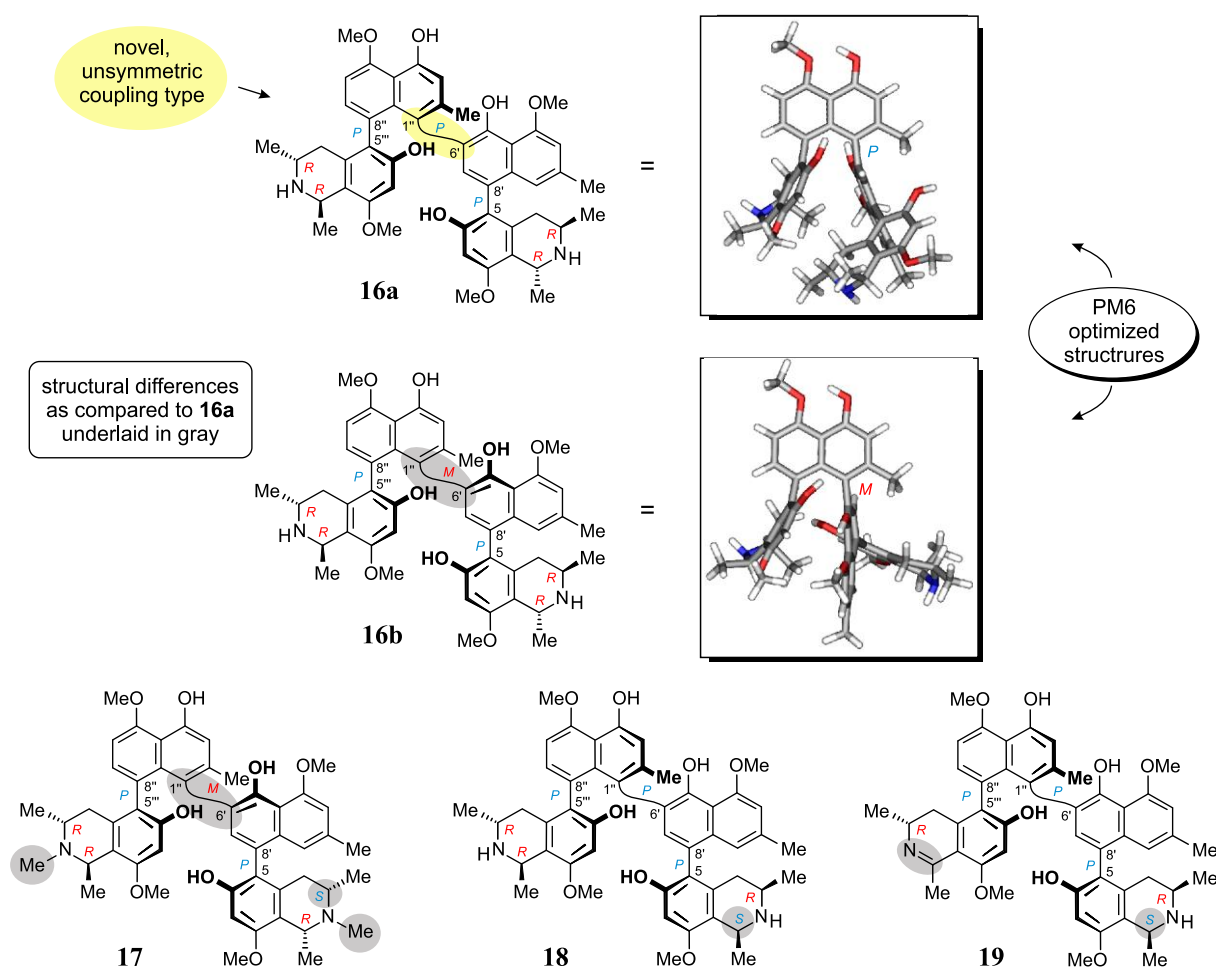
- The second discovered novel type of dimeric NIQs was represented by cyclombandakamines A$_1$ (**20**) and A$_2$ (**21**), which possessed, for the first time, oxygen bridges that link the "northwestern" naphthalene moiety to both the adjacent isoquinoline portion and the other, "southeastern" naphthalene part, resulting in no less than eight condensed rings. Even more thrilling were their stereochemical features, since their annulated molecular architecture showed a total of eight stereogenic elements (six centers and two axes, for one of them the configuration was thermodynamically dictated), the highest number ever encountered in any NIQ. Moreover, the fused pyran-cyclohexenone-dihydrofuran core displayed by these metabolites (see the part highlighted in yellow) was unprecedented among all previously known – natural and artificial – compounds; even as a partial substructure, this structural framework had not previously been detected. The full absolute stereostructures of **20** and **21** were established by spectroscopic, chemical, and chiroptical methods in combination with DFT and TDDFT calculations performed by Dr. T. Bruhn in our group.
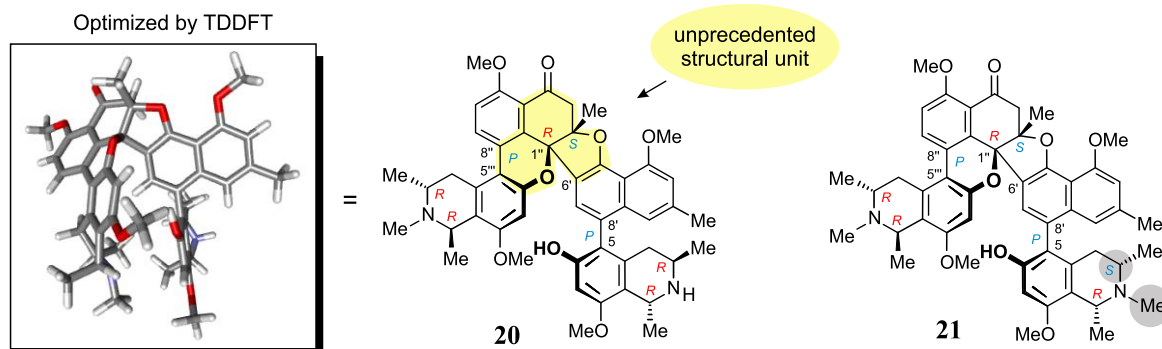
- Spirombandakamines A$_1$ (**22**) and A$_2$ (**23**), both displaying a complex, cage-like molecular framework, represented the third novel type of dimeric NIQs discovered within these doctoral studies. They were the first naphthylisoquinoline alkaloids at all that possessed a five-membered carbon ring, including dimers and monomers. Moreover, the fusion of this uncommon cycle with two, likewise unusual, acetal-fused five- and seven-membered oxygen heterocycles created a unique structural core, which had not been found in any other natural or synthetic compound. In addition, with two chiral biaryl axes and six stereocenters, they had a total of eight stereogenic elements – the highest total number for NIQs, so far displayed only by

the above presented novel cyclombandakamines. Their fascinating absolute stereostructures were established by the fruitful interplay of spectroscopic, chemical, and chiroptical methods with quantum-chemical ECD calculations carried out by Dr. T. Bruhn.
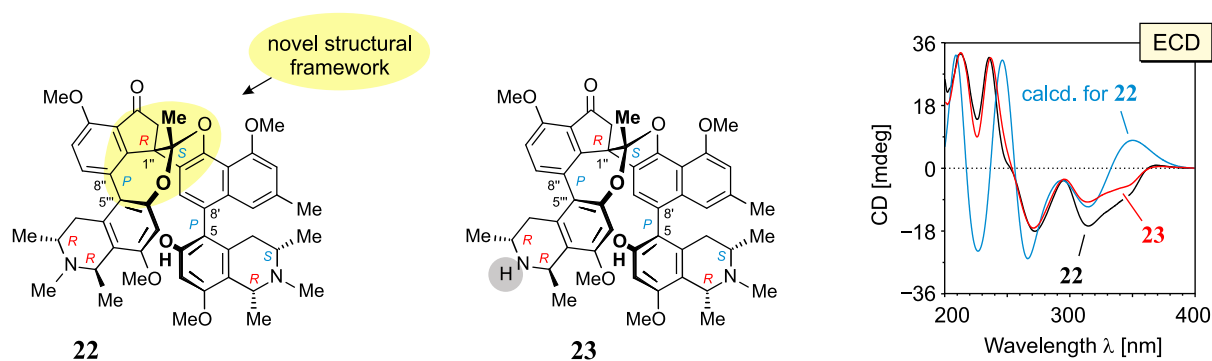
- Biosynthetically, the novel bridged dimeric NIQs, the cyclo- and spirombandakamines, are apparently the products of an oxidation-induced cyclization of the 'open-chain' mbandakamine-type dimers, which, in turn, arise from a previously established and experimentally proven polyketidic route, involving a total of 24 acetate units, which undergo a series of enzyme-catalyzed reactions to yield two intact monomeric NIQs, followed by their cross-coupling. For the cyclized mbandakamines two plausible pathways were postulated in this thesis. The first one proceeds via the formation of phenoxy radicals like **38**, yet leading only to cyclombandakamines, as exemplified for cyclombandakamine A$_1$ (**20**) in the scheme below.
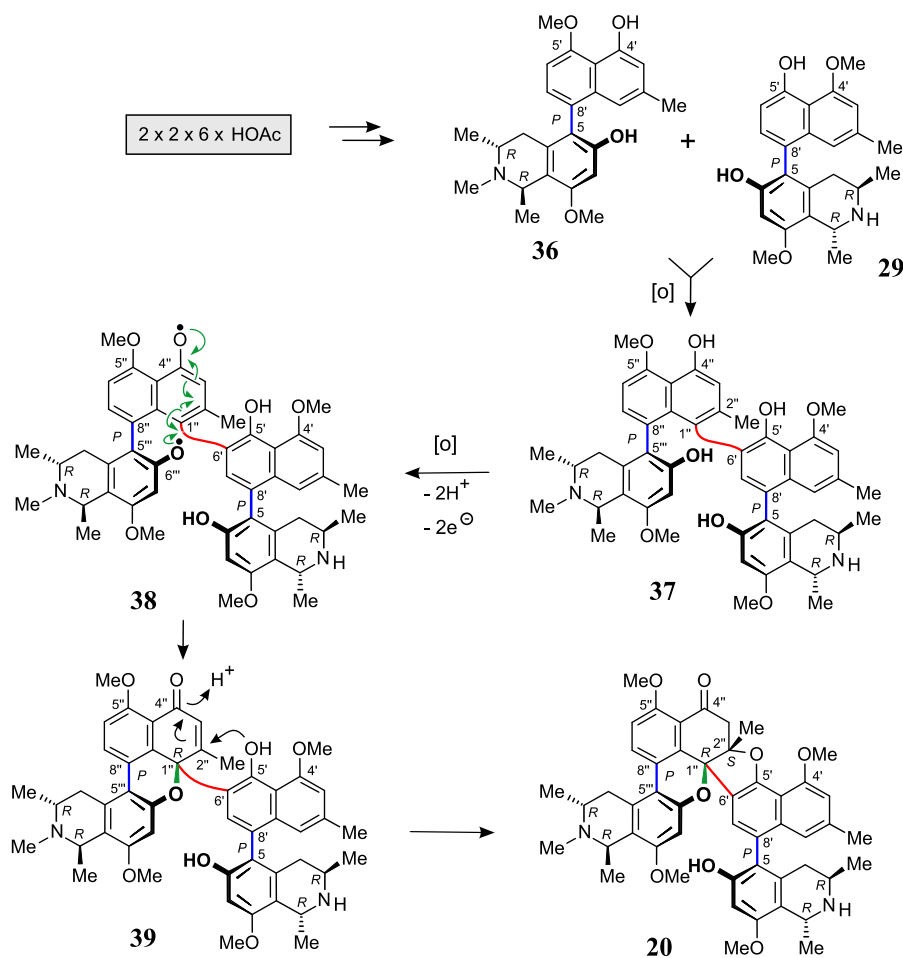
- The second plausible biosynthetic route developed during this work and presented below implied that both, cyclo- and spirombandakamines might arise from joint epoxide precursors. Accordingly, "open-chain" mbandakamines, such as mbandakamine B_2 (**17**), should undergo an epoxidation in the highly strained C-1″ – C-2″ region, leading to a decrease of steric congestion in the central binaphthalene core. Depending on the configuration of the resulting epoxide **40**, its cleavage would then, diastereo-divergently, either lead to cyclombandakamine A_2 (**21**), via **40a** and **41**, or to spirombandakamine A_1 (**22**), with **40b** and **42** as plausible intermediates.
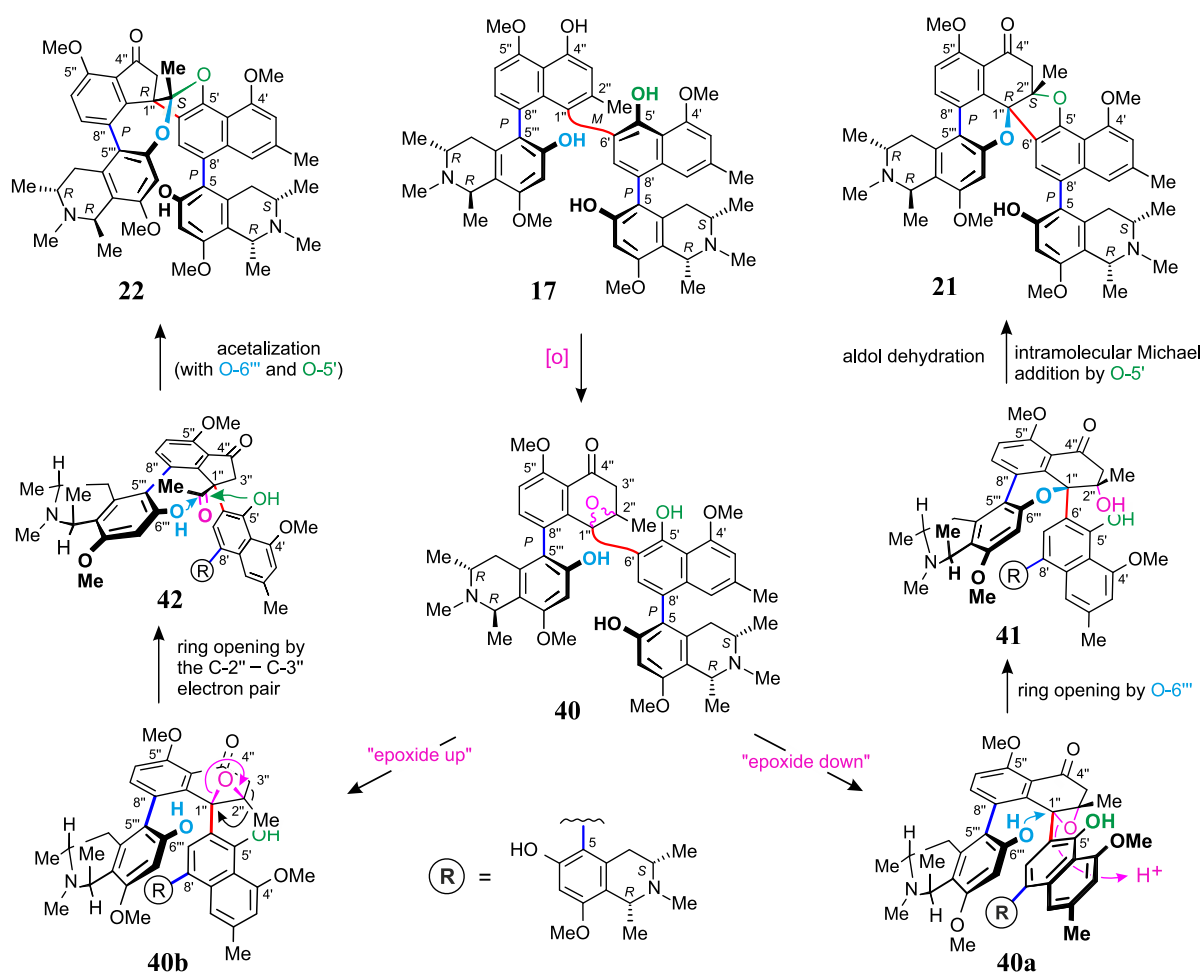
- Preliminary biomimetic semi-synthetic investigations corroborated the formation of both cyclo- and spirombandakamines from the corresponding open-chain mbandakamines. Thus, prolonged treatment of mbandakamine B$_2$ (**17**) with strong aqueous acids at 60°C led to cyclombandakamine A$_1$ (**21**), spirombandakamine A$_1$ (**22**), and further products, among them the atropo-diastereomer of **17** concerning the central axis.

- Pharmacologically, the isolated novel compounds exhibited moderate to strong antiprotozoal activities. Particularly impressive was mbandakamine B$_2$ (**17**), which showed the strongest effects ever found for NIQ alkaloids against the chloroquine-resistance K1 strain of *Plasmodium falciparum* (the pathogen causing malaria), with an excellent IC$_{50}$ value of 4 nM. This dimer was also highly active against *Trypanosoma brucei rhodesiense*, a pathogenic agent causing the deadly African sleeping sickness (IC$_{50}$ = 5 nM). Likewise noteworthy was the strong growth-inhibitory properties of mbandakamine A (**16a**) against HeLa cervical cancer cells (IC$_{50}$ = 1.39 μM).

- Chemotaxonomically, the metabolite profile produced by this *Ancistrocladus* liana showed it to be more closely related to *A. ealaensis* than to any other botanically recognized related taxon. And still there were some significant metabolic and genetic differences between *A. ealaensis* and this as yet unidentified Congolese *Ancistrocladus* plant, which suggested it to be a new subspecies or even a new species. Further investigations are therefore needed to firmly ascertain its taxonomic status.

2) Phytochemical investigations on a further taxonomically as yet undescribed Congolese *Ancistrocladus* liana ("*Ancistrocladus* sp. 105").

- From the leaves of *Ancistrocladus* sp. 105, four new michellamine-type naphthylisoquinoline dimers and two previously unknown monomeric alkaloids were isolated, namely michellamines A_6 (**45**) and A_7 (**46**), the first dimers of 5,8′-coupled NIQs with *cis*-configured stereocenters in both tetrahydroisoquinoline subunits, michellamines B_4 (**47**) and B_5 (**48**), and ancistrobonsolines A_1 (**49**) and A_2 (**50**).
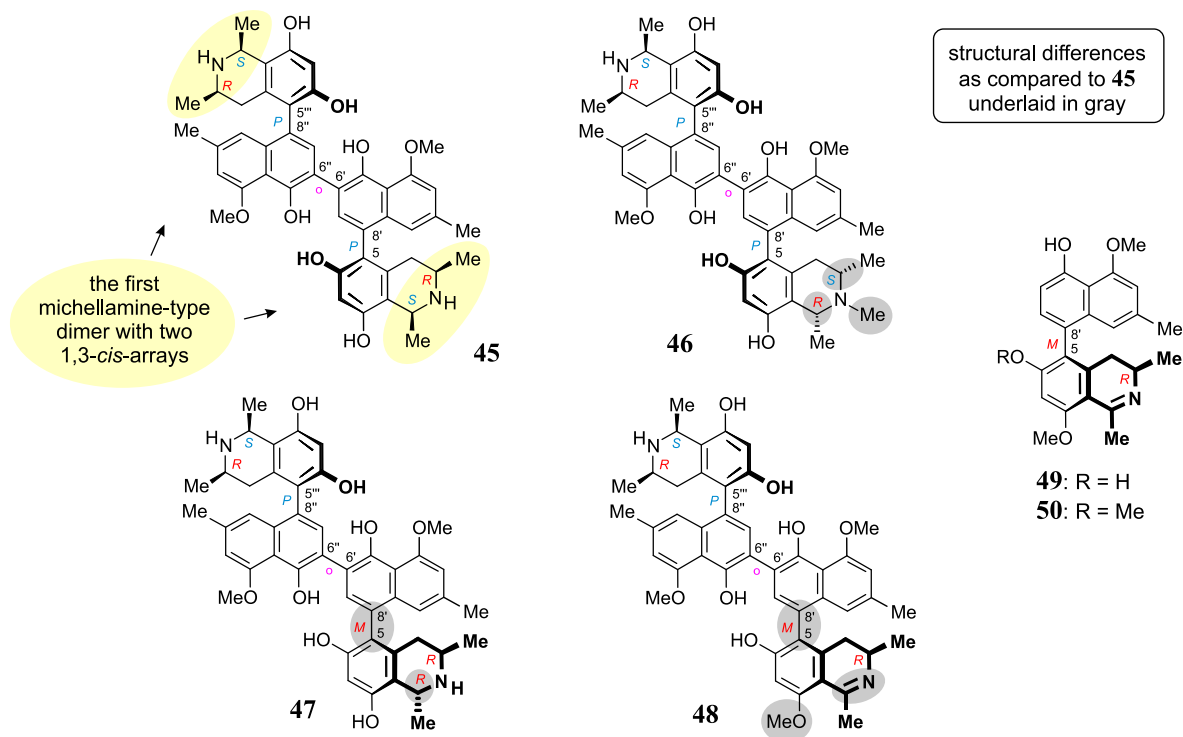
- Moreover, five compounds earlier reported from other *Ancistrocladus* species were identified, ancistroealaine C (**51**), korupensamines A (**52a**) and B (**52b**), and michellamines A_2 (**53**) and E (**54**).
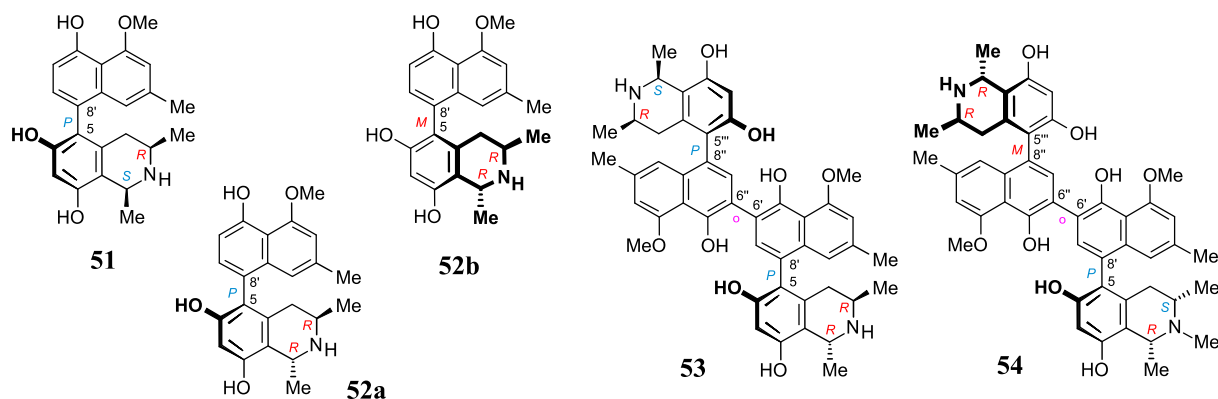
- Chemotaxonomically, the stereostructures of the metabolites clearly delineated this Congolese *Ancistrocladus* liana from all known related species, suggesting that it might be a new taxon. The closest botanically recognized taxa are the Congolese species *A. likoko* and the Cameroonian liana *A. korupensis*.

- The eleven isolated compounds displayed strong to moderate growth-inhibitory properties against cervical HeLa cancer cells. Moreover, some of them were highly active against human PANC-1 pancreatic cancer cells, following the recently developed antiausterity approach, as implemented in the group of Prof. S. Awale (Institute of Natural Medicine, University of Toyama, Japan), where these biological analyses were performed. Particularly noteworthy were ancistrobonsolines A_1 (**49**) and A_2 (**50**), which showed strong preferential cytotoxicities against human PANC-1 pancreatic cancer cells under nutrient-deprived conditions ($PC_{50} = 7.5$ and 12.1 µM, respectively), without displaying toxicity in normal, nutrient-rich medium. Most recent advanced studies on the pharmacological properties of the atropisomer of **50**, ancistrolikokine E_3 (which had lately been isolated from *A. likoko* by S. Fayez), indicated that these compounds were promising lead candidates for the development of anticancer drugs.
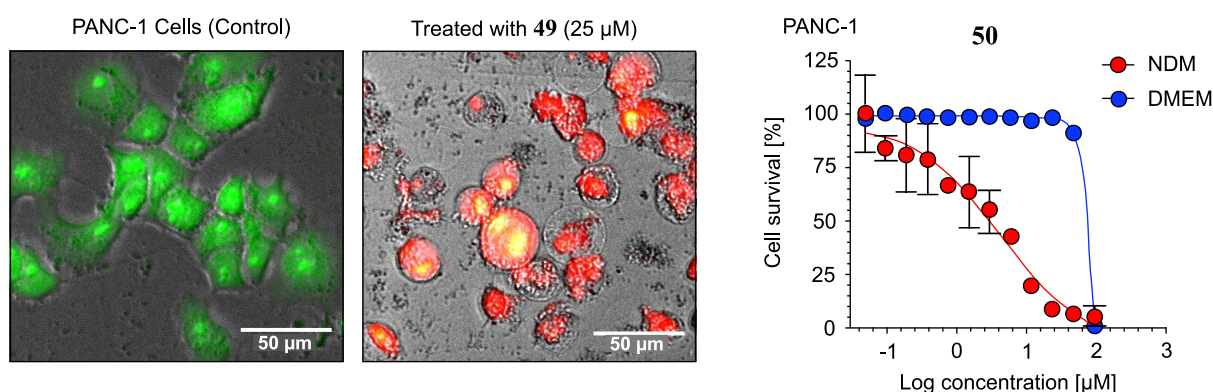
3) Phytochemical investigations on the third botanically as yet undescribed Congolese *Ancistrocladus* liana ("*Ancistrocladus* sp. 106").

- In cooperation with S. M. Kavatsurwa, four new monomeric NIQs, the 5,8′-coupled ancistroyafungines A-C (**56**-**58**) and the 5,1′-linked ancistroyafungine D (**59**), were isolated from the stem bark of *Ancistrocladus* sp. 106, collected in the rainforest near the Congolese village Yafunga.

56   **57**   **58**   **59**

structural differences as compared to **56** underlaid in gray
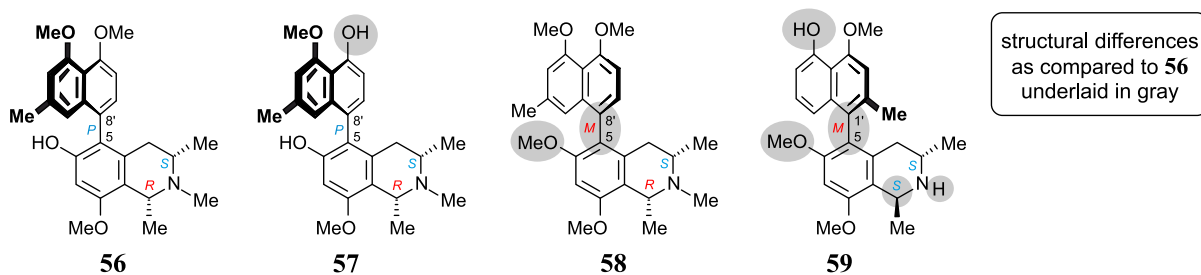
- In addition to the above four new compounds, eleven further NIQs that had previously been identified in related African and Asian *Ancistrocladus* species were obtained. They exhibited five different coupling types, viz., 5,8′, 5,1′, 7,1′, *N*,6′, and *N*,8′.

60   **61**   **62**: R = H   **63**: R = Me

64: R = H   *ent*-**49**: R = H   **67**   **9**
65: R = Me   **66**: R = Me   **68**

∵ configurationally semi-stable
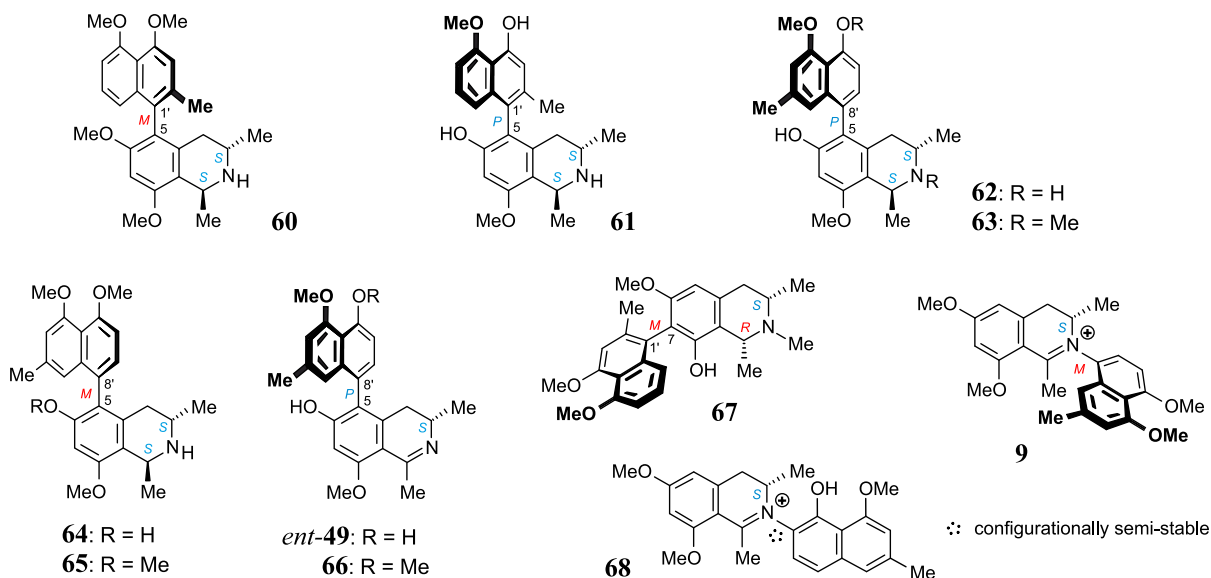
- All of the alkaloids from this plant were *S*-configured at C-3 and possessed an oxygen function at C-6 in the isoquinoline portion, and, thus, belonged to the subclass of "Ancistrocladaceae-type" alkaloids. This finding was geo- and chemotaxonomically remarkable, since – apart from one other *Ancistrocladus* species from the Central Congo Basin – only Southeast Asian and East African

Ancistrocladaceae were known to exclusively produce NIQs with these structural features. Thus, *Ancistrocladus* sp. 106 was clearly distinct from the four taxonomically recognized Congolese *Ancistrocladus* lianas, and might thus represent a new species. Further investigations, including DNA fingerprinting and in-depth studies on its botanical features, will be rewarding.

- The isolated compounds showed strong to moderate antiausterity activities against PANC-1 cancer cells. Within this series of alkaloids, the new NIQs ancistroyafungines B (**57**) and D (**59**) were the most potent ones, with PC_{50} values of 7.6 and 9.7 µM, respectively. Live-cell imaging investigations of the antitumoral potential of ancistroyafungine B in Prof. Awale's group demonstrated that this alkaloid disrupted the integrity of the PANC-1 cell membrane within 4 h, inducing membrane blebbing and rounding, eventually leading to membrane rupture and total cell death within 10 h.
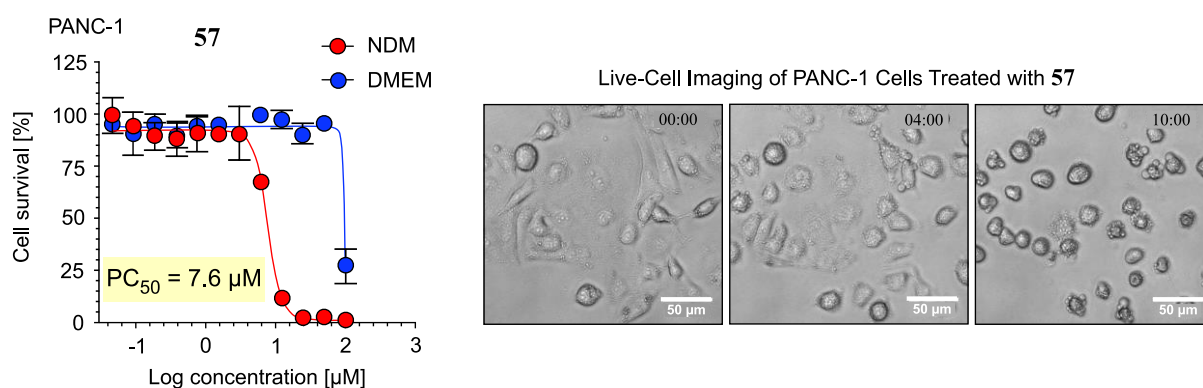
In conclusion, the results from the present thesis are valuable in many respects. Structurally, they provide the scientific community with highly original novel molecular scaffolds, among which some witness intriguing downstream biosynthetic processes that have previously been unknown for naphthylisoquinoline alkaloids. Taxonomically, by evidencing the presence of potentially new *Ancistrocladus* species or subspecies, the findings contribute to the knowledge on the flora from the Congo Basin, warranting further attention from phytogeneticists and botanists, and showing the value of the Congolese rainforest and its need for conservation. Pharmacologically, the discovery of some promising antiplasmodial, antitrypanosomal, and antitumoral agents is of great interest, as it paves the way to further, in-depth efforts for the development of new medicines against protozoic diseases and cancers. Thus, the obtained results open the door to a variety of exciting follow-up research projects, which may lead to further important discoveries.

7. Zusammenfassung

Naphthylisochinolin-Alkaloide (NIQs) sind die einzigen bekannten Isochinoline aus Pflanzen, die nicht aus aromatischen Aminosäuren, sondern aus Polyketidvorstufen aufgebaut werden. Sie weisen einzigartige Molekülgerüste auf, bestehend aus einem Naphthalin- und einem Isochinolin-Baustein. Die beiden Molekülhälften sind durch eine *C*,*C*- oder *N*,*C*-Achse verbunden, die – in den meisten Fällen – rotationsgehindert ist und somit ein Chiralitätselement darstellt. Es gibt sie auch als Dimere, dann können sie bis zu drei aufeinanderfolgende chirale Biarylachsen und vier Stereozentren aufweisen. Abhängig von ihren individuellen Strukturen verfügen einige von ihnen über vielversprechende antiprotozoische, antivirale oder antitumorale Aktivitäten.

Das Vorkommen von NIQs beschränkt sich ausschließlich auf die kleine westafrikanische Pflanzenfamilie Dioncophyllaceae mit nur drei monotypischen Gattungen, *Dioncophyllum* BAILLON, *Habropetalum* AIRY SHAW und *Triphyophyllum* AIRY SHAW sowie auf die eng verwandte Familie Ancistrocladaceae mit nur einer Gattung, *Ancistrocladus* WALLICH.

Der riesige tropische Regenwald der Demokratischen Republik Kongo (DR Kongo) ist Heimat für vier *Ancistrocladus*-Arten, nämlich *A. congolensis* J. LÉONARD, *A. ealaensis* J. LÉONARD, *A. likoko* J. LÉONARD und *A. ileboensis* HEUBL. MUDOGO & G. BRINGMANN. Die jüngste Entdeckung neuer Standorte von *Ancistrocladus*-Lianen in der DR Kongo sowie genetische Analysen von Pflanzenmaterial, das an verschiedenen Standorten im Land gesammelt wurde, lassen jedoch auf das Vorhandensein weiterer, in der botanischen Literatur noch nicht beschriebener *Ancistrocladus*-Arten schließen. Phytochemische Untersuchungen dieser potenziell neuen Arten sind daher eine lohnende Aufgabe, nicht nur im Hinblick auf die chemotaxonomische Charakterisierung der Lianen und ihre mögliche Abgrenzung zu anderen *Ancistrocladus*-Arten, sondern auch für die Erforschung der biologischen Aktivitäten ihrer Inhaltsstoffe.

Das Ziel der vorliegenden Arbeit war die Isolierung und vollständige stereochemische Charakterisierung strukturell neuartiger dimerer NIQs sowie verwandter Sekundärmetabolite aus drei taxonomisch noch nicht beschriebenen kongolesischen *Ancistrocladus*-Arten einschließlich der Testung der neuen Alkaloide auf antiprotozoische und antitumorale Aktivitäten. Ausgehend von den Ergebnissen der phytochemischen Untersuchungen bestand ein weiteres Ziel darin, ein verbessertes Wissen über die chemotaxonomischen Beziehungen

der bislang unbekannten kongolesischen *Ancistrocladus*-Lianen zu den botanisch anerkannten Arten zu erlangen.

Im Detail wurden folgenden Ergebnissen erhalten:

1) HPLC-UV-MS-ECD-Untersuchung der Blätter einer bislang taxonomisch noch nicht näher charakterisierten kongolesischen *Ancistrocladus*-Spezies („*Ancistrocladus* sp. 032/104") führten zur Entdeckung von drei neuen Untergruppen strukturell ganz neuartiger dimerer NIQs.

- Die erste der neu entdeckten Unterklassen umfasste Mbandakamin A (**16a**), B (**16b**), B$_2$ (**17**), C (**18**) und D (**19**). Charakteristisch für alle diese Dimeren war der neuartige 6',1"-Kupplungstyp an der zentralen Achse. Damit waren sie die ersten unsymmetrisch verknüpften dimeren NIQs, die man in der Natur gefunden hatte. Noch bemerkenswerter war, dass dies die ersten Verbindungen überhaupt waren, die einen Naphthalin-Baustein besaßen, der zwei Aryl-Systeme an zwei benachbarten *peri*-Positionen, C-1″ und C-8″, trug. Diese außergewöhnlichen Aryl-Arylbindungen bewirkten eine haarnadelartig gekrümmte Molekülanordnung, in der drei der vier sperrigen bicyclischen Ringsysteme (die beiden Naphthalin-Bausteine und einer der beiden Isochinolin-Einheiten) stark gegeneinander gepresst waren, was zu einer extrem hohen sterischen Hinderung an der zentralen Achse und insgesamt sieben stereogenen Elementen führte. Die Aufklärung der vollständigen dreidimensionalen Strukturen dieser einzigartigen Metaboliten gelang aufgrund des fruchtbaren Zusammenspiels von spektroskopischen, chemischen und chiroptischen Methoden. Die so zugeordneten absoluten Stereostrukturen wurden zudem durch ECD-Berechnungen für **16a** und **16b** (durchgeführt von F. N. Katele) und durch die chemische Totalsynthese von **16a**, welche erst kürzlich in unserer Gruppe von Dr. C. Schies erfolgreich abgeschlossen wurde, bestätigt.

neuer, unsymmetrischer Kupplungstyp

16a

=

PM6-optimierte Strukturen

strukturelle Unterschiede im Vergleich zu **16a** grau hinterlegt

16b

=

17

18

19
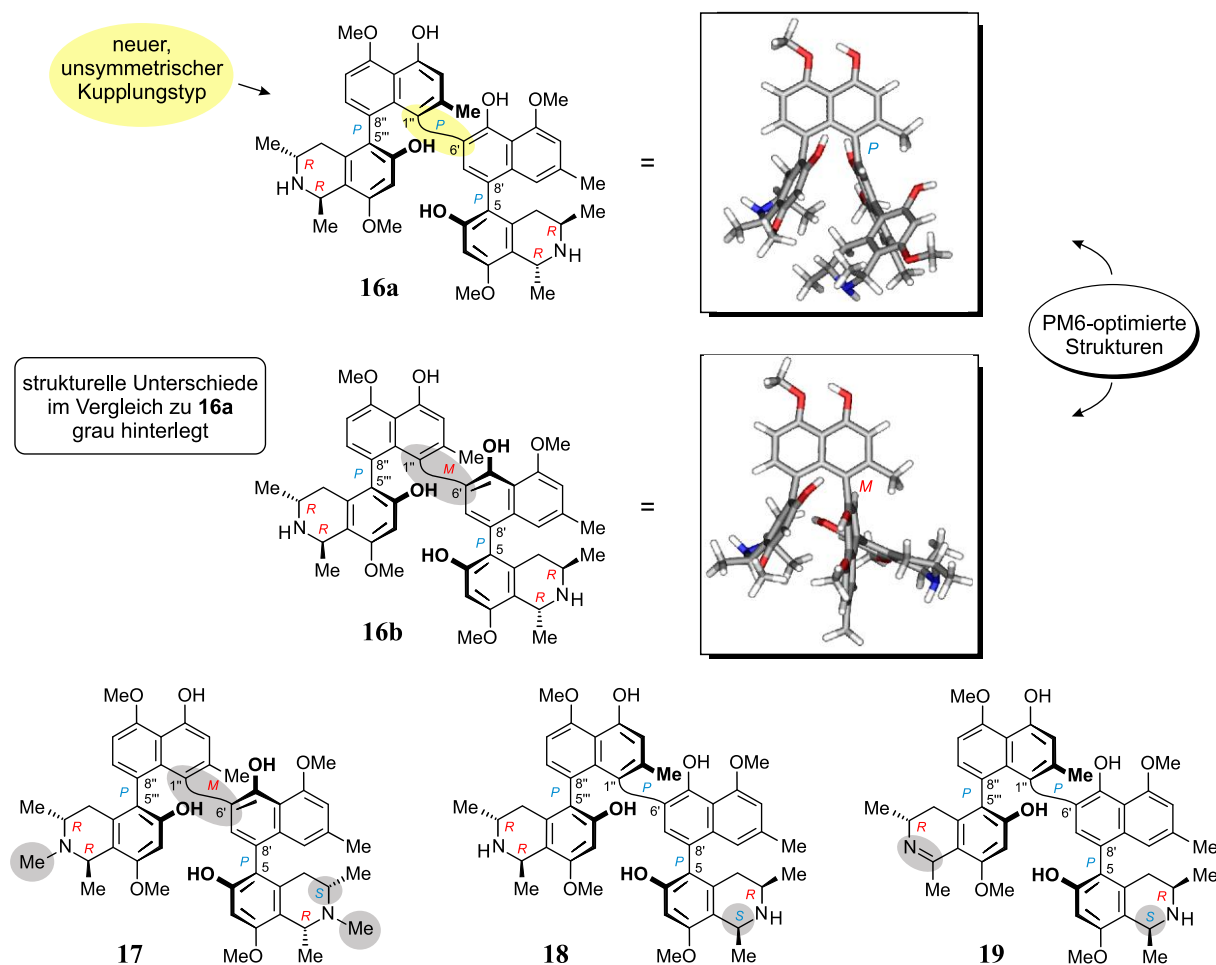
- Zum zweiten neu entdeckten Typ dimerer NIQs gehörten Cyclombandakamin A_1 (**20**) und A_2 (**21**). Diese Alkaloide zeichneten sich dadurch aus, dass sie erstmals Sauerstoffbrücken besaßen, die den „nordwestlichen" Naphthalin-Baustein sowohl mit der benachbarten Isochinolin-Einheit als auch mit dem anderen, „südöstlichen" Naphthalin-Molekülteil verbanden, was zu nicht weniger als acht kondensierten Ringen führte. Noch aufregender waren ihre stereochemischen Eigenschaften, da ihre annulierten Molekülarchitekturen insgesamt acht stereogene Elemente aufwiesen (sechs Zentren und zwei Achsen, bei einer der Achsen war die Konfiguration thermodynamisch diktiert) – die höchste Zahl, die jemals in einem NIQ gefunden wurde. Beispiellos war auch das für diese Metaboliten typische kondensierte Pyran-Cyclohexenon-Dihydrofuran-System (siehe den gelb hervorgehobenen Molekülteil) im Vergleich zu allen bisher bekannten – natürlichen und ausschließlich durch Synthese gewonnenen – Verbindungen; auch als Partialstruktur war dieses Strukturmotiv vor den hier beschriebenen Arbeiten nicht bekannt. Die vollständigen absoluten Stereostrukturen von **20** und **21** wurden durch spektroskopische, chemische und chiroptische Methoden in Kombination mit DFT- und TDDFT-

Berechnungen ermittelt, welche von Dr. T. Bruhn aus unserer Gruppe durchgeführt wurden.

optimiert mittels TDDFT

beispiellose strukturelle Einheit

20

21
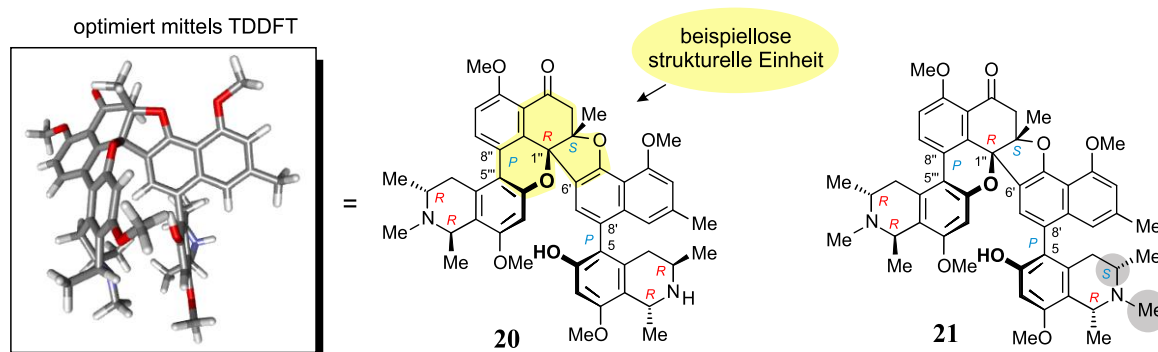
- Die Spirombandakamine A$_1$ (**22**) und A$_2$ (**23**), die beide ein komplexes, käfigartiges Molekülgerüst aufweisen, bildeten den dritten neuartigen Typ dimerer NIQs, die im Rahmen dieser Promotionsarbeit entdeckt wurden. Sie waren die ersten Naphthylisochinoline überhaupt, die einen fünfgliedrigen Kohlenstoffring besaßen, sowohl was dimere als auch monomere Alkaloide anbelangt. Darüber hinaus führte die Fusion dieses ungewöhnlichen Ringsystems über zwei ebenfalls ungewöhnliche Acetal-kondensierte fünf- und siebengliedrige Sauerstoff-Heterocyclen zu einem einzigartigen zentralen Strukturmotiv, das bislang in keiner anderen Verbindung – natürlicher oder synthetischer Herkunft – gefunden wurde. Außerdem wiesen **22** und **23** mit zwei chiralen Biarylachsen und sechs Stereozentren insgesamt acht stereogene Elemente auf – die höchste Gesamtzahl für NIQs, wie sie bisher nur noch bei den oben vorgestellten neuartigen Cyclombandakaminen erreicht wurde. Die faszinierenden absoluten Stereostrukturen der Spirombandakamine A$_1$ (**22**) und A$_2$ (**23**) ergaben sich aus dem fruchtbaren Zusammenspiel spektroskopischer, chemischer und chiroptischer Methoden in Verbindung mit quantenchemischen ECD-Berechnungen, die von Dr. T. Bruhn durchgeführt wurden.

neuartiges strukturelles Motiv

22

23

ECD

ber. für **22**

23

22
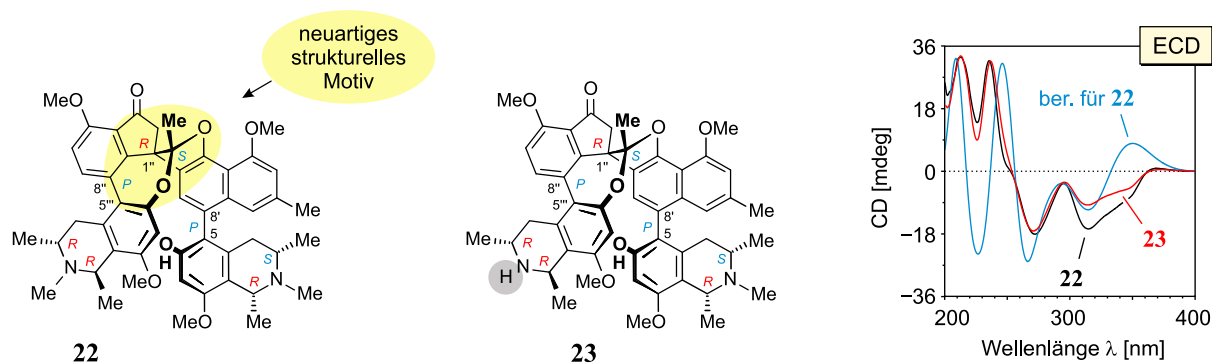
- Biosynthetisch sind die neuartigen verbrückten dimeren NIQs, die Cyclo- und Spirombandakamine, offenbar die Produkte einer Oxidations-induzierten Cyclisierung von 'offenkettigen' Mbandakamin-artigen Dimeren, welche wiederum einem bereits etablierten und experimentell nachgewiesenen polyketidischen Biosyntheseweg folgend aus insgesamt 24 Acetat-Einheiten aufgebaut werden, und zwar durch eine Reihe Enzym-katalysierter Reaktionen zu zwei intakten monomeren NIQs, gefolgt von deren Kreuzkupplung. Für die cyclisierten Mbandakamine wurden in dieser Arbeit zwei plausible Reaktionswege postuliert. Der erste verläuft über Phenoxyradikale wie **38**, die jedoch nur zu Cyclombandakaminen führen, wie im nachstehenden Schema für Cyclombandakamin A$_1$ (**20**) veranschaulicht ist.
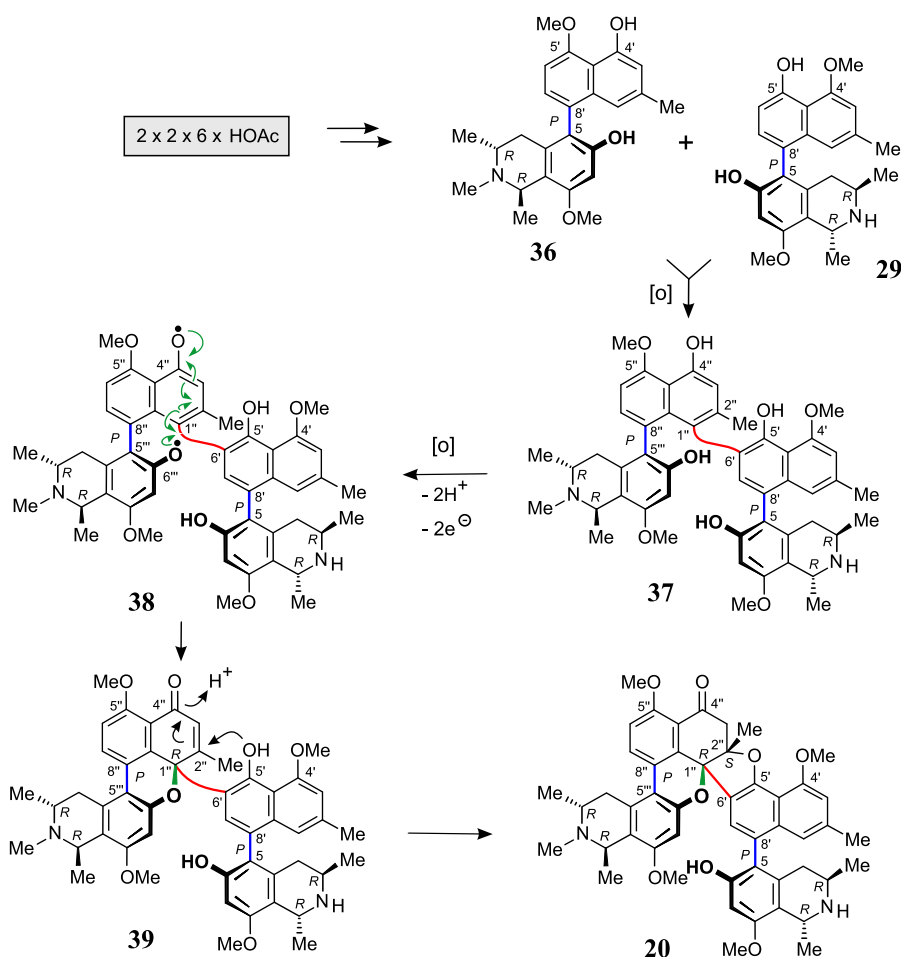
- Der zweite plausible Biosyntheseweg, der während dieser Arbeit entwickelt wurde, implizierte, dass sowohl Cyclo- als auch Spirombandakamine aus gemeinsamen Epoxid-Zwischenstufen entstehen könnten. Dementsprechend sollten 'offenkettige' Mbandakamine wie Mbandakamin B$_2$ (**17**) eine Epoxidierung in der stark gespannten Region C-1''–C-2'' eingehen, was zu einer Verringerung der sterischen Hinderung in

der zentralen Binaphthalin-Einheit führen sollte. Abhängig von der Konfiguration des resultierenden Epoxids **40** würde dessen Spaltung dann diastereo-divergent entweder zu Cyclombandakamin A$_2$ (**21**) über **40a** und **41** oder zu Spirombandakamin A$_1$ (**22**) mit **40b** und **42** als plausiblen Zwischenprodukten führen.
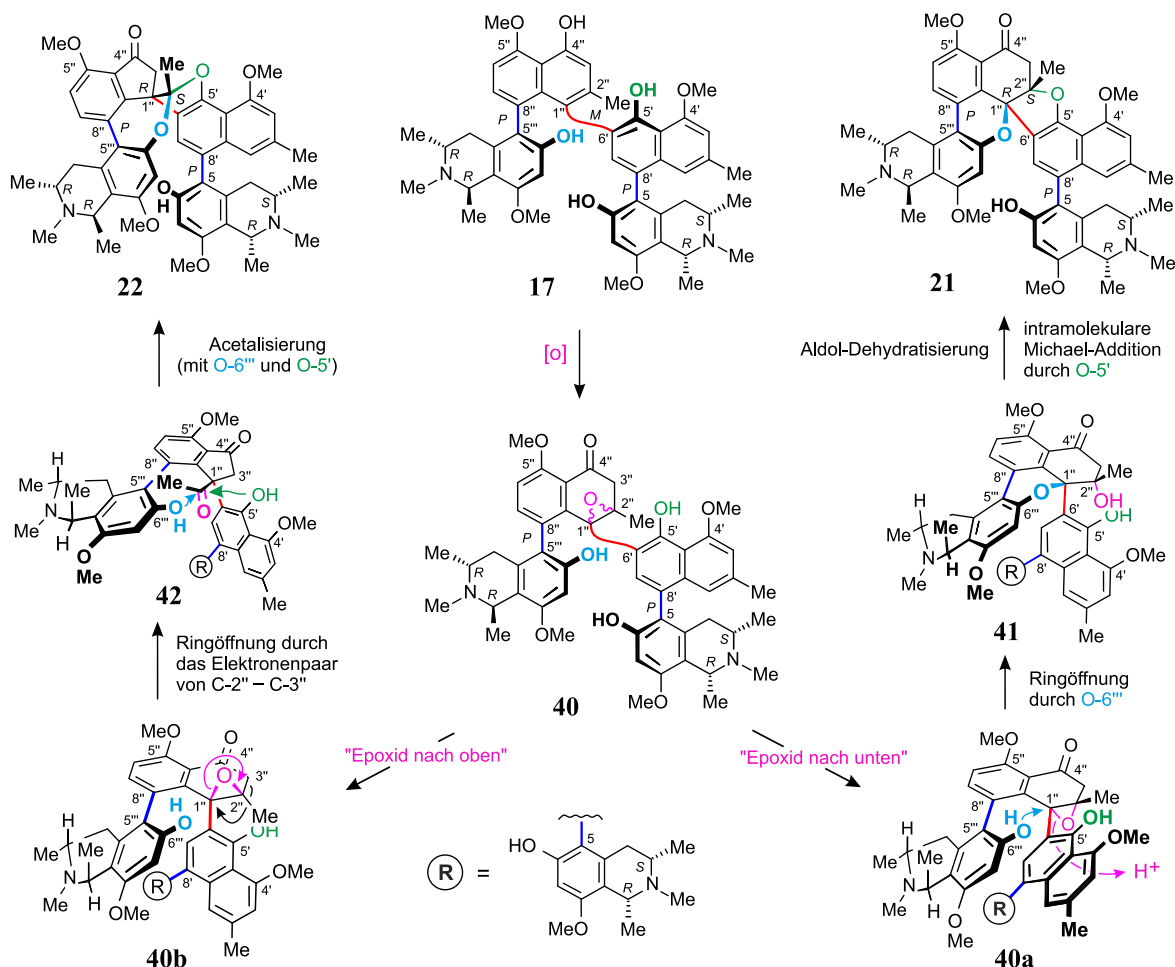
- Erste biomimetische semi-synthetische Untersuchungen bestätigten die Bildung von Cyclo- und Spirombandakaminen aus den entsprechenden offenkettigen Mbandakaminen. So führte eine längere Behandlung von Mbandakamin B$_2$ (**17**) unter stark sauren Bedingungen bei 60° C zu Cyclombandakamin A$_1$ (**21**), Spirombandakamin A$_1$ (**22**) und weiteren Produkten, darunter das Atropo-diastereomer von **17** mit *P*-Konfiguration an der zentralen Achse.

- Pharmakologisch zeigten die isolierten neuen Verbindungen mäßige bis starke antiprotozoische Aktivitäten. Besonders eindrucksvoll war die antiplasmodiale Wirkung von Mbandakamin B$_2$ (**17**), das mit einem hervorragenden IC$_{50}$-Wert von 4

nM die stärkste jemals für NIQs gefundene Aktivität gegen den Chloroquin-resistenten K1-Stamm von *Plasmodium falciparum* (dem Erreger der Malaria) aufwies. Dieses Dimer war auch hochgradig aktiv gegen den Erreger *Trypanosoma brucei rhodesiense* (IC_{50} = 5 nM), der die tödliche Afrikanische Schlafkrankheit verursacht. Bemerkenswert waren auch die stark wachstumshemmenden Eigenschaften von Mbandakamin A (**16a**) gegen HeLa-Gebärmutterhalskrebszellen (IC_{50} = 1.39 μM).

- Aus chemotaxonomischer Sicht wies das Metabolitprofil dieser bislang botanisch noch unbekannten *Ancistrocladus*-Liane, auf eine enge Verwandtschaft zu der gleichfalls im nordwestlichen Kongobecken beheimateten Art *A. ealaensis* hin, denn in *A. ealaensis* wurden mittlerweile ebenfalls mehrere Mbandakamine und Cyclombandakamine entdeckt, während derartige Dimere in allen anderen botanisch anerkannten *Ancistrocladus*-Arten bislang nicht gefunden wurden. Dennoch gibt es einige signifikante metabolische und genetische Unterschiede zwischen *A. ealaensis* und dieser noch nicht identifizierten kongolesischen *Ancistrocladus*-Pflanze, was darauf hindeutet, dass es sich um eine neue Unterart oder sogar um eine neue Art handeln könnte. Für eine eindeutige Klärung des taxonomischen Status sind weitere Untersuchungen notwendig.

2) Phytochemische Untersuchungen an einer weiteren taxonomisch bislang noch nicht beschriebenen kongolesischen *Ancistrocladus*-Liane („*Ancistrocladus* sp. 105").

- Aus den Blättern von *Ancistrocladus* sp. 105 wurden vier neue Michellamin-artige dimere Naphthylisochinoline und zwei bisher unbekannte monomere Alkaloide isoliert, nämlich die Michellamine A_6 (**45**) und A_7 (**46**), die ersten Dimere von 5,8'-gekuppelten NIQs mit *cis*-konfigurierten Stereozentren in beiden Tetrahydroisochinolin-Untereinheiten, die Michellamine B_4 (**47**) und B_5 (**48**), sowie die Ancistrobonsoline A_1 (**49**) und A_2 (**50**).
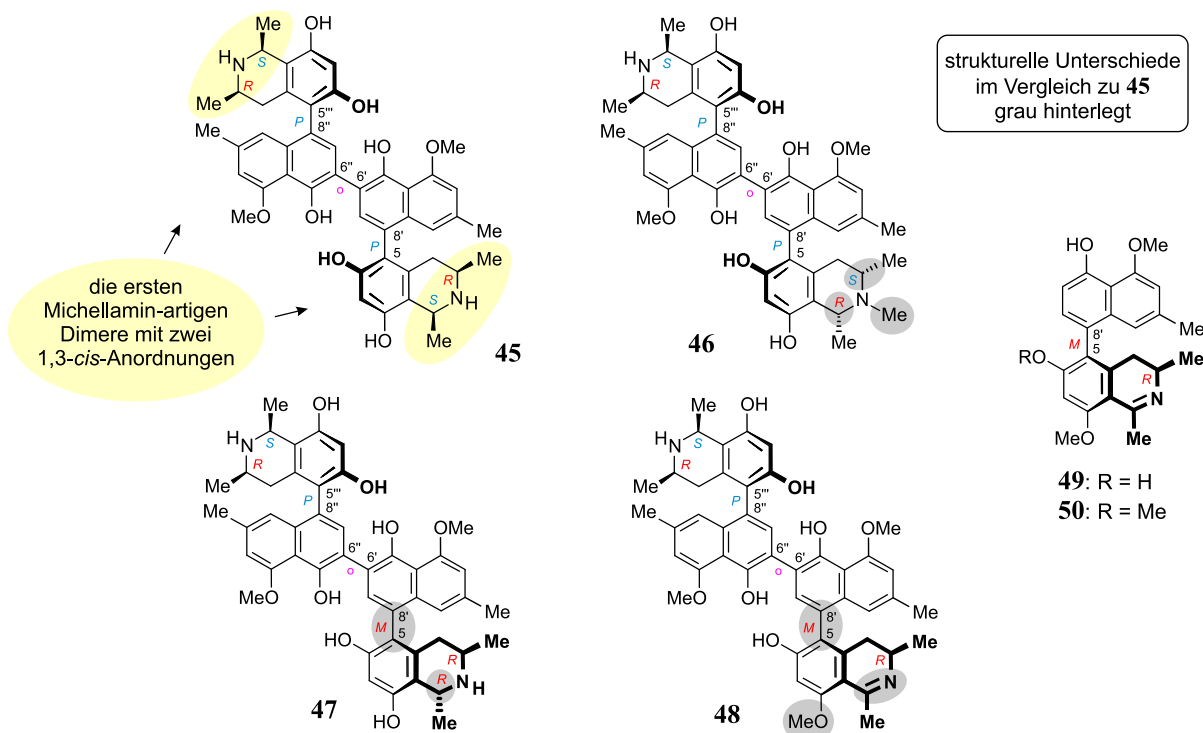
- Darüber hinaus wurden fünf Verbindungen, die bereits aus früheren Arbeiten über andere *Ancistrocladus*-Arten bekannt waren, identifiziert: Ancistroealain C (**51**), die Korupensamine A (**52a**) und B (**52b**) sowie die Michellamine A_2 (**53**) und E (**54**).
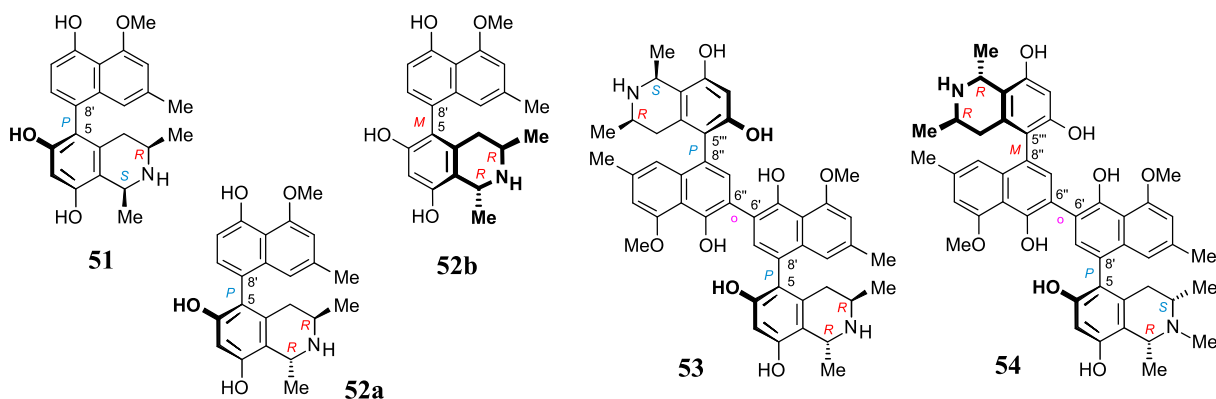
- Chemotaxonomisch ließ sich diese kongolesische *Ancistrocladus*-Liane aufgrund der Stereostrukturen der Metabolite eindeutig von allen bekannten verwandten Arten abgegrenzt, was die Vermutung nahelegt, dass es sich möglicherweise um ein neues Taxon handeln könnte. Die botanisch anerkannten Taxa mit den größten Übereinstimmungen sind die kongolesische Art *A. likoko* und die in Kamerun beheimatete Liane *A. korupensis*.

- Die elf isolierten Verbindungen zeigten starke bis mäßige wachstumshemmende Eigenschaften gegen HeLa-Gebärmutterhalskrebszellen. Darüber hinaus waren einige von ihnen sehr aktiv gegen humane PANC-1-Bauchspeicheldrüsenkrebszellen, und zwar nach dem kürzlich entwickelten 'Antiausteritäts'-Konzept. Dieses dient in der Gruppe von Prof. S. Awale (Institut für Naturmedizin, Universität Toyama, Japan), in der diese biologischen Analysen durchgeführt wurden, als Grundlage für die Suche nach neuen antitumoralen Wirkstoffen. Besonders hervorzuheben waren die Ancistrobonsoline A_1 (**49**) (PC_{50} = 7.5 μM) und A_2 (**50**) (PC_{50} = 12.1 μM), die bevorzugt im nährstoffarmen Medium eine starke cytotoxische Wirkung gegenüber Pankreaskarzinomzellen zeigten, ohne dass dabei toxische Effekte unter normalen, d.h. nährstoffreichen Bedingungen auftraten. Neueste tiefergehende Studien zu den pharmakologischen Eigenschaften des Atropisomers von **50**, Ancistrolikokin E_3 (das kürzlich von S. Fayez aus *A. likoko* isoliert worden war), zeigten, dass solche Naturstoffe vielversprechende Leitstrukturen für die Entwicklung von Krebsmedikamenten darstellen könnten.

PANC-1-Zellen (Kontrolle)   Behandelt mit **49** (25 μM)
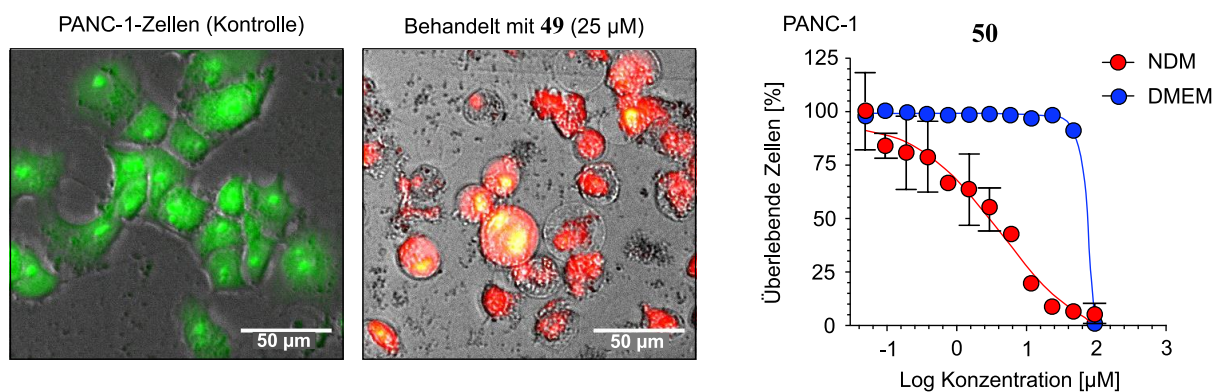
3) Phytochemische Untersuchungen an einer dritten botanisch noch unbeschriebenen kongolesischen *Ancistrocladus*-Liane („*Ancistrocladus* sp. 106").

- In Zusammenarbeit mit S. M. Kavatsurwa an der Universität Pretoria (Südafrika) wurden vier neue monomere NIQs aus der Stammrinde von *Ancistrocladus* sp. 106 isoliert und strukturell aufgeklärt. Es handelte sich dabei um die 5,8'-gekuppelten Ancistroyafungine A-C (**56**-**58**) und das 5,1'-verbrückte Ancistroyafungin D (**59**). Diese Pflanze stammte aus dem Regenwald in der Nähe des kongolesischen Dorfes Yafunga.

56   **57**   **58**   **59**

strukturelle Unterschiede
im Vergleich zu **56**
grau hinterlegt
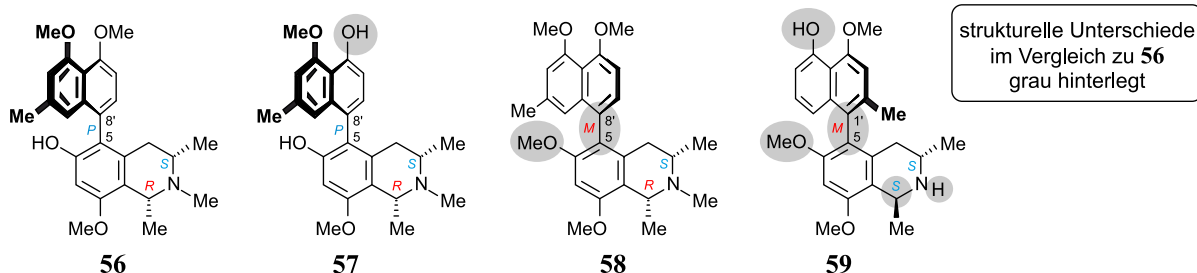
- Zusätzlich zu den oben genannten vier neuen Verbindungen wurden elf weitere NIQs erhalten, die zuvor bereits in verwandten afrikanischen und asiatischen *Ancistrocladus*-Arten identifiziert worden waren. Sie zeigten fünf verschiedene Kupplungstypen, nämlich 5,8', 5,1', 7,1', *N*,6' und *N*,8'.

60   **61**   **62**: R = H   **63**: R = Me

64: R = H   **65**: R = Me   *ent*-**49**: R = H   **66**: R = Me   **67**   **9**

68   ⋰⋱ konfigurativ semistabil
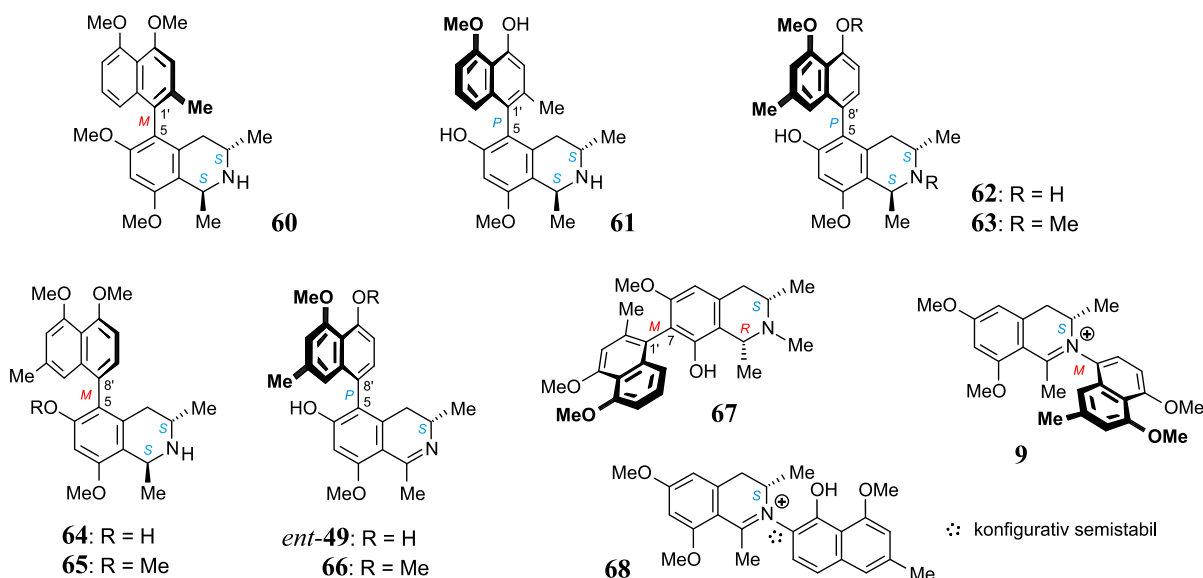
- Alle Alkaloide dieser Pflanze besaßen *S*-Konfiguration an C-3 und eine Sauerstoff-Funktion an C-6 in der Isochinolin-Hälfte und gehörten somit zur Unterklasse der Ancistrocladaceae-Typ-Alkaloide. Dieser Befund ist geo- und chemotaxonomisch bemerkenswert, da – abgesehen von einer anderen *Ancistrocladus*-Art aus dem Zentralkongo-Becken – bekanntermaßen nur südostasiatische und ostafrikanische Ancistrocladaceae ausschließlich NIQs mit diesen Strukturmerkmalen produzieren. Somit unterschied sich *Ancistrocladus* sp. 106 deutlich von den vier taxonomisch anerkannten kongolesischen *Ancistrocladus*-Lianen und könnte somit eine neue Art sein. Daher wären weiterführende Untersuchungen der botanischen Merkmale dieser Pflanze, einschließlich des DNA-Fingerabdrucks, sicherlich lohnenswert.

- Die isolierten Verbindungen zeigten im Sinne des ‚Antiausteritäts-Konzepts' starke bis mäßige Wirkungen gegen PANC-1-Krebszellen. Innerhalb dieser Alkaloid-Serie waren die neuen NIQs Ancistroyafungin B (**57**) und D (**59**) mit PC_{50}-Werten von 7.6 und 9.7 µM die wirksamsten Alkaloide. Untersuchungen in der Gruppe von Prof. Awale zum antitumoralen Potenzial von Ancistroyafungin B in lebenden Zellen zeigten, dass eine Behandlung der Krebszellen mit diesem Alkaloid bereits nach 4 h zu signifikanten Störungen der Membranbeschaffenheit der PANC-1-Zellen führte, Membranbläschen und -rundungen hervorrief und schließlich nach 10 h zu Membranbruch und vollständigem Zelltod führte.

Imaging-Experimente an lebenden PANC-1-Zellen nach Behandlung mit **57**
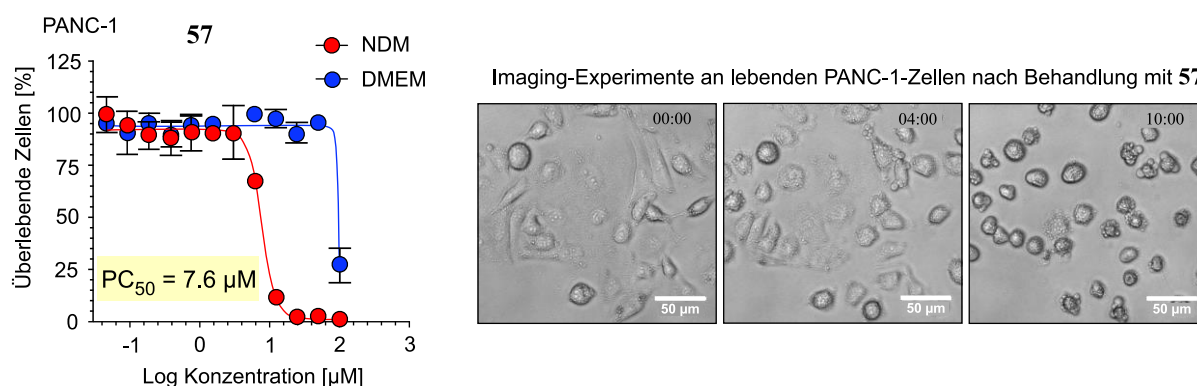
Zusammenfassend sind die Ergebnisse der vorliegenden Arbeit in vielerlei Hinsicht von großem Wert. Aus struktureller Sicht liefern sie der Wissenschaft Naturstoffe mit höchst originellen neuartigen Molekülgerüsten, von denen einige aus faszinierenden ‚downstream'-Biosynthesewegen stammen, die bisher für Naphthylisochinolin-Alkaloide unbekannt waren. In taxonomischer Hinsicht tragen die Ergebnisse durch den Nachweis potenziell neuer *Ancistrocladus*-Arten oder -Unterarten zu den Kenntnissen über die Flora des Kongobeckens bei, was die Aufmerksamkeit von Phytogenetikern und Botanikern auf sich ziehen und die Bedeutung des kongolesischen Regenwaldes und die Notwendigkeit seines Schutzes weiter untermauern wird. Pharmakologisch ist die Entdeckung einiger vielversprechender antiplasmodialer, antitrypanosomaler und antitumoraler Wirkstoffe von großem Interesse, da sie Anreiz für weitere intensive Anstrengungen zur Entwicklung neuer Arzneimittel gegen protozoische Erkrankungen und Krebs sind. Die erzielten Ergebnisse öffnen somit die Tür für eine Vielzahl spannender zukünftiger Forschungsprojekte, die zu weiteren wichtigen Entdeckungen führen könnten.

EXPERIMENTAL PART

1. General Aspects

1.1. Analytical Apparatuses

1.1.1. Optical Rotation

The optical rotation values were measured on a *JASCO* P-1020-polarimeter operating with a sodium light source ($\lambda = 589$ nm).

1.1.2. Infrared Spectroscopy (IR)

The IR spectra were recorded either on a FT-IR-410 or on a FT-IR-4600 type A spectrometer (both from *JASCO*) at room temperature. Measurements were performed using an ATR module, and the wave numbers at the maximum of strong absorption bands are reported (cm^{-1}).

1.1.3. Ultraviolet Spectroscopy (UV)

The UV spectra were taken at room temperature either on a Cary-50-Conc-UVvis spectrophotometer operating with the Cary-WinUV-Simple-scan-Application software (all *Varian* technologies) or on a *Shimadzu* UV-1800 spectrophotometer using the software UVProbe 2.43. In general, the measurements were conducted with a solution of ca. 1 mg/100 mL in spectrophotometric-grade methanol. The wavelengths of maximum absorbance (λ_{max} in nm) are reported along with their corresponding extinction coefficients ($\log \varepsilon$).

1.1.4. Electronic Circular Dichroism (ECD)

ECD spectra were obtained on a *JASCO* J-715 spectropolarimeter at room temperature by using standard quartz crystal cells and spectrophotometric-grade methanol. The scanning speed was set to 200 nm/min and the data pitch at 0.1 nm. The ECD curves were measured 3 times in the interval from 190 to 500 nm. The resulting average curves were corrected by subtracting the solvent effects and were subsequently smoothed by a factor of 5 to 21. They are reported in $\Delta\varepsilon$ values (cm^2/mol) at the given maximum wavelength (λ_{max} in nm).

1.1.5. Nuclear Magnetic Resonance Spectroscopy (NMR)

The ^{1}H NMR (400 MHz, 600 MHz) and ^{13}C NMR (100 MHz, 150 MHz) spectra were recorded at room temperature on either an Avance III HD 400, an Avance III HD 600, or a DMX 600 (all from *Bruker*) machine, using deuterated methanol (MeOD) as the solvent. Chemical shifts (δ) are reported in parts per million (ppm). Calibration of the spectra was carried out by using the ^{1}H and ^{13}C signals of MeOD ($\delta_H = 3.31$ ppm; $\delta_C = 49.15$ ppm) as the internal reference. For the processing of the spectra, the TopSpin 3.0 software from *Bruker* was used. Signal multiplicity is given using the following abbreviations: s = singlet, d = doublet, dd = doublet of doublets, t = triplet, q = quartet, m = multiplet, *p*d = pseudo doublet (or broad, not well-resolved doublet), and *p*t = pseudo triplet (i.e., an irregular, not well-resolved triplet). The coupling constants (*J*) are described in Hertz (Hz).

1.1.6. Mass Spectrometry (MS)

High-resolution electrospray ionization HRMS (ESI) spectra were determined by using either a micrOTOF-focus or a micrOTOF-Q III mass spectrometer (both from *Bruker*). The software modul IsotopePattern of the *Bruker* software Compass 1.1 served for calculation of the respective mass values of the isotopic distribution. For the measurement, samples were dissolved in the spectroscopic-grade methanol.

1.2. Other Apparatuses

For freeze-drying purposes a *Christ*-Alpha 1-4 equipped with a *vacUUbrand* RZ 8 high-vacuum pump was used.

Solvent evaporation or extract concentration was performed by utilizing a *Heidolph* Hei-VAP Value Digital rotary evaporator functioning with a *vacUUbrand* motor pump.

For recording the location of *Ancistrocladus* plants in the Congolese rainforests the Water Resistant Hiking GPS Magellan eXplorist® 100 was employed.

Crushing of plant materials was performed on a MF 10 Basic Microfine Grinder Drive equipped with a Cutting-Grinding Head (both from *IKA-Werke*).

Mechanical shaking during maceration of plant material was applied by means of the Orbital Shaker TR-150 from *INFORS AG*.

1.3. Chromatographic Methods

1.3.1. Thin Layer Chromatography (TLC) and Column Chromatography

Aluminum foil silica gel 60 F_{254} plates from *Merck* were used to monitor some fractionation steps. To detect substances on the TLC plates, fluorescent light at 254 or 365 nm was utilized and staining with Draggendorff reagent was employed to reveal alkaloid-containing fractions.

Amberlyst-15 (Ø 3 cm) for cation-exchange column chromatography was purchased from *Fluka*. For use, the resin on the column was first activated by acidified methanol and then washed with neutral methanol. LiChropep RP® RP-18 (40-63 μm), which was employed for some column fractionation steps, was obtained from *Merck*.

The Sep-Pak® Plus C18 cartridges (from *Waters*) were used to extract and concentrate mbandakamine-type dimers collected after preparative HPLC resolution.

1.3.2. High-Pressure Liquid Chromatography (HPLC)

Analytical HPLC-UV analyses were performed on a *JASCO* system comprising a pump (PU-1580), a four-line degasser unit (DG-2080-54), a quaternary gradient unit (LC-2080-04), an automatic sampler (AS-2055 Plus), a column oven CO-1560, and a DAD (diode-array detector, MD-2010 Plus). The hyphenation of these devises to the computer was assured by a LC-Net II/ADC connector. Measurements and data processing were done using the software Galaxy. Standard analyses (e.g., monitoring of extraction and co-elution experiments) were carried out at room temperature using a Chromolith RP-18e (*Merck*, 100 × 4.6 mm) column with the following gradient: 0 min 10% B, 5.0 min 50% B, 7.0 to 8.0 min 97.0% B and 8.5 to 10 min 10% B, in which A = H_2O + 0.05% trifluoroacetic acid (TFA) and B = MeCN + 0.05% TFA; flow rate: 3 ml/min.

Preparative HPLC-UV separation was performed either on the *JASCO* HPLC system "Prep 1" (PU-2087 Plus, UV-2077 Plus, LC-NetII/ADC) or on the *JASCO* HPLC system "Prep 2" (PU-2087, MD-2010 Plus, LC-NetII/ADC), both with the UV absorption wavelengths set at 232, 254, and 310 nm. The two preparative HPLC instruments were operated with the software Galaxy.

For *online HPLC-ECD analyses*, the analytical system consisted of a motor valve with a 6-port 7010 Rheodyne (from *Besta Motorventile*) connecting the HPLC-DAD to a flow cell

installed in the above described ECD spectrophotometer. This permitted acquisition of the ECD spectrum of the compound of interest directly after identifying its UV curve by the diode array detector. The ECD spectra were measured three times in the interval from 190 to 500 nm, when the respective peaks were at their highest absorbances (typically above 800 mAU). The obtained average ECD curves were subsequently corrected by subtracting the blank recorded at a solvent ratio corresponding to the retention time of the analyzed compound. The HPLC-DAD system used for these analyses consisted of a PU-1580 pump, a three-line degasser unit DG-2080-53, a ternary gradient unit LC-980-025, an automatic sampler AS-2055 Plus, a column oven CO-1560, and a diode-array detector MD-2010 Plus (from *JASCO*).

HPLC-MS (ESI) analyses were carried out on an *Agilent* 1100 Series System consisting of a binary mixing HPLC pump, a degasser module, an autosampler, a DAD (all *Agilent* Technologies), and a *Bruker* Esquire 3000 Plus Ion Trap Mass Spectrometer (capillary temperature: 210 °C; ESI-voltage: 3.5-4.0 kV; N_2 as the heating gas). All measurements were performed on a Symmetry-C_{18} column (Waters, 4.6×250 mm, 5 μm) with the gradient 0 min 5% B, 25 min 70% B, 26 min 100% B, 29 min 100% B, 30 min 5% B, 32 min 5% B, in which A = H_2O + 0.1% formic acid (FA) and B = MeCN + 0.1% FA; flow rate: 0.8 mL/min.

1.3.3.   Gas Chromatography with Mass-Selective Detection (GC-MSD)

GC-MSD analyses were performed either on a GCMS-QP 2010SE (*Shimadzu*) or an a *Hewlett Packard* 5890 II gas chromatographer equipped with a *Hewlett Packard* Ultra 2 (cross linked 5% Ph Me silicone 25 m × 0.32 mm × 0.52 μm Film) capillary column connected to a *Hewlett Packard* 59822B ionization gauge controller and to a *Hewlett Packard* 5917A mass-selective detector.

1.4. Oxidative Degradation

This procedure was carried out as described earlier.[156] Briefly, ca. 0.8 mg of the respective alkaloid were submitted to a ruthenium (III)-catalyzed periodate oxidation, followed by derivatization of the resulting amino acids with MeOH/HCl and (*R*)-α-methoxy-α-trifluoromethylphenylacetyl chloride [(*R*)-MTPA-Cl, prepared from (*S*)-MTPA], and then analysis by GC-MSD.

1.5. Quantum Chemical Calculations

Quantum chemical calculations were carried out by Dr. T. Bruhn, as described in the respective publications.[123,124] Briefly, optimization was done using the B97-D3 functional in combination with def2-TZVP as basis set implemented in ORCA. UV and ECD spectra were computed using TDCAM-B3LYP/def2-TZVP with Gaussian09 and the resulting data were further processed using SpecDis 1.62.[216]

1.6. Assessment of Bioactivities

The testing of the antiprotozoal activities was performed in the group of Prof. R. Brun (Basel, Switzerland), as mentioned in the respective part of this thesis. For these bioassays, a standard protocol described in ref.[217] was used.

The evaluation of the growth-inhibitory potential of the compounds against the human cervical HeLa cell line and against human pancreatic cancer PANC-1 cells was conducted in the group of Prof. S. Awale (Toyama, Japon), as also stated in the respective parts of this thesis. For the protocols employed regarding these experiments, see e.g. the freely available publication indicated in ref.[103]

1.7. Chemicals

All used solvents (acetone, chloroform, dichlormethane, ethanol, ethyl acetate, *n*-hexane, methanol, and petroleum ether 40-60 °C) were analytical grade or distilled prior to use. Water for the HPLC analyses was ultra-purified by using an *Elga* Purelab Classic UV system.

Spectroscopic-grade and HPLC-grade solvents, TFA, FA, HCl, and NaOH were purchased from *Merck*, *Sigma Aldrich*, *VWR Chemicals*, *ITW Reagents*, *Fluka*, or *Acros Organic*.

2. Phytochemical Investigations on a Congolese *Ancistrocladus* Liana Related to *A. ealaensis*

2.1. Plant Material

The *Ancistrocladus* plant material was collected in the neighborhood of the village Bonsolerive, close to the town of Mbandaka in the Province of Equateur in the Democratic Republic of the Congo, in August 2008 (GPS coordinates 00°06.191S, 018°20.506E), by a team led by Prof. V. Mudogo. A voucher specimen (No. 032) has been deposited at the Bringmann Herbarium, University of Würzburg. Further, genetically identical samples were collected at the same site (GPS coordinates 00°06.191S, 018°20.507E) in August 2015 by the author of this thesis accompanied by local helping persons. A voucher specimen (No. 104) has also been deposited at the Bringmann Herbarium, University of Würzburg.

2.2. Extraction and Isolation

Air-dried and powdered leaves (400 g) from the collection of 2008 were exhaustively extracted with an acidified CH_2Cl_2-EtOH mixture (1:1, v/v). After neutralization with sodium hydroxide the suspension was filtered and the solvent evaporated under reduced pressure. The solid crude extract was macerated in chloroform and the remaining residue (3.6 g) was dissolved in methanol and resolved by preparative HPLC operating on a SymmetryPrep C18 column (*Waters*, 7 μm, 19 × 300 mm). The following gradient was used with the solvents (A) H_2O/MeCN (9:1) + 0.05% TFA and (B) H_2O/MeCN (1:9) + 0.05% TFA: 0 min 18% B, 35.5 min 33% B, 36-38 min 100% B, 38.5 min 18% B, and the flow was: 1 mL/min from 0 to 1 min and 8 mL/min from 1 to 40 min. A total of 15 fractions were collected.

Fraction 5 (R_T = 27.1 min) was further resolved on a Chromolith SemiPrep RP-18e (*Merck*, 100 × 10 mm) column using the gradient A/B: 0 min 0% B, 7 min 25% B, 7.5 min 100% B, in which A = H_2O/MeOH (9:1) + 0.05% TFA and B = H_2O/MeOH (1:9) + 0.05% TFA, the flow rate: 10 mL/min, yielding 13 mg of mbandakamine A (**16a**).

Resolution of Fraction 11 (R_T = 33.8 min) on the same HPLC semi-preparative column (Chromolith SemiPrep RP-18e) and the same solvent mixtures, A = H_2O/MeCN (9:1) + 0.05% TFA and B = H_2O/MeCN (1:9) + 0.05% TFA, but with a slightly different gradient: 0 min 15% B, 7 min 25% B, 7.5 min 100% B (flow rate: 8 mL/min), yielded 3.5 mg of mbandakamine B (**16b**).

As already mentioned, the discovery of **16a** and **16b** resulted from the cooperation between the author of this thesis and Dr. C. Steinert, who performed initial plant material extraction and was part of the team that collected the plant material in 2008. The experiments described in the following were conducted solely by the author of this thesis.

The above-mentioned chloroform extract was concentrated under reduced pressure, and was exhaustively washed with petroleum ether. The remaining residue (1 g) was dissolved in methanol and resolved on a SymmetryPrep C18 column (*Waters*, 7 µm, 19 × 300 mm) with the gradient A/B: 0 min 18% B, 35.5 min 33% B, in which A = H_2O/MeCN (9:1) + 0.05% TFA and B = H_2O/MeCN (1:9) + 0.05% TFA, flow: 10 mL/min, providing 15 fractions. Fraction 13 (R_T = 34 min) was further resolved by preparative HPLC on the same column with the gradient A/B: 0 min 38% B, 22 min 70% B, in which A = H_2O/MeOH (9:1) + 0.05% TFA and B = H_2O/MeOH (1:9) + 0.05% TFA, flow rate: 8 mL/min, giving 3 mg of cyclombandakamine A_1 (**20**).

Air-dried and powdered leaves (300 g) from the collection of 2015 were macerated in a neutral mixture of CH_2Cl_2 and MeOH (50:50, 3.2 L) and repeatedly extracted under mechanical agitation (48 h × 3). After filtration, the solvent was evaporated under reduced pressure and the resulting crude extract (28 g) was sonicated in H_2O (300 mL × 5 min × 2). The suspension was then filtrated and the aqueous phase was extracted with CH_2Cl_2, leading to two fractions: the lipophilic or dichloromethane fraction, referred to as F1, and the remaining polar or aqueous phase, addressed as F2.

After concentration under reduced pressure, F1 (1.8 g) was dissolved in the mixture H_2O/MeOH (8:2), filtrated over a 0.2 µm PTFE membrane (*Phenex*), and washed with EtOAc. The obtained alkaloid-enriched phase was concentrated under reduced pressure, dissolved in MeOH and resolved on preparative HPLC column (SymmetryPrep C18, *Waters*, 7 µm, 19 × 300 mm) with the following gradient: A/B: 0 min 18% B, 35 min 40 % B, in which A = H_2O/MeCN (9:1) + 0.05% TFA and B = H_2O/MeCN (1:9) + 0.05% TFA, flow: 10 mL/min. 14 subfractions were collected among which the subfraction 8 (R_T = 26 min), containing cyclombandakamine A_2 (**21**), was further resolved by preparative HPLC and provided 2.1 mg of this alkaloid after two HPLC cycles using the gradient: A/B: 0 min: 20% B and 23 min 38% B, in which A = H_2O/MeCN (9:1) + 0.05% TFA and B = H_2O/MeCN (1:9) + 0.05% TFA, flow: 10 mL/min.

Resolution of Subfraction 7 (R_T = 25 min) in the same chromatographic conditions as above mentioned for Subfraction 8 provided 2.8 mg of spirombandakamine A_1 (**22**). Resolution of Subfraction 5 (R_T = 22.6 min) by preparative HPLC provided spirombandakamine A_1 (**23**) (2.5 mg) after one HPLC cycle on an Xselect® prepHSS PFP column (*Waters*, 5 μm, 10 × 250 mm), using an isocratic gradient 78% of H_2O/MeOH (1:9) + 0.05% TFA; flow rate: 4.3 mL/min. Purification of subfraction 9 (R_T = 27 min) yielded mbandakamine B_2 (**17**) (6 mg) after two HPLC cycles, using the same chromatographic conditions as in the case of **22**.

The above-mentioned Fraction F2 was freeze-dried, giving ca. 30 g of an alkaloid-containing solid extract, which were submitted to a cation-exchange column,[79] in portions of 6 g. After eluting unbound metabolites from the column with MeOH and MeOH/H_2O (1:1), bound compounds were eluted with saturated aqueous sodium chloride solution, yielding ca. 3 g of an alkaloid-containing fraction. The latter was applied on a LiChropep RP® RP-18 (40-63 μm) column to remove further undesired polar material. The remaining alkaloid-enriched portion (0.7 g) was resolved on preparative HPLC column (SymmetryPrep C18, *Waters*, 7 μm, 19 × 300 mm) with the following gradient: A/B: 0 min 18% B, 35 min 40 % B, 36 min 100% B, in which A = H_2O/MeCN (9:1) + 0.05% TFA and B = H_2O/MeCN (1:9) + 0.05% TFA, flow: 10 mL/min, providing 6 mg of mbandakamine A (**16a**, R_T = 21.2 min), 3.1 mg of mbandakamine C (**18**, R_T = 23 min) and 2.6 mg of mbandakamine D (**19**, R_T = 24.4 min).

2.3. New Compounds

2.3.1. Mbandakamine A (16a)

Colorless solid (19 mg).

16a

$[\alpha]_D^{20} = +38$ ($c = 0.1$, MeOH).

HRMS (ESI): *m/z* found = 785.3798 [M+H]$^+$,

$\qquad$ *m/z* calculated for [C$_{48}$H$_{53}$N$_2$O$_8$]$^+$ = 785.3796.

ECD (MeOH): λ_{max} ($\Delta\varepsilon$) = 319 (+4), 290 (−3.6), 248 (+7), 230 (−30), 200 (+32) nm.

UV (MeOH): λ_{max} (log ε) = 348 (3.7), 332 (3.8), 318 (3.8), 290 (3.7), 230 (4.4) nm.

IR (ATM): ν_{max} = 3140, 3047, 2848, 2360, 2336, 1595, 1406, 1108, 1077, 667, 619 cm^{-1}.

Product of the oxidative degradation: (*R*)-3-aminobutyric acid.

^{1}H NMR (600 MHz, MeOD): δ = 1.25 (d, *J* = 6.5 Hz, 3H), 1.49 (d, *J* = 6.5, 3H), 1.53 (d, *J* = 6.7 Hz, 3H), 1.57 (d, *J* = 6.7 Hz, 3H), 1.88 (s, 3H), 1.97 (dd, *J* = 18.0, 4.3 Hz, 1H), 2.34 (s, 3H), 2.42 (dd, *J* = 18.0, 11.7 Hz, 1H), 2.52 (dd, *J* = 18.0, 11.7 Hz, 1H), 3.03 (s, 3H), 3.5 (m, 1H), 3.70 (m, 1H), 3.85 (s, 3H), 3.89 (dd, *J* = 18.1, 4.5 Hz, 1H), 4.09 (s, 3H), 4.15 (s, 3H), 4.64 (q, *J* = 6.7 Hz, 1H), 4.79 (q, *J* = 6.7 Hz, 1H), 5.32 (s, 1H), 6.44 (s, 1H), 6.46 (s, 1H), 6.62 (*p*t, *J* = 1.2 Hz, 1H), 6.74 (d, *J* = 1.2 Hz, 1H), 6.78 (s, 1H), 7.00 (d, *J* = 7.9 Hz, 1H), 7.05 (d, *J* = 7.9 Hz, 1H) ppm.

^{13}C NMR (150 MHz, MeOD): δ = 18.7 (CH$_3$), 18.7 (CH$_3$), 18.8 (CH$_3$), 19.6 (CH$_3$), 21.3 (CH$_3$), 22.0 (CH$_3$), 32.9 (CH$_2$), 33.1 (CH$_2$), 45.6 (CH), 46.1 (CH), 49.4 (CH), 49.9 (CH), 55.3 (CH$_3$), 55.9 (CH$_3$), 56.7 (CH$_3$), 56.8 (CH$_3$), 96.8 (CH), 98.5 (CH), 104.7 (CH), 106.9 (CH), 114.5 (CH), 118.8 (CH), 132.2 (CH), 134.4 (CH), 113.1, 113.4, 114.4, 116.2, 120.5, 122.7, 124.1, 124.3, 126.3, 127.8, 133.5, 133.6, 135.9, 136.4, 138.1, 140.9, 151.0, 154.3, 155.3, 156.5, 157.6, 157.3, 157.4, 158.4 (qC) ppm.

Table 6. NMR data (^{1}H: 600 MHz, ^{13}C: 150 MHz) of mbandakamine A (**16a**) in MeOD.

Position	^{13}C [ppm] (type)	^{1}H [ppm] (mult., J [Hz])	ROESY^{a}	HMBC
1	49.4 (CH)	4.79 (q, 6.7)	Me-1, MeO-8	3, 8, 9, Me-1
3	45.6 (CH)	3.70 (m)	H$_{eq}$-4, Me-1, Me-3	
4	32.9 (CH$_2$)	2.52 (dd, 18.0, 11.7)	H-3, H$_{eq}$-4, H-1', Me-3, **H-7'''**, **MeO-8'''**	3, 9, 10, Me-3
		3.89 (dd, 18.1, 4.5)	H-3, H$_{ax}$-4, **H-7'''**, Me-3	5, 9, 10
5	120.5 (qC)			
6	157.6 (qC)			
7	98.5 (CH)	6.46 (s)	MeO-8	1, 5, 6, 8, 9
8	157.3 (qC)			
9	113.1 (qC)			
10	133.6 (qC)			
1'	118.8 (CH)	6.62 (*p*t, 1.2)	H$_{ax}$-4, Me-2', **MeO-8'''**	3', 4', 8', 9', 10', Me-2'
2'	136.4 (qC)			
3'	106.9 (CH)	6.74 (d, 1.2)	Me-2', MeO-4', **MeO-8'''**	1', 2', 4', 9', Me-2'
4'	157.4 (qC)			
5'	151.0 (qC)			
6'	124.1 (qC)			
7'	134.4 (CH)	6.44 (s)	H$_{eq}$-4, **Me-2''**	
8'	124.3 (qC)			
9'	135.9 (qC)			
10'	114.4 (qC)			
1''	127.8 (qC)			
2''	140.9 (qC)			
3''	114.5 (CH)	6.78 (s)	Me-2''	1'', 4'', 10'', Me-2''
4''	155.3 (qC)			
5''	158.4 (qC)			

Position	δ_C (type)	δ_H (mult, J)	ROESY	HMBC
6"	104.7 (CH)	7.00 (d, 7.9)	MeO-5", H-7"	5", 8", 10"
7"	132.2 (CH)	7.05 (d, 7.9)	H-6", H_{eq}-4'''	5', 9", 5'''
8"	126.3 (qC)			
9"	138.1 (qC)			
10"	116.2 (qC)			
1'''	49.9 (CH)	4.64 (q, 6.7)	**MeO-4'**, Me-1''', MeO-8'''	3''', 8''', 9''', Me-1'''
3'''	46.1 (CH)	3.5 (m)	H_{eq}-4''', Me-1''', Me-3'''	
4'''	33.1 (CH$_2$)	2.42 (dd, 18.0, 11.7)	H-3''', H_{eq}-4''', Me-3'''	3''', 5''', 9''', 10''', Me-3'''
		1.97 (dd, 18.0, 4.3)	H-7", H-3''', H_{ax}-4''', Me-3'''	5''', 9''', 10'''
5'''	122.7 (qC)			
6'''	154.3 (qC)			
7'''	96.8 (CH)	5.32 (s)	**H_{ax}-4, Me-3, MeO-8**, MeO-8'''	8", 5''', 6''', 8''', 9'''
8'''	156.5 (qC)			
9'''	113.4 (qC)			
10'''	133.5 (qC)			
Me-1	18.7 (CH$_3$)	1.57 (d, 6.7)	H-1, H-3, MeO-8	1
Me-3	19.6 (CH$_3$)	1.49 (d, 6.5)	H-3, H_{ax}-4, H_{eq}-4, **H-7''', MeO-8'''**	3, 4
MeO-8	55.9 (CH$_3$)	3.85 (s)	H-1, H-7, Me-1	8
Me-2'	22.0 (CH$_3$)	2.34 (s)	H-1', H-3', **MeO-8'''**	1', 2', 3', 9', 10'
MeO-4'	56.7 (CH$_3$)	4.09 (s)	H-3', **H-1''', MeO-8'''**	4'
Me-2"	21.3 (CH$_3$)	1.88 (s)	**H-7'**, H-3"	6', 1", 2", 3", 8", 9"
MeO-5"	56.8 (CH$_3$)	4.15 (s)	H-6", H-7"	5"
Me-1'''	18.8 (CH$_3$)	1.53 (d, 6.7)	H-1''', H-3''', MeO-8'''	1'''
Me-3'''	18.7 (CH$_3$)	1.25 (d, 6.5)	H-3''', H_{ax}-4''', H_{eq}-4'''	3''', 4'''
MeO-8'''	55.3 (CH$_3$)	3.03 (s)	**H_{ax}-4, H-1', H-3'**, H-1''', H-7''', **Me-3, Me-2', MeO-4'**, Me-1'''	8'''

^{a} ROESY correlations between the two molecular moieties of **16a**, the southeastern portion **16a-I** and the northwestern part **16a-II**, are marked in **bold**.

2.3.2. Mbandakamine B (16b)

Colorless solid (3.5 mg).

16b

$[\alpha]_D^{20} = -38$ ($c = 0.1$, MeOH).

HRMS (ESI): *m/z* found = 785.3790 [M+H]$^+$,

   m/z calculated for $[C_{48}H_{53}N_2O_8]^+$ = 785.3796.
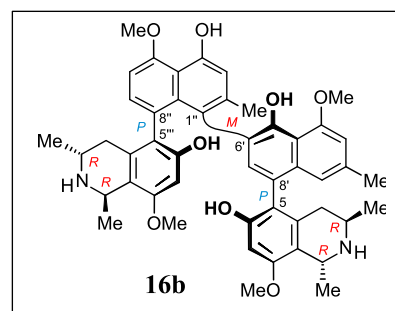
ECD (MeOH): λ_{max} ($\Delta\varepsilon$) = 348 (–0.9), 311 (–1.1), 269 (+1.7), 244 (–3.6), 221 (+6),

   206 (–4) nm.

UV (MeOH): λ_{max} (log ε) = 345 (3.4), 330 (3.5), 319 (3.5), 293 (3.4), 230 (4.2) nm.

IR (ATM): ν_{max} = 2924, 2852, 2360, 2336, 1677, 1204, 1137, 1054, 841, 803, 670 cm^{-1}.

Product of the oxidative degradation: (*R*)-3-aminobutyric acid.

^{1}H NMR (600 MHz, MeOD): δ = 1.13 (d, *J* = 6.4 Hz, 3H), 1.15 (d, *J* = 6.5 Hz, 3H), 1.39 (d, *J* = 6.8 Hz, 3H), 1.56 (d, *J* = 6.8 Hz, 3H), 1.72 (dd, *J* = 18.1, 11.7 Hz, 1H), 1.96 (dd, *J* = 18.2, 10.9 Hz, 1H), 2.01 (s, 3H), 2.22 (dd, *J* = 18.2, 4.1 Hz, 1H), 2.27 (s, 3H), 3.42 (m, 1H), 2.65 (dd, *J* = 18.1, 4.9 Hz, 1H), 3.45 (s, 3H), 3.65 (m, 1H), 3.93 (s, 3H), 4.09 (s, 3H), 4.15 (s, 3H), 4.38 (q, *J* = 6.8 Hz, 1H), 4.73 (q, *J* = 6.8 Hz, 1H), 5.94 (s, 1H), 6.51 (*p*t, *J* = 0.9 Hz), 6.71 (s, 1H), 6.77 (d, *J* = 0.9 Hz, 1H), 6.85 (s, 1H), 6.86 (s, 1H), 6.98 (d, *J* = 8.1 Hz, 1H), 7.01 (d, *J* = 8.1 Hz, 1H) ppm.

^{13}C NMR (150 MHz, MeOD): δ = 18.5 (CH$_3$), 18.6 (CH$_3$), 18.9 (CH$_3$), 19.1 (CH$_3$), 22.2 (CH$_3$), 22.8 (CH$_3$), 33.2 (CH$_2$), 33.6 (CH$_2$), 44.7 (CH), 45.4 (CH), 49.0 (CH), 49.3 (CH), 55.6 (CH$_3$), 56.2 (CH$_3$), 56.9 (CH$_3$), 56.9 (CH$_3$), 98.7 (CH), 98.8 (CH), 104.9 (CH), 107.8 (CH), 114.7 (CH), 118.6 (CH), 132.7 (CH), 133.3 (CH), 113.0, 115.0, 115.4, 116.2, 120.2, 122.9, 123.7, 126.6, 127.4, 131.2, 133.9, 136.1, 137.2, 137.4, 139.63, 139.64, 153.2, 155.6, 155.9, 156.2, 156.3, 157.6, 158.0, 158.1 (qC) ppm.

Table 7. NMR data (^{1}H: 600 MHz, ^{13}C: 150 MHz) of mbandakamine B (**16b**) in MeOD.

Position	^{13}C [ppm] (type)	^{1}H [ppm] (mult., J [Hz])	ROESY ^{a}	HMBC
1	49.0 (CH)	4.73 (q, 6.8)	Me-1, MeO-8	3, 8, 9, 10, Me-1
3	44.7 (CH)	3.65 (m)	H$_{eq}$-4, Me-1, Me-3	
4	33.2 (CH$_2$)	1.72 (dd, 18.1, 11.7)	H$_{eq}$-4, Me-3	3, 10, Me-3
		2.65 (dd, 18.1, 4.9)	H-3, H$_{ax}$-4, H-7', Me-3, **Me-2''**	5, 9, 10
5	120.2 (qC)			
6	155.9 (qC)			
7	98.8 (qC)	6.71 (s)	MeO-8	5, 6, 8, 9
8	157.6 (qC)			
9	115.4 (qC)			
10	133.9 (qC)			
1'	118.6 (CH)	6.51 (*p*t, 0.9)	Me-2'	3', 8', 10', Me-2'
2'	139.6 (qC)			
3'	107.8 (CH)	6.77 (d, 0.9)	Me-2', MeO-4', **MeO-8'''**	1', 4', 10', Me-2'
4'	158.0 (qC)			
5'	153.2 (qC)			
6'	136.1 (qC)			
7'	133.3 (CH)	6.86 (s)	H$_{eq}$-4, Me-2'', **H$_{ax}$-4'''**	5, 5', 6', 6''
8'	122.9 (qC)			
9'	137.2 (qC)			
10'	115.0 (qC)			
1''	126.6 (qC)			
2''	139.6 (qC)			
3''	114.7 (CH)	6.85 (s)	Me-2''	1'', 4'', 5'', 9'', Me-2''
4''	155.6 (qC)			
5''	158.1 (qC)			
6''	104.9 (CH)	7.01 (d, 8.1)	MeO-5''	4'', 8'', 9'', 10''
7''	132.7 (CH)	6.98 (d, 8.1)	MeO-5'', H$_{eq}$-4'''	8'', 9'', 10'', 4''', 5'''
8''	127.4 (qC)			
9''	137.4 (qC)			
10''	116.2 (qC)			
1'''	49.3 (CH)	4.38 (q, 6.8)	Me-1''', MeO-8'''	3''', 8''', 9''', 10''', Me-1'''
3'''	45.4 (CH)	3.42 (m)	H$_{eq}$-4''', Me-1''', Me-3'''	

4'''	33.6 (CH$_2$)	1.96 (dd, 18.2, 10.9)	H$_{eq}$-4''', **H-7'**, Me-3'''	3''', 10'''
		2.22 (dd, 18.2, 4.1)	H-7'', H$_{ax}$-4'''	5''', 9''', 10'''
5'''	123.7 (qC)			
6'''	156.2 (qC)			
7'''	98.7 (CH)	5.94 (s)	**MeO-4'**, MeO-8'''	8'', 5''', 6''', 9''', 10'''
8'''	156.3 (qC)			
9'''	113.0 (qC)			
10'''	131.2 (qC)			
Me-1	18.6 (CH$_3$)	1.56 (d, 6.8)	H-1, H-3, MeO-8	1, 9
Me-3	19.1 (CH$_3$)	1.13 (d, 6.4)	H-3, H$_{ax}$-4, H$_{eq}$-4, **MeO-2''**	3, 4
MeO-8	56.2 (CH$_3$)	3.93 (s)	H-7, Me-1	
Me-2'	22.2 (CH$_3$)	2.27 (s)	H-1', H-3', **MeO-8'''**	1', 2', 3', 9'
MeO-4'	56.9 (CH$_3$)	4.09 (s)	H-3', **H-7'''**, **MeO-8'''**	4'
Me-2''	22.8 (CH$_3$)	2.01 (s)	**H$_{eq}$-4**, H-3'', **Me-1**	1'', 2'', 3''
MeO-5''	56.9 (CH$_3$)	4.15 (s)	H-6'', H-7''	5''
Me-1'''	18.5 (CH$_3$)	1.39 (d, 6.8)	H-1''', H-3'''	1''', 9'''
Me-3'''	18.9 (CH$_3$)	1.15 (d, 6.5)	H-3''', H$_{ax}$-4''', H$_{eq}$-4'''	3''', 4'''
MeO-8'''	55.6 (CH$_3$)	3.45 (s)	**H-1'**, **H-3'**, H-1''', H-7''',**Me-2'**, **MeO-4'**	8'''

[a] ROESY correlations between the two molecular moieties of **16b**, the southeastern portion **16b-I** and the northwestern part **16b-II**, are marked in **bold**.

2.3.3. Mbandakamine B₂ (17)

White amorphous powder (6 mg).

17

$[\alpha]_D^{25} = -107.5$ ($c = 0.05$, MeOH).

HRMS (ESI): *m/z* found = 813.4106 [M+H]⁺,

           m/z calculated for $[C_{50}H_{57}N_2O_8]^+= 813.4109$.
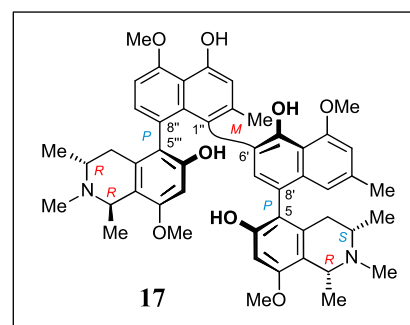
ECD (MeOH): λ_{max} ($\Delta\varepsilon$) = 378 (+1.2), 345 (−10.3), 337 (−9.6), 312 (−15.5), 272 (+1.5), 248

           (−49.0), 219 (+81.2), 205 (−15.5) nm.

UV (MeOH): λ_{max} (log ε) = 345 (3.3), 331 (3.4), 319 (3.6), 293 (3.4), 231 (4.3) nm.

IR (ATR): v_{max} = 3351, 2942, 1670, 1594, 1416, 1312, 1176, 1118, 1075, 956, 830, 798, 719,

           594 cm⁻¹.

Products of the oxidative degradation: (*R*)- and (*S*)-3-aminobutyric acid and (*R*)- and (*S*)-*N*-

           methyl-3-aminobutyric acid.

¹H NMR (600 MHz, MeOD): δ = 1.08 (d, *J* = 6.8 Hz, 3H), 1.21 (d, *J* = 6.1 Hz, 3H), 1.42 (d, *J*

           = 6.8 Hz, 3H), 1.63 (d, *J* = 6.5 Hz, 3H), 1.83 (m, 2H), 2.02 (dd, *J* = 17.0, 2.9 Hz,

           1H), 2.04 (s, 3H), 2.33 (s, 6H), 2.64 (dd, *J* = 17.1, 11.8 Hz, 1H), 2.92 (s, 3H), 2.95

           (m, 1H), 3.40 (s, 3H), 3.63 (m, 1H), 3.93 (s, 3H), 4.06 (s, 3H), 4.16 (s, 3H), 4.48 (q,

           J = 7.0 Hz, 1H), 4.49 (q, *J* = 6.6 Hz, 1H), 5.62 (s, 1H), 6.68 (s, 1H), 6.68 (s, 1H),

           6.81 (s, 1H), 6.82 (d, *J* = 1.0 Hz, 1H), 6.88 (s, 1H), 6.97 (d, *J* = 8.1 Hz, 1H), 7.01

           (d, *J* = 8.1 Hz, 1H) ppm.

¹³C NMR (150 MHz, MeOD): δ = 16.8 (CH₃), 18.1 (CH₃), 19.1 (CH₃), 20.1 (CH₃), 22.3

           (CH₃), 22.7 (CH₃), 29.2 (CH₂), 34.3 (CH₃), 36.2 (CH₂), 41.3 (CH₃), 50.5 (CH), 55.9

           (CH₃), 56.3 (CH₃), 57.1 (CH₃), 57.2 (CH₃), 59.4 (CH), 60.0 (CH), 62.0 (CH), 98.5

           (CH), 98.6 (CH), 105.0 (CH), 108.2 (CH), 114.9 (CH), 119.8 (CH), 133.0 (CH),

           133.6 (CH), 112.0, 115.47, 115.50, 116.1, 119.6, 122.7, 123.0, 123.6, 126.6, 127.3,

           130.5, 136.0, 136.9, 137.9, 139.6, 152.9, 155.8, 155.9, 156.8, 157.3, 157.8, 158.3,
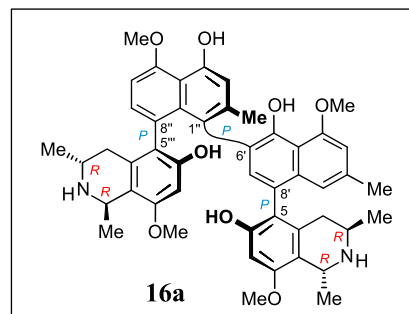
           158.4 (qC) ppm.

Table 8. NMR data (^{1}H: 600 MHz, ^{13}C: 150 MHz) of mbandakamine B$_2$ (**17**) in MeOD.*

Position	^{13}C [ppm] (type)	^{1}H [ppm] (mult., *J* [Hz])	ROESY^a	HMBC
1	62.0 (CH)	4.48 (q, 7.0)	H-3, Me-1, Me-*N*	8, 9, 10, Me-*N*, Me-1
3	60.0 (CH)	2.95 (m)	H$_{eq}$-4, H-1, Me-3, Me-*N*	
4	36.2 (CH$_2$)	2.02 (dd, 2.9, 17.0)	H-3, H$_{ax}$-4, H-7', H-1', Me-3	5, 9, 10
		2.64 (dd, 11.8, 17.1)	H-7', H$_{eq}$-4, Me-3	3, 5, 9, 10
5	119.6 (qC)			
6	156.8 (qC)			
7	98.5 (CH)	6.68 (s)	**Me-*N*'''**, **H-1'''**, MeO-8	1, 5, 6, 8, 9
8	157.8 (qC)			
9	115.5 (qC)			
10	136.8 (qC)			
1'	119.8 (CH)	6.68 (s)	H$_{eq}$-4, Me-2'	3', 8', 10', Me-2'
2'	136.9 (qC)			
3'	108.2 (CH)	6.82 (pd, 1.0)	Me-2', MeO-4'	1', 4', 10', Me-2'
4'	158.3 (qC)			
5'	152.9 (qC)			
6'	122.7 (qC)			
7'	133.6 (CH)	6.81 (s)	H$_{ax}$-4, H$_{eq}$-4, **H$_{eq}$-4'''**, **Me-2''**, **Me-*N*'''**	5, 9', 10', 5', **1''**
8'	123.6 (qC)			
9'	136.0 (qC)			
10'	115.5 (qC)			
1''	126.6 (qC)			
2''	139.6 (qC)			
3''	114.9 (CH)	6.88 (s)	Me-2''	1'', 4'', 10'', Me-2''
4''	155.8 (qC)			
5''	158.4 (qC)			
6''	105.0 (CH)	7.01 (d, 8.1)	H-7'', MeO-5''	5'', 8'', 10''
7''	133.0 (CH)	6.97 (d, 8.1)	H$_{eq}$-4''', H-6''	5''', 5'', 9'', 1'
8''	127.3 (qC)			
9''	137.9 (qC)			
10''	116.1 (qC)			

1'''	59.4 (CH)	4.49 (q, 6.6)	Me-1''', H-**7**, MeO-8''', Me-*N*'''	8''', 9''', 10''', Me-1''', Me-*N*'''
3'''	50.5 (CH)	3.63 (m)	H$_{eq}$-4''', Me-1''', Me-3''', Me-*N*'''	
4'''	29.2 (CH$_2$)	1.83 (dd)^b	H-3''', H$_{ax}$-4''', H-7'', **H-7'**	5''', 9''', 10'''
		1.84 (dd)^b	H$_{eq}$-4''', Me-3''', **H-7'**	3''', 10'''
5'''	123.0 (qC)			
6'''	155.9 (qC)			
7'''	98.6 (CH)	5.62 (s)	MeO-8''', **MeO-4'**	5''', 6''', 8''', 9''', 1'''
8'''	157.3 (qC)			
9'''	112.0 (qC)			
10'''	130.5 (qC)			
Me-1	20.1 (CH$_3$)	1.63 (d, 6.5)	H-1, Me-*N*, MeO-8	1, 9
Me-3	18.1 (CH$_3$)	1.21 (d, 6.1)	H-3, H$_{eq}$-4, H$_{ax}$-4, Me-*N*	3, 4, 10
Me-2'	22.3 (CH$_3$)	2.33 (s)	H-1', H-3', **MeO-8'''**	1', 2', 3'
Me-2''	22.7 (CH$_3$)	2.07 (s)	**H-7'**, H-3''	1'', 2'', 3''
Me-1'''	19.1 (CH$_3$)	1.42 (d, 6.8)	H-1''', H-3''', MeO-8''', Me-*N*'''	1''', 9'''
Me-3'''	16.8 (CH$_3$)	1.08 (d, 6.8)	H-3''', H$_{eq}$-4''', H$_{ax}$-4''', Me-*N*'''	3''', 4'''
MeO-8	56.3 (CH$_3$)	3.93 (s)	H-7, Me-1, *N*'''**-Me**	8
MeO-4'	57.1 (CH$_3$)	4.06 (s)	H-3'	4'
MeO-5''	57.2 (CH$_3$)	4.16 (s)	H-6''	5''
MeO-8'''	55.9 (CH$_3$)	3.40 (s)	H-7''', Me-1'''	8'''
Me-*N*	41.3 (CH$_3$)	2.92 (s)	H-1, H-3, Me-1, Me-3	1, 3
Me-*N*'''	34.3 (CH$_3$)	2.33 (s)	H-1''', H-3''', **H-7''**, **H-7**, **MeO-8**, Me-1''', Me-3'''	1''', 3'''

^{a} ROESY correlations between the two molecular moieties of **17**, the southeastern portion **17-I** and the northwestern part **17-II**, are marked in **bold**. ^{b} These protons overlap each other.

*Slight variations in the chemical shifts for some protons and carbon atoms were observed when the sample was very briefly warmed up before measurements. These changes concerned mainly the southeastern isoquinoline portion: δ_{H-1} = 4.48/4.58, δ_{C-1} = 62.0/62.3; δ_{H-3} = 2.95/3.00, δ_{C-3} = 60.0/60.3, δ_{H-4ax} = 2.64/2.66, δ_{H-4eq} = 2.02/2.05, δ_{C-4} = 36.2/35.8, δ_H for Me-1 = 1.63/1.65, δ_C for Me-1 = 20.1/19.9, δ_H for Me-3 = 1.21/1.24, δ_C for Me-1 = 18.1/17.8, and δ_H for Me-*N* = 2.92/2.99 ppm. These variations are likely to be a consequence of the conformational fluctuations resulting from repulsive interactions between the two isoquinoline portions, which are tightly pressed against each other.

2.3.4. *Mbandakamine C (18)*

Colorless solid (2.3 mg).

$[\alpha]_D^{20} = -10$ (*c* = 0.03, MeOH).

MS (ESI): *m/z* found = 785.2 [M+H]$^+$ (LC-MS),

      m/z calculated for [C$_{48}$H$_{53}$N$_2$O$_8$]$^+$ = 785.4.

18
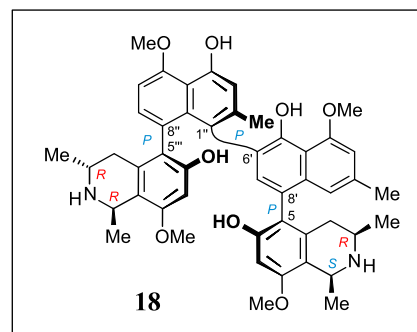
ECD (MeOH): λ_{max} ($\Delta\varepsilon$) = 319 (+8), 290 (−5), 248 (+11), 230 (−43), 200 (+54) nm.

UV (MeCN/H$_2$O, 8:2): λ_{max} (log ε) = 346 (0.31), 331 (0.38), 318 (0.33), 284 (0.41), 230 (0.51), 203 (1.3) nm.

Product of the oxidative degradation: (*R*)-3-aminobutyric acid.

^{1}H NMR (600 MHz, MeOD): δ = 1.25 (d, *J* = 6.6 Hz, 3H), 1.49 (d, *J* = 6.3 Hz, 3H), 1.53 (d, *J* = 6.9 Hz, 3H), 1.76 (d, *J* = 6.6 Hz, 3H), 1.91 (s, 3H), 1.95 (dd, *J* = 17.4, 4.3 Hz, 1H), 2.37 (s, 3H), 2.41 (dd, *J* = 17.4, 12.3 Hz, 1H), 2.54 (dd, *J* = 16.8, 11.7 Hz, 1H), 3.05 (s, 3H), 3.49 (m, 1H), 3.28 (m, 1H), 3.68 (dd, *J* = 17.2, 3.0 Hz, 1H), 3.83 (s, 3H), 4.09 (s, 3H), 4.15 (s, 3H), 4.65 (q, *J* = 6.6 Hz, 1H), 4.66 (q, *J* = 6.6 Hz, 1H), 5.32 (s, 1H), 6.45 (s, 1H), 6.48 (s, 1H), 6.75 (*p*d, *J* = 0.8 Hz, 1H), 6.75 (s, 1H), 6.79 (s, 1H), 6.99 (d, *J* = 7.9 Hz, 1H), 7.04 (d, *J* = 7.9 Hz, 1H) ppm.

^{13}C NMR (150 MHz, MeOD): δ = 18.7 (CH$_3$), 18.8 (CH$_3$), 18.9 (CH$_3$), 20.4 (CH$_3$), 21.4 (CH$_3$), 22.2 (CH$_3$), 33.0 (CH$_2$), 33.1 (CH$_2$), 46.1 (CH), 49.8 (CH), 51.5 (CH), 51.9 (CH), 55.2 (CH$_3$), 55.8 (CH$_3$), 56.7 (CH$_3$), 56.9 (CH$_3$), 96.9 (CH), 99.1 (CH), 104.6 (CH), 106.8 (CH), 114.4 (CH), 118.7 (CH), 132.2 (CH), 134.8 (CH), 113.3, 113.4, 114.4, 116.1, 120.7, 122.7, 124.0, 124.2, 126.3, 127.8, 133.5, 133.8, 136.2, 136.4, 138.0, 140.9, 151.1, 154.4, 155.3, 156.5, 157.4, 157.5, 158.0, 158.4 (qC) ppm.

Table 9. NMR data (^{1}H: 600 MHz, ^{13}C: 150 MHz) of mbandakamine C (**18**) in MeOD.

Position	^{13}C [ppm] (type)	^{1}H [ppm] (mult., J [Hz])	ROESY[a]	HMBC
1	51.9 (CH)	4.66 (q, 6.6)	H-3, MeO-8	3, 8, 9, Me-1
3	51.5 (CH)	3.28 (m)	H-1, Me-3	Me-3
4	33.0 (CH$_2$)	2.54 (dd, 16.8, 11.7)	H-3, H$_{eq}$-4, H-1', **H-7'''**, Me-3, **MeO-8'''**	3, 9, 10, Me-3
		3.68 (dd, 17.2, 3.0)	H-3, H$_{ax}$-4, H-7', **H-7'''**, Me-3	5, 9, 10
5	120.7 (qC)			
6	157.4 (qC)			
7	99.1 (CH)	6.48 (s)	MeO-8	1, 5, 6, 8, 9
8	158.0 (qC)			
9	113.3 (qC)			
10	133.8 (qC)			
1'	118.7 (CH)	6.75 (*p*d, 0.8)	H$_{ax}$-4, Me-2', **MeO-8'''**	3', 4', 8', 9', 10', Me-2'
2'	136.4 (qC)			
3'	106.8 (CH)	6.75 (s)	Me-2', MeO-4', **MeO-8'''**	1', 2', 4', 9', Me-2'
4'	157.5 (qC)			
5'	151.1 (qC)			
6'	124.0 (qC)			
7'	134.8 (CH)	6.45 (s)	H$_{eq}$-4, **Me-2''**	
8'	124.2 (qC)			
9'	136.2 (qC)			
10'	114.4 (qC)			
1''	127.8 (qC)			
2''	140.9 (qC)			
3''	114.3 (CH)	6.79 (s)	Me-2''	1'', 4'', 10'', Me-2''
4''	155.3 (qC)			
5''	158.4 (qC)			
6''	104.6 (CH)	6.99 (d, 7.9)	MeO-5'', H-7''	5'', 8'', 10''
7''	132.3 (CH)	7.04 (d, 7.9)	H-6'', H$_{eq}$-4'''	5'', 9'', 5'''
8''	126.3 (qC)			
9''	138.0 (qC)			

10"	116.1 (qC)			
1'''	49.8 (CH)	4.65 (q, 6.6)	**MeO-4'**, Me-1''', MeO-8'''	3''', 8''', 9''', Me-1'''
3'''	46.1 (CH)	3.49 (m)	H_{eq}-4''', Me-1''', Me-3'''	
4'''	33.1 (CH_2)	2.41 (dd, 17.4, 12.3)	H-3''', H_{eq}-4''', Me-3'''	3''', 5''', 9''', 10''', Me-3'''
		1.95 (dd, 17.4, 4.3)	H-7", H-3''', H_{ax}-4''', Me-3'''	5''', 9''', 10'''
5'''	122.7 (qC)			
6'''	154.4 (qC)			
7'''	96.9 (CH)	5.32 (s)	**H_{ax}-4**, **H_{eq}-4**, **Me-3**, MeO-8'''	8", 5''', 6''', 8''', 9'''
8'''	156.5 (qC)			
9'''	113.4 (qC)			
10'''	133.5 (qC)			
Me-1	20.4 (CH_3)	1.76 (d, 6.6)	H-1, MeO-8	1
Me-3	18.7 (CH_3)	1.49 (d, 6.3)	H-3, H_{ax}-4, H_{eq}-4, **H-7'''**, **MeO-8'''**	3, 4
MeO-8	55.8 (CH_3)	3.83 (s)	H-1, H-7, Me-1	8
Me-2'	22.2 (CH_3)	2.37 (s)	H-1', H-3', **MeO-8'''**	1', 2', 3', 9', 10'
MeO-4'	56.7 (CH_3)	4.09 (s)	H-3', **H-1'''**, **MeO-8'''**	4'
Me-2"	21.4 (CH_3)	1.91 (s)	**H-7'**, H-3"	6', 1", 2", 3", 8", 9"
MeO-5"	56.9 (CH_3)	4.15 (s)	H-6", H-7"	5"
Me-1'''	18.9 (CH_3)	1.53 (d, 6.9)	H-1''', H-3''', MeO-8'''	1'''
Me-3'''	18.8 (CH_3)	1.25 (d, 6.6)	H-3''', H_{ax}-4''', H_{eq}-4'''	3''', 4'''
MeO-8'''	55.2 (CH_3)	3.05 (s)	**H_{ax}-4**, **H-1'**, **H-3'**, H-1''', H-7''', **Me-3**, **Me-2'**, **MeO-4'**, Me-1'''	8'''

[a] ROESY correlations between the two molecular moieties of **18**, the southeastern naphthylisoquinoline portion and the northwestern one, are marked in **bold**.

The physical and spectroscopic data were in good agreement with those reported from parallel studies on *A. ealeansis*.[166]

2.3.5. Mbandakamine D (19)

Colorless solid (2.1 mg).

$[\alpha]_D^{20} = -9$ (c = 0.04, MeOH).

HRMS (ESI): *m/z* found = 783.3642 [M+H]$^+$,

$\qquad$ *m/z* calculated for [C$_{48}$H$_{51}$N$_2$O$_8$]$^+$ = 785.3640.
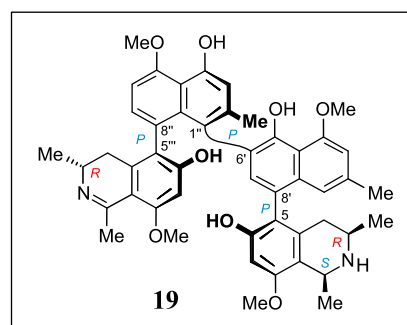
ECD (MeOH): λ_{max} ($\Delta\varepsilon$) = 319 (+8), 290 (−5), 248 (+11), 230 (−43), 200 (+54) nm.

UV (MeCN/H$_2$O, 8:2): λ_{max} (log ε) = 346 (0.23), 332 (0.24), 315 (0.23), 284 (0.11), 230 (0.41), 204 (1.1) nm.

Product of the oxidative degradation: (*R*)-3-aminobutyric acid.

^{1}H NMR (600 MHz, MeOD): δ = 1.26 (d, *J* = 6.6 Hz, 3H), 1.54 (d, *J* = 6.4 Hz, 3H), 1.77 (d, *J* = 6.5 Hz, 3H), 1.90 (s, 3H), 1.98 (dd, *J* = 16.7, 4.7 Hz, 1H), 2.38 (s, 3H), 2.62 (s, 3H), 2.63 (dd, *J* = 17.1, 11.7 Hz, 1H), 2.83 (*p*t, *J* = 16.7 Hz, 1H), 3.26 (s, 3H), 3.34 (m, 1H), 3.48 (m, 1H), 3.61 (dd, *J* = 16.8, 2.8 Hz, 1H), 3.83 (s, 3H), 4.05 (s, 3H), 4.16 (s, 3H), 4.67 (q, *J* = 6.6 Hz, 1H), 5.49 (s, 1H), 6.47 (s, 1H), 6.51 (s, 1H), 6.77 (s, 1H), 6.81 (s, 1H), 6.82 (s, 1H), 7.00 (d, *J* = 7.9 Hz, 1H), 7.06 (d, *J* = 7.9 Hz, 1H) ppm.

^{13}C NMR (150 MHz, MeOD): δ = 18.9 (CH$_3$), 19.0 (CH$_3$), 20.5 (CH$_3$), 21.5 (CH$_3$), 22.3 (CH$_3$), 24.6 (CH$_3$), 33.3 (CH$_2$), 33.9 (CH$_2$), 50.1 (CH), 51.5 (CH), 52.1 (CH), 56.00 (CH$_3$), 56.02 (CH$_3$), 57.3 (CH$_3$), 57.1 (CH$_3$), 99.3 (CH), 98.6* (CH), 104.7 (CH), 107.6 (CH), 114.9 (CH), 119.3 (CH), 131.9 (CH), 136.7 (CH), 108.7*, 113.5, 114.2, 116.2, 120.6, 123.5*,123.7, 124.6, 125.2*, 127.6, 135.5, 136.2, 137.0, 138.0, 143.0*, 141.2, 152.4, 155.5, 157.6, 157.7, 158.2, 158.6, 165.0*, 167.0*, 175.9* (qC) ppm.

* The signal was not visible in the ^{13}C NMR spectrum, but it was evidenced from HMBC cross-peaks, and was ascertained by comparing the chemical shifts with the corresponding ones in michellamine-type dimers displaying a dihydroisoquinoline ring.

Table 10. NMR data (^{1}H: 600 MHz, ^{13}C: 150 MHz) of mbandakamine D (**19**) in MeOD.

Position	^{13}C [ppm] (type)	^{1}H [ppm] (mult., J [Hz])	ROESY ^{a}	HMBC
1	52.1 (CH)	4.67 (q, 6.6)	H-3, MeO-8	3, 8, 9, Me-1
3	51.5 (CH)	3.34 (m)	H-1	
4	33.3 (CH$_2$)	2.63 (dd, 17.1, 11.7)	H-3, H$_{eq}$-4, H-1', **H-7'''**, Me-3	3, 9, 10, Me-3
		3.61 (dd, 16.8, 2.8)	H-3, H$_{ax}$-4, H-7', **H-7'''**, Me-3	5, 9, 10
5	120.6 (qC)			
6	157.7 (qC)			
7	99.3 (CH)	6.47 (s)	MeO-8	1, 5, 6, 8, 9
8	158.2 (qC)			
9	113.5 (qC)			
10	135.5 (qC)			
1'	119.3 (CH)	6.77 (s)	H$_{ax}$-4, Me-2', **MeO-8'''**	3', 4', 8', 9', 10', Me-2'
2'	137.0 (qC)			
3'	107.6 (CH)	6.81 (s)	Me-2', MeO-4', **MeO-8'''**	1', 2', 4', 9', Me-2'
4'	157.6 (qC)			
5'	152.4 (qC)			
6'	123.7 (qC)			
7'	136.7 (CH)	6.51 (s)	H$_{eq}$-4, **Me-2''**	
8'	124.6 (qC)			
9'	136.2 (qC)			
10'	114.2 (qC)			
1''	127.6 (qC)			
2''	141.2 (qC)			
3''	114.9 (CH)	6.82 (s)	Me-2''	1'', 4'', 10'', Me-2''
4''	155.5 (qC)			
5''	158.6,* qC			
6''	104.7 (CH)	7.00 (d, 7.9)	MeO-5'', H-7''	5'', 8'', 10''
7''	131.9 (CH)	7.06 (d, 7.9)	H-6'', H$_{eq}$-4'''	5'', 9'', 5'''
8''	123.5,* qC			
9''	138.0 (qC)			
10''	116.2 (qC)			

1'''	175.9,[*] qC			
3'''	50.1 CH	3.48 (m)	H_{eq}-4''', Me-3'''	
4'''	33.9 (CH$_2$)	2.83 (*p*t, 16.7)	H-3''', H_{eq}-4''', Me-3'''	3''', 5''', 9''', 10''', Me-3'''
		1.98 (dd, 16.7, 4.7)	H-7'', H-3''', H_{ax}-4''', Me-3'''	5''', 9''', 10'''
5'''	125.2,[*] qC			
6'''	167.0,[*] qC			
7'''	98.6,[*] CH	5.49 (s)	**H_{ax}-4**, **H_{eq}-4**, **Me-3**, MeO-8'''	8'', 5''', 6''', 8''', 9'''
8'''	165.0,[*] qC			
9'''	108.7,[*] qC			
10'''	143.0,[*] qC			
Me-1	20.5 (CH$_3$)	1.77 (d, 6.5)	H-1, MeO-8	1
Me-3	19.0 (CH$_3$)	1.54 (d, 6.4)	H-3, H_{ax}-4, H_{eq}-4, **H-7'''**, **MeO-8'''**	3, 4
MeO-8	56.0 (CH$_3$)	3.83 (s)	H-1, H-7, Me-1	8
Me-2'	22.3 (CH$_3$)	2.38 (s)	H-1', H-3', **MeO-8'''**	1', 2', 3', 9', 10'
MeO-4'	57.3 (CH$_3$)	4.05 (s)	H-3', **Me-1'''**, **MeO-8'''**	4'
Me-2''	21.5 (CH$_3$)	1.90 (s)	**H-7'**, H-3''	6', 1'', 2'', 3'', 8'', 9''
MeO-5''	57.1 (CH$_3$)	4.16 (s)	H-6''	5''
Me-1'''	24.6 (CH$_3$)	2.62 (s)	MeO-8''', **MeO-4'**	1'''
Me-3'''	18.9 (CH$_3$)	1.26 (d, 6.6)	H-3''', H_{ax}-4''', H_{eq}-4'''	3''', 4'''
MeO-8'''	56.0 (CH$_3$)	3.26 (s)	**H_{ax}-4**, **H-1'**, **H-3'**, H-7''', **Me-3**, **Me-2'**, **MeO-4'**, Me-1'''	8'''

[a] ROESY correlations between the two molecular portions of **19** are marked in **bold**.

[*] The signal was not visible in the ^{13}C NMR spectrum, but it was evidenced from HMBC cross-peaks, and was ascertained by comparing the values of chemical shifts with the corresponding ones of michellamine-type dimers displaying a dihydroisoquinoline ring.

The physical and spectroscopic data were in good agreement with those reported from parallel studies on *A. ealeansis*.[166]

### 2.3.6. *Cyclombandakamine A₁ (20)*

Beige amorphous powder (3 mg).

$[\alpha]_D^{25} = +34$ (*c* = 0.02, MeOH).

HRMS (ESI): *m/z* found = 797.3783 [M+H]$^+$,

        m/z calculated for $[C_{49}H_{53}N_2O_8]^+$ = 797.3796.
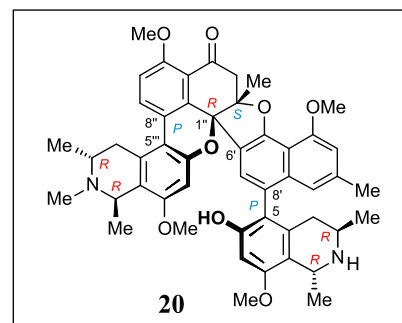
ECD (MeOH): λ_{max} ($\Delta\varepsilon$) = 361 (+2.5), 348 (−1.5), 325 (+4.9), 305 (−10.1), 289 (+3.4), 246
        (−20.8), 233 (+26.2), 220 (+10.2), 217 (+10.9), 206 (−3.5), 195
        (+13.9) nm.

UV (MeOH): λ_{max} (log ε) = 400 (0.03), 344 (0.48), 338 (0.42), 311 (0.66), 293 (0.54), 284
        (0.58), 275 (0.54), 230 (2.6), 214 (2.28), 201 (3.03) nm.

IR (ATM): ν_{max} = 3410, 2962, 2357, 2342, 1683, 1603, 1448, 1260, 1203, 1079, 1026, 799,
        723 cm^{-1}.

Products of the oxidative degradation: (*R*)-3-aminobutyric acid and (*R*)-*N*-methyl-3-
        aminobutyric acid.

^{1}H NMR (600 MHz, MeOD): δ = 0.93 (d, *J* = 6.7 Hz, 3H), 1.09 (d, *J* = 6.4 Hz, 3H), 1.51 (d, *J*
        = 6.7 Hz, 3H), 1.73 (d, *J* = 6.6 Hz, 3H), 1.85 (s, 3H), 1.94 (dd, *J* = 17.9, *J* = 11.4
        Hz, 1H), 2.29 (pd, *J* = 0.3 Hz, 1H), 2.33 (dd, *J* = 17.9, *J* = 4.9 Hz, 1H), 2.92 (s,
        3H), 3.03 (d, *J* = 14.6 Hz, 1H), 3.06 (dd, *J* = 17.1, *J* = 4.5 Hz, 1H), 3.12 (dd, *J* =
        14.6, *J* = 0.7 Hz, 1H), 3.52 (m, 1H), 3.72 (s, 3H), 3.84 (dd, *J* = 17.1, *J* = 5.4 Hz,
        1H), 3.88 (s, 3H), 3.95 (m, 1H), 3.97 (s, 3H), 4.00 (s, 3H), 4.44 (q, *J* = 6.6 Hz,
        1H), 4.68 (q, *J* = 6.8 Hz, 1H), 6.38 (s, 1H), 6.41 (s, 1H), 6.47 (s, 1H), 6.51 (*p*t, *J* =
        1.1 Hz, 1H), 6.80 (d, *J* = 1.2 Hz, 1H), 7.35 (d, *J* = 9.0 Hz, 1H), 8.04 (d, *J* = 9.0
        Hz, 1H) ppm.

^{13}C NMR (150 MHz, MeOD): δ = 12.4 (CH$_3$), 18.2 (CH$_3$), 18.6 (CH$_3$), 18.8 (CH$_3$), 19.0
        (CH$_3$), 22.3 (CH$_3$), 32.6 (CH$_2$), 33.6 (CH$_2$), 38.9 (CH$_3$), 44.8 (CH), 48.9 (CH),
        52.0 (CH$_2$), 55.1 (CH), 56.2 (CH), 56.42 (CH$_3$), 56.43 (CH$_3$), 56.7 (CH$_3$), 57.9
        (CH$_3$), 98.4 (CH), 102.5 (CH), 108.6 (CH), 113.8 (CH), 117.8 (CH), 125.8 (CH),
        135.2 (CH), 85.3, 92.3, 113.9, 114.3, 118.3, 118.4, 119.4, 119.7, 121.0, 124.3,
        126.2, 127.8, 133.1, 138.3, 138.6, 139.6, 154.8, 156.4, 157.2, 157.5, 158.0, 158.4,
        160.6, 196.0 (qC) ppm.

Table 11. NMR data (^{1}H: 600 MHz, ^{13}C: 150 MHz) of cyclombandakamine A$_1$ (**20**) in MeOD.

Position	^{13}C [ppm] (type)	^{1}H [ppm] (mult., *J* [Hz])	ROESY[a]	HMBC
1	48.9 (CH)	4.68 (q, 6.8)	Me-1, MeO-8	3, 8, 9, 10, Me-1
3	44.8 (CH)	3.52 (m)	H$_{eq}$-4, Me-1, Me-3	
4	32.6 (CH$_2$)	2.33 (dd, 4.9, 17.9)	H-3, H$_{ax}$-4, H-7', Me-3	9, 5
		1.94 (dd, 11.4, 17.9)	H-1', H$_{eq}$-4, Me-3	10
5	119.7 (qC)			
6	157.2 (qC)			
7	98.4 (CH)	6.41 (s)	Me-3, Me-*N*''', MeO-8	5, 6, 8, 9
8	157.5 (qC)			
9	113.9 (qC)			
10	133.1 (qC)			
1'	117.8 (CH)	6.51(*p*t, 1.1)	H$_{ax}$-4, Me-2'	3', 8', 10', Me-2'
2'	139.6 (qC)			
3'	108.6 (CH)	6.80 (d, 1.2)	Me-2', MeO-4'	1', 4', 10', Me-2'
4'	158.4 (qC)			
5'	156.4 (qC)			
6'	121.0 (qC)			
7'	125.8 (CH)	6.38 (s)	H$_{eq}$-4, **H$_{eq}$-4'''**, **Me-3'''**, **Me-*N*'''**	5, 9', 10', 5', 1"
8'	126.2 (qC)			
9'	138.6 (qC)			
10'	114.3 (qC)			
1"	85.3 (qC)			
2"	92.3 (qC)			
3"	52.0 (CH$_2$)	3.03 (d, 14.6)	H$_b$-3", Me-2"	1", 2", 4", 10", Me-2"
		3.12 (dd, 0.7, 14.6)	H$_a$-3", Me-2"	1", 4', Me-2'
4"	196.0 (qC)			
5"	160.6 (qC)			
6"	113.8 (CH)	7.35 (d, 9.0)	H-7", MeO-5"	5", 8", 10"
7"	135.2 (CH)	8.04 (d, 9.0)	H$_{eq}$-4''', H$_{ax}$-4''', H-6"	5''', 5", 9"
8"	124.3 (qC)			
9"	138.3 (qC)			

10"	119.4 (qC)			
1'''	57.9 (CH)	4.44 (q, 6.6)	Me-1''', Me-3''', Me-*N*'''	8''', 9''', 10''', Me-1''', Me-*N*'''
3'''	55.1 (CH)	3.95 (m)	H$_{eq}$-4''', Me-1''', Me-3''', Me-*N*'''	-
4'''	33.6 (CH$_2$)	3.06 (dd, 4.5, 17.1)	H-3''', H$_{ax}$-4''', H-7'', Me-3''', **H-7'**	5''', 10'''
		3.84 (dd, 5.4, 17.1)	H$_{eq}$-4''', H-7''	
5'''	118.4 (qC)			
6'''	154.8 (qC)			
7'''	102.5 (CH)	6.47 (s)	MeO-8''', Me-2'''	5''', 6''', 8''', 9'''
8'''	158.0 (qC)			
9'''	118.3 (qC)			
10'''	127.8 (qC)			
Me-1	18.6 (CH$_3$)	1.51 (d, 6.7)	H-1, H-3, MeO-8, **Me-3'''**	1, 9
Me-3	19.0 (CH$_3$)	1.09 (d, 6.4)	H-3, H$_{eq}$-4, H$_{ax}$-4	3, 4
Me-2'	22.3 (CH$_3$)	2.29 (*p*d, 0.3)	H-1', H-3'	1', 2', 3'
Me-2"	18.2 (CH$_3$)	1.85 (s)	H-7''', H$_a$-3", H$_b$-3"	1", 2", 3"
Me-1'''	18.8 (CH$_3$)	1.73 (d, 6.6)	H-1''', H-3''', MeO-8''', Me-*N*'''	1''', 9'''
Me-3'''	12.4 (CH$_3$)	0.93 (d, 6.7)	H-1''', H-3''', H$_{eq}$-4''', **H-7'**, **H-7**, MeO-**8**, **Me-1**, Me-*N*'''	3''', 4'''
MeO-8	56.2 (CH$_3$)	3.88 (s)	H-7, Me-1, **Me-3'''**, **Me-*N*'''**	8'''
MeO-4'	56.4 (CH$_3$)	4.00 (s)	H-3'	4'
MeO-5"	56.7 (CH$_3$)	3.97 (s)	H-6"	5"
MeO-8'''	56.4 (CH$_3$)	3.72 (s)	H-7''', Me-1'''	8'''
Me-*N*'''	38.9 (CH$_3$)	2.92 (s)	H-1''', H-3''', H-**7''**, H-**7**, MeO-**8**, Me-1''', Me-3'''	1''', 3'''

[a] ROESY correlations between the southeastern moiety of **20**, **20-I**, and the northwestern part, **20-II**, are marked in **bold**.

2.3.7. *Cyclombandakamine A₂ (21)*

Beige amorphous powder (2.5 mg).

$[\alpha]_D^{25} = +59$ ($c = 0.06$, MeOH).

HRMS (ESI): *m/z* found = 811.3952 [M+H]⁺,

m/z calculated for $[C_{50}H_{55}N_2O_8]^+$ = 811.3953.
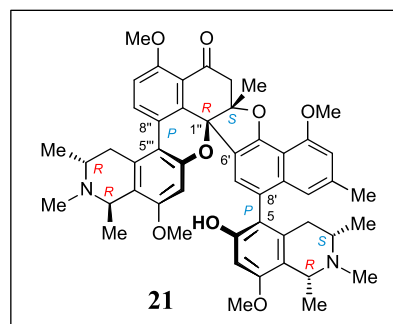
ECD (MeOH): λ_{max} ($\Delta\varepsilon$) = 363 (+1.5), 345 (−0.5), 327 (+1.5), 305 (−8.4), 286 (+1.9), 248 (−16.4), 232 (+28.7), 220 (+11.2), 216 (+11.1), 206 (+1.4), 191 (+20.6) nm.

UV (MeOH): λ_{max} (log ε) = 400 (0.04), 345 (0.50), 339 (0.43), 311 (0.68), 292 (0.56), 285 (0.58), 274 (0.57), 231 (2.62), 214 (2.30), 201 (3.06) nm.

IR (ATR): ν_{max} = 3353, 3064, 2923, 2360, 1676, 1597, 1457, 1274, 1195, 1125, 1073, 1029, 833, 804, 716 cm⁻¹.

Products of the oxidative degradation: (*R*)- and (*S*)-3-aminobutyric acid and (*R*)- and (*S*)-*N*-methyl-3-aminobutyric acid.

¹H NMR (600 MHz, MeOD): δ = 0.84 (d, *J* = 6.7 Hz, 3H), 1.15 (d, *J* = 6.4 Hz, 3H), 1.63 (d, *J* = 6.8 Hz, 3H), 1.72 (d, *J* = 6.6 Hz, 3H), 1.85 (s, 3H), 1.97 (dd, *J* = 17.5, 2.9 Hz, 1H), 2.29 (s, 3H), 2.31 (dd, *J* = 17.5, 11.9 Hz, 1H), 2.85 (s, 3H), 2.96 (s, 3H), 3.03 (d, *J* = 14.7 Hz, 1H), 3.04 (m, 2H), 3.09 (d, *J* = 14.7 Hz, 1H), 3.71 (s, 3H), 3.86 (m, 1H), 3.88 (s, 3H), 3.96 (m, 1H), 3.98 (s, 3H), 4.00 (s, 3H), 4.41 (q, *J* = 6.6 Hz, 1H), 4.56 (q, *J* = 6.8 Hz, 1H), 6.36 (s, 1 H), 6.45 (s, 2H), 6.52 (s, 1H), 6.81 (s, 1H), 7.36 (d, *J* = 8.9 Hz, 1H), 8.05 (d, *J* = 8.9 Hz, 1H) ppm.

¹³C NMR (150 MHz, MeOD): δ = 12.4 (CH₃), 20.0 (CH₃), 18.4 (CH₃), 17.9 (CH₃), 22.5 (CH₃), 18.9 (CH₃), 33.7 (CH₂), 33.8 (CH₂), 39.0 (CH₃), 41.5 (CH₃), 52.2 (CH₂), 55.1 (CH), 56.3 (CH₃), 56.6 (CH₃), 56.6 (CH₃), 56.9 (CH₃), 58.0 (CH), 62.1 (CH), 60.5 (CH), 98.9 (CH), 102.6 (CH), 108.8 (CH), 114.0 (CH), 118.0 (CH), 126.6 (CH), 135.5 (CH), 85.3, 92.5, 114.2, 114.4, 118.4, 118.7, 119.4, 119.4, 126.1, 124.4, 120.9, 127.9, 138.4, 134.9, 138.6, 139.9, 158.1, 157.4, 156.5, 158.4, 154.9, 157.7, 160.7, 196.2 (qC) ppm.

Table 12. NMR data (^{1}H: 600 MHz, ^{13}C: 150 MHz) of cyclombandakamine A$_2$ (**21**) in MeOD.

Position	^{13}C [ppm] (type)	^{1}H [ppm] (mult., J [Hz])	ROESY ^{a}	HMBC
1	62.1 (CH)	4.56 (q, 6.8)	H-3, Me-1, Me-*N*, MeO-8	8, 9, 10, Me-*N*, Me-1
3	60.5 (CH)	3.04 (m)	H$_{eq}$-4, H-1, Me-3, Me-*N*	
4	33.8 (CH$_2$)	1.97 (dd, 2.9, 17.5)	H-3, H$_{ax}$-4, H-1', Me-3	3, 9, 10
		2.31 (dd, 11.9, 17.5)	H-7', H$_{eq}$-4, Me-3	5, 9, 10
5	119.4 (qC)			
6	157.4 (qC)			
7	98.9 (CH)	6.45 (s)	**Me-3'''**, **Me-*N*'''**, MeO-8	1, 5, 6, 8, 9
8	157.7 (qC)			
9	114.2 (qC)			
10	134.9 (qC)			
1'	118.0 (CH)	6.52 (s)	H$_{eq}$-4, Me-2'	3', 8', 10', Me-2'
2'	139.9 (qC)			
3'	108.8 (CH)	6.81 (s)	Me-2', MeO-4'	1', 4', 10', Me-2'
4'	158.4 (qC)			
5'	156.5 (qC)			
6'	120.9 (qC)			
7'	126.6 (CH)	6.36 (s)	H$_{ax}$-4, **H$_{eq}$-4'''**, **Me-3'''**, **Me-*N*'''**	5, 9', 10', 5', 1"
8'	126.1 (qC)			
9'	138.6 (qC)			
10'	114.4 (qC)			
1"	85.3 (qC)			
2"	92.5 (qC)			
3"	52.2 (CH$_2$)	3.03 (d, 14.7)	3"-H$_b$, Me-2"	1", 2", 4", 10", Me-2"
		3.09 (d, 14.7)	H$_a$-3", Me-2"	1", 4', Me-2'
4"	196.2 (qC)			
5"	160.7 (qC)			
6"	114.0 (CH)	7.36 (d, 8.9)	H-7", MeO-5"	5", 8", 10"
7"	135.5 (CH)	8.05 (d, 8.9)	H$_{eq}$-4''', H$_{ax}$-4''', H-6"	5''', 5", 9", 1'

8"	124.4 (qC)			
9"	138.4 (qC)			
10"	119.4 (qC)			
1'''	58.0 (CH)	4.41 (q, 6.6)	Me-1''', Me-3''', Me-N'''	8''', 9''', 10''', Me-1''', Me-N'''
3'''	55.1 (CH)	3.96 (m)	H_{eq}-4''', Me-1''', Me-3''', Me-N'''	
4'''	33.7 (CH_2)	3.04 (dd)[b]	H-3''', H_{ax}-4''', H-7'', Me-3''', **H-7'**	5''', 9''', 10'''
		3.86 (dd)[c]	H_{eq}-4''', H-7''	3''', 10'''
5'''	118.7 (qC)			
6'''	154.9 (qC)			
7'''	102.6 (CH)	6.45 (s)	MeO-8''', Me-2"	5''', 6''', 8''', 9''', 1'''
8'''	158.1 (qC)			
9'''	118.4 (qC)			
10'''	127.9 (qC)			
Me-1	20.0 (CH_3)	1.63 (d, 6.8)	H-1, Me-N, MeO-8	1, 9
Me-3	17.9 (CH_3)	1.15 (d, 6.4)	H-3, H_{eq}-4, H_{ax}-4, Me-N	3, 4
Me-2'	22.5 (CH_3)	2.29 (s)	H-1', H-3'	1', 2', 3'
Me-2"	18.4 (CH_3)	1.85 (s)	H-7''', H_a-3", H_b-3"	1", 2", 3"
Me-1'''	18.9 (CH_3)	1.72 (d, 6.6)	H-1''', H-3''', MeO-8''', Me-N'''	1''', 9'''
Me-3'''	12.4 (CH_3)	0.84 (d, 6.7)	H-1''', H-3''', H_{eq}-4''', **H-7'**, **H-7**, **MeO-8**, Me-N'''	3''', 4'''
MeO-8	56.3 (CH_3)	3.88 (s)	H-7, Me-1, **Me-N'''**	8
MeO-4'	56.6 (CH_3)	4.00 (s)	H-3'	4'
MeO-5"	56.9 (CH_3)	3.98 (s)	H-6"	5"
MeO-8'''	56.6 (CH_3)	3.71 (s)	H-7''', H-1''', Me-1''', **H-1'**, **Me-2'**	8'''
Me-N	41.5 (CH_3)	2.96 (s)	H-1, H-3, Me-1, Me-3	1, 3
Me-N'''	39.0 (CH_3)	2.85 (s)	H-1''', H-3''', Me-1''', Me-3''', H-**7**, **H-7'**, **MeO-8**	1''', 3'''

[a] ROESY correlations between the southeastern moiety and the northwestern part are marked in **bold**.

[b] Overlapped with the signal of H-3. [c] Overlapped with the signal of MeO-8.

2.3.8. *Spirombandakamine A$_1$ (22)*

Beige amorphous powder (3.5 mg).

$[\alpha]_D^{25} = -69.9$ (c = 0.04, MeOH).

HRMS (ESI): *m/z* found = 811.3973 [M+H]$^+$

$\qquad$ *m/z* calculated for [C$_{50}$H$_{55}$N$_2$O$_8$]$^+$ = 811.3953.
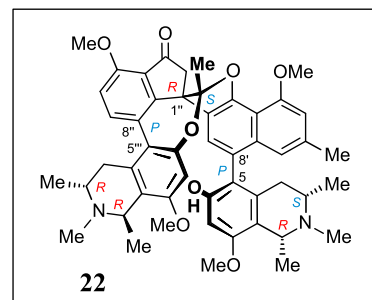
ECD (MeOH): λ_{max} ($\Delta\varepsilon$) = 368 (+7.0), 313 (−38.5), 295 (−10.6), 271 (−46.8), 236 (+83.6), 226 (+25.3), 214 (+101.2), 205 (+55.3) nm.

UV (MeOH): λ_{max} (log ε) = 360 (0.06), 346 (0.72), 331 (0.93), 315 (0.96), 280 (1.3), 226 (3.4), 215 (3.16), 204 (3.8) nm.

IR (ATR): ν_{max} = 3356, 3189, 1660, 1632, 1466, 1424, 1259, 1134, 1030, 801, 721 cm^{-1}.

Products of the oxidative degradation: (*R*)- and (*S*)-3-aminobutyric acid and (*R*)- and (*S*)-*N*-methyl-3-aminobutyric acid.

^{1}H NMR (600 MHz, MeOD): δ = 1.18 (d, *J* = 6.4 Hz, 3H), 1.24 (d, *J* = 6.6 Hz, 3H), 1.54 (d, *J* = 6.8 Hz, 3H), 1.61 (d, *J* = 6.6 Hz, 3H), 1.88 (dd, *J* = 17.3, 2.9 Hz, 1H), 1.94 (s, 3H), 2.03 (dd, *J* = 18.3, *J* = 11.4 Hz, 1H), 2.10 (s, 3H), 2.26 (s, 3H), 2.32 (dd, *J* = 17.3, 11.4 Hz, 1H), 2.66 (d, *J* = 19.5 Hz, 1H), 2.96 (s, 3H), 3.02 (m, 1H), 3.49 (d, *J* = 19.5 Hz, 1H), 3.51 (dd, *J* = 18.3, 4.9 Hz, 1H), 3.78 (s, 3H), 3.87 (s, 3H), 4.00 (m, 1H), 4.01 (s, 3H), 4.03 (s, 3H), 4.38 (q, *J* = 6.8 Hz, 1H), 4.58 (q, *J* = 6.6 Hz, 1H), 6.46 (s, 1H), 6.53 (s, 1H), 6.55 (s, 1H), 6.70 (s, 1H), 6.90 (s, 1H), 7.23 (d, *J* = 8.7 Hz, 1H), 7.86 (d, *J* = 8.7 Hz, 1H) ppm.

^{13}C NMR (150 MHz, MeOD): δ = 16.5 (CH$_3$), 18.0 (CH$_3$), 19.1 (CH$_3$), 19.9 (CH$_3$), 22.4 (CH$_3$), 23.8 (CH$_3$), 29.0 (CH$_2$), 34.0 (CH$_2$), 34.8 (CH$_3$), 41.7 (CH$_3$), 50.6 (CH), 52.4 (CH$_2$), 56.2 (CH$_3$), 56.4 (CH$_3$), 56.5 (CH$_3$), 56.6 (CH$_3$), 58.6 (CH), 60.5 (CH), 62.0 (CH), 58.7, 99.0 (CH), 108.2 (CH), 108.5 (CH), 112.7 (CH), 118.4 (CH), 123.9 (CH), 140.3 (CH), 111.9, 114.8, 118.4, 119.4, 123.4, 125.6, 125.7, 126.3, 127.1, 128.8, 129.6, 135.3, 138.2, 136.5, 154.3, 154.4, 156.8, 157.4, 157.5, 157.6, 157.8, 158.4, 203.2 (qC) ppm.

Table 13. NMR data (^{1}H: 600 MHz, ^{13}C: 150 MHz) of spirombandakamine A$_1$ (**22**) in MeOD.

Position	^{13}C [ppm] (type)	^{1}H [ppm] (mult., J [Hz])	ROESY[a]	HMBC
1	62.0 (CH)	4.58 (q, 6.6)	H-3, Me-1, Me-*N*, MeO-8	8, 9, 10, Me-*N*, Me-1
3	60.5 (CH)	3.02 (m)	H$_{eq}$-4, H-1, Me-3, Me-*N*	
4	34.0 (CH$_2$)	1.88 (dd, 2.9, 17.3)	H-3, H$_{ax}$-4, H-1', Me-3	3, 9, 10
		2.32 (dd, 11.4, 17.3)	H-7', H$_{eq}$-4, Me-3, Me-1	5, 10
5	119.4 (qC)			
6	156.8 (qC)			
7	99.0 (CH)	6.55 (s)	**Me-*N'''***, MeO-8	1, 5, 6, 8, 9
8	157.5 (qC)			
9	114.8 (qC)			
10	135.3 (qC)			
1'	118.4 (CH)	6.53 (s)	H$_{eq}$-4, Me-2', **Me-*N'''***	3', 8', 10', Me-2'
2'	138.2 (qC)			
3'	108.5 (CH)	6.70 (s)	Me-2', MeO-4', **MeO-8'''**	1', 4', 10', Me-2'
4'	157.4 (qC)			
5'	154.4 (qC)			
6'	126.3 (qC)			
7'	123.9 (CH)	6.46 (s)	H$_{ax}$-4, **H$_a$-3''**, **H$_{ax}$-4'''**, **Me-*N'''***	5, 9', 10', 5', 1''
8'	128.8 (qC)			
9'	136.5 (qC)			
10'	111.9 (qC)			
1''	58.7 (qC)			
2''	125.6 (qC)			
3''	52.4 (CH$_2$)	2.66 (d, 19.5)	H$_b$-3'', **H-7'**	6', 1'', 2'', 4'', 9'', 10''
		3.49 (d, 19.5)	H$_a$-3'', Me-2''	1'', 2'', 4'', 10''
4''	203.2 (qC)			
5''	158.4 (qC)			
6''	112.7 (CH)	7.23 (d, 8.7)	H-7'', MeO-5''	5'', 8'', 10'', 4''
7''	140.3 (CH)	7.86 (d, 8.7)	H$_{eq}$-4''', H-6''	5''', 1'', 5'', 9'', 10''
8''	127.1 (qC)			
9''	157.8 (qC)			
10''	125.7 (qC)			

1'''	58.6 (CH)	4.38 (q, 6.8)	Me-1''', MeO-8''', Me-*N*'''	3''', 8''', 9''', 10''', Me-1''', Me-*N*'''
3'''	50.6 (CH)	4.00 (m)	H$_{eq}$-4''', Me-1''', Me-3''', Me-*N*'''	
4'''	29.0 (CH$_2$)	2.03 (dd, 11.4, 18.3)	H-3''', H$_{eq}$-4''', Me-3''', **H-7'**	3''', 5''', 9''', 10'''
		3.51 (dd, 4.9, 18.3)	H-3''', H$_{ax}$-4''', Me-3''', H-7''	5''', 9''', 10'''
5'''	123.4 (qC)			
6'''	154.3 (qC)			
7'''	108.2 (CH)	6.90 (s)	MeO-8''', Me-2'', **MeO-4'**	5''', 6''', 8''', 9''', 1'''
8'''	157.6 (qC)			
9'''	118.4 (qC)			
10'''	129.6 (qC)			
Me-1	19.9 (CH$_3$)	1.61 (d, 6.6)	H-1, Me-*N*, MeO-8	1, 9
Me-3	18.0 (CH$_3$)	1.18 (d, 6.4)	H-3, H$_{eq}$-4, H$_{ax}$-4, Me-*N*, Me-1	3, 4
Me-2'	22.4 (CH$_3$)	2.26 (s)	H-1', H-3'	1', 2', 3'
Me-2''	23.8 (CH$_3$)	1.94 (s)	H-7''', H$_b$-3'', **MeO-4'**	1'', 2'', 3'', **5'**, 6'''
Me-1'''	19.1 (CH$_3$)	1.54 (d, 6.8)	H-1''', H-3''', MeO-8''', Me-*N*'''	1''', 9'''
Me-3'''	16.5 (CH$_3$)	1.24 (d, 6.6)	H-3''', H$_{eq}$-4''', H$_{ax}$-4''', Me-*N*'''	3''', 4'''
MeO-8	56.2 (CH$_3$)	3.87 (s)	H-7, Me-1, H-1	8'''
MeO-4'	56.4 (CH$_3$)	4.01 (s)	H-3', **H-7'''**, **Me-2''**, **MeO-8'''**	4'
MeO-5''	56.6 (CH$_3$)	4.03 (s)	H-6''	5''
MeO-8'''	56.5 (CH$_3$)	3.78 (s)	H-1''', H-7''', Me-1''', **H-3'**, **MeO-4'**	8'''
Me-*N*	41.7 (CH$_3$)	2.96 (s)	H-1, H-3, Me-1, Me-3	1, 3
Me-*N*'''	34.8 (CH$_3$)	2.10 (s)	H-1''', H-3''', **H-7'**, H-7, **H-1'**, **MeO-8**, Me-1''', Me-3'''	1''', 3'''

[a] ROESY correlations between the southeastern moiety of **22**, **22-I**, and the northwestern part, **22-II**, are marked in **bold**.

2.3.9. *Spirombandakamine A₂ (23)*

Beige amorphous powder (2.5 mg).

$[\alpha]_D^{25} = -50.6$ ($c = 0.03$, MeOH).

HRMS (ESI): *m/z* found = 797.3753 [M+H]⁺,

   m/z calculated for $[C_{49}H_{54}N_2O_8]^{2+}$ = 399.1935.
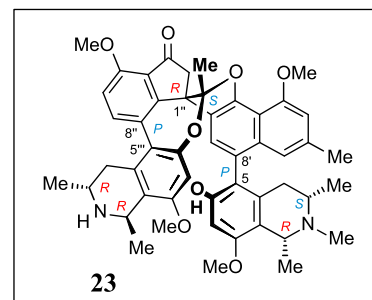
ECD (MeOH): λ_{max} ($\Delta\varepsilon$) = 374 (−0.6), 314 (−41.6), 296 (−15.3), 271 (−71.7), 236 (+124.8), 226 (+33.5), 212 (+130.8), 202 (+70.9) nm.

UV (MeOH): λ_{max} (log ε) = 357 (0.04), 348 (0.65), 332 (0.86), 315 (0.86), 29 (1.1), 228 (3.1), 214 (2.98), 203 (3.4) nm.

IR (ATR): ν_{max} = 3359, 3195, 1661, 1632, 1467, 1424, 1202, 1200, 1135, 802, 721 cm⁻¹.

Products of the oxidative degradation: (*R*)-3-aminobutyric acid and (*R*)-*N*-methyl-3-aminobutyric acid.

¹H NMR (600 MHz, MeOD): δ = 1.12 (d, *J* = 6.5 Hz, 3H), 1.23 (d, *J* = 6.5 Hz, 3H), 1.50 (d, *J* = 6.7 Hz, 3H), 1.63 (d, *J* = 6.7 Hz, 3H), 1.92 (s, 3H), 2.02 (m, 2H), 2.28 (s, 3H), 2.48 (dd, *J* = 17.0, 11.7 Hz, 1H), 2.65 (d, *J* = 19.3 Hz, 1H), 2.98 (s, 3H), 3.05 (m, 1H), 3.49 (d, *J* = 19.3 Hz, 1H), 3.53 (dd, *J* = 17.3, 5.1 Hz, 1H), 3.66 (s, 3H), 3.82 (m, 1H), 3.87 (s, 3H), 4.02 (s, 3H), 4.03 (s, 3H), 4.46 (q, *J* = 6.7 Hz, 1H), 4.58 (q, ³*J* = 6.6 Hz, 1H), 6.43 (s, 1H), 6.54 (s, 1H), 6.59 (s, 1H), 6.74 (s, 1H), 6.78 (s, 1H), 7.24 (d, ³*J* = 8.8 Hz, 1H), 7.80 (d, *J* = 8.8 Hz, 1H) ppm.

¹³C NMR (150 MHz, MeOD): δ = 17.9 (CH₃), 18.7 (CH₃), 18.8 (CH₃), 19.8 (CH₃), 22.4 (CH₃), 22.9 (CH₃), 32.5 (CH₂), 34.4 (CH₂), 41.6 (CH₃), 45.6 (CH₃), 48.3 (CH), 52.3 (CH₂), 56.29 (CH₃), 56.31 (CH₃), 56.5 (CH₃), 56.6 (CH₃), 60.5 (CH), 62.1 (CH), 58.5, 99.9 (CH), 107.4 (CH), 108.6 (CH), 112.8 (CH), 118.5 (CH), 123.60 (CH), 140.3 (CH), 112.2, 116.0, 120.1, 120.5, 123.59, 125.89, 125.92, 126.1, 127.1, 128.2, 130.2, 135.3, 136.4, 138.3, 154.4, 154.8, 155.7, 156.9, 157.2, 157.5, 157.6, 158.4, 203.0 (qC) ppm.

Table 14. NMR data (^{1}H: 600 MHz, ^{13}C: 150 MHz) of spirombandakamine A$_2$ (**23**) in MeOD.

Position	^{13}C [ppm] (type)	^{1}H [ppm] (mult., J [Hz])	ROESY^a	HMBC
1	62.1 (CH)	4.58 (q, 6.6)	H-3, Me-1, Me-*N*, MeO-8	8, 9, 10, Me-*N*, Me-1
3	60.5 (CH)	3.05 (m)	H$_{eq}$-4, H-1, Me-3, Me-*N*	
4	34.4 (CH$_2$)	2.02^b	H-3, H$_{ax}$-4, H-1', Me-3	3, 9, 10
		2.48 (dd, 11.7, 17.0)	H-7', H$_{eq}$-4, Me-3, Me-1	5, 10
5	120.5 (qC)			
6	155.7 (qC)			
7	99.9 (CH)	6.59 (s)	**Me-3'''**, MeO-8	1, 5, 6, 8, 9
8	157.6 (qC)			
9	116.0 (qC)			
10	135.3 (qC)			
1'	118.5 (CH)	6.54 (s)	H$_{eq}$-4, Me-2'	3', 8', 10', Me-2'
2'	138.3 (qC)			
3'	108.6 (CH)	6.74 (s)	Me-2', MeO-4', **MeO-8'''**	1', 4', 10', Me-2'
4'	157.5 (qC)			
5'	154.8 (qC)			
6'	126.1 (qC)			
7'	123.6 (CH)	6.43 (s)	H$_{ax}$-4, **H$_a$-3''**, **H$_{ax}$-4'''**, **Me-3'''**	5, 9', 10', 5', 1''
8'	128.2 (qC)			
9'	136.4 (qC)			
10'	112.2 (qC)			
1''	58.5 (qC)			
2''	125.9 (qC)			
3''	52.3 (CH$_2$)	2.65 (d, 19.3)	H$_b$-3'', **H-7'**	6', 1'', 2'', 4'', 9'', 10''
		3.49 (d, 19.3)	H$_a$-3'', Me-2''	1'', 2'', 4'', 10''
4''	203.0 (qC)			
5''	158.4 (qC)			
6''	112.8 (CH)	7.24 (d, 8.8)	H-7'', MeO-5''	5'', 8'', 10'', 4''
7''	140.3 (CH)	7.80 (d, 8.8)	H$_{eq}$-4''', H-6''	5''', 1'', 5'', 9'', 10''
8''	127.1 (qC)			
9''	157.2 (qC)			

10"	125.9 (qC)			
1'''	48.3 (CH)	4.46 (q, 6.7)	Me-1''', MeO-8'''	3'', 8''', 9''', 10'', Me-1''', Me-*N*'''
3'''	45.6 (CH)	3.82 (m)	H$_{eq}$-4''', Me-1''', Me-3'''	
4'''	32.5 (CH$_2$)	2.01[b]	H-3''', H$_{eq}$-4''', Me-3''', **H-7'**	3''', 5''', 9''', 10'''
		3.53 (dd, 5.1, 17.3)	H-3''', H$_{ax}$-4''', Me-3''', H-7"	5''', 9''', 10'''
5'''	123.6 (qC)			
6'''	154.4 (qC)			
7'''	107.4 (CH)	6.78 (s)	MeO-8''', Me-2", **MeO-4'**	5''', 6''', 8''', 9''', 1'''
8'''	156.9 (qC)			
9'''	120.1 (qC)			
10'''	130.2 (qC)			
Me-1	19.8 (CH$_3$)	1.63 (d, 6.7)	H-1, Me-*N*, MeO-8	1, 9
Me-3	17.9 (CH$_3$)	1.23 (d, 6.5)	H-3, H$_{eq}$-4, H$_{ax}$-4, Me-*N*	3, 4
Me-2'	22.4 (CH$_3$)	2.28 (s)	H-1', H-3'	1', 2', 3'
Me-2"	22.9 (CH$_3$)	1.92 (s)	H-7''', H$_b$-3", **MeO-4'**	1", 2", 3", 6'''
Me-1'''	18.7 (CH$_3$)	1.50 (d, 6.7)	H-1''', H-3''', MeO-8'''	1''', 9'''
Me-3'''	18.8 (CH$_3$)	1.12 (d, 6.5)	H-3''', H$_{eq}$-4''', H$_{ax}$-4''', H-**7**, **H-7'**	3''', 4'''
MeO-8	56.3 (CH$_3$)	3.87 (s)	H-7, Me-1, H-1	8'''
MeO-4'	56.5 (CH$_3$)	4.02 (s)	H-3', **H-7'''**, **Me-2"**, **MeO-8'''**	4'
MeO-5"	56.6 (CH$_3$)	4.03 (s)	H-6"	5"
MeO-8'''	56.3 (CH$_3$)	3.66 (s)	H-1''', H-7", Me-1''', **H-3'**, **MeO-4'**	8'''
Me-*N*	41.6 (CH$_3$)	2.98 (s)	H-1, H-3, Me-1, Me-3	1, 3

[a] ROESY correlations between the southeastern moiety and the northwestern part of **23** are marked in **bold**. [b] The signals of these protons overlapped each other.

3. Phytochemical Investigations on a Congolese *Ancistrocladus* Liana Related to *A. likoko*

3.1. Plant Material

Material of an *Ancistrocladus* plant, morphologically related to *A. likoko*, was collected in August 2015 (Global Positioning System coordinates: 00°06.572S, 018°20.146E, 315±22 m) by the author of this thesis in the vicinity of the village Bonsolerive, which is located at about 20 km southeast of the town of Mbandaka in the Democratic Republic of the Congo. A voucher specimen (No. 105) has been deposited at the Bringmann Herbarium, Institute of Organic Chemistry, University of Würzburg.

3.2. Extraction and Isolation

Air-dried leaves (200 g) were ground and repeatedly extracted by maceration with a neutral mixture of MeOH − CH$_2$Cl$_2$ (1:1, 2 L) with mechanical shaking. After three cycles of 24 h each, the filtrates were evaporated to dryness and the marc was extracted with an acidified (HCl) mixture of MeOH − CH$_2$Cl$_2$ (1:1, pH = 2-3, 2 L), again with mechanical shaking, for 48 h. The acidified extract was neutralized with NaOH and mixed with the neutral one, after the similarity between the two extracts had been established by analytical HPLC. The resulting total crude residue was submitted to a cation-exchange column (Amberlyst-15 from *Fluka*, Ø 3 cm) to remove undesired, non-basic metabolites.[79] The obtained alkaloid-enriched fraction was partitioned between water and dichloromethane, giving, after evaporation of the evaporation, 800 mg of an aqueous subfraction and 30 mg of a dichloromethane subfraction. The polar subfraction was dissolved in methanol and resolved by preparative HPLC operating with a SymmetryPrep C18 column (*Waters*, 7 μm, 19 x 300 mm), using the following gradient: A/B: 0 min 10% B; 25 min 25% B; 30 min 28% B; 31 min 100% B; 34 min 100% B; 35 min 10% B, in which H$_2$O/MeCN (9:1) + 0.05% TFA and B = H$_2$O/MeCN (1:9) + 0.05% TFA. From this subfraction, eight metabolites were obtained, including the alkaloids **45**-**48** and **51**-**54**. Resolution of the lipophilic subfraction by preparative HPLC yielded compounds **49** and **50**. The following gradient was used with the solvents (A) H$_2$O/MeCN (9:1) + 0.05% TFA and (B) H$_2$O/MeCN (1:9) + 0.05% TFA: 0 min 20% B, 5 min 30% B, 19 min 38% B, 20.5 min 100% B; flow: 10 mL/min; column: SymmetryPrep C18 (*Waters*, 7 μm, 19 x 300 mm).

3.3. New Compounds

3.3.1. *Michellamine A₆ (45)*

Brown amorphous powder (8 mg).

45

$[\alpha]_D^{25} = -35$ ($c = 0.01$, MeOH).

HRMS (ESI): *m/z* found = 757.3486 [M+H]⁺,

$\qquad$ *m/z* calculated for [C₄₆H₄₉N₂O₈]⁺ = 757.3483.
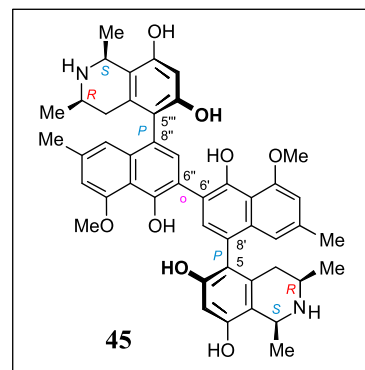
ECD (MeOH): λ_{max} $(\Delta\varepsilon)^* = 200$ (−5.0), 212 (−30.7), 247 (+15.0), 297 (−12.7), 331

$\qquad$ (+3.9) nm.

UV (MeOH): λ_{max} (log ε) = 200 (2.50), 228 (2.31), 263 (2.01), 302 (1.63), 311 (1.62),

$\qquad$ 316 (1.63), 331 (1.63), 333 (1.62), 344 (1.64) nm.

IR (ATM): ν_{max} = 3329, 1672, 1600, 1418, 1359, 1249, 1181, 1138, 1071, 836, 799,

$\qquad$ 722 cm⁻¹.

Product of the oxidative degradation: (*R*)-3-aminobutyric acid.

¹H NMR (400 MHz, MeOD): δ = 1.26 (d, *J* = 6.5 Hz, 6H), 1.82 (d, *J* = 6.5 Hz, 6H),

$\qquad$ 2.27 (dd, *J* = 17.3, 12.0 Hz, 2H), 2.37 (s, 6H), 2.64 (dd, *J* = 17.3, 3.3 Hz,

$\qquad$ 2H), 3.27 (m, 2H), 4.10 (s, 6H), 4.64 (q, *J* = 6.5 Hz, 2H), 6.47 (s, 2H), 6.84

$\qquad$ (*p*t, *J* = 0.9 Hz, 2H), 6.86 (d, *J* = 1.3 Hz, 2H), 7.29 (s, 2H) ppm.

¹³C NMR (100 MHz, MeOD): δ = 18.9 (CH₃), 20.0 (CH₃), 22.3 (CH₃), 33.3 (CH₂),

$\qquad$ 51.0 (CH), 52.4 (CH), 57.1 (CH₃), 102.9 (CH), 108.1 (CH), 119.3 (CH),

$\qquad$ 134.9 (CH), 113.0, 115.3, 119.4, 120.4, 124.3, 135.2, 137.1, 137.7, 152.4,

$\qquad$ 156.5, 156.8, 158.2 (qC) ppm.

---

*Note that the $\Delta\varepsilon$ values previously reported[103] were expressed in "mdeg", but not "cm²mol⁻¹",
as mentioned therein.

Table 15. NMR data (^{1}H: 400 MHz, ^{13}C: 100 MHz) of michellamine A$_6$ (**45**) in MeOD.[a]

Position	^{13}C [ppm] (type)	^{1}H [ppm] (mult., J [Hz])	ROESY	HMBC
1	52.4 (CH)	4.64 (q, 6.5)	H-3, Me-1	9, 10, Me-1
3	51.0 (CH)	3.27 (m)	H-1, H$_{eq}$-4, Me-3	
4	33.3 (CH$_2$)	2.64 (dd, 3.3, 17.3)	H-3, H$_{ax}$-4, H-7', Me-3	5, 9, 10, Me-3
		2.27 (dd, 12.0, 17.3)	H-3, H$_{eq}$-4, H-1', Me-3	3, 9, 10, Me-3
5	119.4 (qC)			
6	156.8 (qC)			
7	102.9 (CH)	6.47 (s)		1, 5, 6, 8, 9
8	156.5 (qC)			
9	113.0 (qC)			
10	135.2 (qC)			
1'	119.3 (CH)	6.84 (*p*t, 0.9)	H$_{eq}$-4, Me-2'	3', 8', 9', 10', Me-2'
2'	137.7 (qC)			
3'	108.1 (CH)	6.86 (*p*d, 1.3)	Me-2', MeO-4'	1', 2', 4', 10', Me-2'
4'	158.2 (qC)			
5'	152.4 (qC)			
6'	120.4 (qC)			
7'	134.9 (CH)	7.29 (s)	H$_{eq}$-4	5, 5', 6', 9'
8'	124.3 (qC)			
9'	137.1 (qC)			
10'	115.3 (qC)			
Me-1	20.0 (CH$_3$)	1.82 (d, 6.5)	H-1	1, 9
Me-3	18.9 (CH$_3$)	1.26 (d, 6.5)	H-3, H$_{eq}$-4, H$_{ax}$-4	3, 4, 10
Me-2'	22.3 (CH$_3$)	2.37 (s)	H-1', H-3'	1', 2', 3'
MeO-4'	57.1 (CH$_3$)	4.10 (s)	H-3'	4'

[a] These data were identical for the second molecular half of the C_2-symmetric dimer **45**.

3.3.2. *Michellamine A₇ (46)*

Beige amorphous powder (5 mg).

$[\alpha]_D^{25} = -41$ ($c = 0.08$, MeOH).

HRMS (ESI): *m/z* found = 771.3655 [M+H]$^+$,

           m/z calculated for $[C_{47}H_{51}N_2O_8]^+$ = 771.3640.
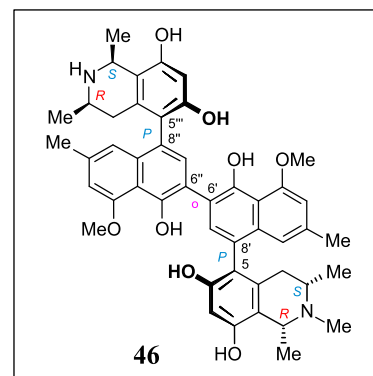
ECD (MeOH): λ_{max} $(\Delta\varepsilon)^*$ = 200 (–5), 210 (–21.5), 243 (+18.7), 300 (–12.6),

           340 (+4.6) nm.

UV (MeOH): λ_{max} (log ε) = 203 (2.61), 231 (2.47), 261 (2.15), 302 (1.75), 311 (1.7),

           315 (1.7), 330 (1.67), 333 (1.70), 345 (1.72) nm.

IR (ATM): ν_{max} = 3329, 1672, 1600, 1418, 1359, 1249, 1181, 1138, 1071, 836, 799,

           722 cm^{-1}.

Products of the oxidative degradation: (*R*)-3-aminobutyric acid and (*S*)-*N*-methyl-3-aminobutyric acid.

^{1}H NMR (600 MHz, MeOD): δ = 1.27 (d, *J* = 6.5 Hz, 3H), 1.33 (d, *J* = 6.6 Hz, 3H),

        1.77 (d, *J* = 6.7 Hz, 3H), 1.82 (d, *J* = 6.6 Hz, 3H), 2.28 (dd, *J* = 17.8, 12.2

        Hz, 1H), 2.36 (s, 3H), 2.36 (dd**, 1H), 2.37 (s, 3H), 2.65 (dd, *J* = 17.8, 4.3

        Hz, 1H), 2.69 (dd, *J* = 18.0, 11.4 Hz, 1H), 3.04 (s, 3H), 3.23 (m, 1H), 3.29

        (m, 1H), 4.10 (s, 3H), 4.12 (s, 3H), 4.64 (m, 2H), 6.47 (s, 2H), 6.78 (s, 1H),

        6.85 (s, 1H), 6.87 (s, 1H), 6.86 (s, 1H), 7.33 (s, 1H), 7.29 (s, 1H), ppm.

^{13}C NMR (150 MHz, MeOD): δ = 18.2 (CH$_3$), 18.9 (CH$_3$), 19.6 (CH$_3$), 20.0 (CH$_3$),

        22.28 (CH$_3$), 22.31 (CH$_3$), 33.4 (CH$_2$), 34.5 (CH$_2$), 41.4 (CH$_3$), 51.0 (CH),

        52.5 (CH), 57.1 (CH$_3$), 57.1 (CH$_3$), 60.6 (CH), 62.6 (CH), 102.6 (CH),

        102.9 (CH), 108.1 (CH), 108.2 (CH), 119.39 (CH), 119.5 (CH), 135.0 (CH),

        135.7 (CH), 113.0, 113.4, 115.2, 115.3, 119.1, 119.37, 124.0, 124.3, 135.2,

        136.5, 137.1, 137.6, 137.7, 152.4, 152.5, 155.7, 156.5, 156.8, 157.0, 158.2,

        158.3 (qC) ppm.

---

*The $\Delta\varepsilon$ values previously reported$^{[103]}$ were expressed in "mdeg", but not in "cm^{2}mol^{-1}", as mentioned therein.

** This signal was overlapped by that of Me-2′, but was deduced to be a dd, from the respective 2D NMR cross peaks.

Table 16. NMR data (^{1}H: 600 MHz, ^{13}C: 150 MHz) of michellamine A$_7$ (**46**) in MeOD.[a]

Position	^{13}C [ppm] (type)	^{1}H [ppm] (mult., *J* [Hz])	ROESY	HMBC
1	62.6 (CH)	4.64 (q, 6.6)	Me-1, Me-*N*	9, 10, Me-1, 8
3	60.6 (CH)	3.23 (m)	Me-*N*, H$_{eq}$-4, Me-3	
4	34.5 (CH$_2$)	2.36 (dd)[a]	H-3, H$_{ax}$-4, H-1', Me-3	5, 9, 10, Me-3
		2.69 (dd, 11.4; 18.0)	H-3, H$_{eq}$-4, H-7', Me-3	3, 9, 10, Me-3
5	119.1 (qC)			
6	157.0 (qC)			
7	102.6 (CH)	6.47 (s)		1, 5, 6, 8, 9
8	155.7 (qC)			
9	113.4 (qC)			
10	135.2 (qC)			
1'	119.5 (CH)	6.78 (s)	H$_{eq}$-4, Me-2'	3', 8', 9', 10', Me-2'
2'	137.6 (qC)			
3'	108.2 (CH)	6.87 (s)	Me-2', MeO-4'	1', 2', 4', 10', Me-2'
4'	158.3 (qC)			
5'	152.5 (qC)			
6'	120.4 (qC)			
7'	135.7 (CH)	7.33 (s)	H$_{ax}$-4	5, 5', 6'', 9'
8'	124.0 (qC)			
9'	136.5 (qC)			
10'	115.2 (qC)			
1''	119.4 (CH)	6.85 (s)	H$_{ax}$-4''', Me-2''	3'', 8'', 9'', 10'', Me-2''
2''	137.7 (qC)			
3''	108.1 (CH)	6.86 (s)	Me-2'', MeO-4''	1'', 2'', 4'', 10'', Me-2''
4''	158.2 (qC)			
5''	152.4 (qC)			
6''	120.4 (qC)			
7''	135.0 (CH)	7.29 (s)	H$_{eq}$-4'''	5''', 5'', 6', 9''
8''	124.3 (qC)			
9''	137.1 (qC)			

10″	115.3 (qC)			
1‴	52.5 (CH)	4.64 (q, 6.6)	H-3‴, Me-1‴	9‴, 10″, Me-1‴
3‴	51.0 (CH)	3.29 (m)	H-1‴, H_{eq}-4‴, Me-3‴	
4‴	33.4 (CH_2)	2.65 (dd, 4.3, 17.8)	H-3‴, H_{ax}-4‴, H-7″, Me-3‴	5‴, 9‴, 10″, Me-3‴
		2.28 (dd, 12.2, 17.8)	H-1″, H_{eq}-4‴, Me-3‴	3‴, 9‴, 10″, Me-3‴
5‴	119.4 (qC)			
6‴	156.8 (qC)			
7‴	102.9 (CH)	6.47 (s)		1‴, 5‴, 6‴, 8‴, 9‴
8‴	156.5 (qC)			
9‴	113.0 (qC)			
10‴	135.2 (qC)			
Me-1	19.6 (CH_3)	1.77 (d, 6.7)	Me-N, H-1	1, 9
Me-3	18.2 (CH_3)	1.33 (d, 6.6)	Me-N, H-3, H_{eq}-4, H_{ax}-4	3, 4
Me-2′	22.3 (CH_3)	2.36 (s)	H-1′, H-3′	1′, 2′, 3′
Me-2″	22.3 (CH_3)	2.37 (s)	H-1″, H-3″	1″, 2″, 3″
Me-1‴	20.0 (CH_3)	1.82 (d, 6.6)	H-1‴	1‴, 9‴
Me-3‴	18.9 (CH_3)	1.27 (d, 6.5)	H-1‴, H-3‴	3‴, 4‴, 10‴
MeO-4′	57.1 (CH_3)	4.12 (s)	H-3′	4′
MeO-4″	57.1 (CH_3)	4.10 (s)	H-3″	4″
Me-N	41.4 (CH_3)	3.04 (s)	Me-3, Me-1, 1, 3	1, 3

[a] This signal was overlapped by that of Me-2′, but was deduced to be a dd, from the respective 2D NMR cross peaks.
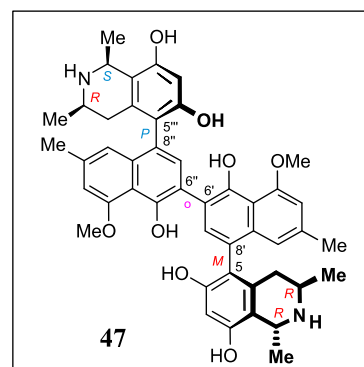
3.3.3. Michellamine B₄ (47)

Beige amorphous powder (9 mg).

$[\alpha]_D^{25} = -25$ ($c = 0.03$, MeOH).

HRMS (ESI): *m/z* found = 757.3475 [M+H]⁺,

   m/z calculated for $[C_{46}H_{49}N_2O_8]^+$ = 757.3483.

ECD (MeOH): λ_{max} ($\Delta\varepsilon$) = 207 (+2.0), 230 (–5.7), 316 (+1.0), 353 (–0.4) nm.

UV (MeOH): λ_{max} (log ε) = 202 (2.50), 228 (2.32), 263 (2.05), 302 (1.60), 311 (1.61), 316 (1.60), 331 (1.60), 333 (1.60), 344 (1.61) nm.

IR (ATM): ν_{max} = 3335, 1672, 1617, 1418, 1360, 1251, 1200, 1137, 1072, 837, 800, 722 cm⁻¹.

Product of the oxidative degradation: (*R*)-3-aminobutyric acid.

¹H NMR (600 MHz, MeOD): δ = 1.24 (d, *J* = 6.4 Hz, 3H), 1.28 (d, *J* = 6.3 Hz, 3H), 1.70 (d, *J* = 6.7 Hz, 3H), 1.82 (d, *J* = 6.5 Hz, 3H), 2.26 (dd, *J* = 17.4, 12.0 Hz, 1H), 2.37 (s, 6H), 2.37 (dd*, 1H), 2.53 (dd, *J* = 18.1, 11.7 Hz, 1H), 2.61 (dd, *J* = 17.4, 3.3 Hz, 1H), 3.29 (m, 1H), 3.66 (m, 1H), 4.11 (s, 6H), 4.64 (q, *J* = 6.5 Hz, 1H), 4.74 (q, *J* = 6.7 Hz, 1H), 6.46 (s, 1H), 6.48 (s, 1H), 6.84 (s, 2H), 6.87 (s, 2H), 7.27 (s, 1H), 7.30 (s, 1H) ppm.

¹³C NMR (150 MHz, MeOD): δ = 18.5 (CH₃), 18.9 (CH₃), 19.4 (CH₃), 20.0 (CH₃), 22.3 (2 CH₃), 33.3 (CH₂), 34.1 (CH₂), 45.4 (CH), 49.5 (CH), 50.9 (CH), 52.4 (CH), 57.29 (CH₃), 57.30 (CH₃), 102.2 (CH), 102.9 (CH), 108.2 (CH), 108.3 (CH), 119.3 (CH), 119.4 (CH), 134.9 (CH), 135.2 (CH), 113.0, 113.4, 115.3, 115.4, 119.1, 119.2, 120.29, 120.30, 124.30, 124.29, 133.2, 135.3, 136.6, 137.2, 137.81, 137.80, 152.4, 152.4, 155.7, 156.5, 156.8, 157.0, 158.2, 158.2 (qC) ppm.

* This signal was overlapped by that of Me-2' (δ_H = 2.37 ppm), but was deduced to be a dd, from the respective 2D NMR cross peaks.

Table 17. NMR data (^{1}H: 600 MHz, ^{13}C: 150 MHz) of michellamine B$_5$ (**47**) in MeOD.

Position	^{13}C [ppm] (type)	^{1}H [ppm] (mult., J [Hz])	ROESY	HMBC
1	49.5 (CH)	4.74 (q, 6.7)	Me-1	9, 10, Me-1, 8
3	45.4 (CH)	3.66 (m)	Me-1, H$_{eq}$-4, Me-3	
4	34.1 (CH$_2$)	2.37 (dd)^a	H-3, H$_{ax}$-4, H-1', Me-3	5, 9, 10, Me-3
		2.53 (dd, 11.7, 18.1)	H-3, H$_{eq}$-4, H-7', Me-3	3, 9, 10, Me-3
5	119.1 (qC)			
6	157.0 (qC)			
7	102.2 (CH)	6.46 (s)		1, 5, 6, 8, 9, 8'
8	155.7 (qC)			
9	113.4 (qC)			
10	133.2 (qC)			
1'	119.4 (CH)	6.84 (s)	H$_{eq}$-4, Me-2'	3', 8', 9', 10', Me-2'
2'	137.8 (qC)			
3'	108.3 (CH)	6.87 (s)	Me-2', MeO-4'	1', 2', 4', 10', Me-2'
4'	158.2 (qC)			
5'	152.4 (qC)			
6'	120.3 (qC)			
7'	135.3 (CH)	7.27 (s)	H$_{ax}$-4	5, 5', 6'', 9'
8'	124.3 (qC)			
9'	136.6 (qC)			
10'	115.4 (qC)			
1''	119.3 (CH)	6.84 (s)	H$_{ax}$-4''', Me-2''	3'', 8'', 9'', 10'', Me-2''
2''	137.8 (qC)			
3''	108.1 (CH)	6.87 (s)	Me-2'', MeO-4''	1'', 2'', 4'', 10'', Me-2''
4'''	158.2 (qC)			
5''	152.4 (qC)			
6''	120.3 (qC)			
7''	134.9 (CH)	7.30 (s)	H$_{eq}$-4'''	5''', 5'', 6', 9''
8''	124.3 (qC)			
9''	137.2 (qC)			
10''	115.3 (qC)			

1‴	52.4 (CH)	4.64 (q, 6.5)	H-3‴, Me-1‴	9‴, 10‴, Me-1‴
3‴	50.9 (CH)	3.29 (m)	H-1‴, H$_{eq}$-4‴, Me-3‴	
4‴	33.3 (CH$_2$)	2.61 (dd, 3.3, 17.4)	H-3‴, H$_{ax}$-4‴, H-7″, Me-3‴	5‴, 9‴, 10‴, Me-3‴
		2.26 (dd, 12.0, 17.4)	H-1″, H$_{eq}$-4‴, Me-3‴	3‴, 9‴, 10‴, Me-3‴
5‴	119.2 (qC)			
6‴	156.8 (qC)			
7‴	102.9 (CH)	6.48 (s)		1‴, 5‴, 6‴, 8‴, 9‴
8‴	156.5 (qC)			
9‴	113.0 (qC)			
10‴	135.2 (qC)			
Me-1	18.5 (CH$_3$)	1.70 (d, 6.7)	H-1, H-3	1, 9
Me-3	19.4 (CH$_3$)	1.28 (d, 6.3)	H-3, H$_{eq}$-4, H$_{ax}$-4	3, 4
Me-1‴	20.0 (CH$_3$)	1.82 (d, 6.5)	H-1‴	1‴, 9‴
Me-3‴	18.9 (CH$_3$)	1.24 (d, 6.4)	H$_{ax}$-4‴, H-3‴	4‴, 10‴, 3‴
Me-2′	22.3 (CH$_3$)	2.37 (s)	H-1′	1′, 2′, 3′
Me-2″	22.3 (CH$_3$)	2.37 (s)	H-1″, H-3″	1″, 2″, 3″
MeO-4′	57.2 (CH$_3$)	4.11 (s)	H-3′	4′
MeO-4″	57.2 (CH$_3$)	4. 11 (s)	H-3″	4″

[a] This signal was overlapped by that of Me-2′, but was deduced to be a dd, from the respective 2D NMR cross peaks.
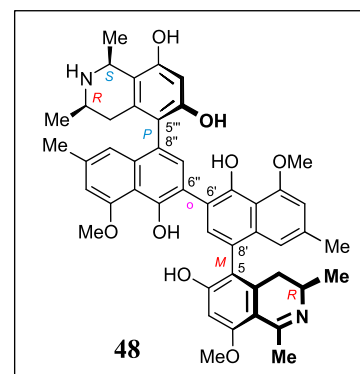
3.3.4. Michellamine B₅ (48)

Beige amorphous powder (7 mg).

$[\alpha]_D^{25} = -32$ ($c = 0.008$, MeOH).

HRMS (ESI): *m/z* found = 769.3484 [M+H]$^+$,

   m/z calculated for $C_{47}H_{49}N_2O_8$ = 769.3483.

ECD (MeOH): λ_{max} ($\Delta\varepsilon$)* = 200 (–3), 210 (–12.0), 229 (–0.8), 237 (–2.3), 262 (+5.4), 304 (–1.5), 327 (–0.3), 350 (–3.1) nm.

UV (MeOH): λ_{max} (log ε) = 200 (2.80), 231 (2.60), 265 (2.14), 302 (1.75), 311 (1.76), 331 (1.75), 335 (1.75), 344 (1.78) nm.

IR (ATM): ν_{max} = 3354, 1670, 1625, 1577, 1408, 1354, 1326, 1262, 1199, 1132, 1071, 957, 832, 798, 720 cm^{-1}.

Product of the oxidative degradation: (*R*)-3-aminobutyric acid.

^{1}H NMR (600 MHz, MeOD): δ = 1.24 (d, *J* = 6.5 Hz, 3H), 1.28 (d = *J* = 6.7 Hz, 3H), 1.82 (d, *J* = 6.6 Hz, 3H), 2.25 (dd, *J* = 17.2, 11.9 Hz, 1H), 2.37 (s, 6H), 2.52 (dd**, 1H), 2.59 (dd**, 1H), 2.61 (m, 1H), 2.77 (d, *J* = 1.4 Hz, 3H), 3.29 (m, 1H), 3.72 (m, 1H), 4.03 (s, 3H), 4.10 (s, 3H), 4.11 (s, 3H), 4.64 (q, *J* = 6.6 Hz, 1H), 6.48 (s, 1H), 6.69 (s, 1H), 6.77 (*p*t, *J* = 1.2 Hz, 1H), 6.84 (*p*t, *J* = 1.2 Hz, 1H), 6.86 (d, *J* = 1.4 Hz, 1H), 6.88 (d, *J* = 1.2 Hz, 1H), 7.30 (s, 2 H) ppm.

^{13}C NMR (100 MHz, MeOD): δ = 18.2 (CH$_3$), 18.9 (CH$_3$), 20.0 (CH$_3$), 22.3 (CH$_3$), 22.3 (CH$_3$), 24.9 (CH$_3$), 33.3 (CH$_2$), 33.6 (CH$_2$), 49.4 (CH), 50.9 (CH), 52.4 (CH), 56.8 (CH$_3$), 57.1 (CH$_3$), 57.2 (CH$_3$), 99.4 (CH), 102.9 (CH), 108.1 (CH), 108.3 (CH), 118.9 (CH), 119.4 (CH), 134.9 (CH), 135.2 (CH), 108.8, 113.0, 115.2, 115.3, 119.2, 120.0, 120.4, 122.3, 122.6, 124.3, 135.2, 136.1, 137.2, 137.8, 138.2, 143.0, 152.5, 152.9, 156.5, 156.8, 158.2, 158.3, 165.8, 167.8, 175.8 (qC) ppm.

---

*Note that the $\Delta\varepsilon$ values previously reported[103] were expressed in "mdeg", but not "cm^{2}mol^{-1}", as mentioned therein.
**These signals overlapped each other.

Table 18. NMR data (^{1}H: 600 MHz, ^{13}C: 150 MHz) of michellamine B$_5$ (**48**) in MeOD.

Position	^{13}C [ppm] (type)	^{1}H [ppm] (mult., J [Hz])	ROESY	HMBC
1	175.8 (qC)			
3	49.4 (CH)	3.72 (m)	H$_{eq}$-4, Me-3	
4	33.6 (CH)	2.52 (dd)^c	H-3, H$_{ax}$-4, H-1′, Me-3	5, 9, 10, Me-3
		2.61 (dd)^c	H-3, H$_{eq}$-4, H-7′, Me-3	3, 9, 10, Me-3
5	122.3 (qC)			
6	167.8 (qC)			
7	99.4 (CH)	6.69 (s)	MeO-8	1, 5, 6, 8, 9, 8′
8	165.8 (qC)			
9	108.8 (qC)			
10	143.0 (qC)			
1′	118.9 (CH)	6.77 (pt, 1.2)	H$_{eq}$-4, Me-2′	3′, 8′, 9′, 10′, Me-2′
2′	138.2 (qC)			
3′	108.3 (CH)	6.88 (d, 1.2)	Me-2′, MeO-4′	1′, 2′, 4′, 10′, Me-2′
4′	158.2 (qC)			
5′	152.5 (qC)			
6′	120.0 (qC)			
7′	135.2 (CH)	7.30 (s)	H$_{ax}$-4	5, 5′, 6″, 9′
8′	122.6 (qC)			
9′	136.1 (qC)			
10′	115.2 (qC)			
1″	119.4 (CH)	6.84 (pt, 1.2)	H$_{ax}$-4‴, Me-2″	3″, 8″, 9″, 10″, Me-2″
2″	137.8 (qC)			
3″	108.1 (CH)	6.86 (d, 1.4)	Me-2″, MeO-4″	1″, 2″, 4″, 10″, Me-2″
4″	158.3 (qC)			
5″	152.9 (qC)			
6″	120.4 (qC)			
7″	134.9 (CH)	7.30 (s)	H$_{eq}$-4‴	5‴, 5″, 6′, 9″
8″	124.3 (qC)			
9″	137.2 (qC)			
10″	115.3 (qC)			

1‴	52.4 (CH)	4.64 (q, 6.6)	H-3‴, Me-1‴	9‴, 10‴, Me-1‴
3‴	50.9 (CH)	3.29 (m)	H-1‴, H$_{eq}$-4‴, Me-3‴	
4‴	33.3 (CH$_2$)	2.59 (dd)^c	H-3‴, H$_{ax}$-4‴, H-7″, Me-3‴	5‴, 9‴, 10‴, Me-3‴
		2.25 (dd, 11.9, 17.2)	H-1″, H$_{eq}$-4‴, Me-3‴	3‴, 9‴, 10‴, Me-3‴
5‴	119.2 (qC)			
6‴	156.8 (qC)			
7‴	102.9 (CH)	6.48 (s)		1‴, 5‴, 6‴, 8‴, 9‴
8‴	156.5 (qC)			
9‴	113.0 (qC)			
10‴	135.2 (qC)			
Me-1	24.9 (CH$_3$)	2.77 (d, 1.4)	MeO-8	1, 9
Me-3	18.2 (CH$_3$)	1.28 (d, 6.7)	H-3, H$_{eq}$-4, H$_{ax}$-4	3, 4
Me-1‴	20.0 (CH$_3$)	1.82 (d, 6.6)	H-1‴	1‴, 9‴
Me-3‴	18.9 (CH$_3$)	1.24 (d, 6.5)	H$_{ax}$-4‴, H-3‴	4‴, 10‴, 3‴
Me-2′	22.3 (CH$_3$)	2.37 (s)	H-1′	1′, 2′, 3′
Me-2″	22.3 (CH$_3$)	2.37 (s)	H-1″, H-3″	1″, 2″, 3″
MeO-8	56.8 (CH$_3$)	4.03 (s)	H-7, Me-1	8
MeO-4′	57.1 (CH$_3$)	4.11 (s)	H-3′	4′
MeO-4″	57.2 (CH$_3$)	4.10 (s)	H-3″	4″

^{c} These signals overlapped each other.

3.3.5. Ancistrobonsoline A₁ (49)

Yellow amorphous powder (10 mg).

$[\alpha]_D^{25}$ = +75 (c = 0.01, MeOH).

HRMS (ESI): *m/z* found = 392.1843 [M+H]⁺,

        m/z calculated for $[C_{24}H_{26}NO_4]^+$ = 392.1856.

ECD (MeOH): λ_{max} ($\Delta\varepsilon$) = 211 (–10.1), 229 (+5.7), 244 (–2.9), 269 (+0.6), 281 (+0.5), 320 (+2.8) nm.

UV (MeOH): λ_{max} = 336 (0.30), 325 (0.27), 315 (0.37), 312 (0.31), 236 (1.01) nm.

IR (ATM): ν_{max} = 3382, 1671, 1625, 1575, 1400, 1352, 1326, 1297, 1264, 1198, 1132, 1084, 956, 832, 799, 720 cm⁻¹.

Product of the oxidative degradation: (*R*)-3-aminobutyric acid.

¹H NMR (400 MHz, MeOD): δ = 1.26 (d, *J* = 6.6 Hz, 3H), 2.34 (d, *J* = 0.6 Hz, 3H), 2.41 (dd, *J* = 16.9, *J* = 5.8 Hz, 1H), 2.48 (dd, *J* = 16.9, 11.3 Hz, 1H), 2.79 (d, *J* = 1.5 Hz, 3H), 3.70 (m, 1H), 4.04 (s, 3H), 4.10 (s, 3H), 6.67 (s, 1H), 6.72 (*p*t, *J* = 1.1 Hz, 1H), 6.80 (d, *J* = 7.9 Hz, 1H), 6.83 (d, *J* = 0.9 Hz, 1H), 7.05 (d, *J* = 7.9 Hz, 1H) ppm.

¹³C NMR (100 MHz, MeOD): δ = 18.2 (CH₃), 22.3 (CH₃), 24.8 (CH₃), 33.6 (CH₂), 49.5 (CH), 56.8 (CH₃), 57.0 (CH₃), 99.3 (CH), 107.9 (CH), 110.4 (CH), 118.7 (CH), 131.7 (CH), 115.0, 108.8, 122.5, 123.1, 136.7, 138.2, 142.9, 156.4, 158.2, 165.8, 167.8, 175.8 (qC) ppm.
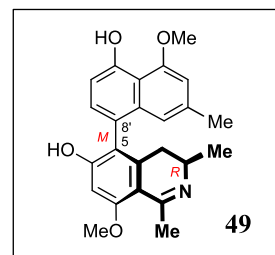
Table 19. NMR data (^{1}H: 400 MHz, ^{13}C: 100 MHz) of ancistrobonsoline A$_1$ (**49**) in MeOD.

Position	^{13}C [ppm] (type)	^{1}H [ppm] (mult., J [Hz])	NOESY	HMBC
1	175.8 (qC)			
3	49.5 (CH)	3.70 (m)	H$_{eq}$-4, Me-3	
4	33.6 (CH$_2$)	2.41 (dd, 5.8, 16.9)	H-3, H$_{ax}$-4, H-1′, Me-3	5, 9, 10, Me-3
		2.48 (dd, 11.3, 16.9)	H$_{eq}$-4, H-7′, Me-3	5, 3, 9, 10, Me-3
5	122.5 (qC)			
6	167.8 (qC)			
7	99.3 (CH)	6.67 (s)	MeO-8	1, 5, 6, 8, 9
8	165.8 (qC)			
9	108.8 (qC)			
10	142.9 (qC)			
1'	118.7 (CH)	6.72 (*p*t, 1.1)	H$_{eq}$-4, Me-2′	3′, 8′, 9′, 10′, Me-2′
2'	138.2 (qC)			
3'	107.9 (CH)	6.83 (*p*d, 0.9)	Me-2′, MeO-4′	1′, 2′, 4′, 10′, Me-2′
4'	158.2 (qC)			
5'	156.4 (qC)			
6'	110.4 (CH)	6.80 (d, 7.9)	H-7′	5′, 8′, 10′
7'	131.7 (CH)	7.05 (d, 7.9)	H$_{ax}$-4, H-6′	5, 5′, 6′, 9′
8'	123.1 (qC)			
9'	136.7 (qC)			
10'	115.0 (qC)			
Me-1	24.8 (CH$_3$)	2.79 (*p*d, 1.5)	MeO-8	1, 9
Me-3	18.2 (CH$_3$)	1.26 (d, 6.6)	H$_{eq}$-4, H$_{ax}$-4, H-3	4, 3
Me-2'	22.3 (CH$_3$)	2.34 (*p*d, 0.6)	H-1′, H-3′	1′, 2′, 3′
MeO-8	56.8 (CH$_3$)	4.04 (s)	H-7, Me-1	8
MeO-4'	57.0 (CH$_3$)	4.10 (s)	H-3′	4′

3.3.6. *Ancistrobonsoline A₂ (50)*

Yellow amorphous powder (7 mg).

$[\alpha]_D^{25}$ = +56 (c = 0.009, MeOH).

HRMS (ESI): *m/z* found = 406.2013 [M+H]$^+$,

        m/z calculated for $[C_{25}H_{28}NO_4]^+$ = 406.2013.

ECD (MeOH): λ_{max} ($\Delta\varepsilon$) = 210 (–12.1), 229 (+4.7), 242 (–1.9), 262 (+1.6), 286 (+0.6),

        314 (+2.6) nm.

UV (MeOH): λ_{max} (log ε) = 336 (0.30), 325 (0.27), 315 (0.37), 313 (0.31), 237 (1.01)

        nm.

IR (ATM): ν_{max} = 3384, 1670, 1626, 1577, 1457, 1263, 1200, 1130, 1084, 1052, 956,

        834, 798, 719 cm^{-1}.

Product of the oxidative degradation: (*R*)-3-aminobutyric acid.

^{1}H NMR (400 MHz, MeOD): δ = 1.27 (d, *J* = 6.6 Hz, 3H), 2.32 (d, *J* = 0.8 Hz, 3H),

        2.42 (dd, *J* = 16.9, 5.8 Hz, 1H), 2.49 (dd, *J* = 16.9, 11.3 Hz, 1H), 2.82 (d, *J* =

        1.5 Hz, 3H), 3.71 (m, 1H), 3.83 (s, 3H), 4.10 (s, 3H), 4.15 (s, 3H), 6.64 (*p*t, *J*

        = 1.1 Hz, 1H), 6.78 (d, *J* = 7.9 Hz, 1H), 6.82 (d, *J* = 0.9 Hz, 1H), 6.83 (s,

        1H), 7.00 (d, *J* = 7.9 Hz, 1H) ppm.

^{13}C NMR (100 MHz, MeOD): δ = 18.1 (CH$_3$), 22.3 (CH$_3$), 24.9 (CH$_3$), 33.4 (CH$_2$),

        49.6 (CH), 57.01 (CH$_3$), 57.02 (CH$_3$), 57.2 (CH$_3$), 95.9 (CH), 107.8 (CH),

        110.3 (CH), 118.6 (CH), 131.4 (CH), 109.2, 114.8, 123.3, 123.6, 138.2,

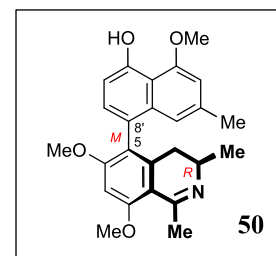   136.6, 141.6, 156.2, 158.1, 166.4, 168.7, 176.3 (qC) ppm.

Table 20. NMR data (^{1}H: 400 MHz, ^{13}C: 100 MHz) of ancistrobonsoline A$_2$ (**50**) in MeOD.

| Position	^{13}C [ppm] (type)	^{1}H [ppm] (mult., J [Hz])	NOESY	HMBC
1	176.3 (qC)			
3	49.6 (CH)	3.71 (m)	H$_{eq}$-4, Me-3	
4	33.4 (CH$_2$)	2.42 (dd, 5.8, 16.9)	H-3, H$_{ax}$-4, H-1′, Me-3	5, 9, 10, Me-3
		2.49 (dd, 11.3, 16.9)	H$_{eq}$-4, H-7′, Me-3	5, 3, 9, 10, Me-3
5	123.6 (qC)			
6	168.7 (qC)			
7	95.9 (CH)	6.83 (s)	MeO-8, MeO-6	1, 5, 6, 8, 9
8	166.4 (qC)			
9	109.2 (qC)			
10	141.6 (qC)			
1'	118.6 (CH)	6.64 (*p*t, 1.1)	H$_{eq}$-4, Me-2′, MeO-6	3′, 8′, 9′, 10′, Me-2′
2'	138.2 (qC)			
3'	107.8 (CH)	6.82 (*p*d, 0.9)	Me-2′, MeO-4′	1′, 2′, 4′, 10′, Me-2′
4'	158.1 (qC)			
5'	156.2 (qC)			
6'	110.3 (CH)	6.78 (d, 7.9)	H-7′	5′, 8′, 10′
7'	131.4 (CH)	7.00 (d, 7.9)	H$_{ax}$-4, H-6′, MeO-6	5, 5′, 6′, 9′
8'	123.3 (qC)			
9'	136.6 (qC)			
10'	114.8 (qC)			
Me-1	24.9 (CH$_3$)	2.82 (*p*d, 1.5)	MeO-8	1, 9
Me-3	18.1 (CH$_3$)	1.27 (d, 6.6)	H$_{eq}$-4, H$_{ax}$-4, H-3	4, 3
Me-2'	22.3 (CH$_3$)	2.32 (*p*d, 0.8)	H-1′, H-3′	1′, 2′, 3′
MeO-6	57.2 (CH$_3$)	3.83 (s)	H-7, H-7′, H-1′	6
MeO-8	57.0 (CH$_3$)	4.15 (s)	H-7, Me-1	8
MeO-4'	57.0 (CH$_3$)	4.10 (s)	H-3′	4′

3.4. Known Compounds

3.4.1. *Ancistroealaine C (51)*

Brown amorphous powder (11 mg).

HRMS (ESI): *m/z* found = 380.1853 [M+H]$^+$,

  m/z calculated for [C$_{23}$H$_{26}$NO$_4$]$^+$ = 380.1856.
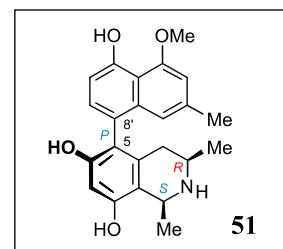
ECD (MeOH): λ_{max} ($\Delta\varepsilon$) = 200 (+5.0), 213 (−5.1), 227 (−10.8), 245 (+2.5), 282 (−0.5), 306 (+0.3), 338 (−0.09) nm.

Product of the oxidative degradation: (*R*)-3-aminobutyric acid.

^{1}H NMR (400 MHz, MeOD): δ = 1.20 (d, *J* = 6.5 Hz, 3H), 1.80 (d, *J* = 6.5 Hz, 3H), 2.18 (dd, *J* = 11.9, 17.3 Hz, 1H), 2.33 (s, 3H), 2.42 (dd, *J* = 3.4, 17.3 Hz, 1H), 3.25 (m, 1H), 4.09 (s, 3H), 4.63 (q, *J* = 6.4 Hz, 1H), 6.47 (s, 1H), 6.79 (*p*t, *J* = 1.0 Hz, 1H), 6.79 (d, *J* = 7.7 Hz, 1H), 6.80 (s, 1H), 7.07 (d, *J* = 7.7 Hz, 1H) ppm.

^{13}C NMR (100 MHz, MeOD): δ = 20.0 (CH$_3$), 18.8 (CH$_3$), 22.4 (CH$_3$), 33.3 (CH$_2$), 52.4 (CH), 50.9 (CH), 56.9 (CH$_3$), 102.9 (CH), 107.6 (CH), 110.5 (CH), 119.3 (CH), 131.5 (CH), 112.8, 115.1, 119.5, 125.0, 135.1, 137.6, 137.7, 155.8, 156.4, 156.8, 158.1 (qC) ppm.
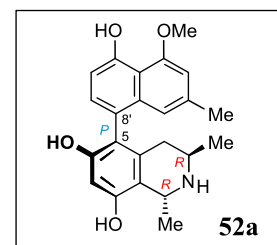
The physical and spectroscopic data were in good agreement with those previously published.[166]

3.4.2. *Korupensamine A (52a)*

Brown amorphous powder (2.1 mg).

HRMS (ESI): *m/z* found = 380.1845 [M+H]$^+$,

  m/z calculated for [C$_{23}$H$_{26}$NO$_4$]$^+$ = 380.1856.

ECD (MeOH): λ_{max} ($\Delta\varepsilon$) = 200 (+3.3), 211 (−7.2), 217 (−5.7), 221 (−6.0), 238 (+3.1), 283 (−0.3), 312 (+0.1) nm.

Product of the oxidative degradation: (*R*)-3-aminobutyric acid.

^{1}H NMR (400 MHz, MeOD): δ = 1.20 (d, J = 6.6 Hz, 3H), 1.65 (d, J = 6.6 Hz, 3H), 2.06 (dd, J = 11.7, 18.0 Hz, 1H), 2.31 (s, 3H), 2.62 (dd, J = 4.7, 17.9 Hz, 1H), 3.66 (m, 1H), 4.09 (s, 3H), 4.76 (q, J = 6.8 Hz, 1H), 6.45 (s, 1H), 6.69 (*p*t, J = 1.2 Hz, 1H), 6.79 (s, 1H), 6.80 (d, J = 7.8 Hz, 1H), 7.10 (d, J = 7.8 Hz) ppm.

^{13}C NMR (100 MHz, MeOD): δ = 18.4 (CH$_3$), 19.2 (CH$_3$), 22.3 (CH$_3$), 33.0 (CH$_2$), 45.1 (CH), 49.5 (CH), 56.8 (CH$_3$), 102.0 (CH), 107.5 (CH), 119.0 (CH), 110.4 (CH), 131.3 (CH), 113.1, 115.0, 119.1, 124.8, 132.1, 137.3, 137.4, 155.5, 155.7, 156.9, 158.0 (qC) ppm.

The physical and spectroscopic data fitted with those previously reported.[196,218]

3.4.3. *Korupensamine B (52b)*

Brown amorphous powder (3.5 mg).

HRMS (ESI): *m/z* found = 380.1859 [M+H]$^{+}$,

m/z calculated for [C$_{23}$H$_{26}$NO$_4$]$^{+}$ = 380.1856.
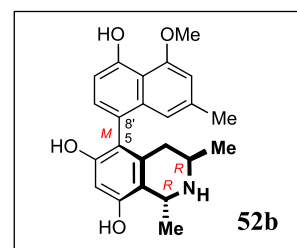
ECD (MeOH): λ_{max} ($\Delta\varepsilon$) = 200 (–2.7), 212 (+6.5), 236 (–5.8), 262 (+1.6), 283 (+1.2) nm.

Product of the oxidative degradation: (*R*)-3-aminobutyric acid.

^{1}H NMR (600 MHz, MeOD): δ = 1.24 (d, J = 6.2 Hz, 3H), 1.68 (d, J = 6.8 Hz, 3H), 2.24 (dd, J = 4.8, 18.0 Hz, 1H), 2.34 (s, 3H), 2.38 (dd, J = 11.6, 18.0 Hz, 1H), 3.65 (m, 1H), 4.09 (s, 3H), 4.75 (q, J = 6.78 Hz, 1H), 6.45 (s, 1H), 6.78 (*p*t, J = 1.1 Hz, 1H), 6.79 (d, J = 7.8 Hz, 1H), 6.80 (*p*d, J = 1.1 Hz, 1H), 7.03 (d, J = 7.8 Hz, 1H) ppm.

^{13}C NMR (150 MHz, MeOD): δ = 18.4 (CH$_3$), 19.3 (CH$_3$), 22.2 (CH$_3$), 33.9 (CH$_2$), 45.2 (CH), 49.6 (CH), 56.9 (CH$_3$), 102.0 (CH), 107.6 (CH), 119.0 (CH), 110.4 (CH), 131.5 (CH), 113.1, 115.0, 119.2, 124.8, 132.1, 137.0, 137.6, 155.5, 155.7, 156.9, 157.9 (qC) ppm.

The physical and spectroscopic data were in agreement with the previously reported ones.[196]
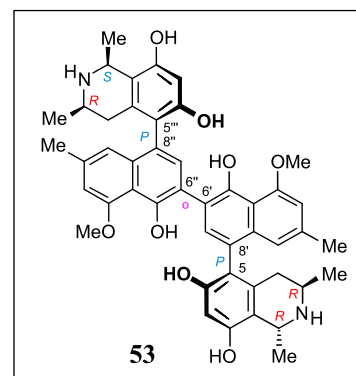
3.4.4. Michellamine A₂ (53)

Beige amorphous powder (3 mg).

53

MS (ESI): *m/z* found = 757.6 [M+H]⁺ (LC-MS),

   m/z calculated for $[C_{46}H_{49}N_2O_8]^+$ = 757.3.

ECD (MeOH): λ_{max} $(\Delta\varepsilon)$ = 200 (−10), 208 (−37.2), 243 (+14.5), 300 (−9.5), 333 (+2.6) nm.

Product of the oxidative degradation: (*R*)-3-aminobutyric acid.

¹H NMR (600 MHz, MeOD): δ = 1.24 (d, *J* = 6.2 Hz, 3H), 1.25 (d, *J* = 6.5 Hz, 3H), 1.64 (d, *J* = 6.8 Hz, 3H), 1.82 (d, *J* = 6.6 Hz, 3H), 2.15 (dd, *J* = 11.7, 18.0 Hz, 1H), 2.28 (dd, *J* = 12.1, 17.3 Hz, 1H), 2.34 (s, 3H), 2.37 (s, 3H), 2.65 (dd, *J* = 3.4, 17.5 Hz, 1H), 2.83 (dd, *J* = 4.9, 18.2 Hz, 1H), 3.30 (m, 1H), 3.70 (m, 1H), 4.10 (s, 3H), 4.11 (s, 3H), 4.64 (q, *J* = 6.7 Hz, 1H), 4.77 (q, *J* = 6.5 Hz, 1H), 6.45 (s, 1H), 6.47 (s, 1H), 6.74 (s, 1H), 6.84 (m, 1H), 6.86 (s, 2H), 7.29 (s, 1H), 7.31 (s, 1H) ppm.

¹³C NMR (150 MHz, MeOD): δ = 18.3 (CH₃), 18.8 (CH₃), 19.3 (CH₃), 19.8 (CH₃), 22.1 (CH₃), 22.2 (CH₃), 33.1 (CH₂), 33.2 (CH₂), 45.1 (CH), 49.6 (CH), 50.9 (CH), 52.3 (CH), 57.0 (2CH₃), 102.0 (CH), 102.8 (CH), 107.97 (CH), 107.99 (CH), 119.10 (CH), 119.3 (CH), 134.7 (CH), 134.8 (CH), 137.49 (CH), 137.52 (CH), 112.8, 112.9, 115.18, 115.19, 119.14, 119.2, 120.3, 120.4, 124.2, 124.2, 133.1, 135.0, 136.7, 136.9, 152.2, 152.3, 155.5, 156.3, 156.7, 156.9, 158.12, 158.13 (qC) ppm.

The physical and spectroscopic data fitted with those previously reported.[172,218]
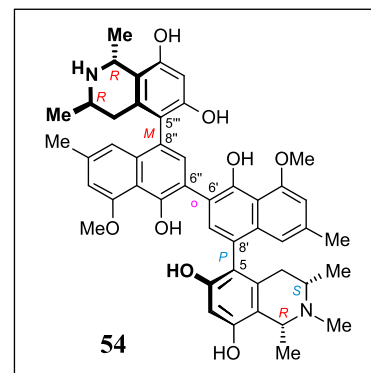
3.4.5. Michellamine E (54)

Beige amorphous powder (4 mg).

54

MS (ESI): *m/z* found = 771.7 [M+H]⁺ (LC-MS),

   m/z calculated for $[C_{47}H_{51}N_2O_8]^+$ = 771.4

ECD (MeOH): λ_{max} $(\Delta\varepsilon)$ = 200 (+3.8), 212 (−1.5), 219 (−0.4), 224 (−0.8), 245 (+1.8), 268 (+0.2), 281 (+0.4) nm.

Product of the oxidative degradation: (*R*)-3-aminobutyric acid and (*S*)-*N*-methyl-3-aminobutyric acid.

^{1}H NMR (600 MHz, MeOD): $\delta = 1.26$ (d, $J = 6.2$ Hz, 3H), 1.30 (d, $J = 6.5$ Hz, 3H), 1.68 (d, $J = 6.8$ Hz, 3H), 1.76 (d, $J = 6.5$ Hz, 3H), 2.31 (dd, $J = 17.3$, 3.1 Hz, 1H), 2.35 (dd*, 1H), 2.36 (s, 3H), 2.37 (s, 3H), 2.54 (dd, $J = 18.2$, 11.6 Hz, 1H), 2.66 (dd, $J = 17.5$, 11.6 Hz, 1H), 3.03 (s, 3H), 3.22 (m, 1H), 3.65 (m, 1H), 4.10 (s, 3H), 4.11 (s, 3H), 4.63 (q, $J = 6.6$ Hz, 1H), 4.73 (q, $J = 6.8$ Hz, 1H), 6.46 (s, 1H), 6.47 (s, 1H), 6.78 (s, 1H), 6.84 (s, 1H), 6.87 (s, 1H), 7.27 (s, 1H), 7.33 (s, 1H), ppm.

^{13}C NMR (150 MHz, MeOD): $\delta = 18.0$ (CH$_3$), 18.4 (CH$_3$), 19.3 (CH$_3$), 19.5 (CH$_3$), 22.16 (CH$_3$), 22.19 (CH$_3$), 34.0 (CH$_2$), 34.4 (CH$_2$), 41.2 (CH$_3$), 45.2 (CH), 49.6 (CH), 57.00 (CH$_3$), 57.01 (CH$_3$), 60.4 (CH), 62.5 (CH), 102.1 (CH), 102.5 (CH), 108.08 (CH), 108.10 (CH), 119.2 (CH), 119.4 (CH), 135.1 (CH), 135.5 (CH), 113.2, 113.3, 115.1, 115.2, 118.9, 119.0, 120.11, 120.12, 123.9, 124.1, 133.0, 134.7, 136.4, 136.5, 137.57, 137.61, 152.27, 152.34, 155.5, 155.6, 156.85, 156.86, 158.02, 158.03 (qC) ppm.

*This signal was overlapped by that of the three-proton singlet (at 2.36 ppm), but was deduced to be a dd, from the respective 2D NMR cross peaks.

The physical and spectroscopic data fitted with those previously reported.[75]

4. Phytochemical Investigations on a Congolese *Ancistrocladus* Liana Related to *A. congolensis*

4.1. Plant Material

Stem bark material of an as yet botanically unidentified *Ancistrocladus* plant was collected by S. M. Kavatsurwa in the rainforest surrounding the village Yafunga, Tshopo Province, Democratic Republic of the Congo, in December 2014 (Global Position System coordinates: 00°43'46.6", 024°20'16.8"). A voucher specimen (No. 106) has been deposited at the Bringmann Herbarium, University of Würzburg.

4.2. Extraction and Isolation

As already mentioned in the result and discussion part, first phytochemical investigations on this plant were done by S. M. Kavatsurwa in cooperation with the author of this thesis, leading to the isolation and structural elucidation of four NIQs. Details on this work can be found in the PhD thesis of S. M. Kavatsurwa. Below are described the experiments carried out later on solely by the author of this thesis, which provided additional material of the four previously isolated compounds and yielded eleven further NIQs.

Air-dried stem bark material (100 g) was powdered and exhaustively extracted with a CH_2Cl_2/MeOH mixture (1:1), with mechanical shaking (160 RPM) at room temperature. The resulting extract was concentrated *in vacuo*, giving 6 g of a solid crude residue, which was washed with *n*-hexane to remove the most lipophilic compounds. The remaining, defatted residue was suspended in H_2O and sonicated (2×15 minutes). After decantation and filtration, the resulting aqueous filtrate was exhaustively extracted with CH_2Cl_2. The organic phase was concentrated to dryness, yielding 1.2 g of a crude extract, of which 1 g was dissolved in a mixture of H_2O and MeOH (8:2), filtered over a 0.2 μm PTFE membrane (*Phenex*), and extracted with EtOAc. The upper, organic phase was concentrated under reduced pressure, dissolved in MeOH and resolved on a preparative HPLC SymmetryPrep C18 column (*Waters*, 19×300 mm, 7 μm) using the following gradient: A/B: 0 min 20% B, 22 min 30 % B, 35 min 60 % B, and 37 min 100 % B, where A = H_2O/MeCN (9:1) + 0.05% TFA and B = H_2O/MeCN (1:9) + 0.05% TFA; flow: 10 mL/min. This chromatographic separation provided 2.8 mg of 4′-*O*-demethylancistrocladine (**61**, R_T = 19.4 min), 3.5 mg of 7-*epi*-ancistrobrevine D (**67**, R_T = 21.9 min), 2.1 mg of 6,5′-*O*,*O*-didemethylancistroealaine A (*ent*-**49**, R_T = 24.0 min), 7 mg of

ancistrocladinium A (**9**, R$_T$ = 35.9 min), 13 mg of ancistrocladinium B (**68**, R$_T$ = 39.6 min), and eleven other fractions.

Fraction 1 (15-18 min) was further resolved by preparative HPLC using 20% of MeCN (flow: 12 mL/min) to give ancistrobrevine B (**64**, 2.3 mg, R$_T$ = 17.1 min), ancistroyafungine A (**56**, 9 mg, R$_T$ = 19.7 min), and ancistrobertsonine A (**63**, 4 mg, R$_T$ = 22.6 min). Fraction 4 (20-21.5 min; flow: 8 mL/min) was resolved by isocratic HPLC, using MeOH/H$_2$O as the eluent (54:46), which provided ancistroguineine A (**62**, R$_T$ = 9.3 min, 1.9 mg), ancistroyafungine B (**56**, R$_T$ = 10.8 min, 2.1 mg), and 6-*O*-demethylancistroealaine A (**66**, R$_T$ = 12.4 min, 3.5 mg). The same chromatographic conditions were applied to resolve Fraction 7 (25.1-26.5 min), giving 6 mg of 6-*O*-methylhamatine (**60**, R$_T$ = 15.3 min) and 7 mg of ancistrotectoriline A (**65**, R$_T$ = 16.2 min). Ancistroyafungine C (**58**, 5.1 mg) was obtained from Fraction 8 (26.5-28.1 min), following its elution with 56 % aqueous MeOH (R$_T$ = 14.5 min). From Fraction 9 (28.1-29.8 min) ancistroyafungine D (**59**, 2.5 mg) was isolated by isocratic HPLC with 58 % aqueous MeOH, R$_T$ of **59** = 12.1 min.

4.3. New Compounds

4.3.1. Ancistroyafungine A (56)

Beige amorphous powder (9 mg).

$[\alpha]_D^{25} = +16.1$ ($c = 0.10$, MeOH).

HRMS (ESI): *m/z* found = 422.2333 [M+H]$^+$,

        m/z calculated for [C$_{26}$H$_{32}$NO$_4$]$^+$ = 422.2326.

ECD (MeOH): λ_{max} ($\Delta\varepsilon$) = 196 (+17.4), 211 (–17.4), 217 (–14.9), 224 (–17.3), 239
        (+18.2), 286 (–0.87), 307 (–0.84) nm.

UV (MeOH): λ_{max} (log ε) = 204 (1.43), 231 (1.51), 306 (0.32), 321 (0.25), 335 (0.18)
        nm.

IR (ATM): ν_{max} = 3430, 1669, 1582, 1448, 1273, 1173, 1132, 830, 798, 719 cm^{-1}.

Products of the oxidative degradation: (*S*)-3-aminobutyric acid and (*S*)-*N*-methyl-3-
        aminobutyric acid.

^{1}H NMR (600 MHz, MeOD): δ = 1.26 (d, *J* = 6.5 Hz, 3H), 1.72 (d, *J* = 6.5 Hz, 3H),
        2.21 (dd, *J* = 17.3, 3.1 Hz, 1H), 2.31 (s, 3H), 2.58 (dd, *J* = 17.2, 11.5 Hz,
        1H), 3.02 (s, 3H), 3.16 (m, 1H), 3.92 (s, 3H), 3.93 (s, 3H), 3.96 (s, 3H), 4.65
        (q, *J* = 6.6 Hz, 1H), 6.60 (s, 1H), 6.69 (s, 1H), 6.79 (s, 1H), 6.94 (d, *J* = 7.9
        Hz, 1H), 7.16 (d, *J* = 7.9 Hz, 1H) ppm.

^{13}C NMR (150 MHz, MeOD): δ = 18.1 (CH$_3$), 20.0 (CH$_3$), 22.1 (CH$_3$), 34.2 (CH$_2$),
        41.5 (CH$_3$), 56.2 (CH$_3$), 56.9 (CH$_3$), 57.1 (CH$_3$), 60.5 (CH), 62.3 (CH), 99.1
        (CH), 106.8 (CH), 110.1 (CH), 118.5 (CH), 131.1 (CH), 114.4, 117.6,
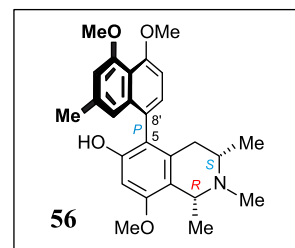   120.1, 126.2, 134.8, 137.7, 138.1, 157.4, 157.7, 158.6, 158.9 (qC) ppm.

Table 21. NMR data (^{1}H: 600 MHz, ^{13}C: 150 MHz) of ancistroyafungine A (**56**) in MeOD.

Position	^{13}C [ppm] (type)	^{1}H [ppm] (mult., J [Hz])	NOESY	HMBC
1	62.3 (CH)	4.65 (q, 6.6)	H-3, Me-1, Me-N	9, 10, Me-1, Me-N, 8
3	60.5 (CH)	3.16 (m)	H-1, Me-N, H$_{eq}$-4, Me-3	
4	34.2 (CH$_2$)	2.21 (dd, 3.1, 17.3)	H-3, H$_{ax}$-4, H-1', Me-3	5, 9, 10, Me-3
		2.58 (dd, 11.5, 17.2)	H-3, H$_{eq}$-4, H-7', Me-3	3, 9, 10, Me-3
5	120.1 (qC)			
6	157.7 (qC)			
7	99.1 (CH)	6.60 (s)	MeO-8	1, 5, 6, 8, 9
8	157.4 (qC)			
9	114.4 (qC)			
10	134.8 (qC)			
1'	118.5 (CH)	6.69 (s)	H$_{eq}$-4, Me-2'	3', 8', 9', 10', Me-2'
2'	137.7 (qC)			
3'	110.1 (CH)	6.79 (s)	Me-2', MeO-4'	1', 2', 4', 10', Me-2'
4'	158.9 (qC)			
5'	158.6 (qC)			
6'	106.8 (CH)	6.94 (d, 7.9)	H-7', MeO-5'	5', 8', 10'
7'	131.1 (CH)	7.16 (d, 7.9)	H-6', H$_{ax}$-4	5, 5', 6', 9'
8'	126.2 (qC)			
9'	138.1 (qC)			
10'	117.6 (qC)			
Me-1	20.0 (CH$_3$)	1.72 (d, 6.5)	MeO-8, Me-N, H-1	1, 9
Me-3	18.1 (CH$_3$)	1.26 (d, 6.5)	H$_{eq}$-4, H$_{ax}$-4, H-3, Me-N	4, 3
Me-2'	22.2 (CH$_3$)	2.31 (s)	H-1', H-3'	1', 2', 3'
MeO-8	56.2 (CH$_3$)	3.92 (s)	H-7, Me-1, H-1	8
MeO-4'	57.1 (CH$_3$)	3.93 (s)	H-3'	4'
MeO-5'	56.9 (CH$_3$)	3.96 (s)	H-6'	5'
Me-N	41.5 (CH$_3$)	3.02 (s)	Me-1, Me-3, H-1, H-3	1, 3

4.3.2. *Ancistroyafungine B (57)*

Yellow amorphous powder (2.1 mg).

57

$[\alpha]_D^{25} = +8.1$ ($c = 0.40$, MeOH).

HRMS (ESI): *m/z* found = 408.2173 [M+H]$^+$,

m/z calculated for $[C_{25}H_{30}NO_4]^+ = 408.2169$.

ECD (MeOH): λ_{max} ($\Delta\varepsilon$) = 192 (+8.8), 209 (–9.2), 216 (–6.9), 223 (–7.6), 238 (+10.8), 286 (–0.6) nm.

UV (MeOH): λ_{max} (log ε) = 206 (1.63), 231 (1.61), 306 (0.34), 321 (0.28), 336 (0.21) nm.

IR (ATM): ν_{max} = 3372, 1671, 1583, 1448, 1364, 1273, 1196, 1134, 1093, 832, 799, 720 cm^{-1}.

Products of the oxidative degradation: (*S*)-3-aminobutyric acid and (*S*)-*N*-methyl-3-aminobutyric acid.

^{1}H NMR (600 MHz, MeOD): δ = 1.27 (d, *J* = 6.6 Hz, 3H), 1.72 (d, *J* = 6.6 Hz, 3H), 2.22 (dd, *J* = 17.3, 3.1 Hz, 1H), 2.32 (s, 3H), 2.57 (dd, *J* = 17.3, 11.4 Hz, 1H), 3.03 (s, 3H), 3.16 (m, 1H), 3.91 (s, 3H), 4.09 (s, 3H), 4.65 (q, *J* = 6.6 Hz, 1H), 6.59 (s, 1H), 6.69 (*p*t, *J* = 1.1 Hz, 1H), 6.80 (d, *J* = 7.9 Hz, 1H), 6.81 (s, 1H), 7.10 (d, *J* = 7.9 Hz, 1H) ppm.

^{13}C NMR (150 MHz, MeOD): δ = 18.1 (CH$_3$), 20.0 (CH$_3$), 22.3 (CH$_3$), 34.3 (CH$_2$), 41.5 (CH$_3$), 56.2 (CH$_3$), 56.9 (CH$_3$), 60.5 (CH), 62.3 (CH), 99.1 (CH), 107.7 (CH), 110.5 (CH), 119.2 (CH), 132.1 (CH), 114.5, 115.0, 119.9, 124.3, 134.9, 137.0, 137.8, 156.1, 157.4, 157.7, 158.1 (qC) ppm.
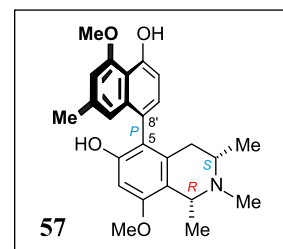
Table 22. NMR data (^{1}H: 600 MHz, ^{13}C: 150 MHz) of ancistroyafungine B (**57**) in MeOD.

Position	^{13}C [ppm] (type)	^{1}H [ppm] (mult., J [Hz])	NOESY	HMBC
1	62.3 (CH)	4.65 (q, 6.6)	H-3, Me-1, Me-N	9, 10, Me-1, Me-N, 8
3	60.5 (CH)	3.16 (m)	H-1, Me-N, H$_{eq}$-4, Me-3	
4	34.3 (CH$_2$)	2.22 (dd, 3.1, 17.3)	H-3, H$_{ax}$-4, H-1', Me-3	5, 9, 10, Me-3
		2.57 (dd, 11.4, 17.3)	H-3, H$_{eq}$-4, H-7', Me-3	3, 9, 10, Me-3
5	119.9 (qC)			
6	158.1 (qC)			
7	99.1 (CH)	6.59 (s)	MeO-8	1, 5, 6, 8, 9
8	157.7 (qC)			
9	114.5 (qC)			
10	134.9 (qC)			
1'	119.2 (CH)	6.69 (pt, 1.1)	H$_{eq}$-4, Me-2′	3', 8', 9', 10', Me-2′
2'	137.8 (qC)			
3'	107.8 (CH)	6.81 (s)	Me-2′, MeO-4′	1', 2', 4', 10', Me-2′
4'	157.4 (qC)			
5'	156.1 (qC)			
6'	110.5 (CH)	6.80 (d, 7.9)	H-7′	5', 8′, 10'
7'	132.1 (CH)	7.10 (d, 7.9)	H-6′, H$_{ax}$-4	5, 5', 6′, 9'
8'	124.3 (qC)			
9'	137.0 (qC)			
10'	115.0 (qC)			
Me-1	20.0 (CH$_3$)	1.72 (d, 6.6)	MeO-8, Me-N, H-1	1, 9
Me-3	18.1 (CH$_3$)	1.26 (d, 6.6)	H$_{eq}$-4, H$_{ax}$-4, H-3, Me-N	4, 3
Me-2'	22.3 (CH$_3$)	2.32 (s)	H-1′, H-3′	1′, 2′, 3′
MeO-8	56.2 (CH$_3$)	3.91 (s)	H-7, Me-1, H-1	8
MeO-4'	57.1 (CH$_3$)	4.09 (s)	H-3'	4′
Me-N	41.5 (CH$_3$)	3.03 (s)	Me-1, Me-3, H-1, H-3	1, 3

4.3.3. *Ancistroyafungine C (58)*

Beige amorphous powder (5.1 mg).

$[\alpha]_D^{25} = -5.9$ ($c = 0.43$, MeOH).

HRMS (ESI): *m/z* found = 436.2486 [M+H]$^+$,

$\qquad$ *m/z* calculated for [C$_{27}$H$_{34}$NO$_4$]$^+$ = 436.2482.

ECD (MeOH): λ_{max} ($\Delta\varepsilon$) = 201 (−10.4), 228 (+22.9), 243 (−8.3), 281 (+0.5) nm.

UV (MeOH): λ_{max} (log ε) = 206 (1.56), 231 (1.54), 306 (0.32), 321 (0.26),

$\qquad$ 336 (0.19) nm.

IR (ATM): ν_{max} = 3388, 1671, 1583, 1451, 1316, 1274, 1199, 1133, 1093, 1061, 966,

$\qquad$ 832, 800, 720 cm^{-1}.

Products of the oxidative degradation: (*S*)-3-aminobutyric acid and (*S*)-*N*-methyl-3-

$\qquad$ aminobutyric acid.

^{1}H NMR (400 MHz, MeOD): δ = 1.29 (d, *J* = 6.7 Hz, 3H), 1.77 (d, *J* = 6.5 Hz, 3H),

$\qquad$ 2.30 (d, *J* = 0.3 Hz, 3H), 2.35 (dd, *J* = 17.3, 11.0 Hz, 1H), 2.49 (dd, *J* = 17.3,

$\qquad$ 3.3 Hz, 1H), 3.02 (s, 3H), 3.23 (m, 1H), 3.69 (s, 3H), 3.93 (s, 3H), 3.95 (s,

$\qquad$ 3H), 4.00 (s, 3H), 4.67 (q, *J* = 6.4 Hz, 1H), 6.65 (*p*t, *J* = 0.9 Hz, 1H), 6.78

$\qquad$ (d, *J* = 1.2 Hz, 1H), 6.79 (s, 1H), 6.91 (d, *J* = 8.1 Hz, 1H), 7.10 (d, *J* = 8.1

$\qquad$ Hz, 1H) ppm.

^{13}C NMR (100 MHz, MeOD): δ = 18.1 (CH$_3$), 20.1 (CH$_3$), 22.2 (CH$_3$), 33.1 (CH$_2$),

$\qquad$ 41.6 (CH$_3$), 56.4 (CH$_3$), 56.5 (CH$_3$), 56.9 (CH$_3$), 57.1 (CH$_3$), 60.2 (CH),

$\qquad$ 61.9 (CH), 96.2 (CH), 106.7 (CH), 109.9 (CH), 118.4 (CH), 130.2 (CH),

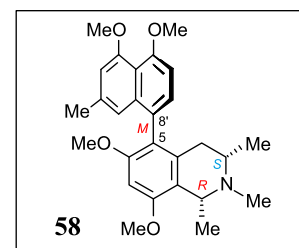$\qquad$ 114.9, 117.6, 122.0, 126.5, 134.8, 137.96, 138.01, 157.9, 158.3, 158.9,

$\qquad$ 160.0 (qC) ppm.

Table 23. NMR data (^{1}H: 400 MHz, ^{13}C: 100 MHz) of ancistroyafungine C (**58**) in MeOD.

Position	^{13}C [ppm] (type)	^{1}H [ppm] (mult., J [Hz])	NOESY	HMBC
1	61.9 (CH)	4.67 (q, 6.4)	H-3, Me-1, Me-*N*	9, 10, Me-1, 8, Me-*N*
3	60.2 (CH)	3.23 (m)	H-1, Me-*N*, H$_{eq}$-4, Me-3	
4	33.1 (CH$_2$)	2.35 (dd, 11.1, 17.3)	H-3, H$_{ax}$-4, H-1', Me-3	5, 9, 10, Me-3
		2.49 (dd, 3.3, 17.3)	H-3, H$_{eq}$-4, H-7', Me-3	3, 9, 10, Me-3
5	122.0 (qC)			
6	160.0 (qC)			
7	96.2 (CH)	6.79 (s)	MeO-6, MeO-8	1, 5, 6, 8, 9
8	157.9 (qC)			
9	114.9 (qC)			
10	134.8 (qC)			
1'	118.4 (CH)	6.65 (t, 0.9)	H$_{ax}$-4, Me-2', MeO-6	3', 8', 9', 10', Me-2'
2'	138.0 (qC)			
3'	109.9 (CH)	6.78 (d, 1.2)	Me-2', MeO-4'	1', 2', 4', 10', Me-2'
4'	158.9 (qC)			
5'	158.3 (qC)			
6'	106.7 (CH)	6.91 (d, 8.1)	H-7', MeO-5'	5', 8', 10'
7'	130.2 (CH)	7.10 (d, 8.1)	H-6', H$_{eq}$-4, MeO-6	5, 5', 6', 9'
8'	126.5 (qC)			
9'	138.0 (qC)			
10'	117.6 (qC)			
Me-1	20.1 (CH$_3$)	1.77 (d, 6.5)	MeO-8, Me-*N*, H-1	1, 9
Me-3	18.1 (CH$_3$)	1.29 (d, 6.7)	H$_{eq}$-4, H$_{ax}$-4, H-3, Me-*N*	4, 3
Me-2'	22.2 (CH$_3$)	2.30 (d, 0.7)	H-1', H-3'	1', 2', 3'
MeO-6	56.5 (CH$_3$)	3.69 (s)	H-6, H-1', H-7'	6
MeO-8	56.4 (CH$_3$)	4.00 (s)	H-7, Me-1, H-1	8
MeO-4'	57.1 (CH$_3$)	3.93 (s)	H-3'	4'
MeO-5'	56.9 (CH$_3$)	3.95 (s)	H-6'	5'
Me-*N*	41.6 (CH$_3$)	3.02 (s)	Me-1, Me-3, H-1, H-3	1, 3

4.3.4. *Ancistroyafungine D (59)*

Yellow amorphous powder (2.5 mg).

$[\alpha]_D^{25}$ = +5.9 (*c* = 0.41, MeOH).

HRMS (ESI): *m/z* found = 408.2168 [M+H]$^+$,

   m/z calculated for [C$_{25}$H$_{30}$NO$_4$]$^+$ = 408.2169.

ECD (MeOH): λ_{max} ($\Delta\varepsilon$) = 200 (–7.2), 227 (+18.8), 241 (–8.6), 284 (+0.3) nm.

UV (MeOH): λ_{max} (log ε) = 204 (0.3), 230 (0.22), 288 (0.05), 305 (0.04), 322 (0.03), 336 (0.03) nm.

IR (ATM): ν_{max} = 3431, 1673, 1584, 1450, 1364, 1316, 1273, 1200, 1134, 834, 800, 720 cm^{-1}.

Product of the oxidative degradation: (*S*)-3-aminobutyric acid.

^{1}H NMR (400 MHz, MeOD): δ = 1.20 (d, *J* = 6.4 Hz, 3H), 1.64 (d, *J* = 6.9 Hz, 3H), 2.09 (s, 3H), 2.10 (dd, *J* = 18.0, 11.3 Hz, 1H), 2.42 (dd, *J* = 17.3, 4.8 Hz, 1H), 3.68 (s, 3H), 3.70 (m, 1H), 4.01 (s, 3H), 4.12 (s, 3H), 4.80 (q, *J* = 6.6 Hz, 1H), 6.53 (dd, *J* = 8.4, 1.0 Hz, 1H), 6.70 (dd, *J* = 7.7, 1.1 Hz, 1H), 6.78 (s, 1H), 6.92 (s, 1H), 7.11 (dd, *J* = 8.4, 7.7 Hz, 1H) ppm.

^{13}C NMR (100 MHz, MeOD): δ = 18.7 (CH$_3$), 20.7 (CH$_3$), 20.7 (CH$_3$), 32.9 (CH$_2$), 45.1 (CH), 48.9 (CH)*, 56.38 (CH$_3$), 56.42 (CH$_3$), 56.9 (CH$_3$), 95.6 (CH), 108.1 (CH), 110.5 (CH), 116.9 (CH), 128.9 (CH), 115.16, 115.17, 120.5, 126.6, 132.9, 136.1, 137.3, 156.3, 157.1, 158.1, 159.7 (qC) ppm.

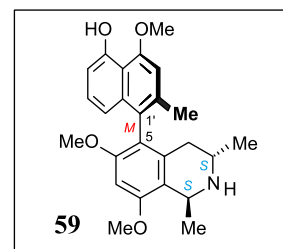   *This signal was overlapped by the solvent peak, but it was detected by HMBC and HSQC measurements.

Table 24. NMR data (^{1}H: 400 MHz, ^{13}C: 100 MHz) of ancistroyafungine D (**59**) in MeOD.

| Position	^{13}C [ppm] (type)	^{1}H [ppm] (mult., *J* [Hz])	NOESY	HMBC
1	48.9 (CH)	4.80 (q, 6.8)	H-3, Me-1	9, 10, Me-1
3	45.1 (CH)	3.70 (m)	H-1, H-4, Me-3, Me-1	
4	32.9 (CH$_2$)	2.10 (dd, 18.0, 11.3)	H-3, H$_{ax}$-4, H-8′, Me-3	5, 9, 10, Me-3
		2.42 (dd, 17.3, 4.8)	H-3, H$_{eq}$-4, Me-2′, Me-3	3, 9, 10, Me-3
5	120.5 (qC)			
6	159.7 (qC)			
7	95.6 (CH)	6.78 (s)	MeO-6, MeO-8	5, 6, 8, 9
8	158.1 (qC)			
9	115.2 (qC)			
10	132.9 (qC)			
1′	126.6 (qC)			
2′	136.1 (qC)			
3′	108.1 (CH)	6.92 (s)	Me-2′, MeO-4′	1′, 2′, 4′, 10′, Me-2′
4′	157.1 (qC)			
5′	156.3 (qC)			
6′	110.5 (CH)	6.70 (dd, 7.7, 1.0)	H-7′	5′, 8′, 10′
7′	128.9 (CH)	7.11 (dd, 8.4, 7.7)	H-6′, H-8′	5′, 6′, 8′, 9′
8′	116.9 (CH)	6.53 (dd, 8.4, 1.0)	H-7′, H$_{ax}$-4	1′, 6′, 9′, 10′
9′	137.3 (qC)			
10′	115.2 (qC)			
Me-1	18.7 (CH$_3$)	1.64 (d, 6.9)	MeO-8, H-1, H-3	1, 9
Me-3	19.3 (CH$_3$)	1.20 (d, 6.4)	H$_{eq}$-4, H$_{ax}$-4, H-3,	4, 3
Me-2′	20.7 (CH$_3$)	2.09 (s)	H-3′, H$_{eq}$-4	1′, 2′, 3′
MeO-6	56.4 (CH$_3$)	3.68 (s)	H-7, Me-2′, H-8′	6
MeO-8	56.4 (CH$_3$)	4.01 (s)	H-7, Me-1, H-1	8
MeO-4′	56.9 (CH$_3$)	4.12 (s)	H-3′	4′

4.4. Known Compounds

4.4.1. Ancistrocladinium A (9)

Yellow amorphous powder (7 mg).

MS (ESI): m/z found = 420.5 [M+H]$^+$ (LC-MS),

m/z calculated for [C$_{26}$H$_{30}$NO$_4$]$^+$ = 420.2.
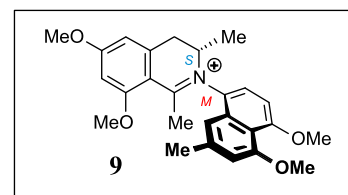
ECD (MeOH): λ_{max} ($\Delta\varepsilon$) = 213 (+5.0), 230 (−3.6), 238 (+1.9), 311 (−3.3) nm.

Product of the oxidative degradation: (*S*)-3-aminobutyric acid.

^{1}H NMR (400 MHz, MeOD): δ = 1.31 (d, J = 6.5 Hz, 3H), 2.51 (*p*d, J = 0.7 Hz, 3H), 2.52 (d, J = 4.9 Hz, 3H), 3.13 (dd, J = 17.0, 2.5 Hz, 1H), 3.84 (dd, J = 17.0, 6.7 Hz, 1H), 3.97 (s, 3H), 4.01 (s, 3H), 4.03 (s, 3H), 4.05 (s, 3H), 4.25 (m, 1H), 6.74 (*p*d, J = 2.1 Hz, 1H), 6.77 (*p*t, J = 0.8 Hz, 1H), 6.97 (d, J = 8.1 Hz, 1H), 6.98 (s, 1H), 7.09 (*p*t, J = 1.1 Hz, 1H), 7.47 (d, J = 8.4 Hz, 1H) ppm.

Key NOESY interactions: H-3 (4.25 ppm) ↔ H-1′ (7.09 ppm) ↔ Me-2′ (2.51 ppm) ↔ H-3′ (6.98 ppm) ↔ MeO-4′ (3.97 ppm); Me-3 (1.31 ppm) ↔ H-7′ (7.47 ppm) ↔ H-6′ (6.97 ppm) ↔ MeO-5′ (4.01 ppm).

The physical chromatographic, and spectroscopic data were in good agreement with the ones previously published.[56]

4.4.2. 6-O-Methylhamatine (60)

Yellow amorphous powder (6 mg).

MS (ESI): m/z found = 422.4 [M+H]$^+$ (LC-MS),

m/z calculated for [C$_{26}$H$_{32}$NO$_4$]$^+$ = 422.23.
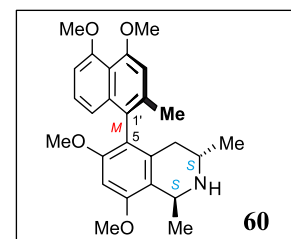
ECD (MeOH): λ_{max} ($\Delta\varepsilon$) = 200 (−7.6), 228 (+18.9), 241 (−9.3), 284 (+0.3) nm.

Product of the oxidative degradation: (*S*)-3-aminobutyric acid.

^{1}H NMR (400 MHz, MeOD): δ = 1.19 (d, *J* = 6.5 Hz, 3H), 1.64 (d, *J* = 6.5 Hz, 3H), 2.07 (s, 3H), 2.08 (dd, *J* = 17.9, 11.9 Hz, 1H), 2.40 (dd, *J* = 18.0, 4.8 Hz, 1H), 3.68 (s, 3H), 3.70 (m, 1H), 3.92 (s, 3H), 3.96 (s, 3H), 4.02 (s, 3H), 4.80 (q, *J* = 6.7 Hz, 1H), 6.67 (dd, *J* = 8.5, 1.0 Hz, 1H), 6.78 (s, 1H), 6.85 (d, *J* = 7.1 Hz, 1H), 6.91 (s, 1H), 7.15 (dd, *J* = 8.4, 7.8 Hz, 1H) ppm.

Key NOESY interactions: H-3 (3.70 ppm) $\leftrightarrow$ Me-1 (1.64 ppm) $\leftrightarrow$ MeO-8 (4.02 ppm) $\leftrightarrow$ H-7 (6.78 ppm) $\leftrightarrow$ MeO-6 (3.68 ppm) $\leftrightarrow$ H-8′ (6.67 ppm) $\leftrightarrow$ H-7′ (7.15 ppm) $\leftrightarrow$ H-6′ (6.85) $\leftrightarrow$ MeO-5′ (3.92 ppm);

H_{ax}-4 (2.08 ppm) $\leftrightarrow$ H-8′;

H_{eq}-4 (2.40 ppm) $\leftrightarrow$ Me-2′ (2.07 ppm) $\leftrightarrow$ H-3′ (6.91 ppm) $\leftrightarrow$ MeO-4′ (3.96 ppm).

The physical and spectroscopic data were in good agreement with the ones previously published.[218,219]

4.4.3. 4′-*O*-Demethylancistrocladine A (61)

Yellow amorphous powder (2.8 mg).

MS (ESI): *m/z* found = 394.2 [M+H]$^+$ (LC-MS),

   m/z calculated for [$C_{24}H_{28}NO_4$]$^+$ = 394.5.
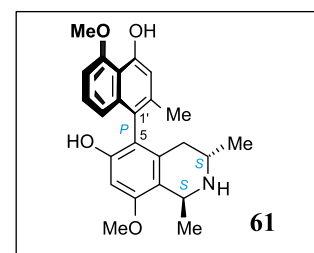
ECD (MeOH): λ_{max} ($\Delta\varepsilon$) = 200 (+15.1), 228 (−14.9), 241 (+7.5), 284 (−1.7) nm.

Product of the oxidative degradation: (*S*)-3-aminobutyric acid.

^{1}H NMR (400 MHz, MeOD): δ = 1.21 (d, *J* = 6.4 Hz, 3H), 1.64 (d, *J* = 6.7 Hz, 3H), 2.06 (s, 3H), 2.14 (dd, *J* = 17.7, 11.4 Hz, 1H), 2.26 (dd, *J* = 17.5, 5.5 Hz, 1H), 3.62 (m, 1H), 3.92 (s, 3H), 4.09 (s, 3H), 4.77 (q, *J* = 6.6 Hz, 1H), 6.60 (s, 1H), 6.81 (s, 1H), 6.85 (dd, *J* = 8.5, 0.9 Hz, 1H), 6.88 (*p*d, *J* = 7.2 Hz, 1H), 7.21 (dd, *J* = 8.5, 7.8 Hz, 1H) ppm.

Key NOESY interactions: H-3 (3.62 ppm) $\leftrightarrow$ Me-1 (1.64 ppm) $\leftrightarrow$ MeO-8 (3.92 ppm) $\leftrightarrow$ H-7 (6.60 ppm);

H_{eq}-4 (2.26 ppm) $\leftrightarrow$ H-8′ (6.85 ppm) $\leftrightarrow$ H-7′ (7.21 ppm) $\leftrightarrow$ H-6′ (6.88) $\leftrightarrow$ MeO-5′ (4.09 ppm);

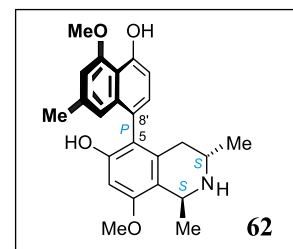H$_{ax}$-4 (2.14 ppm) ↔ Me-2′ (2.06 ppm) ↔ H-3′ (6.81 ppm).

The physical and spectroscopic data were in good agreement with the ones previously published.[202,219]

4.4.4. *Ancistroguineine A (62)*

Beige amorphous powder (1.9 mg).

MS (ESI): *m/z* found = 394.2 [M+H]$^+$ (LC-MS),

        m/z calculated for [C$_{24}$H$_{28}$NO$_4$]$^+$ = 394.5.

ECD (MeOH): λ$_{max}$ (Δε) = 200 (+5.4), 211 (–10.4), 224 (–16.3), 238 (+14.7),

        287 (–0.9) nm.

Product of the oxidative degradation: (*S*)-3-aminobutyric acid.

^{1}H NMR (400 MHz, MeOD): δ = 1.24 (d, *J* = 6.5 Hz, 3H), 1.65 (d, *J* = 6.7 Hz, 3H),

        2.27 (dd, *J* = 18.1, 5.0 Hz, 1H), 2.33 (*p*d, *J* = 0.7 Hz, 3H), 2.41 (dd, *J* = 18.2,

        11.5 Hz, 1H), 3.64 (m, 1H), 3.92 (s, 3H), 4.09 (s, 3H), 4.76 (q, *J* = 6.8 Hz,

        1H), 6.58 (s, 1H), 6.75 (*p*t, *J* = 1.1 Hz, 1H), 6.80 (d, *J* = 8.0 Hz, 1H), 6.81

        (s, 1H), 7.03 (d, *J* = 7.8 Hz, 1H) ppm.

Key NOESY interactions: H-3 (3.64 ppm) ↔ Me-1 (1.65 ppm) ↔ MeO-8 (3.92 ppm)

        ↔ H-7 (6.58 ppm);

        H$_{eq}$-4 (2.27 ppm) ↔ H-1′ (6.75 ppm) ↔ Me-2′ (2.33 ppm) ↔ H-3′ (6.81) ↔

        MeO-4′ (4.09 ppm);

        H$_{ax}$-4 (2.41 ppm) ↔ H-7′ (7.03 ppm) ↔ H-6′ (6.80 ppm).

^{13}C NMR (100 MHz, MeOD): δ = 18.8 (CH$_3$), 19.3 (CH$_3$), 22.4 (CH$_3$), 34.0 (CH$_2$),

        45.2 (CH), 48.6 (CH)*, 56.2 (CH$_3$), 56.9 (CH$_3$), 98.8 (CH), 107.8 (CH),

        110.5 (CH), 119.0 (CH), 131.6 (CH), 114.3, 115.1, 120.1, 124.6, 133.2,

        137.1, 137.8, 156.0, 157.4, 157.7, 158.1 (qC) ppm.

    *This signal was overlapped by the solvent peak, but it was detected from HMBC and
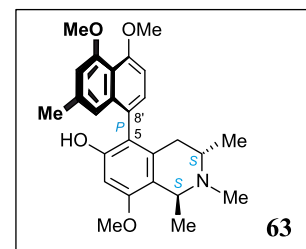   HSQC measurements.

The physical and spectroscopic data corroborated the previously published ones.[213]

4.4.5. Ancistrobertsonine A (63)

Beige amorphous powder (4 mg).

MS (ESI): *m/z* found = 422.2332 [M+H]$^+$ (LC-MS),

      m/z calculated for [C$_{26}$H$_{32}$NO$_4$]$^+$ = 422.2326.

ECD (MeOH): λ_{max} ($\Delta\varepsilon$) = 200 (+19.2), 212 (–14.9), 224 (–15.4), 239 (+17.0),

            286 (–0.9) nm.

Products of the oxidative degradation: (*S*)-3-aminobutyric acid and (*S*)-*N*-methyl-3-
aminobutyric acid.

^{1}H NMR (400 MHz, MeOD): δ = 1.23 (d, *J* = 6.6 Hz, 3H), 1.71 (d, *J* = 6.6 Hz, 3H),

      2.22 (dd, *J* = 18.6, 4.8 Hz, 1H), 2.32 (s, 3H), 2.47 (dd, *J* = 18.6, 12.0 Hz,

      1H), 2.75 (s, 3H), 3.65 (m, 1H), 3.92 (s, 3H), 3.93 (s, 3H), 3.96 (s, 3H), 4.73

      (q, *J* = 6.7 Hz, 1H), 6.61 (s, 1H), 6.74 (*p*t, *J* = 1.1 Hz, 1H), 6.79 (*p*d, *J* = 1.1

      Hz, 1H), 6.94 (d, *J* = 8.2 Hz, 1H), 7.15 (d, *J* = 7.9 Hz, 1H) ppm.

^{13}C NMR (150 MHz, MeOD): δ = 16.9 (CH$_3$), 19.5 (CH$_3$), 22.2 (CH$_3$), 29.9 (CH$_2$),

      34.2 (CH$_3$), 50.6 (CH), 56.3 (CH$_3$), 56.9 (CH$_3$), 57.1 (CH$_3$), 59.8 (CH), 99.2

      (CH), 106.9 (CH), 110.1 (CH), 118.3 (CH), 130.7 (CH), 112.1, 117.8,

      120.4, 126.3, 132.4, 137.6, 138.1, 157.6, 158.4, 158.6, 158.9 (qC) ppm.
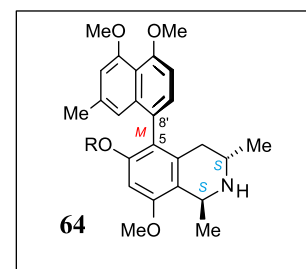
The spectroscopic data were in good agreement with the previously published ones.[203]

4.4.6. Ancistrobrevine B (64)

Yellow amorphous powder (2.3 mg).

MS (ESI): *m/z* found = 408.4 [M+H]$^+$ (LC-MS),

      m/z calculated for [C$_{25}$H$_{30}$NO$_4$]$^+$ = 408.2

ECD (MeOH): λ_{max} ($\Delta\varepsilon$) = 200 (–5.6), 210 (+11.3), 228 (+19.9), 242 (–10.6), 285

            (+0.4) nm.

Product of the oxidative degradation: (*S*)-3-aminobutyric acid.

^{1}H NMR (400 MHz, MeOD): δ = 1.19 (d, [3]*J* = 6.4 Hz, 3H), 1.63 (d, *J* = 6.7 Hz, 3H), 2.08 (dd, *J* = 18.2, 11.3 Hz, 1H), 2.29 (s, 3H), 2.66 (dd, *J* = 18.0, 4.9 Hz, 1H), 3.67 (m, 1H), 3.92 (s, 3H), 3.93 (s, 3H), 3.96 (s, 3H), 4.77 (q, *J* = 6.6 Hz, 1H), 6.59 (s, 1H), 6.66 (*p*t, *J* = 0.9 Hz, 1H), 6.78 (*p*d, *J* = 1.0 Hz, 1H), 6.95 (d, *J* = 8.0 Hz, 1H), 7.15 (d, *J* = 7.9 Hz, 1H) ppm.

Key NOESY interactions: H-3 (3.67 ppm) ↔ Me-1 (1.63 ppm) ↔ MeO-8 (3.92 ppm) ↔ H-7 (6.59 ppm); H$_{ax}$-4 (2.08 ppm) ↔ H-1′ (6.66 ppm) ↔ Me-2′ (2.29 ppm) ↔ H-3′ (6.78 ppm) ↔ MeO-4′ (3.93 ppm); H$_{eq}$-4 (2.66 ppm) ↔ H-7′ (7.15 ppm) ↔ H-6′ (6.95 ppm) ↔ MeO-5′ (3.96 ppm).

The spectroscopic data were in good agreement with the ones previously published.[204,218]

4.4.7. *Ancistrotectoriline A (65)*

Yellow amorphous powder (7 mg).

MS (ESI): *m/z* found = 422.5 [M+H]$^+$ (LC-MS), *m/z* calculated for [C$_{26}$H$_{32}$NO$_4$]$^+$ = 422.2.
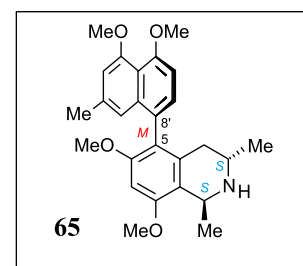
ECD (MeOH): λ_{max} ($\Delta\varepsilon$) = 200 (−8.6), 228 (+21.9), 240 (−13.5) nm.

Product of the oxidative degradation: (*S*)-3-aminobutyric acid.

^{1}H NMR (400 MHz, MeOD): δ = 1.18 (d, *J* = 6.4 Hz, 3H), 1.64 (d, *J* = 6.6 Hz, 3H), 2.08 (dd, *J* = 17.8, 11.5 Hz, 1H), 2.27 (s, 3H), 2.66 (dd, *J* = 18.0, 4.8 Hz, 1H), 3.66 (m, 1H), 3.66 (s, 3H), 3.92 (s, 3H), 3.93 (s, 3H), 4.01 (s, 3H), 4.81 (q, *J* = 6.8 Hz, 1H), 6.56 (*p*q, *J* = 0.9 Hz, 1H), 6.76 (s, 1H), 6.77 (*p*d, *J* = 1.0 Hz, 1H), 6.92 (d, *J* = 8.0 Hz, 1H), 7.09 (d, *J* = 7.9 Hz, 1H) ppm.

Key NOESY interactions: H-3 (3.66 ppm) ↔ Me-1 (1.64 ppm) ↔ MeO-8 (4.01 ppm) ↔ H-7 (6.76 ppm) ↔ MeO-6 (3.66 ppm) ↔ H-1′ (6.56 ppm); H$_{ax}$-4 (2.08 ppm) ↔ H-1′ ↔ Me-2′ (2.27 ppm) ↔ H-3′ (6.77 ppm) ↔ MeO-4′ (3.92 ppm); H$_{eq}$-4 (2.66 ppm) ↔ H-7′ (7.09 ppm) ↔ H-6′ (6.92 ppm) ↔ MeO-5′ (3.93 ppm).

The spectroscopic data were in good agreement with the ones previously published.[210]

4.4.8. 6,5'-O,O-didemethylancistroealaine A (ent-49)

Beige amorphous powder (2.1 mg).

MS (ESI): *m/z* found = 392.4 [M+H]$^+$ (LC-MS),

   m/z calculated for [$C_{24}H_{26}NO_4$]$^+$ = 392.2.
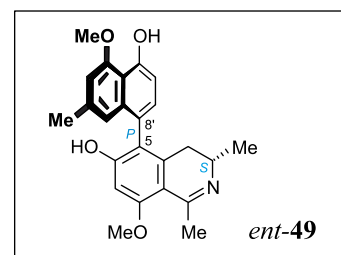
ECD (MeOH): λ_{max} ($\Delta\varepsilon$) = 211 (+12.3), 229 (–7.1), 244 (+5.2), 269 (–0.3),

   281 (–0.4) nm.

Product of the oxidative degradation: (*S*)-3-aminobutyric acid.

^{1}H NMR (400 MHz, MeOD): δ = 1.26 (d, *J* = 6.6 Hz, 3H), 2.34 (d, *J* = 0.6 Hz, 3H),

   2.41 (dd, *J* = 16.9, *J* = 5.8 Hz, 1H), 2.48 (dd, *J* = 16.9, 11.3 Hz, 1H), 2.79

   (d, *J* = 1.5 Hz, 3H), 3.70 (m, 1H), 4.04 (s, 3H), 4.10 (s, 3H), 6.67 (s, 1H),

   6.72 (*p*t, *J* = 1.1 Hz, 1H), 6.80 (d, *J* = 7.9 Hz, 1H), 6.83 (d, *J* = 0.9 Hz, 1H),

   7.05 (d, *J* = 7.9 Hz, 1H) ppm.

Key NOESY interactions: H_{eq}-4 (2.41 ppm) ↔ H-1' (6.72 ppm) ↔ Me-2' (2.34 ppm)

   ↔ H-3' (6.83 ppm) ↔ MeO-4' (4.10 ppm);

   H_{ax}-4 (2.48 ppm) ↔ H-7' (7.05 ppm) ↔ H-6' (6.80 ppm).

The spectroscopic data were in good agreement with the previously published ones.[102] They also corroborated those of its new enantiomer[103] herein described (see compound **48**).

4.4.9. 6-O-demethylancistroealaine A (66)

Beige amorphous powder (3.5 mg).

MS (ESI): *m/z* found = 406.5 [M+H]$^+$ (LC-MS),

   m/z calculated for [$C_{25}H_{28}NO_4$]$^+$ = 406.2.
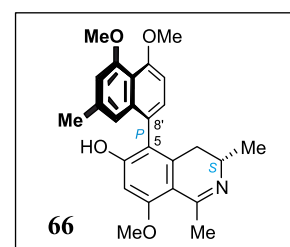
ECD (MeOH): λ_{max} ($\Delta\varepsilon$) = 212 (+16.1), 231 (–15.0), 246 (+10.2), 281 (–3.4) nm.

Product of the oxidative degradation: (*S*)-3-aminobutyric acid.

^{1}H NMR (400 MHz, MeOD): δ = 1.25 (d, *J* = 6.9 Hz, 3H), 2.33 (d, *J* = 0.5 Hz, 3H),

   2.41 (dd, *J* = 17.1, *J* = 6.3 Hz, 1H), 2.48 (dd, *J* = 16.7, 11.4 Hz, 1H), 2.79

   (d, *J* = 1.1 Hz, 3H), 3.68 (m, 1H), 3.94 (s, 3H), 3.96 (s, 3H), 4.05 (s, 3H),

6.67 (s, 1H), 6.71 (*p*q, *J* = 1.1 Hz, 1H), 6.81 (d, *J* = 0.9 Hz, 1H), 6.93 (d, *J* = 8.1 Hz, 1H), 7.10 (d, *J* = 8.0 Hz, 1H) ppm.

Key NOESY interactions: H$_{eq}$-4 (2.41 ppm) ↔ H-1′ (6.71 ppm) ↔ Me-2′ (2.33 ppm) ↔ H-3′ (6.81 ppm) ↔ MeO-4′ (3.94 ppm); H$_{eq}$-4 (2.48 ppm) ↔ H-7′ (7.10 ppm) ↔ H-6′ (6.93 ppm) ↔ MeO-5′ (3.96 ppm).

^{13}C NMR (100 MHz, MeOD): δ = 18.2 (CH$_3$), 22.2 (CH$_3$), 24.8 (CH$_3$), 33.6 (CH$_2$), 49.6 (CH), 56.8 (CH$_3$), 57.1 (CH$_3$), 99.3 (CH), 106.5 (CH), 110.2 (CH), 118.0 (CH), 130.8 (CH), 108.8, 117.6, 122.6, 125.0, 137.3, 138.5, 142.8, 158.99, 159.04, 165.8, 167.8, 175.8 (qC) ppm.

The spectroscopic data were in good agreement with the previously published ones.[102]

4.4.10. 7-epi-ancistrobrevine D (67)

Yellow amorphous powder (3.5 mg).

MS (ESI): *m/z* found = 422.4 [M+H]$^+$ (LC-MS),
　　　m/z calculated for [C$_{26}$H$_{32}$NO$_4$]$^+$ = 422.2.
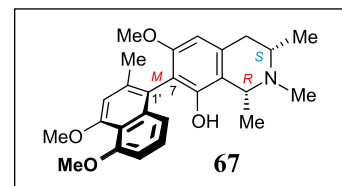
ECD (MeOH): λ_{max} ($\Delta\varepsilon$) = 200 (+2.5), 211 (–7.6), 230 (+10.1), 252 (–0.2), 282 (+1.6) nm.

Products of the oxidative degradation: (*S*)-3-aminobutyric acid and (*S*)-*N*-methyl-3-aminobutyric acid.

^{1}H NMR (400 MHz, MeOD): δ = 1.60 (d, *J* = 6.5 Hz, 3H), 1.77 (d, *J* = 6.6 Hz, 3H), 2.13 (s, 3H), 3.08 (m, 2H), 3.11 (s, 3H), 3.50 (m, 1H), 3.60 (s, 3H), 3.92 (s, 3H), 3.97 (s, 3H), 4.63 (q, 6.5 Hz, 1H), 6.56 (s, 1H), 6.77 (dd, *J* = 8.4, 0.9 Hz, 1H), 6.85 (*p*d, *J* = 7.4 Hz, 1H), 6.92 (s, 1H), 7.15 (dd, *J* = 8.6, 7.5 Hz, 1H) ppm.
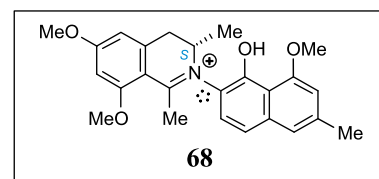
Key NOESY interactions: Me-3 (1.60 ppm) ↔ Me-*N* (3.11 ppm) ↔ Me-1 (1.77 ppm) ↔ Me-2′ (2.13 ppm) ↔ H-3′ (6.92 ppm) ↔ MeO-4′ (3.97 ppm); H-1 (4.63 ppm) ↔ H-3 (3.50 ppm).

The spectroscopic data were in good agreement with the previously published ones.[207,219]

4.4.11. Ancistrocladinium B (68)

Yellow amorphous powder (13 mg).

68

MS (ESI): *m/z* found = 406.5 [M+H]$^+$ (LC-MS),

   m/z calculated for [C$_{26}$H$_{32}$NO$_4$]$^+$ = 406.2.

Product of the oxidative degradation: (*S*)-3-aminobutyric acid.

A slow atropisomerization typical of this compound was detected by HPLC-UV, leading to a mixture of ca. 1:1 ratio of the *P*- and *M*-atropisomers at room temperature.

^{1}H NMR (400 MHz, MeOD): δ = 1.21 (d, *J* = 7.1 Hz, 3H), 1.30 (d, *J* = 6.9 Hz, 3H), 2.52 (s, 6H), 2.57 (s, 3H), 2.66 (s, 3H), 3.05 (dd, *J* = 16.6, 2.6 Hz, 1H), 3.07 (dd, *J* = 16.6, 2.6 Hz, 1H), 3.66 (dd, *J* = 16.4, 6.0 Hz, 1H), 3.70 (dd, *J* = 16.5, 5.9 Hz, 1H), 4.00 (s, 3H), 4.01 (s, 3H), 4.04 (s, 6H), 4.11 (s, 3H), 4.12 (s, 3H), 4.38 (m, 1H), 4.48 (m, 1H), 6.72 (s, 3H), 6.99 (dd, *J* = 4.2. 0.9 Hz, 2H), 7.33 (s, 1H), 7.34 (s, 1H), 7.47 (m, 3H) ppm.

The physical chromatographic, and spectroscopic data were in good agreement with those previously published.[56]

NOTES AND REFERENCES

[1]   G. L. Drusano, *J. Infect. Dis.* **2017**, *216*, 150-152.

[2]   J. H. McKerrow, *Nat. Prod. Rep.* **2015**, *32*, 1610-1611.

[3]   N. M. Revie, K. R. Iyer, N. Robbins, L. E. Cowen, *Curr. Opin. Microbiol.* **2018**, *45*, 70-76.

[4]   I. Roca, M. Akova, F. Baquero, J. Carlet, M. Cavaleri, S. Coenen, J. Cohen, D. Findlay, I. Gyssens, O. E. Heure, G. Kahlmeter, H. Kruse, R. Laxminarayan, E. Liébana, L. López-Cerero, et al., *New Microbes New Infect.* **2015**, *6*, 22-29.

[5]   World Health Organization, *Antimicrobial Resistance: Global Report on Surveillance 2014*, can be found under: https://www.who.int/drugresistance/documents/surveillancereport/en/

[6]   C. Holohan, S. Van Schaeybroeck, D. B. Longley, P. G. Johnston, *Nat. Rev. Cancer* **2013**, *13*, 714.

[7]   P. Padiyara, H. Inoue, M. Sprenger, *Infect. Dis. Res. Treat.* **2018**, *11*, 1178633718767887.

[8]   O. B. Jonas, A. Irwin, F. C. J. Berthe, F. G. Le Gall, P. V. Marquez, *Drug-Resistant Infections : A Threat to Our Economic Future (Vol. 2): Final Report (English)*, 2017, can be found, via the World Bank Group, under: http://documents.worldbank.org/curated/en/323311493396993758/final-report

[9]   World Health Organization, *World Malaria Report 2017*, can be found under: https://www.who.int/malaria/publications/world-malaria-report-2017/en/

[10]   S. M. Rich, F. H. Leendertz, G. Xu, M. LeBreton, C. F. Djoko, M. N. Aminake, E. E. Takang, J. L. D. Diffo, B. L. Pike, B. M. Rosenthal, P. Formenty, C. Boesch, F. J. Ayala, N. D. Wolfe, *Proc. Natl. Acad. Sci. U.S.A.* **2009**, *106*, 14902-14907.

[11]   H. Noedl, Y. Se, K. Schaecher, B. L. Smith, D. Socheat, M. M. Fukuda, *New Engl. J. Med.* **2008**, *359*, 2619-2620.

[12]   E. A. Ashley, M. Dhorda, R. M. Fairhurst, C. Amaratunga, P. Lim, S. Suon, S. Sreng, J. M. Anderson, S. Mao, B. Sam, C. Sopha, C. M. Chuor, C. Nguon, S. Sovannaroth, S. Pukrittayakamee, et al., *New Engl. J. Med.* **2014**, *371*, 411-423.

[13] A. M. Thu, A. P. Phyo, J. Landier, D. M. Parker, F. H. Nosten, *FEBS J.* **2017**, *284*, 2569-2578.

[14] N. J. White, *Lancet Infect. Dis.* **2017**, *17*, e15-e20.

[15] Y. Tu, *Angew. Chem. Int. Ed.* **2016**, *55*, 10210-10226.

[16] N. R. Farnsworth, *Ciba Found. Symp.* **1990**, *154*, 2-11.

[17] L. Hoareau, E. J. DaSilva, *Electron. J. Biotechnol.* **1999**, *2*, 3-4.

[18] G. M. Cragg, P. G. Grothaus, D. J. Newman, *Chem. Rev.* **2009**, *109*, 3012-3043.

[19] D. S. Fabricant, N. R. Farnsworth, *Environ. Health Perspect.* **2001**, *109*, 69-75.

[20] M. J. Miller, J. Albarracin-Jordan, C. Moore, J. M. Capriles, *Proc. Natl. Acad. Sci. U.S.A.* **2019**, 201902174.

[21] P. Talalay, P. Talalay, *Acad. Med.* **2001**, *76*, 238-247.

[22] L. Wang, J. Zhang, Y. Hong, Y. Feng, M. Chen, Y. Wang, *Evid. Based Complement. Alternat. Med.* **2013**, *2013*, 16.

[23] G. K. Daikos, *Int. J. Antimicrob. Agents* **2007**, *29*, 617-620.

[24] M. Ekor, *Front. Pharmacol.* **2014**, *4*.

[25] D. J. Newman, G. M. Cragg, *J. Nat. Prod.* **2016**, *79*, 629-661.

[26] H. Itokawa, S. L. Morris-Natschke, T. Akiyama, K.-H. Lee, *J. Nat. Med.* **2008**, *62*, 263-280.

[27] N. J. White, T. T. Hien, F. H. Nosten, *Trends Parasitol.* **2015**, *31*, 607-610.

[28] Z. Guo, *Acta Pharm. Sin. B* **2016**, *6*, 115-124.

[29] WHO, *Guidelines for the treatment of malaria*, 3 ed., **2015**.

[30] T. S. Kaufman, E. A. Rúveda, *Angew. Chem. Int. Ed.* **2005**, *44*, 854-885.

[31] R. Schmitz, *Pharm. Hist.* **1985**, *27*, 61-74.

[32] R. J. Huxtable, S. K. Schwarz, *Mol. Interv.* **2001**, *1*, 189-191.

[33] N. Kuhnert, *Chem. unserer Zeit* **1999**, *33*, 213-220.

[34] J. G. Mahdi, A. J. Mahdi, A. J. Mahdi, I. D. Bowen, *Cell Prolif.* **2006**, *39*, 147-155.

[35]   J. Schlauer, *CPN* **1997**, *26*, 34-38.

[36]   H. Meimberg, P. Dittrich, G. Bringmann, J. Schlauer, G. Heubl, *Plant Biol.* **2000**, *2*, 218-228.

[37]   M. W. C. K. M. Cameron, S. M. Swensen, *Am. J. Bot.* **1995**, *82*, 117-118.

[38]   G. Bringmann, F. Pokorny, H. Reuscher, D. Lisch, L. Aké Assi, *Planta Med.* **1990**, *56*, 496-497.

[39]   H. K. Airy Shaw, *Kew Bull.* **1951**, *6*, 327-347.

[40]   C. Taylor, R. Gereau, G. Walters, *Ann. Missouri Bot. Gard.* **2005**, *92*, 360-399.

[41]   C. Wiart, S. Mogana, S. Khalifah, M. Mahan, S. Ismail, M. Buckle, A. K. Narayana, M. Sulaiman, *Fitoterapia* **2004**, *75*, 68-73.

[42]   I. M. Said, I. B. Ahmad, M. D. Yahya, A. M. Marini, *Pharm. Biol.* **2001**, *39*, 357-363.

[43]   G. François, G. Bringmann, J. D. Phillipson, L. Aké Assi, C. Dochez, M. Rübenacker, C. Schneider, M. Wéry, D. C. Warhurst, G. C. Kirby, *Phytochemistry* **1994**, *35*, 1461-1464.

[44]   G. Bringmann, F. Pokorny, in *The Alkaloids: Chemistry and Pharmacology, Vol. 46* (Ed.: G. A. Cordell), Academic Press Inc., New York, **1995**, pp. 127-271.

[45]   G. Bringmann, C. Günther, M. Ochse, O. Schupp, S. Tasler, in *Progress in the Chemistry of Organic Natural Products* (Eds.: W. Herz, H. Falk, G. W. Kirby, R. E. Moore), Springer Vienna, Vienna, **2001**, pp. 1-249.

[46]   J. Ziegler, P. J. Facchini, R. Geißler, J. Schmidt, C. Ammer, R. Kramell, S. Voigtländer, A. Gesell, S. Pienkny, W. Brandt, *Phytochemistry* **2009**, *70*, 1696-1707.

[47]   R. B. Herbert, in *The Chemistry and Biology of Isoquinoline Alkaloids* (Eds.: J. D. Phillipson, M. F. Roberts, M. H. Zenk), Springer Berlin Heidelberg, Berlin, Heidelberg, **1985**, pp. 213-228.

[48]   G. Bringmann, M. Wohlfarth, H. Rischer, M. Grüne, J. Schlauer, *Angew. Chem. Int. Ed.* **2000**, *39*, 1464-1466.

[49]   G. Bringmann, J. Mutanyatta-Comar, M. Greb, S. Rüdenauer, T. F. Noll, A. Irmer, *Tetrahedron* **2007**, *63*, 1755-1761.

[50]   S. R. M. Ibrahim, G. A. Mohamed, *Fitoterapia* **2015**, *106*, 194-225.

[51]   K. Kaur, M. Jain, T. Kaur, R. Jain, *Biorg. Med. Chem.* **2009**, *17*, 3229-3256.

[52]   M. M. Salem, K. A. Werbovetz, *Curr. Med. Chem.* **2006**, *13*, 2571-2598.

[53]   G. François, G. Timperman, W. Eling, L. Aké Assi, J. Holenz, G. Bringmann, *Antimicrob. Agents Chemother.* **1997**, *41*, 2533-2539.

[54]   G. François, G. Timperman, J. Holenz, L. Aké Assi, T. Geuder, L. Maes, J. Dubois, M. Hanocq, G. Bringmann, *Ann. Trop. Med. Parasitol.* **1996**, *90*, 115-123.

[55]   G. Bringmann, C. Günther, W. Saeb, J. Mies, A. Wickramasinghe, V. Mudogo, R. Brun, *J. Nat. Prod.* **2000**, *63*, 1333-1337.

[56]   G. Bringmann, I. Kajahn, M. Reichert, S. E. H. Pedersen, J. H. Faber, T. Gulder, R. Brun, S. B. Christensen, A. Ponte-Sucre, H. Moll, G. Heubl, V. Mudogo, *J. Org. Chem.* **2006**, *71*, 9348-9356.

[57]   G. Bringmann, M. Rübenacker, J. R. Jansen, D. Scheutzow, L. Aké Assi, *Tetrahedron Lett.* **1990**, *31*, 639-642.

[58]   G. Bringmann, J. R. Jansen, H. Reuscher, M. Rübenacker, K. Peters, H. G. von Schnering, *Tetrahedron Lett.* **1990**, *31*, 643-646.

[59]   G. Bringmann, G. François, L. Aké Assi, J. Schlauer, *Chimia* **1998**, *52*, 18-28.

[60]   J. Li, R. Seupel, D. Feineis, V. Mudogo, M. Kaiser, R. Brun, D. Brünnert, M. Chatterjee, E.-J. Seo, T. Efferth, G. Bringmann, *J. Nat. Prod.* **2017**, *80*, 443-458.

[61]   K. P. Manfredi, J. W. Blunt, J. H. Cardellina II, J. B. McMahon, L. L. Pannell, G. M. Cragg, M. R. Boyd, *J. Med. Chem.* **1991**, *34*, 3402-3405.

[62]   M. R. Boyd, Y. F. Hallock, J. H. Cardellina II, K. P. Manfredi, J. W. Blunt, J. B. McMahon, R. W. Buckheit, G. Bringmann, M. Schäffer, G. M. Cragg, D. W. Thomas, J. G. Jato, *J. Med. Chem.* **1994**, *37*, 1740-1745.

[63]   J. B. McMahon, M. J. Currens, R. J. Gulakowski, R. W. Buckheit, Jr., C. Lackman-Smith, Y. F. Hallock, M. R. Boyd, *Antimicrob. Agents Chemother.* **1995**, *39*, 484-488.

[64]   G. Bringmann, S. Harmsen, J. Holenz, T. Geuder, R. Götz, P. A. Keller, R. Walter, Y. F. Hallock, J. H. Cardellina II, M. R. Boyd, *Tetrahedron* **1994**, *50*, 9643-9648.

[65]   G. Bringmann, R. Götz, G. François, *Tetrahedron* **1996**, *52*, 13419-13426.

[66]   P. D. Hobbs, V. Upender, J. Liu, D. J. Pollart, D. W. Thomas, M. I. Dawson, *Chem. Commun.* **1996**, 923-924.

[67]   G. Bringmann, R. Götz, S. Harmsen, J. Holenz, R. Walter, *Liebigs Annalen* **1996**, *1996*, 2045-2058.

[68]   V. Upender, D. J. Pollart, J. Liu, P. D. Hobbs, C. Olsen, W.-R. Chao, B. Bowden, J. L. Crase, D. W. Thomas, A. Pandey, J. A. Lawson, M. I. Dawson, *J. Heterocycl. Chem.* **1996**, *33*, 1371-1384.

[69]   G. Bringmann, R. Götz, P. A. Keller, R. Walter, M. R. Boyd, F. Lang, A. Garcia, J. J. Walsh, I. Tellitu, K. V. Bhaskar, T. R. Kelly, *J. Org. Chem.* **1998**, *63*, 1090-1097.

[70]   T. R. Hoye, M. Chen, B. Hoang, L. Mi, O. P. Priest, *J. Org. Chem.* **1999**, *64*, 7184-7201.

[71]   G. Bringmann, W. Saeb, J. Mies, K. Messer, M. Wohlfarth, R. Brun, *Synthesis* **2000**, *2000*, 1843-1847.

[72]   G. Bringmann, M. Wohlfarth, H. Rischer, M. Heubes, W. Saeb, S. Diem, M. Herderich, J. Schlauer, *Anal. Chem.* **2001**, *73*, 2571-2577.

[73]   G. Bringmann, M. Rückert, J. Schlauer, M. Herderich, *J. Chromatogr. A* **1998**, *810*, 231-236.

[74]   T. G. McCloud, J. R. Britt, L. K. Cartner, K. C. Pearl, F. D. Majadly, G. M. Muschik, P. A. Klueh, G. M. Cragg, D. W. Thomas, J. G. Jato, J. E. Simon, *Phytochem. Anal.* **1997**, *8*, 120-123.

[75]   Y. F. Hallock, K. P. Manfredi, J.-R. Dai, J. H. Cardellina II, R. J. Gulakowski, J. B. McMahon, M. Schäffer, M. Stahl, K.-P. Gulden, G. Bringmann, G. François, M. R. Boyd, *J. Nat. Prod.* **1997**, *60*, 677-683.

[76]   Y. F. Hallock, J. H. Cardellina II, M. Schäffer, G. Bringmann, G. François, M. R. Boyd, *Bioorg. Med. Chem. Lett.* **1998**, *8*, 1729-1734.

[77]   G. Bringmann, M. Wohlfarth, H. Rischer, J. Schlauer, R. Brun, *Phytochemistry* **2002**, *61*, 195-204.

[78]   M. Xu , T. Bruhn, B. Hertlein, R. Brun, A. Stich, J. Wu, G. Bringmann, *Chem. Eur. J.* **2010**, *16*, 4206-4216.

[79]   G. Bringmann, G. Zhang, T. Büttner, G. Bauckmann, T. Kupfer, H. Braunschweig, R. Brun, V. Mudogo, *Chem. Eur. J.* **2013**, *19*, 916-923.

[80]   G. Bringmann, B. K. Lombe, C. Steinert, K. Ndjoko Ioset, R. Brun, F. Turini, G. Heubl, V. Mudogo, *Org. Lett.* **2013**, *15*, 2590-2593.

[81] F. G. Turini, C. Steinert, G. Heubl, G. Bringmann, B. K. Lombe, V. Mudogo, H. Meimberg, *Taxon* **2014**, *63*, 329-341.

[82] G. Heubl, F. Turini, V. Mudogo, I. Kajahn, G. Bringmann, *Plant Ecol. Evol.* **2010**, *143*, 63-69.

[83] H. Rischer, G. Heubl, H. Meimberg, M. Dreyer, H. A. Hadi, G. Bringmann, *Blumea* **2005**, *50*, 357-365.

[84] G. Bringmann, H. Rischer, J. Schlauer, K. Wolf, A. Kreiner, M. Duschek, L. Aké Assi, *CPN* **2002**, *31*, 44-52.

[85] G. Bringmann, J. Schlauer, K. Wolf, H. Rischer, U. Buschbom, A. Kreiner, F. Thiele, M. Duschek, L. Aké Assi, *CPN* **1999**, *28*, 7-13.

[86] G. Heubl, G. Bringmann, H. Meimberg, *Plant Biol. (Stuttg.)* **2006**, *8*, 821-830.

[87] Thanks to Prof. D. L. Nickrent for allowing the use of its picture, which can be found under: www.phytoimages.siu.ed

[88] H. Meimberg, H. Rischer, F. G. Turini, V. Chamchumroon, M. Dreyer, M. Sommaro, G. Bringmann, G. Heubl, *Plant Syst. Evol.* **2010**, *284*, 77-98.

[89] S. Porembski, in *Flowering Plants Dicotyledons: Malvales, Capparales and Non-betalain Caryophyllales* (Eds.: K. Kubitzki, C. Bayer), Springer Berlin Heidelberg, Berlin, Heidelberg, **2003**, pp. 25-27.

[90] N. Wallich, *Numerical List of Dried Specimens of Plants in the Museum of the Honl. East India Company*, 1828, a lithographed manuscript that can be found under: https://doi.org/10.5962/bhl.title.1917

[91] J.-E. Planchon, *Ann. Sci. Nat., Bot. sér.* **1849**, *3*, 316-320.

[92] I. M. Turner, *Gard. Bull. Singapore* **2015**, *67*, 35-37.

[93] G. E., in *Die natürlichen Pflanzenfamilien, Vol. 21*, 2 ed. (Eds.: A. Engler, K. Prantl), Engelmann, Leipzig, **1925**, pp. 589-592.

[94] A. Cronquist, *An Integrated System of Classification of Flowering Plants*, Columbia University Press, New York, **1981**.

[95] J. Léonard, in *Flora of Tropical East Africa* (Ed.: R. M. Polhill), A. A. Balkema, Boston, **1986**.

[96] M. Cheek, *Kew Bull.* **2000**, *55*, 871-882.

[97] R. E. Gereau, *Novon* **1997**, *7*, 242-245.

[98] J. C. Dagar, N. T. Singh, *Plant Resources of the Andaman & Nicobar Islands: Enumeration & utilisation of vascular plants Vol. 2*, Bishen Singh Mahendra Pal Singh, **1999**.

[99] R. Freson, *Bull. Jard. Bot. Natl. Belg.* **1967**, *37*, 73-76.

[100] J. Léonard, in *Flore d'Afrique Centrale (Zaïre-Rwanda-Burundi), Spermatophytes* (Ed.: P. Bamps), Jardin Botanique National de Belgique, **1982**.

[101] M. Unger, M. Dreyer, S. Specker, S. Laug, M. Pelzing, C. Neusüß, U. Holzgrabe, G. Bringmann, *Phytochem. Anal.* **2004**, *15*, 21-26.

[102] G. Bringmann, J. Spuziak, J. H. Faber, T. Gulder, I. Kajahn, M. Dreyer, G. Heubl, R. Brun, V. Mudogo, *Phytochemistry* **2008**, *69*, 1065-1075.

[103] B. K. Lombe, D. Feineis, V. Mudogo, R. Brun, S. Awale, G. Bringmann, *RSC Adv.* **2018**, *8*, 5243-5254.

[104] S. M. Kavatsurwa, B. K. Lombe, D. Feineis, D. F. Dibwe, V. Maharaj, S. Awale, G. Bringmann, *Fitoterapia* **2018**, *130*, 6-16.

[105] F. G. Turini, PhD thesis, Ludwig-Maximilians University Munich **2014**.

[106] C. de Wasseige, P. de Marcken, N. Bayol, H.-H. F., P. Mayaux, B. Desclee, R. Nasi, A. Billand, P. Defourny, R. Eba'a Atyi, *Les Forêts du Bassin du Congo - Etat des Forêts 2010*, Office des publications de l'Union Européenne, Luxembourg, **2012**.

[107] R. A. Mittermeier, C. G. Mittermeier, T. M. Brooks, J. D. Pilgrim, W. R. Konstant, G. A. B. da Fonseca, C. Kormos, *Proc. Natl. Acad. Sci. U.S.A.* **2003**, *100*, 10309-10313.

[108] C. Shumway, D. Musibono, S. Ifuta, J. Sullivan, R. C. Schelly, J. Punga, J. C. Palata, V. Puema, *Biodiversity Survey: Systematics, Ecology, and Conservation Along the Congo River. Research Report for Congo River Environment and Development Project,* 2003, can be found under: https://www.researchgate.net/publication/301684734_Biodiversity_Survey_Systematics_Ecology_and_Conservation_Along_the_Congo_River_Research_report_for_Congo_River_Environment_and_Development_Project_CREDP.

[109] M. Leal, *PhytoKeys* **2014**, *42*, 49-55.

[110] H. Taedoumg, B. Sonké, P. Hamon, P. De Block, *PhytoKeys* **2017**, *83*, 103-118.

[111] K. K. H. Belesi, P. Stoffelen, *Plant Ecol. Evol.* **2011**, *144*, 237-239.

[112] E. Fischer, B. Kirunda, C. Ewango, M. Leal, D. Kujirakwinja, A. Bamba, A. J. Plumptre, *Phytotaxa* **2017**, *298*, 277-282.

[113] G. A. Levin, J. K. Morton, E. Robbrecht, *Syst. Bot.* **2007**, *32*, 576-582.

[114] J. Léonard, *Bull. Soc. R. Bot. Belge* **1949**, *82*, 27-40.

[115] Y. F. Hallock, C. B. Hughes, J. H. Cardellina II, M. Schäffer, K.-P. Gulden, G. Bringmann, M. R. Boyd, *Nat. Prod. Lett.* **1995**, *6*, 315-320.

[116] C. Schlötterer, *Chromosoma* **2000**, *109*, 365-371.

[117] M. L. C. Vieira, L. Santini, A. L. Diniz, C. d. F. Munhoz, *Genet. Mol. Biol.* **2016**, *39*, 312-328.

[118] P. Jarne, P. J. L. Lagoda, *Trends Ecol. Evol.* **1996**, *11*, 424-429.

[119] E. J. Oliveira, J. G. Pádua, M. I. Zucchi, R. Vencovsky, M. L. C. Vieira, *Genet. Mol. Biol.* **2006**, *29*, 294-307.

[120] K. A. Selkoe, R. J. Toonen, *Ecol. Lett.* **2006**, *9*, 615-629.

[121] P. M. Abdul-Muneer, *Genet. Res. Int.* **2014**, *2014*, 691759.

[122] B. K. Lombe, Master thesis, University of Kinshasa **2013**.

[123] B. K. Lombe, T. Bruhn, D. Feineis, V. Mudogo, R. Brun, G. Bringmann, *Org. Lett.* **2017**, *19*, 6740-6743.

[124] B. K. Lombe, T. Bruhn, D. Feineis, V. Mudogo, R. Brun, G. Bringmann, *Org. Lett.* **2017**, *19*, 1342-1345.

[125] Part of the results from this cooperation (i.e., on the discovery of mbandakamines A and B) has been presented by Dr. C. Steinert in her doctoral thesis and also in the master dissertation of the author of this thesis.

[126] B. K. Lombe, D. Feineis, G. Bringmann, *Nat. Prod. Rep.* **2019**, DOI: 10.1039/c1039np00024k.

[127] G. Bringmann, J. Mutanyatta-Comar, K. Maksimenka, J. M. Wanjohi, M. Heydenreich, R. Brun, W. E. G. Müller, M. G. Peter, J. O. Midiwo, A. Yenesew, *Chem. Eur. J.* **2008**, *14*, 1420-1429.

[128] H. O. House, R. W. Magin, H. W. Thompson, *J. Org. Chem.* **1963**, *28*, 2403-2406.

[129] H. O. House, R. W. Bashe, *J. Org. Chem.* **1967**, *32*, 784-791.

[130] C. Wolf, X. Mei, *J. Am. Chem. Soc.* **2003**, *125*, 10651-10658.

[131] I. Eiichi, O. Shigeru, F. Yasuhiro, M. Hiroshi, *Bull. Chem. Soc. Jpn.* **1982**, *55*, 845-851.

[132] G. Bringmann, W. Saeb, J. Kraus, R. Brun, G. François, *Tetrahedron* **2000**, *56*, 3523-3531.

[133] F. Z. Katele, M.Sc thesis, University of Pretoria **2015**.

[134] J. J. P. Stewart, *J. Mol. Model.* **2007**, *13*, 1173-1213.

[135] S. Grimme, *J. Comput. Chem.* **2006**, *27*, 1787-1799.

[136] A. Schäfer, C. Huber, R. Ahlrichs, *J. Chem. Phys.* **1994**, *100*, 5829-5835.

[137] G. Bringmann, T. Bruhn, K. Maksimenka, Y. Hemberger, *Eur. J. Org. Chem.* **2009**, *2009*, 2717-2727.

[138] J. E. Ridley, M. C. Zerner, *Theor. Chim. Acta* **1976**, *42*, 223-236.

[139] C. Schies, R. Seupel, D. Feineis, A. Gehrold, M. Schraut, M. Kaiser, R. Brun, G. Bringmann, *ChemistrySelect* **2018**, *3*, 940-945.

[140] Y. F. Hallock, J. H. Cardellina II, M. Schäffer, M. Stahl, G. Bringmann, G. François, M. R. Boyd, *Tetrahedron* **1997**, *53*, 8121-8128.

[141] V. Balasubramaniyan, *Chem. Rev.* **1966**, *66*, 567-641.

[142] S. Görög, *Ultraviolet-Visible Spectrophotometry in Pharmaceutical Analysis*, 1 ed., CRC Press, Inc, Boca Raton, **1995**.

[143] K. Krohn, A. Michel, U. Flörke, H.-J. Aust, S. Draeger, B. Schulz, *Liebigs Ann. Chem.* **1994**, *1994*, 1093-1097.

[144] S. Grimme, J. Antony, S. Ehrlich, H. Krieg, *J. Chem. Phys.* **2010**, *132*, 154104.

[145] F. Weigend, R. Ahlrichs, *PCCP* **2005**, *7*, 3297-3305.

[146] F. Neese, *WIREs Comput. Mol. Sci.* **2012**, *2*, 73-78.

[147] T. Yanai, D. P. Tew, N. C. Handy, *Chem. Phys. Lett.* **2004**, *393*, 51-57.

[148] D. T. Tshitenge, D. Feineis, V. Mudogo, M. Kaiser, R. Brun, G. Bringmann, *Sci. Rep.* **2017**, *7*, 5767.

[149] The atomic numbering style follows that of "normal" mono- and dimeric naphthylisoquinolines (including biosynthetic considerations).

[150] G. Bringmann, S. Schneider, *Liebigs Ann. Chem.* **1985**, *1985*, 765-774.

[151] G. Bringmann, J. R. Jansen, *Liebigs Ann. Chem.* **1985**, *1985*, 2116-2125.

[152] G. Bringmann, *Liebigs Ann. Chem.* **1985**, *1985*, 2126-2134.

[153] G. Bringmann, F. Pokorny, M. Wenzel, K. Wurm, C. Schneider, *J. Labelled Compd. Radiopharmaceut.* **1997**, *39*, 29-38.

[154] G. Bringmann, A. Irmer, S. Rüdenauer, J. Mutanyatta-Comar, R. Seupel, D. Feineis, *Tetrahedron* **2016**, *72*, 2906-2912.

[155] G. Bringmann, T. Geuder, M. Rübenacker, R. Zagst, *Phytochemistry* **1991**, *30*, 2067-2070.

[156] G. Bringmann, R. God, M. Schäffer, *Phytochemistry* **1996**, *43*, 1393-1403.

[157] K. R. Wilson, R. E. Pincock, *J. Am. Chem. Soc.* **1975**, *97*, 1474-1478.

[158] G. Bringmann, W. Saeb, D. Koppler, G. François, *Tetrahedron* **1996**, *52*, 13409-13418.

[159] G. Bringmann, A. J. Price Mortimer, P. A. Keller, M. J. Gresser, J. Garner, M. Breuning, *Angew. Chem. Int. Ed.* **2005**, *44*, 5384-5427.

[160] G. Bringmann, T. Gulder, T. A. M. Gulder, M. Breuning, *Chem. Rev.* **2011**, *111*, 563-639.

[161] E. P. Kyba, G. W. Gokel, F. De Jong, K. Koga, L. R. Sousa, M. G. Siegel, L. Kaplan, G. D. Y. Sogah, D. J. Cram, *J. Org. Chem.* **1977**, *42*, 4173-4184.

[162] A. K. Yudin, L. J. P. Martyn, S. Pandiaraju, J. Zheng, A. Lough, *Org. Lett.* **2000**, *2*, 41-44.

[163] F. Octa-Smolin, F. van der Vight, R. Yadav, J. Bhangu, K. Soloviova, C. Wölper, C. G. Daniliuc, C. A. Strassert, H. Somnitz, G. Jansen, J. Niemeyer, *J. Org. Chem.* **2018**, *83*, 14568-14587.

[164] A. M. Genaev, G. E. Salnikov, A. V. Shernyukov, Z. Zhu, K. Y. Koltunov, *Org. Lett.* **2017**, *19*, 532-535.

[165] D. T. Tshitenge, PhD thesis, Julius-Maximilians-Universität Würzburg **2017**.

[166] D. T. Tshitenge, D. Feineis, V. Mudogo, M. Kaiser, R. Brun, E.-J. Seo, T. Efferth, G. Bringmann, *J. Nat. Prod.* **2018**, *81*, 918-933.

[167] S. Fayez, D. Feineis, V. Mudogo, S. Awale, G. Bringmann, *RSC Adv.* **2017**, *7*, 53740-53751.

[168] S. Fayez, D. Feineis, V. Mudogo, E.-J. Seo, T. Efferth, G. Bringmann, *Fitoterapia* **2018**, *129*, 114-125.

[169] S. Awale, D. F. Dibwe, C. Balachandran, S. Fayez, D. Feineis, B. K. Lombe, G. Bringmann, *J. Nat. Prod.* **2018**, *81*, 2282-2291.

[170] G. Bringmann, W. Saeb, M. Rückert, J. Mies, M. Michel, V. Mudogo, R. Brun, *Phytochemistry* **2003**, *62*, 631-636.

[171] G. Bringmann, K. Messer, R. Brun, V. Mudogo, *J. Nat. Prod.* **2002**, *65*, 1096-1101.

[172] G. Bringmann, C. Steinert, D. Feineis, V. Mudogo, J. Betzin, C. Scheller, *Phytochemistry* **2016**, *128*, 71-81.

[173] J. Li, R. Seupel, T. Bruhn, D. Feineis, M. Kaiser, R. Brun, V. Mudogo, S. Awale, G. Bringmann, *J. Nat. Prod.* **2017**, *80*, 2807-2817.

[174] G. Bringmann, A. Hamm, C. Günther, M. Michel, R. Brun, V. Mudogo, *J. Nat. Prod.* **2000**, *63*, 1465-1470.

[175] Thanks to Dr. R. E. Gereau (Missouri Botanical Garden, USA) for helping to figure out these morphologic features.

[176] E. Izumi, T. Ueda-Nakamura, B. P. Dias Filho, V. F. Veiga Junior, C. V. Nakamura, *Nat. Prod. Rep.* **2011**, *28*, 809-823.

[177] C. L. Arteaga, P. C. Adamson, J. A. Engelman, M. Foti, R. B. Gaynor, S. G. Hilsenbeck, P. J. Limburg, S. W. Lowe, E. R. Mardis, S. Ramsey, T. R. Rebbeck, A. L. Richardson, E. H. Rubin, G. J. Weiner, *Clin. Cancer. Res.* **2014**, *20*, S1-S112.

[178] K. Strong, C. Mathers, J. Epping-Jordan, S. Resnikoff, A. Ullrich, *Eur. J. Cancer Prev.* **2008**, *17*, 153-161.

[179] V. Surlin, V. Bintintan, F. D. Petrariu, R. Dobrin, R. Lefter, A. Ciobica, D. Timofte, *Rev. Med. Chir. Soc. Med. Nat. Iasi* **2014**, *118*, 924-931.

[180] M. Ilic, I. Ilic, *World J. Gastroenterol.* **2016**, *22*, 9694-9705.

[181] F. Bray, J. Ferlay, I. Soerjomataram, R. L. Siegel, L. A. Torre, A. Jemal, *CA Cancer J. Clin.* **2018**, *68*, 394-424.

[182] V. L. Gordon-Dseagu, S. S. Devesa, M. Goggins, R. Stolzenberg-Solomon, *Int. J. Epidemiol.* **2018**, *47*, 427-439.

[183] L. Rahib, B. D. Smith, R. Aizenberg, A. B. Rosenzweig, J. M. Fleshman, L. M. Matrisian, *Cancer Res.* **2014**, *74*, 2913-2921.

[184] D. Li, K. Xie, R. Wolff, J. L. Abbruzzese, *Lancet* **2004**, *363*, 1049-1057.

[185] A. Maitra, R. H. Hruban, *Annu. Rev. Pathol.* **2008**, *3*, 157-188.

[186] J.-P. Gillet, M. M. Gottesman, in *Multi-Drug Resistance in Cancer* (Ed.: J. Zhou), Humana Press, Totowa, NJ, **2010**, pp. 47-76.

[187] K. Izuishi, K. Kato, T. Ogura, T. Kinoshita, H. Esumi, *Cancer Res.* **2000**, *60*, 6201-6207.

[188] J. Magolan, M. J. Coster, *Curr. Drug Del.* **2010**, *7*, 355-369.

[189] S. Awale, E. M. N. Nakashima, S. K. Kalauni, Y. Tezuka, Y. Kurashima, J. Lu, H. Esumi, S. Kadota, *Bioorg. Med. Chem. Lett.* **2006**, *16*, 581-583.

[190] H. Esumi, K. Izuishi, K. Kato, K. Hashimoto, Y. Kurashima, A. Kishimoto, T. Ogura, T. Ozawa, *J. Biol. Chem.* **2002**, *277*, 32791-32798.

[191] S. Awale, J. Lu, S. K. Kalauni, Y. Kurashima, Y. Tezuka, S. Kadota, H. Esumi, *Cancer Res.* **2006**, *66*, 1751-1757.

[192] A. S. Strimpakos, M. W. Saif, *J. Pancreas* **2013**, *14*, 354-358.

[193] D. T. Tshitenge, D. Feineis, S. Awale, G. Bringmann, *J. Nat. Prod.* **2017**, *80*, 1604-1614.

[194] S. Fayez, D. Feineis, L. Aké Assi, M. Kaiser, R. Brun, S. Awale, G. Bringmann, *Fitoterapia* **2018**, *131*, 245-259.

[195] D. B. Longley, D. P. Harkin, P. G. Johnston, *Nat. Rev. Cancer* **2003**, *3*, 330.

[196] Y. F. Hallock, K. P. Manfredi, J. W. Blunt, J. H. Cardellina II, M. Schaeffer, K.-P. Gulden, G. Bringmann, A. Y. Lee, J. Clardy, G. François, M. R. Boyd, *J. Org. Chem.* **1994**, *59*, 6349-6355.

[197] This signal was overlapped by that of Me-2′, but could be deduced to be dd, from the respective 2D NMR cross peaks.

[198] G. Bringmann, K.-P. Gulden, Y. F. Hallock, K. P. Manfredi, J. H. Cardellina II, M. R. Boyd, B. Kramer, J. Fleischhauer, *Tetrahedron* **1994**, *50*, 7807-7814.

[199] G. Van Zant, C. G. Fry, *Cytometry* **1983**, *4*, 40-46.

[200] J. K. Pritchard, M. Stephens, P. Donnelly, *Genetics* **2000**, *155*, 945-959.

[201] Further details on this work can be found in the PhD thesis of S. M. Kavatsurwa, which is currently under preparation.

[202] A. Montagnac, A. H. A. Hadi, F. Remy, M. Païs, *Phytochemistry* **1995**, *39*, 701-704.

[203] G. Bringmann, F. Teltschik, M. Schäffer, R. Haller, S. Bär, S. A. Robertson, M. A. Isahakia, *Phytochemistry* **1998**, *47*, 31-35.

[204] G. Bringmann, R. Zagst, H. Reuscher, L. Aké Assi, *Phytochemistry* **1992**, *31*, 4011-4014.

[205] G. Bringmann, B. Hertlein-Amslinger, I. Kajahn, M. Dreyer, R. Brun, H. Moll, A. Stich, K. Ndjoko Ioset, W. Schmitz, L. H. Ngoc, *Phytochemistry* **2011**, *72*, 89-93.

[206] R. Seupel, Y. Hemberger, D. Feineis, M. Xu, E.-J. Seo, T. Efferth, G. Bringmann, *Org. Biomol. Chem.* **2018**, *16*, 1581-1590.

[207] N. H. Anh, A. Porzel, H. Ripperger, G. Bringmann, M. Schäffer, R. God, T. Van Sung, G. Adam, *Phytochemistry* **1997**, *45*, 1287-1291.

[208] C. Jiang, Z.-L. Li, P. Gong, S.-L. Kang, M.-S. Liu, Y.-H. Pei, Y.-K. Jing, H.-M. Hua, *Fitoterapia* **2013**, *91*, 305-312.

[209] G. Bringmann, F. Teltschik, M. Michel, S. Busemann, M. Rückert, R. Haller, S. Bär, S. A. Robertson, R. Kaminsky, *Phytochemistry* **1999**, *52*, 321-332.

[210] C.-P. Tang, Y.-P. Yang, Y. Zhong, Q.-X. Zhong, H.-M. Wu, Y. Ye, *J. Nat. Prod.* **2000**, *63*, 1384-1387.

[211] G. Bringmann, R. Seupel, D. Feineis, G. Zhang, M. Xu, J. Wu, M. Kaiser, R. Brun, E.-J. Seo, T. Efferth, *Fitoterapia* **2016**, *115*, 1-8.

[212] G. Bringmann, M. Dreyer, J. H. Faber, P. W. Dalsgaard, J. W. Jaroszewski, H. Ndangalasi, F. Mbago, R. Brun, M. Reichert, K. Maksimenka, S. B. Christensen, *J. Nat. Prod.* **2003**, *66*, 1159-1165.

[213] G. Bringmann, C. Günther, S. Busemann, M. Schäffer, J. D. Olowokudejo, B. I. Alo, *Phytochemistry* **1998**, *47*, 37-43.

[214] G. Bringmann, R. Seupel, D. Feineis, M. Xu, G. Zhang, M. Kaiser, R. Brun, E.-J. Seo, T. Efferth, *Fitoterapia* **2017**, *121*, 76-85.

[215] The movie is available at: https://vimeo.com/283591161

[216] T. Bruhn, A. Schaumlöffel, Y. Hemberger, G. Bringmann, *Chirality* **2013**, *25*, 243-249.

[217] I. Orhan, B. Şener, M. Kaiser, R. Brun, D. Tasdemir, *Mar. Drugs* **2010**, *8*, 47-58.

[218] C. Steinert, PhD thesis, Julius-Maximilians-Universität Würzburg **2015**.

[219] G. Zhang, PhD thesis, Julius-Maximilians-Universität Würzburg **2012**.

ACKNOWLEDGMENTS

- The University of Würzburg and the DFG-funded program SFB630;

- The *Else-Kröner-Fresenius-Stiftung*, the *Holger-Pöhlmann Stiftung*, and the NGO *Förderverein Uni Kinshasa e.V.*, which generously provided financial assistance via the Excellence Scholarship Program BEBUC (www.foerderverein-uni-kinshasa.de); and

- The German Academic Exchange Service (Deutscher Akademischer Austauschdienst (DAAD).

To Sylvia Pöhlmann ("my German mother"), I have no words that would appropriately acknowledge her most incredible manifold assistance. Simply, thank you SO much!

I am highly grateful to Prof. K. Ndjoko Ioset (University of Würzburg, Germany, and University of Lubumbashi, D.R. Congo), to Prof. M. Mavoko (University of Kinshasa, D.R. Congo), to Christine and Mechtild Wolf and all the Wolf Family, and to late Prof. F. Schneider, for their strong support.

Particular thank to Profs. P. T. Mpiana and C. N. Kabele (University of Kinshasa, D.R. Congo), and to Asst. Prof. D. F. Dibwe (Hokkaido University, Japan) for their continued support. I am also indebted to many wonderful persons from the region of Mbandaka who helped me during the field trips.

To my former and current colleagues in the Bringmann Group, I am appreciative for the nice and supportive research atmosphere. A particularly big shout out to J. P. Mufusama and Dr. D. Tshitenge, for the memorable cheerful time spent in the laboratory and outside. I also extend my gratitude to S. M. Kavatsurwa, not only for the nice joint cooperation, but also for many wonderful moments shared in Würzburg.

I would like also to thank all the friends who made my life in Germany joyful (Vincent Fungula, Dr. Sibu Mabuza, Lea Fouefack, Maria Vitale, Erick Aroko, and the Congolese and Cameroonian Student Communities in Würzburg) and those who have been strongly supporting me away from Africa (Jentho Mulangua, Edmond Ntambue, Félix Katele, Alexis Ngoyi, and many others).

Last but not least, I extend my deepest gratitude to my beloved parents, Théophile Lombe Kimbadi and Julie Njima Kasendue, to Gylaine Vanissa Tchuisseu Tchakounté, and to all my Family for their unconditional love, support, concern, and understanding!

LIST OF PUBLICATIONS

1. Peer-Reviewed Journal Articles

8) B. K. Lombe, D. Feineis, G. Bringmann; Dimeric naphthylisoquinoline alkaloids: polyketide-derived axially chiral bioactive quateraryls; *Natural Product Reports* **2019** (in press, doi: 10.1039/c9np00024k)

7) S. Awale, C. Balachandran, D. F. Dibwe, S. Fayez, D. Feineis, B. K. Lombe, G. Bringmann; Ancistrolikokine E$_3$, a 5,8′-coupled naphthylisoquinoline alkaloid, eliminates the tolerance of cancer cells to nutrition starvation by inhibition of the Akt/mTOR/Autophagy signaling pathway; *Journal of Natural Products* **2018**, *81*, 2282 – 2291

6) S. M. Kavatsurwa[1], B. K. Lombe[1], D. Feineis, D. F. Dibwe, V. Maharaj, S. Awale, G. Bringmann; Ancistroyafungines A-D, 5,8′- and 5,1′-coupled naphthylisoquinoline alkaloids from a Congolese *Ancistrocladus* species, with antiausterity activities against human PANC-1 pancreatic cancer cells; *Fitoterapia* **2018**, *130*, 6 – 16 ([1]Co-first authors)

5) B. K. Lombe, D. Feineis, V. Mudogo, R. Brun, S. Awale, G. Bringmann; Michellamines A$_6$ and A$_7$, and further mono- and dimeric naphthylisoquinolines from a Congolese *Ancistrocladus* liana and their antiausterity activities against pancreatic cancer cells; *RSC Advances* **2018**, *8*, 5243 – 5254

4) B. K. Lombe, T. Bruhn, D. Feineis, V. Mudogo, R. Brun, G. Bringmann; Antiprotozoal spirombandakamines A$_1$ and A$_2$, fused naphthylisoquinoline dimers from a Congolese *Ancistrocladus* plant; *Organic Letters* **2017**, *19*, 6740 – 6743

3) B. K. Lombe, T. Bruhn, D. Feineis, V. Mudogo, R. Brun, G. Bringmann; Cyclombandakamines A$_1$ and A$_2$, oxygen-bridged naphthylisoquinoline dimers from a Congolese *Ancistrocladus* liana; *Organic Letters* **2017**, *19*, 1342 – 1345

2) F. G. Turini, C. Steinert, G. Heubl, G. Bringmann, B. K. Lombe, V. Mudogo, H. Meimberg; Microsatellites facilitate species delimitation in Congolese *Ancistrocladus* (Ancistrocladaceae), a genus with pharmacologically potent naphthylisoquinoline alkaloids; *Taxon* **2014**, *63*, 329 – 341

1) G. Bringmann, <u>B. K. Lombe</u>, C. Steinert, K. N. Ioset, R. Brun, F. Turini, G. Heubl, V. Mudogo; Mbandakamines A and B, unsymmetrically coupled dimeric naphthylisoquinoline alkaloids, from a Congolese *Ancistrocladus* species; *Organic Letters* **2013***, 15,* 2590 – 2594

2. Oral Talks

9) Naphthylisoquinoline alkaloids as potent antiausterity agents against human pancreatic cancer cells; at the *55th Natural Products Meeting: Chemistry, Biology and Ecology*; Bayreuth (Germany), April 20, **2018** (jointly animated with S. Fayez, from University of Würzburg)

8) Structures, chemotaxonomic implications, and antitumor activities of mono- and dimeric naphthylisoquinoline alkaloids from a Congolese *Ancistrocladus* liana; at the *Department of Chemistry, University of Kinshasa*; Kinshasa (D.R. Congo), April 13, **2018**

7) Spirombandakamine A, an unprecedented fused dimer from a Congolese *Ancistrocladus* plant; at the *53th Natural Products Meeting: Chemistry, Biology and Ecology*; Munich (Germany), April 28, **2017**

6) Absolute stereostructures and possible biosynthetic origins of the novel cage-like naphthylisoquinoline alkaloid dimers, cyclombandakamines A_1 and A_2; 5-minute talk at the *Chem-SyStM Symposium*; Würzburg (Germany), December 6, **2016**

5) Cyclombandakamine A_1, the first caged dimeric naphthylisoquinoline Alkaloid; at the *50th Natural Products Meeting: Chemistry, Biology and Ecology*; Würzburg (Germany), October 9, **2015**

4) Systematic search and elucidation of the absolute stereostructures of novel bioactive natural products; at the *Department of Chemistry, University of Kinshasa*; Kinshasa (D.R. Congo), February 11, **2015** (jointly animated with F.Z. Katele, from University of Pretoria, South Africa)

3) Bioactive naphthylisoquinoline alkaloids isolated from Congolese Ancistrocladus plants; at the *5th SOCHIMICO Symposium*; Kinshasa (D.R. Congo), December 13, **2013**

2) Novel-type dimeric naphthylisoquinoline alkaloids from a Congolese *Ancistrocladus* species; at the *12th International Conference Chemistry Africa*; Pretoria (South Africa), July 11, **2013**

1) Search for novel therapeutic agents: isolation and complete structural elucidation of a novel antiplasmodial alkaloid; at the Workshop of *the Fédération des Entreprises du Congo*; Kinshasa (D.R. Congo), March 1, **2013**

3. Poster Presentations

(Only those personally presented by the author of the thesis)

6) B. K. Lombe, S. Fayez, D. Feineis, T. Bruhn, V. Mudogo, S. Awale, G. Bringmann; Mono- and dimeric naphthylisoquinoline alkaloids from Congolese *Ancistrocladus* plants and mechanistic studies on their anticancer activities; at the *31st Irsee Natural Product Meeting*; Irsee (Germany), **2019**

5) B. K. Lombe, T. Bruhn, D. Feineis, V. Mudogo, G. Bringmann; Novel naphthylisoquinoline dimers, from a Congolese *Ancistrocladus* plant, with antiprotozoal activities; at the *Chem-SyStM Symposium*; Würzburg (Germany), **2018**

4) B. K. Lombe, T. Bruhn, D. Feineis, V. Mudogo, G. Bringmann; LC-UV-MS-CD-assisted discovery of novel-type naphthylisoquinoline dimers in a Congolese *Ancistrocladus* plant; at the *3rd European Conference on Natural Products*; Frankfurt (Germany), **2018**

3) B. K. Lombe, T. Bruhn, D. Feineis, V. Mudogo, G. Bringmann; Naphthylisoquinoline dimers with novel scaffolds, from a Congolese *Ancistrocladus* plant; at the *66th Gordon Research Conference on Natural Products and Bioactive Compounds* and at the *1st Gordon Research Seminar on Natural Products and Bioactive Compounds*; Andover NH (USA), **2017**

2) B. K. Lombe, T. Bruhn, D. Feineis, V. Mudogo, G. Bringmann; Absolute stereostructures and possible biosynthetic origins of novel cage-like naphthylisoquinoline alkaloid dimers; at the *Chem-SyStM Symposium*; Würzburg (Germany), **2016**

1) B. K. Lombe, C. Schies, C. Steinert, V. Mudogo, K. N. Ioset, G. Bringmann; Mbandakamines A and B: new dimeric naphthylisoquinoline alkaloids; at the *8th Joint PhD Students Meeting of the SFB 630 and 766 and FOR 854*; Retzbach (Germany), **2014**